Fakultät für Maschinenwesen

Lehrstuhl für Flugsystemdynamik

A Rapid Robust Fault Detection Algorithm for Flight Control Reconfiguration

Markus Kaminski

Vollständiger Abdruck der von der Fakultät für Maschinenwesen
der Technischen Universität München
zur Erlangung des akademischen Grades eines
Doktor-Ingenieurs (Dr.-Ing.) genehmigten Dissertation.

Vorsitzender:	apl. Prof. Dr.-Ing. Christian Breitsamter
Prüfer der Dissertation:	1. Prof. Dr.-Ing. Florian Holzapfel
	2. Prof. Dr.-Ing. Manfred Hajek

Die Dissertation wurde am 27.12.2017 bei der Technischen Universität München eingereicht und durch die Fakultät für Maschinenwesen am 10.12.2018 angenommen.

Acknowledgements

For his professional assistance I am deeply grateful to my doctoral thesis supervisor Prof. Dr.-Ing. Florian Holzapfel from the Technical University of Munich. The numerous fruitful discussions on the subject greatly helped me to develop new views on the topic. Furthermore I would like to thank all my colleagues at Airbus that supported me. Foremost my bosses Dr. Johann Krammer, Wolfgang Schirdewahn, and Rudi Bischoff who allowed me to work part of my time on the Sagitta research project. The latter facilitated the preparatory activities that laid the early basis for the content presented herein. I am also very thankful to Dr. Hans-Christoph Oelker for the comments received after reviewing the draft of this text.
Finally I would like to thank my girlfriend Juliane for her patience and encouragement throughout the years where this thesis project came into life. It was written in parallel to the author's normal work at Airbus and I would like to especially thank her for accepting the uncounted hours of our home life that went into this thesis.

Markus Kaminski
Munich 2017

Abstract

This thesis resides in the area of fault-tolerant flight control. It was inspired by the idea to combine a Conventional Flight Control System (CFCS) with an active fault-tolerant one. The latter is only activated in case that the conventional FCS is no longer able to provide an acceptable closed-loop performance, e.g. due to severe aircraft damage. Such an approach would potentially permit keeping the Active fault-tolerant FCS (AFCS) largely outside certification scope and thus help to avoid/limit problems that may arise from the immature certification experience with respect to AFCS. Furthermore it will allow to *augment* the existing certified and proven CFCS of operational aircraft instead of replacing them entirely, thus leading to significantly reduced costs and development risks. Of course such a setup warrants reliable means to detect a CFCS problem that is severe enough so that it warrants switching to the AFCS. This thesis suggests a possible approach to this fault detection problem utilizing a *model-based* approach. The major focus to this effect is in the task of *residual evaluation*, which, in general has only been very sparsely investigated in the past (cf. Ding, 2013, p. 17).
Driven by the certification requirement the primary goal of this work was to provide an approach that guarantees a user selectable False Alarm Rate (FAR). A false alarm would lead to an inadvertent activation of the AFCS and is therefore certification relevant. A secondary objective was to limit conservatism in the assumptions in order to provide a fault detection performance that promises practical benefits of the suggested system. Both goals have, to the author's opinion, been achieved. Concerning the secondary objective several potential additional improvements have been identified, that could be investigated in a follow-on work. The suggested approach has been tested in a linear simulation case study based on a public F-16 model provided e.g. by Klein and Morelli (2006).

The primary research contributions provided by this thesis are:

- The idea of combining a CFCS with an AFCS, albeit not complete new, has only been very sparsely investigated in the past and none of the work known to the author (cf. chapter 1.4) do treat the problem of how to define a useable switching logic/threshold beyond mentioning its existence. This thesis focusses especially on the switching, i.e. fault detection, algorithm. The above mentioned reasoning chain implies that the possibility that the fault-tolerant flight control system is *inadvertently activated* must be very remote, i.e. the False Alarm Rate (FAR) must be very low. To judge the possibility for inadvertent activation, the FAR must be quantifiable by a number. This work *uses a strict, state of the art FAR-based design approach,* as suggested by Ding (2013), and applies it to the aircraft fault detection problem on hand. This strict FAR-based

design approach is, to the author's knowledge, new in the context of aircraft fault detection.

- Most of the current Fault Detection and Diagnosis (FDD) work treats the problem detecting faults in the uncontrolled plant. In case of aircraft, and potentially in many other applications, the user (e.g. pilot) is much more interested in the *closed-loop* performance of the system, because that is what is visible to him/her. The author therefore suggests to model *the acceptable closed-loop performance, directly derived from the respective flying qualities standards, as deterministic model uncertainties of reference model* used for fault detection. The approach to use the flying quality standard derived CAP-ζ_{SP} combination to define the parameter polytope of acceptable reference model uncertainties and consequently derive the norm-based residual threshold based on this reference model was developed by the author and is, to the author's knowledge, new.
- The aforementioned approach for the fault detection system required the extension of the combined stochastic/norm-based fault detection approach for deterministic and stochastic unknown *inputs,* as suggested by Ding (2013, pp. 339-345), to the much more complex case of deterministic/stochastic unknown inputs and *deterministic model uncertainties*. Several extensions are suggested in this work with respect to the aircraft application discussed above. The work thus adds research results to the, as highlights by Ding (2013, p. 17), very sparsely investigated FDD research area of *residual evaluation*.
- The FD system proposed in this thesis is to author opinion, very flexible to adapt to different practical demands. Adaptations are easily done by just changing the range of acceptable *closed-loop* natural frequencies and damping ratios. Most important, those two parameters can be readily interpreted in physical and flying quality context and they allow a direct comparison with the flying quality standards MIL-F-8785C (US DoD, 1996) and MIL-STD-1797B[1] (US DoD, 2012). To the author's opinion this is a significant practical advantage and gives the aerospace engineer a direct understanding what the effect of the parameter changes are.

Furthermore the work provides several secondary contributions, which are summarized in chapter 1.5.

[1] Restricted distribution, therefore information from MIL-F-8785C is used within this text.

Table of Contents

List of Tables

List of Figures

List of Acronyms

Acronym	Description
Act.	Actuator
ACTIVE	Advanced Control Technology for Integrated Vehicles
ADS	Air Data System
AFCS	Active Fault-Tolerant Flight Control System
AFTC	Active Fault-Tolerant Control
AGARD	Advisory Group for Aerospace Research and Development
AirSTAR	Airborne Subscale Transport Aircraft Research
AMC	Acceptable Means of Compliance
AoA	Angle of Attack
ARRC	Adaptive Retrofit Reconfigurable Control
ATTAS	Advanced Technologies Testing Aircraft System
CAP	Control Anticipation Parameter
CAT	Category
CDF	Cumulative Distribution Function
CFCS	Conventional Flight Control System
CG	Centre of Gravity
DLR	Deutschen Zentrums für Luft- und Raumfahrt (German)
DoD	Department of Defence
DOF	Degrees Of Freedom
DS	Data Source
DT1	Differential, 1st order lag control element
EAS	Equivalent Air Speed
EASA	European Aviation Safety Agency
ECEF	Earth Centred Earth Fixed
EOM	Equations of Motion
Eq.	Equation
FAR	False Alarm Rate
FC	Flight Condition
FCS	Flight Control System
FD	Fault Detection
FDD	Fault Detection & Diagnosis
FDI	Fault Detection and Identification
FDIA	Fault Detection Isolation and Analysis
FDIE	Fault Detection Isolation and Estimation
FLARE	Fast on-Line Actuator Reconfiguration Enhancement
FMEA	Failure Mode and Effect Analysis

Acronym	Description
FS	Force Source
FTC	Fault-Tolerant Control
GLR	Generalized (log) Likelihood Ratio
HIDEC	Highly Integrated Digital Electronic Control
ID	Identification
IDF	Israeli Defence Forces
IFC	Intelligent Flight Control
ILS	Instrument Landing System
IMM	Interacting Multiple Models
ISA	International Standard Atmosphere
KEAS	Knots Equivalent Air Speed
KTAS	Knots True Air Speed
LMI	Linear Matrix Inequality
LOC	Loss-Of-Control
LOES	Low Order Equivalent System
LPV	Linear Parameter Varying
LR	Likelihood Ratio
LTI	Linear Time Invariant
MC	Monte Carlo
MDR	Missed Detection Rate
MIMO	Multiple Input Multiple Output
ML	Maximum Likelihood
MM	Multi Model
MMS	Multi Model Switching
MMST	Multiple Model Switching and Tuning
MPC	Model Predictive Control
MRAC	Model Reference Adaptive Control
MS	Moment Source
MSLS	Modified Sequential Least Square
MT	Motion Type
NASA	National Aeronautics and Space Administration
NATO	North Atlantic Treaty Organization
NED	North East Down
NF	Notation Frame
NTSB	National Transportation Safety Board
PCA	Propulsion Controlled Aircraft
PFTC	Passive Fault-Tolerant Control
PIO	Pilot Induced Oscillations

Acronym	Description
PL	Position Limit (of actuator/control surface)
PSD	Power Spectral Density
PT0	Proportional control element (without lag)
PT1	Proportional, 1st order lag control element
PT2	Proportional, 2nd order lag control element
PTNN	Pre-Trained Neural Network
RCM	Retrofit Control Module
RFTFC	Reconfigurable Fault-Tolerant Flight Control
RHOC	Receding Horizon Optimal Control
RL	Rate Limit (of actuator/control surface)
RMS	Root Mean Squared
RP	Reference Point
RTO	Research and Technology Organisation (of NATO)
SAE	Society of Automotive Engineers
SDFCS	Self-Designing Flight Control System
SISO	Single Input Single Output
SL	Sea Level
SMC	Sliding Mode Control
SOFFT	Stochastic Optimal Feed-forward and Feedback Technique
SRFCS	Self-Repairing Flight Control System
STC	Self-Tuning Controller
SW	Sliding Window
TAFA	Tailless Advanced Fighter Aircraft
TAS	True Air Speed
TC	Test Case
TCAS	Traffic Alert and Collision Avoidance System
TIFS	Total In-Flight Simulator
TUM	Technical University of Munich
UAS	Unmanned Aerial System
UAV	Unmanned Aerial Vehicle
UB	Universitätsbibliothek (German)
UCAV	Unmanned Combat Aerial Vehicle
US	United States of America
USAF	United States Air Force
USN	United States Navy
VISTA	Variable Stability In-flight Simulator Test Aircraft
ZOH	Zero Order Hold element

Nomenclature

For the Euclidian vector space a declaration scheme based on (Holzapfel, 2011, pp. 5/1-15/1) is applied.

Latin letters:

Symbol	Description
$\vec{\boldsymbol{a}}_K$	Linear Acceleration. Abbreviation for $(\vec{\boldsymbol{a}}_K^G)^{II}$.
$\boldsymbol{A}, \boldsymbol{B}, \boldsymbol{C}, \boldsymbol{D}$	System matrices of state space model.
b	Wing span
CAP	Control Anticipation Parameter
C_{ik}	Aerodynamic non-dimensional coefficient of reference value i due to k.
$\bar{c}$	Mean aerodynamic cord
d_i	Decision function with respect to i
$\hat{d}_i$	Decision function with respect to i based on generalized likelihood ratio estimate
$\boldsymbol{d}$	Deterministic disturbance input vector
$e, \boldsymbol{e}$	Scalar/vector error signal
$\boldsymbol{E}_i$	Disturbance input matrix for input i. Affecting state equation.
$\boldsymbol{f}$	Fault input vector
FAR	False Alarm Rate
$\widehat{FAR}$	False Alarm Rate estimated from simulation
$\boldsymbol{F}_i$	Disturbance input matrix for input i. Affecting output equation.
$\left(\vec{\boldsymbol{F}}_{FS}^{RP}\right)_{NF}$	Force of type FS applied at reference point RP and listed in notation frame NF.
g	Earth gravitational acceleration
$\vec{\boldsymbol{g}}_0$	Gravitational acceleration in the 0 notation frame.
$G_{yu}, \boldsymbol{G}_{yu}$	Transfer function/matrix from input u to output y.
h_A	Pressure altitude
h_P	Angular momentum of engine
H_q	Feed-forward gain
$\boldsymbol{H}_0, \boldsymbol{H}_1$	Null hypothesis and alternative hypothesis
$\mathcal{H}_\infty$	$\mathcal{H}_\infty \equiv \left\|\boldsymbol{G}_{rq_{cmd}}\right\|_\infty$

Symbol	Description
$\mathcal{H}_{\infty,max}$	Maximum $\mathcal{H}_{\infty,\max}$-norm of all systems inside model uncertainty parameter polytope, i.e. $\mathcal{H}_{\infty,max} \equiv \left\|\boldsymbol{G}_{rq_{cmd}}\right\|_{\infty,max}$
$\boldsymbol{I}$	Identity Matrix
J_{th}	Fault detection threshold (general)
$J_{th,RMS}$	Deterministic fault detection threshold based on RMS-value
J_{th,χ^2}	Integrated stochastic/deterministic fault detection threshold
$\tilde{J}_{th,\chi^2}$	Integrated stochastic/deterministic fault detection threshold for colored-noise corrected variance
$(\boldsymbol{J}^{RP})_{XY}$	Moments of inertia around point RP with coordinate system of input vector X and coordinate system of output vector Y.
k	Sample number
$\boldsymbol{K}_i$	Controller gain
$\mathcal{K}$	System gain
L_{w_W}	Turbulence scale length
$\boldsymbol{L}$	Observer gain matrix
Ma_A	Mach Number
m	Mass of air vehicle
m_{χ^2}	Degree of freedom of chi-square distribution
M_i	Aerodynamic dimensional pitch moment coefficient of reference value i.
$\left(\vec{\boldsymbol{M}}_{MS}^{RP}\right)_{NF}$	Moment of type MS around reference point RP and listed in notation frame NF.
$\boldsymbol{M}_{XY}$	Transformation matrix with coordinate system of input vector X and coordinate system of output vector Y.
$(n_z)_{NF}$	Normal load factor. Abbreviation for $\left(n_{K,z}^{G}\right)_{NF}$ given in notation frame NF.
N_i	Number of samples used with respect to i
$N(s)$	Transfer function nominator
$\mathcal{N}(\boldsymbol{\mu}, \boldsymbol{\Sigma})$	Gaussian normal distribution with mean $\boldsymbol{\mu}$ and covariance $\boldsymbol{\Sigma}$
p_θ	Probability of parameter θ
p	Roll component of $(\vec{\omega}_K^{OB})_B$
$\boldsymbol{P}_i$	Co-variance matrix for system i
P_a	Actual power level of engine

Symbol	Description
P_c	Commanded power level of engine
q^*	Dimensionless pitch rate
q_K	Pitch component of $(\vec{\omega}_K^{OB})_B$
q_{cmd}	(Pilot) pitch rate command input
$\check{q}_{cmd}$	(Pilot) pitch rate command amplitude
$\bar{q}_A$	Dynamic pressure
$\overline{\boldsymbol{Q}}$	Discrete state-covariance of residual dynamic system
r	Yaw component of $(\vec{\omega}_K^{OB})_B$
$\tilde{\boldsymbol{r}}, \tilde{r}_i$	Vector residual signal $\tilde{\boldsymbol{r}}$ with components $\tilde{r}_i$ at residual post filter input
$\check{\boldsymbol{r}}, \check{r}_i$	Vector residual signal $\check{\boldsymbol{r}}$ with components $\check{r}_i$ at residual post filter output
$\boldsymbol{r}, r_i$	Vector residual signal $\boldsymbol{r}$ with components r_i at variance scaling filter output
$(\check{\boldsymbol{r}}_{det})_{sim}$	Residual deterministic signal amplitude
s	Continuous time Laplace operator
$s(y_i)$	Log Likelihood Ratio (LR) for sample y_i
$S(\boldsymbol{Y})$	Log Likelihood Ratio (LR) for sample vector $\boldsymbol{Y}$
$\hat{S}(\boldsymbol{Y})$	Log Likelihood Ratio (LR) estimate for sample vector $\boldsymbol{Y}$
S	Wing reference area
t_{TI}	Time. Time identifier TI (see table below).
T_{TI}	Time constant. Time identifier TI (see table below).
T_{w_W}	Turbulence period
$\boldsymbol{u}$	Input vector (general context)
V_A	True airspeed (TAS). Abbreviation for $V_A = \lvert(\vec{\boldsymbol{v}}_A^G)_A\rvert$.
V_{EAS}	Equivalent Air Speed (EAS). $V_{EAS} = V_A \cdot \sqrt{\rho_A(h_A)/\rho_{A,ISA\,SL}}$.
$V(\boldsymbol{x})$	Lyapunov function
$\overline{\boldsymbol{V}}$	Discrete time residual variance scaling filter matrix
$\mathcal{V}_i$	Vertex system i (see polytopic model uncertainties)
$\mathcal{V}_{\infty,max}$	The vertex that leads to $\lVert\boldsymbol{G}_{rq_{cmd}}\rVert_{\infty,max}$
$y, \boldsymbol{y}$	Scalar/vector system output
$\hat{y}, \hat{\boldsymbol{y}}$	Scalar/vector system output estimate

Symbol	Description
$x, \boldsymbol{x}$	State scalar/vector
$\hat{x}, \hat{\boldsymbol{x}}$	State scalar/vector estimate
$x_0, \boldsymbol{x_0}$	Initial state
$(x^G)_B$	Position of the centre of gravity in the B coordinate system, commonly referred to as CG position.
X_i	Aerodynamic dimensional X-force coefficient of reference value i.
z	Discrete time Laplace operator
Z_i	Aerodynamic dimensional Z-force coefficient of reference value i.
$\|.\|_2$	2-Norm of signal
$\|.\|_{RMS}$	Root Mean Square (RMS) value of signal
$\|.\|_\infty$	Peak norm of signal for a vector, $\mathcal{H}_\infty$-Norm for a transfer matrix

Greek letters:

Symbol	Description
α_{NF}	Angle of attack. Notation is NF.
$\alpha_0(d)$	Size or level of significance of statistical test, i.e. False Alarm Rate (FAR) of test d
$\alpha_1(d)$	Missed Detection Rate (MDR) of test d
β_{NF}	Angle of sideslip. Notation is NF.
$\beta(d)$	Power of test d
γ_{NF}	Flight path angle
δ_T	Thrust lever position
$\boldsymbol{\delta}, \delta_i$	Parameter vector with components δ_i
Δ	Deviation from trim condition (if preceding sinal/value)
$\boldsymbol{\Delta}$	Model uncertainty identifier (if preceding matrix)
ε_i	Error correction factor for reference value i
ζ_i	Damping ratio of dynamic system i.
$\tilde{\zeta}_i$	Damping ratio of dynamic system i for model uncertainty polytope approximation.
η	Elevator deflection angle
$\boldsymbol{\theta}_i$	Parameter vector for reference value i
$\widehat{\boldsymbol{\theta}}_i$	Estimate of parameter vector $\boldsymbol{\theta}_i$

Symbol	Description
κ	Flap deflection angle
λ_{χ^2}	Non-centrality parameter of chi-square distribution
$\mu, \boldsymbol{\mu}$	Scalar/vector arithmetic mean
μ_{χ^2}	Mean of chi-square distribution
$\boldsymbol{\nu}_P$	Process noise in state space context
$\boldsymbol{\nu}_M$	Measurement noise in state space context
$\boldsymbol{\nu}_N$	White noise (N for normal distribution)
$\boldsymbol{\nu}_i, \vec{\boldsymbol{\nu}}_i$	Noise vector of reference value i in sensor context
$\boldsymbol{\Sigma}_i$	Co-variance matrix of reference value i.
$\boldsymbol{\Sigma}_{\boldsymbol{P}}$	Process noise covariance matrix of process i (Kalman filter)
σ_i	Standard deviation of reference value i
σ_{max}	Maximum singular value
Σ	Variance
$\tilde{\Sigma}_{\chi^2}$	Estimated variance of chi-square distribution
$\hat{\Sigma}_{\chi^2}$	Colored noise corrected variance of chi-square distribution
Φ_i	Power spectral density for signal i
χ^2_m	Central chi-square distribution with m degrees of freedom
$\chi^2_m(\lambda)$	Non-central chi-square distribution with m degrees of freedom and non-centrality parameter λ
ω_i	Angular rate of system i
$\omega_{\mathcal{H}_{\infty,max}}$	$\omega_{\mathcal{H}_{\infty,max}} \equiv \omega_{\left\|\boldsymbol{G}_{rq_{cmd}}\right\|_{\infty,max}}$
$\vec{\boldsymbol{\omega}}_{K,DS}$	Abbreviation of $(\vec{\omega}_K^{OB})_B$.
$\dot{\vec{\boldsymbol{\omega}}}_{K,DS}$	Abbreviation of $\left(\dot{\vec{\omega}}_K^{OB}\right)_B^B$.
$(\vec{\boldsymbol{\omega}}_{MT}^{XY})_{NF}$	Angular rate of the axis system Y around the axis system X and listed in notation frame NF. Type of Motion MT.
$\left(\dot{\vec{\boldsymbol{\omega}}}_{MT}^{XY}\right)_{NF}^{Z}$	Angular acceleration of the axis system Y around the axis system X derived in coordinate system Z and listed in notation frame NF. Type of Motion MT.

Indices for Reference Points (RP):

Index	Description
E_0	Origin of ECEF Frame E (center of earth)
G	Centre of Gravity
N_0	Origin of Navigation Frame N

Indices for Motion Types (MT), Force Sources (FS) and Moment Sources (MS):

Index	Description
A	Aerodynamic
G	Gravitational
K	Kinematic
P	Propulsive

Indices for notation frames (X, Y, Z, NF):

Index	Description
0	Local NED system
A	Aerodynamic
B	Air vehicle body coordinate system
E	ECEF coordinate system
N	Navigation Frame
W	Wind

System, Signal and Value identifiers:

Index	Description
∞	Stationary value for $t \to \infty$.
lim	Limit value
det	Deterministic signal
max	Maximum value
cmd	Command input
env	Signal envelope (obtained by envelope detector)
nom	Nominal value
FD	Fault Detection
FCS	FCS Override Activation
L1	ω_{SP} and ζ_{SP} bounds derived from L1 flying qualities requirements

Index	Description
req	Requirement
RMS	Root Mean Square Signal
PF	Residual Post Filter
F	Fault Occurence
W	Wind System
HP	High Pass
LP	Low Pass
OL	Open-loop system
CL	Closed-loop system
SP	Longitudinal short period system
u	Unknown input
k	Known input
No index	True value
0	Trim value
10%	ω_{SP} and ζ_{SP} bounds derived from allowing 10% deviation from nominal values

Indices for Times (TI):

Index	Description
$n_z = 1$	Time when $(n_z)_K$ = 1 g has been reached/passed during recovery
$q_k = 0$	Time when the pitch-up rotation has been stopped during recovery
2	Time to double
D	Delay
F	Time of Fault occurrence
FCS	Time of CFCS Override Activation
FD	Time of Fault Detection
s	Sample time
η	Time when the elevator has reached its full recovery deflection

Citations and quotations rules and style follow the citation guideline of the "Technische Universität München" (TUM UB, 2014).

Definitions of Terms

Agility
The ability of the air vehicle to change its flight path vector $(\vec{v}_K^G)^E$ rapidly.

Flight Control System (FCS)
The term *flight control system*, as used in this text, refers to modern digital full authority control architectures where no direct mechanical connection between the input element (e.g. stick) and the control effector (e.g. the aerodynamic control surface) exists. Those systems are typically also called fly-by-wire or fly-by-light flight control systems.

Active fault-tolerant Flight Control System (AFCS)
The term *active fault-tolerant flight control system* refers to flight control systems which are able to adapt themselves to changes of the plants dynamic behaviour that have *not been pre-modelled* (e.g. structural damage of the air vehicle).

Conventional Flight Control System (CFCS)
The term *conventional flight control system*, as used in this text, refers to flight control systems which are only able to react on changes of the plants dynamic behaviour that *have been pre-modelled*. Those changes can, for example, result from different flight conditions (e.g. dynamic pressure, angle of attack, Mach number) or failures of system components (e.g. sensors, actuators).

Flying Qualities vs. Handling Qualities
This text uses the following definition:
Flying qualities are the characteristics, or the dynamics, of the airplane.
Handling qualities are the characteristics, or the dynamics, of the pilot plus airplane.

Fault:
"An unpermitted deviation of at least one characteristic property or parameter of the system from the acceptable / usual / standard condition." (R. Isermann & Ballé, 1997, p. 710)

Failure:
"A permanent interruption of a system's ability to perform a required function under specified operating conditions. (R. Isermann & Ballé, 1997, p. 710)

Error:
"A deviation between a measured or computed value (of an output variable) and the true, specified or theoretically correct value." (R. Isermann & Ballé, 1997, p. 710)

Disturbance:
"An unknown (and uncontrolled) input acting on a system." (R. Isermann & Ballé, 1997, p. 710)

Residual:
"A fault indicator, based on a deviation between measurements and model-equation-based computations." (R. Isermann & Ballé, 1997, p. 710)

Fault detection:
"Determination of the faults present in a system and the time of detection." (R. Isermann & Ballé, 1997, p. 710)

Fault isolation:
"Determination of the kind, location and time of detection of a fault. Follows fault detection." (R. Isermann & Ballé, 1997, p. 710)

Fault identification:
"Determination of the size and time-variant behaviour of a fault. Follows fault isolation." (R. Isermann & Ballé, 1997, p. 710)

Fault diagnosis:
"Determination of the kind, size, location and time of detection of a fault. Follows fault detection. Includes fault identification." (R. Isermann & Ballé, 1997, p. 710)

Analytical redundancy:
"Use of two or more (but not necessarily identical) ways to determine a variable, where one way uses a mathematical process model in analytical form." (R. Isermann & Ballé, 1997, p. 710)

Safety:
"Ability of a system not to cause danger to persons or equipment or the environment." (R. Isermann & Ballé, 1997, p. 710)

1 Introduction

The topic of this thesis resides in the large research field of fault-tolerant control which is mainly composed of the three research areas of Fault Detection and Diagnosis (FDD), Robust Control and Reconfigurable Control (Figure 1). This work picks up the only very sparsely investigated idea of augmenting a contemporary conventional flight control system with a fault-tolerant one. Beside the important practical and economic advantage that such a system could relatively easily be retrofitted to existing flight control systems it also has, to the author's opinion, some significant advantages with respect to certification. The reader may imagine it would be possible to develop a fault detection system that only activates the fault-tolerant flight control system when the conventional one is no longer able to deliver a sufficient closed loop performance. In this case we could argue that this should never happen in the certified envelope and only in case of a malfunction that was not foreseen during design and certification phase (e.g. severe structural damage). A respective fault detection system would of course be obliged to have a very low false alarm rate in order to ensure that the risk of unintentionally activating the fault-tolerant system is sufficiently low. This thesis addresses the question of how to approach the design of such a system using state of the art FDD techniques. It proposes a new way to fault detection based on monitoring of the closed-loop aircraft response to pilot commands. However, before going into the details of fault detection in dynamic systems, it is worth discussing the importance of fault-tolerant flight control in general as well as some more details on the motivation for this thesis.

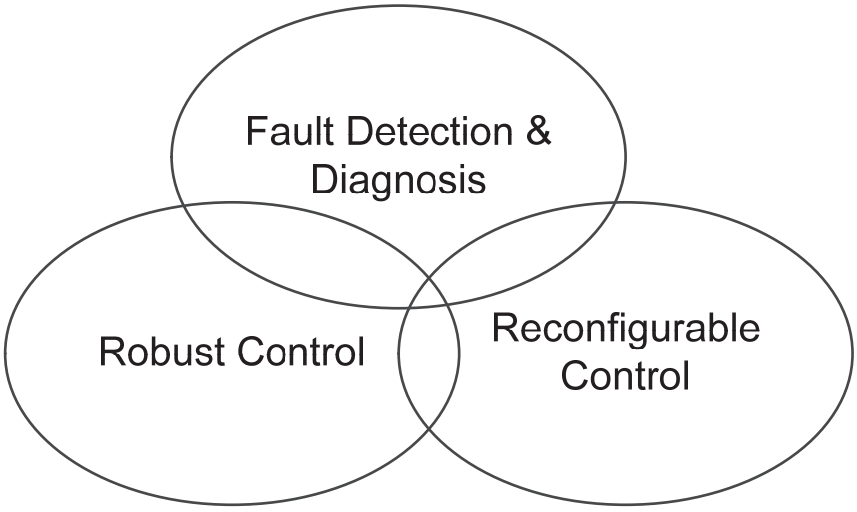

Figure 1 Areas of fault-tolerant control (based on Patton, 1997, p. 1035)

1.1 Why Fault-Tolerant Flight Control?

In the last three decades so called fault-tolerant flight control systems have drawn significant attention of the research community, authorities, and industry. The term fault-tolerant thereby refers to the potential of those systems to tolerate faults that cannot be dealt with by conventional flight control systems therefore reducing the risk of losing an aircraft due to loss of control.
Before looking at the fault-tolerant flight control systems it is worth discussing the different reasons why the loss of an aircraft must be prevented by all available means. The first, and most important one, is obvious for manned aircraft. The lives of the occupants must be protected by all feasible means. However one must not forget that an aircraft crash even in sparsely populated areas also poses a significant risk to people on ground. This risk is the same for manned and unmanned aircraft[2]. As the hazard of being injured must be the same or even less for uninvolved persons on ground than for those on-board, the loss of an aircraft must be prevented for both, manned and unmanned systems. The second reason, why losing an aircraft is unacceptable, is related to financial considerations. Both manned and unmanned aircraft are getting more and more expensive. This is above all true for military systems due to their, compared to civilian ones, low production quantities and more complex on-board systems. The loss of two RQ-4A Global Hawk UAVs in 2001 and 2002, for example, was quoted at $40.6 million each (USAF, 2001, 2002), and the loss of a B-2A stealth bomber in 2008 at $1.4 *billion* (USAF, 2008). Moreover the air segments of current UAS are comparatively simple designs but they will, especially with the introduction of Unmanned Combat Aerial Vehicles (UCAV), become significantly more complex and thus expensive. Therefore, also from a financial point of view, it will be less and less acceptable to lose an air vehicle neither a manned nor an unmanned one. Finally, in a military context, the complete loss of an air vehicle results in a significant tactical and strategic disadvantage, especially in a large scale conflict, where the amount of aircraft damaged and lost tend to be very high at the beginning of the crisis (Pywell, Alonze, Hurricks, & Wellings, 1999, p. 23-6). Pywell et al. point out that "since the accumulative damage and loss rates could be very high, aircraft availability is critical. This emphasises the need to avoid damage as far as is practical and the equally important need to conserve and re-cycle valuable damaged aircraft. *It is essential that damaged aircraft can return to base and can be repaired quickly.* [emphasis added] Remembering that the purpose of the aircraft is to generate successful combat missions, survivability is fundamental to this aim." To the author's opinion, the situation is even worse nowadays and will continue to

[2] The risk is the same when comparing manned and unmanned aircraft that have the same reliability and physical characteristics i.e. mass, dimensions.

worsen in the future because, as mentioned before, military systems become more and more expensive and thus the total numbers of units produced are constantly decreasing. An extreme example is again the B-2 fleet. Only 21 B-2s have been built and only 20 of them are in operational service with the USAF. Loosing just a single airplane hence already leads to a significant reduction of the B-2 fleets fighting power.

While this shows that everything possible must be done to prevent the complete loss of an aircraft the question remains how the later can be avoided i.e. the survivability of the system can be increased. In principal two basic concepts exists: to avoid damage or to make the system more tolerant to possible damage. Both terms have been coined by the military community in the more specific context of man-made threats as "Battle Damage Avoidance" and "Battle Damage Tolerance" but can be readily extended to the more general case of avoiding or tolerating damage in general, no matter what the reason for it is i.e. damage avoidance and damage tolerance. Examples for damage avoidance provisions are anti-collision systems like the Traffic Alert and Collision Avoidance System (TCAS), self-defence systems, engine fire extinguishers, armoured protection or weather radars. Damage tolerance is typically increased by hardware redundancy (e.g. duplication of engines, important sensors, actuators, and structural load paths) or more intelligent use of the existing on-board resources (e.g. smarter logics and algorithms). Under the latter fall fault-tolerant flight control systems as defined in the first paragraph of this chapter

So what is the difference between conventional flight control systems and fault-tolerant ones? It is certainly true that also the former are able to react on faults. However fault detection and identification is limited on detecting failures of certain system components. Continuous system operation, after a fault, is then achieved by using a redundant backup system (e.g. flight control computer, sensor, and actuator) or by switching to a pre-defined backup mode where the failed system is not required. An example for the latter would be a gain scheduled Angle of Attack (AoA) command system that, after detecting an AoA measurement failure, switches to a rate command pitch attitude hold demand systems and to AoA-independent controller gains. The current industrial state-of-the-art is also well summarized by Goupil and Marcos (2010, p. 522):

> The state-of-practice for an aircraft manufacturer to diagnose and to tolerate faults, and then to obtain full flight envelope protection under all possible external disturbances, is to provide high levels of hardware redundancy. Relying on this strong redundancy, fault detection is mainly performed by cross checks, consistency checks, voting mechanisms and built-in test techniques of varying sophistication […]. Fault tolerance relies mainly on hardware redundancy, stringent safety analysis, dissimilarity, physical installation segregation

and hardware/software reconfiguration. Here reconfiguration means automatic management following a failure.

This conventional approach to fault tolerance has certain disadvantages. First of all, as Goupil and Marcos point out, it requires a comparably high amount of hardware redundancy but, more important, it cannot deal with faults that have not been foreseen or were too complex to be pre-modelled during flight control system design. The most illustrative example is an air vehicle subject to some form of structural damage. If, for example due to a mid-air collision, a part of a wing is torn off the air vehicle it is virtually impossible to foresee and detect all possible wing structure failures, build a plant model, and design a control system in advance for it. In addition it is also not possible to switch to a redundant backup system because that would require a backup airframe, which is, for obvious reasons, not available. Fault-tolerant control systems approach this deficiency by accounting for that kind of damage either *during the controller off-line design* i.e. passive fault-tolerant control or by installing means that allow controller adaptation to unforeseen dynamic behaviour *during* controller operation i.e. active fault-tolerant control. The advantages and disadvantages of both approaches will be discussed in more detail in chapter 2.3 however it must be noted here that the possibilities of passive fault-tolerant control, which is based on robust control, are limited as there is fundamental trade-off between robust stability and robust performance. Furthermore the separation between passive fault-tolerant control and conventional control is diffuse. Of course also for the design of conventional control systems parameter uncertainties have to be taken into account. However those uncertainties have classically been relatively small model uncertainties related to the fact that even the model of the undamaged aircraft will not be perfect. In contrast, with passive fault-tolerant control, the concept of model uncertainty has been systematically applied to explicitly treat air vehicle damage.

Before moving on it is important to note that historically there has always been an active fault-tolerant control element inside the aircraft: Pilots in a manned aircraft can, within their physiological limits, adapt to the changed dynamics of even severely damaged aircraft. This has been demonstrated several times in the past (cf. Edwards, Lombaerts, & Smaili, 2010, pp. 21-38). Probably the most noteworthy events where the landing of an IDF F-15 (no. 957) which lost the whole right wing due to a mid-air collision (Aloni, 2006, p. 70; Mason, 1985, p. 29; Tomayko, 2003, pp. 1-4), American Airlines flight UA232 where the crew managed to fly the aircraft for approximately 45 min even after a complete hydraulic failure only by engine thrust modulation (NTSB, 1990, pp. 1-5), and the very well documented B-52H (no. 61-023) test flight on Jan 10, 1964 where the aircraft vertical stabilizer was torn off as a result of strong clear air turbulences (Hartnett, 2006; USAF, 1964). The possi-

bility for successful pilot intervention will however be more and more limited. First of all due to the growing number of unmanned air systems, where the pilot is on ground and therefore virtually outside the control systems inner loops, and second due to the many air vehicle configurations that cannot be controlled by a pilot without the help of a control system i.e. strongly unstable aircraft. This means that fault-tolerant flight control systems, besides being just a valuable aid to the pilot, will become more and more essential to sustain the damage tolerance of stable contemporary manned aircraft configurations.
This chapter tried to show that human safety, financial and military considerations force us to prevent the loss of an aircraft by all feasible means. Furthermore the increasing numbers of unmanned aircraft and naturally unstable configurations, which cannot be controlled without the aid of a flight control system, limit the possibility of active fault-tolerant control by human pilots. Hence fault-tolerant flight control becomes an important cornerstone of sustaining and increasing air systems survivability.

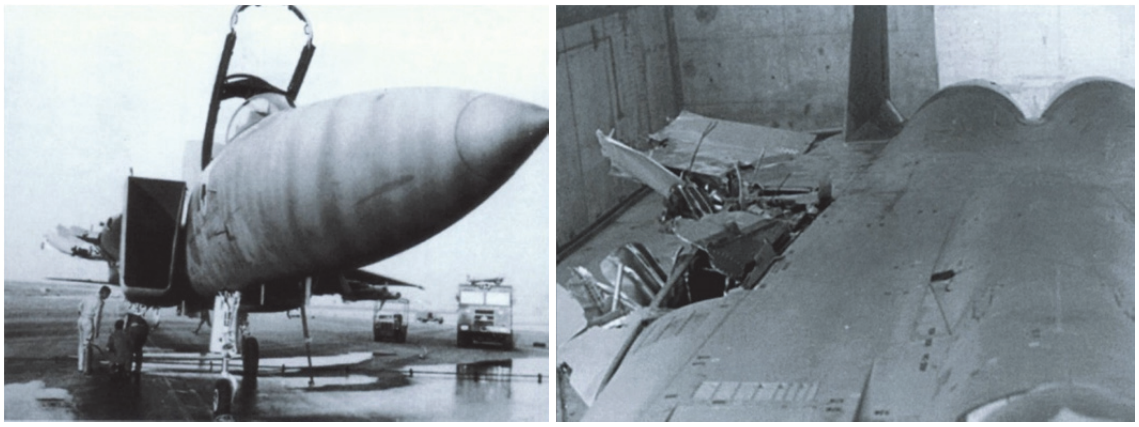

Figure 2 IDF F-15 (no. 957) after landing without right wing. The right wing was nearly completely torn off by a mid-air collision (Unknown, 2014)

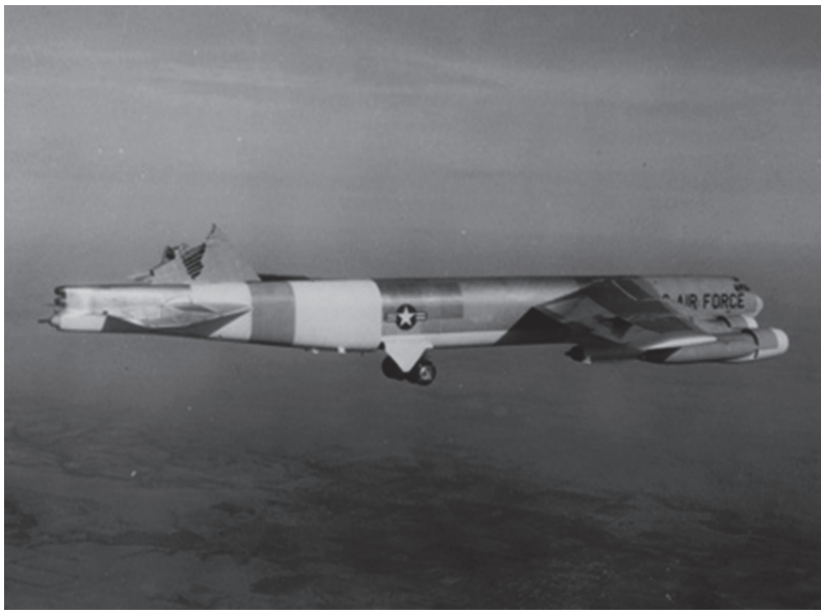

Figure 3 USAF B-52H (no. 61-023) after losing its vertical stabilizer on a test flight to investigate the effects of clear air turbulence on the fin structure (Unknown, 1964). Lateral stability was augmented by increasing the drag aft of the Centre of Gravity (CG). Hence only the aft landing gear was lowered, till shortly before landing, and the outboard speed brakes were deflected. In addition a forward CG position was maintained by pumping fuel from the aft to the forward fuel groups. Furthermore the angle of sideslip was actively controlled by differential thrust. (USAF, 1964).

1.2 Motivation for this Thesis

Despite their advantages fault-tolerant flight control systems have not yet seen widespread use beyond the scope of experimental aircraft, small UAVs, and a few fault-tolerant elements to detect actuator and sensor failures in production aircraft. One of the rare examples of the latter is the actuator oscillatory failure detection algorithm implemented in the Airbus A380 flight control system as described by Goupil (2010) and Lavigne, Cazaurang, Fadiga, and Goupil (2014).
To the author's opinion there exist two major reasons for the current situation:

1. Most active fault-tolerant methods are not yet compatible to the certification demands. Although there have been recently some improvements in this regard, the certification experience remains limited.
2. Most current approaches aim at *replacing* the *certified* conventional flight control systems already installed in current production aircraft or aircraft families.

Let us discuss the certification aspect first. In aviation, and many other industries, certification is an inevitable requirement for all safety critical systems and the certification requirements with respect to a catastrophic failure, i.e. one that causes multiple fatalities, are quite demanding. For large aeroplanes, for example, EASA AMC 25.1309 requires that the average probability of *any* catastrophic failure is less than 10^{-9} per flight hour (EASA, 2013, p. 2-F-45). This probability includes hardware failures (e.g. a flight control computer malfunction) but also "design" failures (e.g. the inability of an algorithm to deal with a certain situation). EASA AMC 25.1309 further states that, "the required substantiation of the proper functioning of equipment, systems, and installations under the operating and environmental conditions approved for the aeroplane may be shown by test and/or analysis or reference to comparable service experience on other aeroplanes." (EASA, 2013, p. 2-F-46). Those requirements pose a problem for many *active* fault-tolerant methods because they adapt the controller during system operation in an *autonomous* way. This shall be illustrated by the following example: For the same operating point[3], a conventional gain scheduled control system will always use the same gain, as long as scheduling variables are correctly measured. The system behaviour is very predictable hence validation and verification will simply aim at showing that the gain value is correct and that measurements, used for gain scheduling, are sufficiently accurate and reliable. An active *adaptive* controller, on the other hand, will autonomously calculate the gain based on the system behaviour observed *during operation*. This dependence on the observed behaviour is desired because it is the basis for the systems fault-tolerance, but it also makes it less predictable. The number of required validation and verification test points is now in principle unlimited. Furthermore the control system by itself, and not only the plant, is non-linear and cannot be approximated as quasi-LTI. As a result there is only limited use of the well-developed linear control theory to backup any reasoning which might be used to overcome the testability problem. Non-linear control theory, on the other hand, is not as well developed yet because it covers a much larger and complex group of systems. This finally leads to the situation that correct functioning of the system in many cases cannot sufficiently be proven "by test and/or analysis". In other words there often exists a validation and verification "gap" and this gap cannot be closed yet. The severity of this gap depends on the *active* fault-tolerant control method chosen. In comparison to *adaptive* methods, so called *projection based* methods rely on the identification of pre-modelled faults to activate a pre-modelled controller. In this case the controller behaviour becomes better predictable because there is just a limited, and therefore testable, set of controller/model combinations for the faulty and the nominal situations. However, in this case, the correct function of the Fault Detection (FD) algo-

[3] normally given by angle of attack, Mach number and dynamic pressure

rithm, required to select the appropriate controller, must be proven to achieve a false alarm rate lower than 10^{-9} per flight hour, so that at least no fault is detected if the system operates under non-fault operating conditions. *Passive* fault-tolerant control systems do not suffer from the same problems because there is just one offline designed, fixed gain or gain scheduled, controller that covers the nominal as well as the fault situation. From a certification point of view that would be ideal but unfortunately passive methods are hardly able to deliver the required performance even for the case of comparably small modelling uncertainties. Thus they are normally not able to deliver the required control performance when they are made robust enough to cover fault situations (see also chapter 2.3.4)

The second reason mentioned is related to economic aspects and those are, for a practical application, as important as the first one. Most of the current research focusses on the development of the fault-tolerant methods in a way that aims at replacing current industry practices of how control systems are designed. While this is certainly a valid long-term goal it neglects an important practical truth: There already exist many excellent, certified, and operational proven conventional flight control systems installed in current production aircraft that have been designed by classical control methods. Virtually no aircraft manufacturer will consider replacing them completely by new systems or developing a new FCS by solely relying on new control approaches. Why not? Because for industry the development of a completely new flight control system means mainly two things: an enormous financial effort and a significantly increased risk that something goes wrong, possibly with a catastrophic outcome. The financial aspect may be illustrated by the development of the Eurofighter flight control system. The active development began in 1982 with the Experimental Aircraft Programme (Kaul, Sella, & Walker, 1985) for a first flight of the Eurofighter prototype in 1994 and this first flight, by far, did not mark the end of the operational FCS development. For civil transport aircraft another important aspect to be considered is that a major part of the flight control system is common within an aircraft family. The flight control systems of the A380/A340/A330, for example, are in large parts based on the A320 one, with only small continuous improvements for every new family (Brockhaus, Alles, & Luckner, 2011, pp. 878-880). The increase in risk when developing a new flight control system is unfortunately well documented by some FCS induced accidents. Examples are the PIO related accidents of the Saab Gripen in February 1989 and April 1990 as well as the YF-22 accident in April 1992 (NATO RTO, 2000, pp. 12-18). This means that from an industry point of view the complete replacement of an existing FCS by an entirely new developed system is in nearly all cases not a realistic option. Some exceptions to this might exist for small UAV and/or purely experimental projects like the X-36 (see for example J. S. Brinker & Wise, 2001) but virtually not for larger scale production aircraft programmes.

Because of the described certification challenges and economic constraints it is the author's strong believe that any change can thus only come in the form of FCS additions to existing systems and careful introduction of fault-tolerant control methods in certain areas of the classical control system design process.
The idea for this work arose from a review of fault-tolerant control methods that could increase the aircraft survivability in case of structural damage. The focus was placed on structural damage because an increased FCS tolerance against it would mean a significant extension of current systems capabilities. No doubt also fault-tolerant control research on actuator and sensor faults is an important aspect but many of those faults are already covered by hardware redundancy in existing flight control systems. A high level of hardware redundancy is certainly not desirable because of weight, cost, and maintenance constraints but at least a solution exists for those kinds of problems. Structural damage on the other hand can, for obvious reasons, normally not be covered by hardware redundancy because that would mean a backup airframe is required. The risk of structural damage is certainly relatively low for civil transport aircraft. It is increased for military aircraft during peacetime, mainly because of mid-air collisions during close formation flying and close-in combat training but it is, for obvious reasons, significant during wartime. Increasing the aircraft survivability against loss of control due to structural damage would therefore form an important aspect for a noteworthy increase of aircraft survivability which leads to a major tactical and strategic advantage (cf. chapter 1.1).
The considerations above lead the author to the idea of combining the advantages of a conventional and fault-tolerant flight control systems with the goal of an increased damage tolerance of the overall systems. The idea is to augment a conventional control system that can be or is already certified according to standard certification procedures by a fault-tolerant control system that will only be activated if the conventional flight control system can no longer handle the situation. This should never happen in the certified operating envelope if the conventional FCS was correctly designed. As the active fault-tolerant FCS will never be activated for the certified operating conditions, i.e. for the undamaged aircraft, it should be possible to keep it largely outside of the certification scope and thus help to avoid/limit problems that may arise from the immature certification experience with respect to AFCS. Furthermore it will allow to *augment* the existing certified and proven CFCS of operational aircraft instead of replacing them entirely, thus leading to significantly reduced costs and development risks. To be able to use the described argumentation chain, it is important to find a reliable and certifiable switching logic, i.e. fault detection system. The latter would of course be obliged to have a very low false alarm rate, given by the applicable certification requirements, in order to ensure that the risk of unintentionally activating the fault-tolerant system is sufficiently low. This thesis addresses the question of how to approach the design of such a system using

state of the art FDD techniques. It proposes a new way to fault detection based on monitoring of the closed-loop aircraft response to pilot commands.
The author later discovered that the idea of combing a conventional FCS with an active fault-tolerant one by itself is, even if only sparsely investigated in the past, not new. However earlier work did either not focus on the required switching logic (Wohletz, Paduano, & Annaswamy, 1999; Wohletz, Paduano, & Maine, 2000) or selected an approach where the fault-tolerant flight control system always works in parallel to the conventional one (for example D. G. Ward & Monaco, 2005) which has certain advantages but inhibits a clear segregation of both systems. The differences between this work and the existing contribution of others will be discussed further in Chapter 1.4. *The research contributions of this thesis are summarized in chapter 5.2.*

1.3 Problem Statement and Objectives

This work mainly investigates two ideas, one that has been only sparsely investigated in the past and one that, to the author knowledge is a new idea or questions:

1. The dynamic behaviour that we want to achieve in case of aircraft is most of the time fairly simple, i.e. the response of a conventional aircraft beside the unconventional configuration of modern airframes. For the longitudinal axis the goal can be described by linear second or fourth order system.
2. There exist many certified aircraft with certified conventional flight control systems. While those flight control systems are very reliable as long as the plant behaviour matches the model behaviour, the ability of those systems to react on unforeseen faults is limited. It is important to realise that conventional flight control systems do not measure or check the dynamic performance of the aircraft in flight. They assume that the latter is correct because the model has been correct. Fault-tolerant control systems on the other hand can better deal with unforeseen faults because they measure the dynamic response of the aircraft during operation and, if required, adapt themselves in order to achieve the desired control performance. However there exists only limited experience how to certify such systems that change their behaviour during operation and they also tend to be less reliable because they are more complex. Therefore it seems reasonable to the author to combine both approaches in order to try to profit from the respective advantage. This could be achieved by using a conventional flight control system during fault-free operation and switching to a fault-tolerant, adaptive flight control system if a fault is detected that could *not* be dealt with by the conventional flight control system.

To keep the approach consistent with typical design demands, the following requirements have been identified by the author and shall be investigated in detail:

Requirement 1-1: The probability that the AFCS is inadvertently activated by the fault detection system shall be equal or less 10^{-6} per flight hour. This shall be proven by stochastic and/or logical reasoning that supports a possible certification.

Rationale: Using the assumption that only the CFCS has been certified it must be ensured that the probability that the AFCS is inadvertently activated is small enough to fulfil typical safety requirements.

Requirement 1-2: The developed architecture must be able to be retrofitted to a conventional flight control systems.

Rationale: As explained above the approach relies on a CFCS being used during fault-free operation. Thus the fault detection system must be retrofitable to existing CFCS. Furthermore, as mentioned in chapter 1.2, certification challenges and economic constraints make an extension of an existing system more interesting than its entire replacement.

Requirement 1-3: The architecture shall allow safe and efficient flight testing.

Rationale: Verification of the correct function of architecture in a laboratory setup up will most likely be difficult, as it incorporates the real system behaviour that can only be partly simulated. Therefore flight test will form an important part of verification testing.

Requirement 1-4: The fault detection system shall minimize the amount of measurements required to function correctly.

Rationale: With an increasing number of measurements the reliability of the system will be reduced as more measurements must be accurate and available for the system to work correctly i.e. the failure probabilities multiply.

Requirement 1-5: The fault detection system should not require angle of attack measurements to work correctly.

Rationale: Angle of attack measurement probes are prone to damage because of their exposed position. Furthermore accurate measurements can normally only be obtained by model-based estimation/calibration algorithms. The validity of those models in a fault case cannot be assured.

Requirement 1-6: The system shall not rely on an off-line defined set of failure models.

Rationale: It is very unlikely that different forms of faults can be modelled accurately enough with a reasonable number of pre-defined failure models. Furthermore there is no proof that such a system would work properly in case of a combination of the different faults.

Requirement 1-7: The fault detection must not rely on the AFCS.

Rationale: As the AFCS is deemed not certified this would make the certification argumentation chain invalid.

Requirement 1-8: The fault detection by the fault detection system shall be fast enough to give the active fault-tolerant flight control system a realistic chance to recover control of the air vehicle.

Rationale: Activation of the AFCS does not help if it is too late for the AFCS to recover the aircraft to a safe flight condition.

Requirement 1-9: The fault detection by the fault detection system shall be fast enough to give the active fault-tolerant flight control system a realistic chance to recover control of the air vehicle *within* acceptable normal load factor limits.

Rationale: Activation of the AFCS does not help if it is too late for the AFCS to recover the aircraft within acceptable normal load factor limit, i.e. the structure fails.

1.4 Related Work

Large scale work on fault-tolerant flight control systems began in 1984 with the USAFs Self-Repairing Flight Control System (SRFCS) program (Chandler, 1984). Inspired by the idea of reducing hardware redundancy the program only focussed on control effector failures. Flight control reconfiguration was based on a pseudo-inverse approach with explicit Fault Detection and Identification (FDI). Early flight test where conducted in 1985 on the NC-131H Total In-Flight Simulator (TIFS) aircraft. The program was finished in 1990 with 25 flight tests on NASA Dryden's F-15 HIDEC (Highly Integrated Digital Electronic Control, Figure 4). It confirmed the effectiveness of the pseudo-inverse approach for cases where the FDI worked properly (Steinberg, 2005, pp. 265-267). Steinberg points out that "both reconfiguration and pilot-alert were dependent on reliable FDIE [Fault Detection Isolation and Estimation] and that was the least successful part of the program. FDIE required substantial tuning of threshold parameters and it was difficult to get both fast detection and low false alarm rates". This highlights the fact that the system was far from working reliable and also far from being certifiable. Boeing later also looked into extending their approach, developed for effector damage during SRFCS, to incorporate structural damage but has not been successful (Tomayko, 2003, p. 31).
Another significant milestone for fault-tolerant flight control for a very specific damage case came in the form of the Propulsion Controlled Aircraft (PCA) programme. The programme was driven by the American Airlines UA232 accident in Sioux City, already mentioned in chapter 1.1, and the related NTSB recommendation to "encourage research and development of backup flight control systems for newly certificated wide-body airplanes that utilize an alternative source of motive power separate from that source used for the conventional control system" (NTSB, 1990, p. 102). The PCA approach only focussed on a complete hydraulic system loss and was based on a second FCS using only the engines as control effectors. The system was supposed to be switched on by the pilot. In 1993 a successful landing without using any of the aerodynamic control surfaces was demonstrated on NASAs F-15 HIDEC (Figure 4) (Steinberg, 2005, p. 267). Later more demonstrations followed on a MD-11 transport aircraft which successfully conducted two ILS and one piloted landing (J. Burken, Maine, Burcham, & Kahler, 1996). To the author's opinion the PCA architecture could be certifiable as the FDI function is allocated to the pilot and both control systems, the regular one and the one using only the engines, can be designed off-line using conventional control design techniques. However the very limited scope on complete loss of hydraulics and concerns about the effectiveness with different CG position probably prevented the concept from entering into production aircraft (Steinberg, 2005, p. 267).

Figure 4 NASAs F-15A HIDEC during a landing for the PCA programme (NASA, 1993)

The beginning of the 1990s saw the introduction of the first adaptive approaches to fault-tolerant flight control. One of the first architectures flight tested was developed during the USAFs Self-Designing Flight Control System (SDFCS) programme and based on the Self Tuning Controller (STC) or indirect adaptive principle that relies on accurate online estimation of the plant model parameters. The identified plant model is then used to calculate the controller gains during system operation. The process is therefore comparable to conventional off-line control design however the online parameter estimation is anything but straight forward. The main problem is related to insufficient excitation which leads to bad estimation results. Many approaches have been suggested to deal with the problem by halting the estimation process when the excitation is insufficient. To the author's knowledge all of them rely on tuning parameters, like "forgetting factors", that must be determined in an iterative, empirical way (Chandler, Pachter, & Mears, 1995; Klein & Morelli, 2006, pp. 285-286; D. G. Ward, Barron, Carley, & Curtis, 1994). Proving reliability of a flight control system based on this approach seems therefore cumbersome if not impossible (cf. Steinberg, 2005, p. 268). Therefore, with the online parameter estimation methods available today, it is unlikely that such a system can be certified. Nevertheless a STC system based on the Modified Sequential Least Square (MSLS) algorithm (D. G. Ward et al., 1994) and a Receding Horizon Optimal Controller (RHOC, D. G. Ward & Barron, 1995) has been successfully flight tested on the VISTA F-16 aircraft during the SDFCS programme (J. Monaco, Ward, Barron, & Bird, 1997; David G. Ward, Monaco, & Bodson, 1998).

Figure 5 USAFs F-16 VISTA (left, USAF, 2012) and NASAs X-36 (right, NASA, 1997)

In 1993 the DLR in Germany conducted flight tests on the ATTAS (Advanced Technologies Testing Aircraft System, Figure 6) research aircraft using an active fault-tolerant control system based on an explicit model-following approach. The controller adaptation was limited to the feed-forward path to prevent any stability problems which might be encountered with feedback path adaptation. By the use of direct feed-forward control gain identification, inverting the control matrix ($\boldsymbol{B}$) was prevented. A "genetic algorithm" was used to update the reference model and the feedforward controller. The configuration has been flight tested for a simulated failure case where the elevator effectiveness ($\boldsymbol{M_\eta}$) was reduced by 50%. The system notably reduced the pitch angle tracking error but adaptation was comparably slow (Baumgarten, Buchholz, & Heine, 1995; Buchholz, Heine, & Baumgarten, 1996). Heine (1999, p. 12-4) later states: "Nevertheless the growing computational burden when trying to cover additional failure cases and necessary certification efforts make it unlikely to combine genetic online optimization with current control law design and its certification process." In 2008 another test flight of a model-following architecture augmented by an MPC/RHOC controller was conducted on the ATTAS. The goal was to optimize tracking of a pre-defined trajectory under a control effector fault. The setup relied on an accurate FDI system that has not been implement-

ed for the flights. Instead perfect knowledge of the control effector status was assumed. The system demonstrated satisfactory performance with a simulated aileron fault. Simulator studies did also demonstrate the use of differential thrust as active control element in case of a rudder and aileron failure. (F. de Almeida & Leißling, 2009; F. A. de Almeida & Leißling, 2010).

Figure 6 DLRs VFW614 ATTAS (DLR, 2008)

Another adaptive control approach has been developed under the USN Intelligent Flight Control (IFC) program and was based on an adaptive neural network control law (Anthony Calise, Kim, Kam, & Azam, 1992; Kim & Calise, 1997). It was applied to the Boeing's Tailless Advanced Fighter Aircraft (TAFA) high-fidelity simulation under the USAF RESTORE programme (J. Brinker & Wise, 1998; A. Calise, Lee, & Sharma, 1998; Wise et al., 1999) and in 1999 flight tested on the X-36 (J. Brinker & Wise, 2000; J. S. Brinker & Wise, 2001).
In parallel McDonnell Douglas and NASA teamed to develop the so called Intelligent Flight Control System (IFCS). The system was supposed to be tested on a highly modified F-15B prototype. The aircraft was equipped with a full authority digital fly-by-wire control system, canards and two dimensional thrust-vectoring and thrust-reverse capable nozzles and subsequently became the NASA F-15B ACTIVE (Advanced Control Technology for Integrated Vehicles, Figure 7). The first set of IFCS flights occurred in March and April 1999. They were intended to proof the concept of the Stochastic Optimal Feed-forward and Feedback Technique (SOFFT) based flight controller. The later was in principle an on-line LQR implementation that uses a plant model, in this case 26 stability and control derivatives, to calculate the correct surface commands. For the 1999 flights the derivatives were provided by a static Pre-Trained Neural Network (PTNN) obtained from wind-tunnel measure-

ments. A second set of flights was finished in 2003 with an on-line parameter identification and neural network-based learning functionality implemented. However the on-line identified plant model was not actually used by the SOFFT controller i.e. the control system was not yet adaptive. The system setup was subsequently named "Gen 1" (Hageman, Smith, & Stachowiak, 2003, pp. 1-3; Williams-Hayes, 2004, p. 2).
The situation in the early years of 2000 is appropriately described by Steinberg (2005, p. 271) from the USN:

> By the end of the 1990s, continuously adaptive and intelligent control techniques had been flight tested successfully for reconfigurable flight control. Progress had been made on many key areas. However, the flight testing had been fairly limited in many respects and concerns still remained about factors such as how to do flight certification to ensure safety, how to set design parameters that impact on adaptation, and how to incorporate all of the many qualitative and quantitative requirements that go into practical flight-control design. Although the potential benefits were significant, control designers interested in using these approaches on production aircraft would still need to be cautious.

NASA meanwhile continued their efforts in the IFCS programme with a direct adaptive control architecture based on dynamic inversion augmented by a neural network. This architecture was subsequently named "Gen 2" (J. J. Burken, Williams-Hayes, Kaneshige, & Stachowiak, 2006; Williams-Hayes, 2005). In comparison to the indirect "Gen1" architecture "Gen 2" is based on a modified version of the direct neural network approach developed by A. Calise et al. (1998) for the above mentioned TAFA simulation study. The configuration has also been applied by Rysdyk and Calise (1998) to the XV-15 tilt rotor aircraft simulation. In 2006 flight testing of the "Gen 2" IFCS started on the F-15B ACTIVE. The flights included a simulated failure case where the stabilator was stuck (Buschbacher & Maliska, 2006). The results were mixed (J. T. Bosworth & Williams-Hayes, 2007). In 2008 some more flights where conducted this time using the canards to destabilize the plant in the longitudinal axis (J. Bosworth, 2008). Bosworth summarized the results as follows: "The convergent properties of this initial system warrant additional improvement since continued maneuvering caused continued adaptation change. Compared to the non-adaptive system the adaptive system provided better closed-loop behavior with improved matching of the onboard reference model." (J. Bosworth, 2008, p. 1). Because of the mixed results during the "Gen 2" flights with the simulated stabilator failure the system was modified and entitled "Gen 2a". Subsequent flight test have shown a significant improvement over the "Gen 2" system (J. Burken,

Hanson, Lee, & Kaneshige, 2009). With the retirement of the F-15B ACTIVE in January 2009 the largest active fault-tolerant flight test program came at least to a preliminary end.

Figure 7 NASAs F-15B ACTIVE (NASA, 1998)

While all those flight test projects, without any doubt, have been remarkable achievements and very important milestones for active fault-tolerant flight control none of them sufficiently matured the technology for a large scale use on production aircraft.

By the year 2000 a limited number of researchers started to bring up the idea of augmenting existing conventional flight control systems with an active fault-tolerant one. To the author's knowledge the first to discuss this thought were (Wohletz et al., 1999) and (Wohletz et al., 2000). They suggest a Retrofit Control Module (RCM) as shown in Figure 8 that is based on a Model Reference Adaptive Controller (MRAC) and a LOES reference model inferred from on-line parameter estimation.

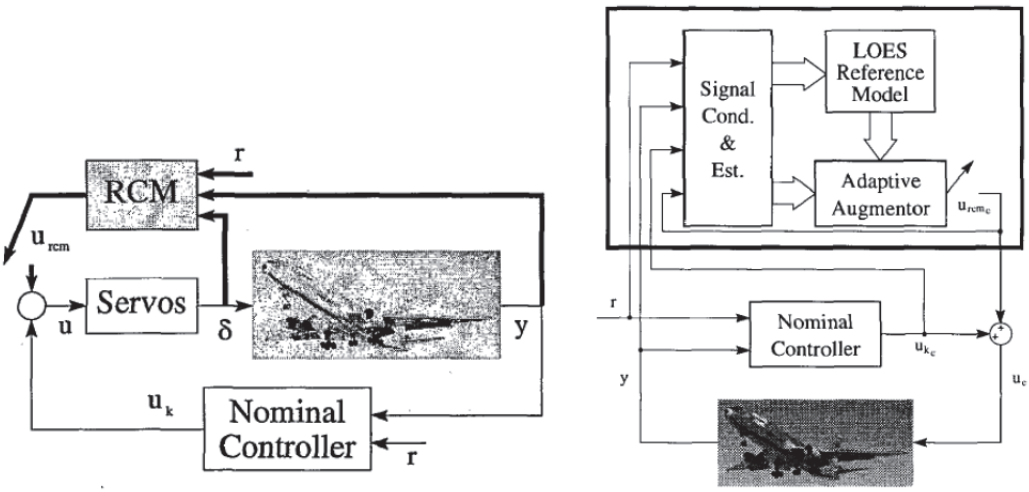

Figure 8 Retrofit architecture suggested by Wohletz et al. (1999, left) and Wohletz et al. (2000, right)

For estimation the MSLS algorithm flight tested on the F-16 VISTA was used (D. G. Ward et al., 1994; David G. Ward et al., 1998). More important than the actual mechanization of the fault-tolerant controller is however the idea that the nominal controller, i.e. the certified production control system, must be clearly separated from the fault-tolerant system as indicated by the switch in Figure 8: "It [the RCM] must also introduce no command signals in the unfailed case; we presume that the primary control laws work well when no failures exist. This also helps encapsulate the verification and validation task." (Wohletz et al., 1999, p. 996). The author fully agrees with this segregation idea. However the mechanization of the switching (or better activation) logic is not sufficiently addressed in both papers. They suggest to use the difference between the measured angular accelerations and the reference angular accelerations from the reference model i.e. the input error as base for switching (Wohletz et al., 2000, p. 5). This choice probably came naturally during design of the adaptive controller because they use an input error approach as suggested by Bodson and Groszkiewicz (1997). The author independently came up with the same idea but based on physical reasoning: Any deviation from a desired movement must first show up in a deviation of the actual from the desired accelerations i.e. the transfer function from the disturbance to the acceleration has a pole-zero-difference of zero (cf. Brockhaus et al., 2011, p. 341). Unfortunately the switching logic suggested by Wohletz et al. has two weak points: First of all no suggestion is made how to determine the switching threshold and second the parameters of the LOES model are estimated online. The latter, to the author's opinion, is as of today not certifiable because of the problems involved online parameter estimation. Furthermore the on-line estimation of the LOES model must be halted once a failure occurs. This requires another logic that has to be certifiable. Finally

the work only covered open-loop stable plants and control effector failures. This text will also use the idea of combining a conventional certified control system with an active fault-tolerant control system by keeping the fault-tolerant control system inactive if no fault occurs *but will focus on the switching logic* as this is the most important aspect concerning certifiability.
J. D. Boskovic and Mehra (2002) later slightly modified the architecture of Wohletz et al. by using the nominal controller output u_N (Figure 9) instead of the measured control surface position δ (Figure 8). They furthermore used a different approach for designing the fault-tolerant controller. However again the problem of how to design the switching or activation logic was not addressed: "The switch shown in the Figure [Figure 9] is used to disconnect the ARRC [Adaptive Retrofit Reconfigurable Control] module in the case with no failures, while in the case of failures, a suitably chosen detection mechanism is used to connect the ARRC module." (J. D. Boskovic & Mehra, 2002, p. 1257). Moreover the paper only addresses a loss of effectiveness of the control effector as fault case.

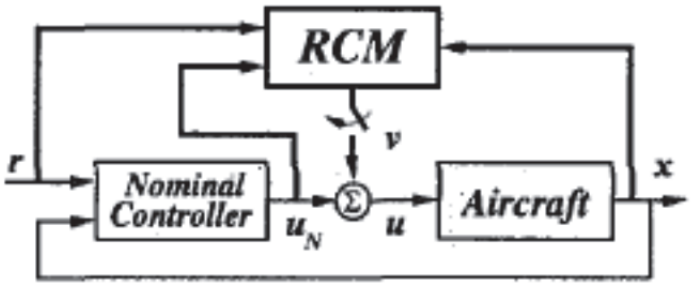

Figure 9 Retrofit architecture suggested by J. D. Boskovic and Mehra (2002)

In subsequent work the switch is removed from the architecture and the approach is extended to a larger group of fault cases and more sophisticated algorithms (J. Boskovic, S. Bergstrom, et al., 2005; J. Boskovic, Prasanth, & Mehra, 2005; J. Boskovic, Redding, & Knoebel, 2009; J. D. Boskovic, S. Bergstrom, & R. K. Mehra, 2005; J. D. Boskovic, S. E. Bergstrom, & R. K. Mehra, 2005; Jovan D. Boskovic, Prasanth, & Mehra, 2007; Jovan, Joshua, & Raman, 2007; Jovan, Ravi, & Raman, 2006). The architecture was subsequently entitled FLARE (Fast on-Line Actuator Reconfiguration Enhancement). The problem of validation and verification for certification is not suitably addressed beside the following remark: "An alternative solution [to designing a new control system] is to retain the nominal controller and add a retrofit feedback control module that is active only if the system state leaves the nominal state set. Such an augmented controller would need to be tested only for the operating regimes for which the retrofit module was designed." (Jovan D. Boskovic et al., 2007, p. 703). This statement is only true if it can be proven that the

system cannot interfere with the nominal controller during nominal i.e. fault-free operations. However this topic is not addressed.
In 2002 A. J. Calise, Bong-Jun, and Craig (2002, p. 1549) realize that "particularly within the aircraft and automobile industries, there is a legacy of experience with existing control system architectures, and these industries would much prefer to augment their plants with an adaptive process, rather than replace them with a totally new architecture." As discussed in chapter 1.2 the author fully agrees with this statement. They propose to compensate the output error between an online plant model and the real plant by a neural network based adaptation algorithm. Later they largely extended the concept of augmenting an existing linear controller by an adaptive neural network one. However none of the papers addresses the problem of validation, verification, and certification.
Idan, Johnson, and Calise (2002, p. 1013) suggest retrofitting an adaptive neural network based control system to an existing conventional flight control system to deal with actuator failures. They state that "a central feature of the proposed hierarchical flight control architecture is its capability to enhance the safety of conventional, previously certified flight control systems. The secondary control channels of this methodology can simply be added to an existing system, without intervening with its normal operation. The hierarchical switching between the various secondary channels will be introduced only after a failure occurs and has been identified." No details on the implementation of the "hierarchical switching" are given, even if the switching logic is very important because it ensures that the non-certified "secondary channel" is not intervening with the certified conventional flight control system during fault-free operation. Again certification is mentioned but not really addressed.
Another interesting retrofit approach was initially suggested by Jeffrey Monaco, Ward, and Bateman (2004) and later refined by D. G. Ward and Monaco (2005) for an in-flight demonstration on the F/A-18 (Figure 10). According D. G. Ward and Monaco (2005, p. 64) the F/A-18 was selected because "the F/A-18 technology roadmap has listed fault-tolerant control as an important future capability for the aircraft." The fault-tolerant control law works in parallel to the production control law but the AFCS interferes via the reference signal r and not directly via the actuator input u.

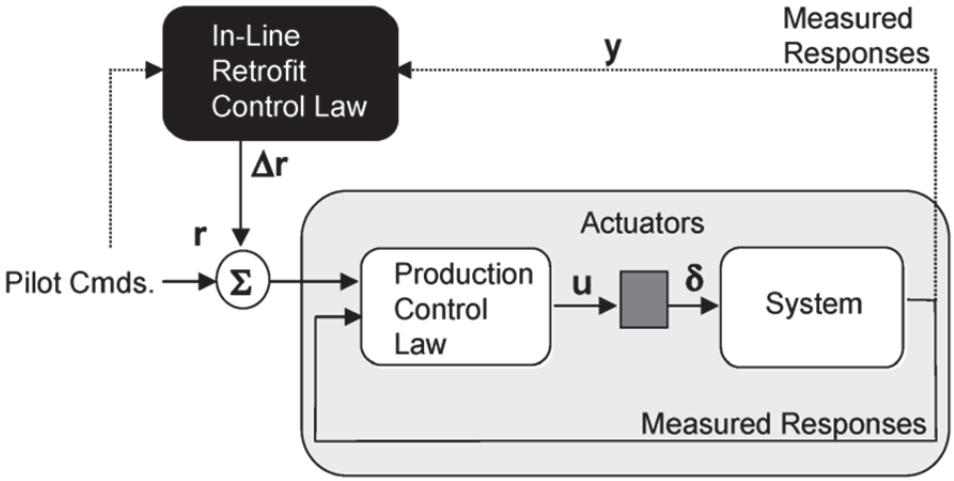

Figure 10 Retrofit architecture suggested by D. G. Ward and Monaco (2005, p. 64)

The fault-tolerant control system itself is based on the STC approach. The actual aircraft closed-loop behaviour is described by a time-varying Low Order Equivalent System (LOES). The LOES model parameters are estimated on-line. A set of off-line estimated LOES models describes the desired system behaviour i.e. forms the reference model. A RHOC is used to minimize the tracking error between the reference model and the measured aircraft behaviour. The MSLS algorithm, used for on-line parameter estimation, and the RHOC are largely based on the ones developed for the F-16 VISTA flight tests described above (D. G. Ward & Barron, 1995; D. G. Ward et al., 1994; David G. Ward et al., 1998). According to D. G. Ward and Monaco (2005, p. 64) it was the aim "to balance certification requirements and reconfiguration performance of revolutionary flight control designs." Assuming that fault-tolerant retrofit control system cannot be certified, the author is sceptical that such a setup would be really certifiable. Even if the possible inputs of the retrofit system are limited by the protection mechanisms of the production control system, the retrofit system has full authority within the operational envelope and it is always activated. For example an erroneous full-nose down command by the retrofit control system may not lead to overstressing the structure but can be highly safety critical during the approach and landing phase. Four flights on an F/A-18C have been conducted out of the Naval Test Center at Patuxent River. Page, Monaco, and Meloney (2006, p. 15) summarize the results as follows:

> The results validate the performance benefits of the retrofit system as compared with the baseline system for a range and variety of simulated surface failures. Although several compromises were required for flight test imple-

> mentation, the retrofit system was shown to be capable of improving post-failure handling qualities.

They furthermore conclude:

> Most importantly, significant additional work to address certification issues is necessary. The current work presents a candidate flight control architecture that is theoretically more amenable to use in a flight critical role. However, the focus of the research has been to establish performance bounds of such a system rather than address the methods that must be undertaken to complete the verification and validation process.

This suggests that the author's concerns related to certifiability of the architecture are not arbitrary. Besides that, to the author's opinion, the architecture is a very interesting approach to optimize the undamaged aircraft performance of a conventional control system by compensating for small modelling uncertainties or difference between individual productions aircraft in a fleet. In such a case the authority of the system might be limited to a level that is acceptable from a flight safety point of view.

By 1998 some active fault-tolerant flight control system elements have entered into the F/A-18E/F production programme. However the algorithm only deals with one specific horizontal stabilizer actuator failure case. Steinberg and Tomayko report that the system has demonstrated its effectiveness in flight test as well as with a real actuator failure during one of the development flights (Steinberg, 2005, pp. 263, 272; Tomayko, 2003, p. 46). Another comparable example of fault-tolerant control technology that entered into a production aircraft is the actuator oscillatory failure detection algorithm implemented in the Airbus A380 flight control system as described by Goupil (2010).

The discussion of this chapter focused on fault-tolerant control approaches that have been flight tested on larger scale aircraft and on research dealing with so called retrofit architectures because both areas are closely related to the topic of this text i.e. how to combine a conventional with an active fault-tolerant control system and how to approach the certification problem of active fault-tolerant control systems for production aircraft. This, of course, only scratches on the surface of all the great work conducted on fault-tolerant, robust, and adaptive control in general. The last years have also seen remarkable in-flight demonstrations on smaller unmanned air vehicles like Rockwell Collins demonstration of a damage tolerant control system on a subscale F-18 model (Jourdan, Piedmonte, Gavrilets, Vos, & McCormick, 2010) and the L1 adaptive control test on NASAs AirSTAR subscale transport aircraft

model (Gregory, Cao, Xargay, Hovakimyan, & Zou, 2009; Gregory, Xargay, Cao, & Hovakimyan, 2010) to mention just a view of them.
Despite all those efforts fault-tolerant flight control systems have not seen widespread use in production systems. This is also summarized by Lombaerts, Smaili, and Breeman (2010, p. 40) who state that

> Reconfigurable flight control systems have been successfully flight tested […] and evaluated in manned simulations […], but up to date, no RFTFC [Reconfigurable Fault-Tolerant Flight Control] has been certified or applied in both commercial and military aircraft.

To the authors opinion a major reason for this is the fact that current research focuses on replacing conventional flight control systems instead of, at least in the first instance, augmenting them. Looking at the history of aviation nearly all successful advances were made in small well-defined steps. Flight controls are no exception to this. The first production autopilot was developed by Sperry in 1912 for the Curtiss F Flying Boat. It lowered the pilot workload by introducing a control system in the "outer loop". In 1942 the first control element found its way into the "inner loop" in form of yaw damper in the Me 262. It augmented the mechanical flight control system but did not replace it. In 1974, with the introduction of the F-16, the mechanical flight control system was the first time replaced by a full authority fly-by-wire one. The introduction of active fault-tolerant control systems will have to be done in a stepwise approach as well. It is therefore the author's opinion that research should more focus on how to augment existing conventional flight control systems with active fault-tolerant ones. To use a conventional flight control system, that can be qualified and certified with well proven means, when the aircraft is not or just slightly damaged and the fault-tolerant flight control system only in the case when the aircraft is severely damaged seems to be the most promising way to foster the larger scale, i.e. production, use of fault-tolerant flight control technology.
While such an approach would relieve the certification and qualification requirements on the fault-tolerant control system it puts the fault detection algorithm into certification focus. To the author's knowledge the aspects of when the switching shall occur and how the reliability, i.e. the false alarm rate, of such an algorithm can be quantified has not been investigated in detail before. This question forms the heart of this thesis.

1.5 Research Contributions

This chapter shall give a short summary of the research contributions provided by this thesis. A more detailed discussion can be found in chapter 5.2.

Primary research contributions:

- The idea of combining a CFCS with an AFCS, albeit not complete new, has only been very sparsely investigated in the past and none of the work known to the author (cf. chapter 1.4) do treat the problem of how to define a useable switching logic/threshold beyond mentioning its existence. This thesis focusses especially on the switching, i.e. fault detection, algorithm. The above mentioned reasoning chain implies that the possibility that the fault-tolerant flight control system is *inadvertently activated* must be very remote, i.e. the False Alarm Rate (FAR) must be very low. To judge the possibility for inadvertent activation, the FAR must be quantifiable by a number. This work *uses a strict, state of the art FAR-based design approach,* as suggested by Ding (2013), and applies it to the aircraft fault detection problem on hand. This strict FAR-based design approach is, to the author's knowledge, new in the context of aircraft fault detection.
- Most of the current Fault Detection and Diagnosis (FDD) work treats the problem detecting faults in the uncontrolled plant. In case of aircraft, and potentially in many other applications, the user (e.g. pilot) is much more interested in the *closed-loop* performance of the system, because that is what is visible to him/her. The author therefore suggests to model *the acceptable closed-loop performance, directly derived from the respective flying qualities standards, as deterministic model uncertainties of reference model* used for fault detection. The approach to use the flying quality standard derived CAP-ζ_{SP} combination to define the parameter polytope of acceptable reference model uncertainties and consequently derive the norm-based residual threshold based on this reference model was developed by the author and is, to the author's knowledge, new.
- The aforementioned approach for the fault detection system required the extension of the combined stochastic/norm-based fault detection approach for deterministic and stochastic unknown *inputs,* as suggested by Ding (2013, pp. 339-345), to the much more complex case of deterministic/stochastic unknown inputs and *deterministic model uncertainties*. Several extensions are suggested in this work with respect to the aircraft application discussed above. The work thus adds research results to the, as highlights by Ding (2013, p. 17), very sparsely investigated FDD research area of *residual evaluation*.

- The FD system proposed in this thesis is to author opinion, very flexible to adapt to different practical demands. Adaptations are easily done by just changing the range of acceptable *closed-loop* natural frequencies and damping ratios. Most important, those two parameters can be readily interpreted in physical and flying quality context and they allow a direct comparison with the flying quality standards MIL-F-8785C (US DoD, 1996) and MIL-STD-1797B[4] (US DoD, 2012). To the author's opinion this is a significant practical advantage and gives the aerospace engineer a direct understanding what the effect of the parameter changes are.

Furthermore the work provides some secondary contributions:

- To overcome the problem of a non-convex model uncertainty parameter space, the author suggests the use of an approximated parameter polytope. In terms of the problem on hand, i.e. the aircraft longitudinal short period motion, this means that the allowable range of damping ratios ζ_{SP} is slightly reduced. However it is ensured that the approximation stays in the area of the desired level of flying qualities, i.e. on the "safe side". To the author's knowledge using such an approach in the context of a flying quality model is also new.
- Due to the incorporation of model uncertainties into the reference model, also known system inputs affect the residual dynamics. A new adaptive threshold (threshold generator) in the form of an input energy signal envelope detector is suggested to account for this effect.
- The approach chosen for deterministic fault detection uses the signal energy or RMS-value. Of course the practical application warrants a limited observation time. This violates the theoretical definition of the energy and RMS-signal. To the author's knowledge the implications for fault detection when using a limited RMS-window size are not discussed in current FDD literature. This work will discuss the implications and suggest a possible solution in form of the input energy detector mentioned above.
- This work incorporates the known colored noise Kalman filter extensions in the residual generation process in order to deal with colored process noise from atmospheric disturbances. This extension is to the author's knowledge, also new in a fault detection context.

[4] Restricted distribution, therefore information from MIL-F-8785C is used within this text.

- The aircraft application warrants the use of a residual band-pass post filter to supress the impact of steady and very low frequency gains on the residual and to limit the higher frequency noise. Unfortunately, due to auto-correlation, the filtered residual noise is no longer white but colored, therefore violating one of the underlying assumptions of the χ^2-distribution required for stochastic residual evaluation.. In this regard the author suggests the use of a colored noise corrected variance together with the normal distribution approximation of the χ^2-distribution as a possible solution to the issues resulting from the colored noise.

1.6 Summary and Outline

Chapter 1.1 discussed why fault-tolerant flight control systems are important, while chapter 1.2 explained the motivation for the topic of this, i.e. to investigate a fault detection system to combine a Conventional Flight Control System (CFCS) with an active fault-tolerant one while ensuring a user selectable False Alarm Rate (FAR). Chapter 1.3 summarized the goals for this thesis. A brief outline of larger scale fault-tolerant flight control programs was given in chapter 1.4. Finally chapter 1.5 gave a résumé of the research contribution provided by this thesis.
The remainder of the text will be structured as follows: We will start with an introduction on typical design goals and architectures for conventional flight control systems, a high-level overview of common Fault-Tolerant Control (FTC) approaches, and a discussion of different approaches to fault detection and diagnosis (Chapter 2). Chapter 3 summarizes the theoretical studies conducted with respect to contemporary model-based fault detection and finally describes the fault detection system proposed in this work (chapter 3.5) including the detailed research contributions by the author. The results of the simulation case study, conducted to verify the theoretical results and to demonstrate the performance of the fault detection system for a realistic failure case, are described in chapter 4. Chapter 5 will discuss the overall results as wll as the research contributions and summarize possible areas for a follow on work. Finally a summary and concluding remarks are given in chapter 6.

2 Basic Aspects of Fault-Tolerant Control and Fault Detection and Diagnosis

2.1 Motivation and Scope of Discussion

Fault-tolerant control systems in general are highly integrated systems. Therefore the activities lumped together under the term fault-tolerant control in fact touch many different *research areas* that historically have been considered more or less separate from each other, namely: Fault Detection and Diagnosis (FDD), Robust Control, and Reconfigurable/Adaptive Control (Figure 11).

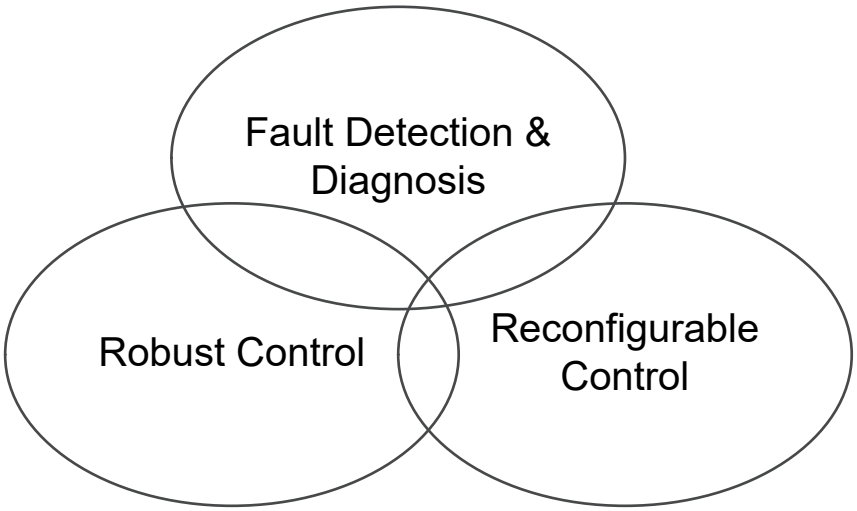

Figure 11 Areas of fault-tolerant control (based on Patton, 1997, p. 1035)

Chapter 2.2.1 will give a brief outline why digital flight control systems have become so important in contemporary aircrafts. Typical primary design goals for the aircraft longitudinal motion, especially the Control Anticipation Parameter (CAP) as one the most important flying qualities metrics for this axis, will be discussed in chapter 2.2.2. Because of its importance the CAP forms the basis of the fault detection algorithm proposed in this text (chapter 3.5). The considerations made for the CAP are therefore very important for the remainder of this work. Chapter 2.2.3 briefly outlines redundancy setups in current production flight control systems in order for the reader to understand the difference to model-based redundancy as introduced in chapter 2.4. Some important FTC methods are introduced in chapter 2.3. This chapter is, to author's opinion, important to understand the basic idea behind different FTC approaches as well as the difference to conventional FCS. Chapter 2.4 will then have a closer look on the subject of FDD which is major focus of this text.

2.2 Thoughts on Typical Conventional Production Flight Control Systems

2.2.1 Typical Challenges of Modern Aircraft Designs

As already mentioned in the introduction (chapter 1.1) many modern airframe designs yield unfortunate dynamic behaviours up to instability. Therefore a control system is required to achieve

- stabilisation and
- the desired dynamic behaviour, i.e. flying qualities

Static instability in the longitudinal axis, for example, is a common design feature of many modern military aircraft. There are two major reasons for this situation. The first one is related to aerodynamic performances. A statically unstable design, when compared to a stable one, provides a lower trimmed drag coefficient for the same lift coefficient as well as a higher maximum lift coefficient. This leads to a significantly better ability to change the flight path vector, commonly referred to as *agility*. The latter is of special importance for fighter aircraft and becomes particularly apparent in a considerable increase of the sustained and instantaneous turn performance. Overall this means a significant size/mass decrease for the same performance requirements or a significant performance increase for the same aircraft size/mass (NATO AGARD, 1991b, pp. 52-53). The second reasons is related to some modern combat aircraft design features, like for example stealth, that lead to aircraft shapes that are unstable, e.g. the B-2 (Britt, Volk, Dreim, & Applewhite, 2000). The most obvious implication for flight control system design is that the aircraft becomes uncontrollable[5] without the FCS and thus high reliability of the latter has to be achieved for flight safety reasons. However of same importance, even if less obvious, are the more stringent requirements on the accuracy of sensor measurements, the pitch control power and its build up rate as well as the sensitivity to time delays. Those requirements increase with the worst-case time to double of the open loop plant, i.e. the time till the angle of attack α doubles after it has been perturbed from its equilibrium point (Brockhaus et al., 2011, pp. 820-821; NATO AGARD, 1991a, p. 22-21). Table 1 shows some values of the worst-case time to double for some modern fighter-type aircraft (NATO RTO, 2000).

[5] in a flying quality sense

Table 1 Pitch motion worst case time to double of some modern fighter-type aircraft (NATO AGARD, 1991b; NATO RTO, 2000, p. 22)

Aircraft	Worst Case Time to Double
X-29	0,15 sec
FBW-Jaguar	0,25 sec
EAP	0,18 sec
Rafale A	0,40 sec
F-16C	1,5 sec

2.2.2 Typical Design Goals for the Longitudinal Axis

In all cases the control goal for the inner loop of a flight control system is to achieve an aircraft response that ensures good flying qualities. There exist certain standards that relate the goodness of flying qualities to certain design parameters. For manned aircraft by far most widely used ones are MIL-F-8785C (US DoD, 1996) and MIL-STD-1797B[6] (US DoD, 2012). To the author's knowledge there exist no comparable standard for unmanned aircraft however it is reasonable to assume that in many cases the flying quality requirement for unmanned aircraft, in terms of aircraft dynamic response, will be comparable to the ones of manned aircraft. This text, which deals with longitudinal motion, will therefore refer to the requirements of the above-mentioned documents for the dynamics of the short period motion.
It is worth noting that the basic flying quality requirements have not changed with the introduction of highly augmented fly-by-wire aircraft although their flight control system would allow creating response types that are very different from conventional ones. It seems that the pilots can best handle the conventional response types. One reason might be that this is simply the type of response they are most used to. The implication for flight control design is thus, in the vast majority of cases, the goal is to achieve a response fairly similar to that of a conventional aircraft with good flying qualities (Hodgkinson, 1999, p. 14; NATO RTO, 2000, p. 33). To underline this important point the author wants to cite NATO RTO (2000, p. 34):

> Summary of F-22 Flying Qualities: The F-22 control law design was based on goals derived from the guidelines provided by existing alternate handling qualities/PIO metrics, with specific control law architecture changes made to satis-

[6] Restricted distribution, therefore information from MIL-F-8785C is used within this text.

> fy these goals. *In particular, the F-22 was designed to have a low order, classical aircraft response* [accentuation added]. Elimination of integrator dynamics from the closed-loop response of the aircraft allowed the designer to increase the bandwidth of the system, lower equivalent system time delay and achieve satisfactory performance trends with respect to these handling qualities/PIO metrics.

The goal for the reference control system designed for this case study was therefore to create a closed loop pitch rate response close to that of a linear second order system with damping ratio $\zeta_{SP} = 0{,}707$ and a natural frequency to achieve $CAP = 1$, where CAP stands for the so called Control Anticipation Parameter. The CAP is defined at the ratio of the immediate pitch rate acceleration to the quasi-stationary normal acceleration

$$CAP = \frac{\dot{q}(t \to 0)}{n_z(t \to \infty)} = \frac{\Delta \dot{q}_0}{\Delta n_{z,\infty}} \tag{2-1}$$

For most contemporary aircraft only the elevator is used as primary control input for the longitudinal axis, i.e. for rapid control. Flaps (if not combined with the elevator, i.e. flaperon) and slat settings for example rather follow manual control inputs or a certain schedule and the thrust response is normally to slow for controlling the short period motion. Therefore it is a common assumption to ignore the effect of flaps and thrust inputs when dealing with the short period related CAP. Furthermore with classical elevator configurations the direct influence of $\Delta\eta$ on the force in z-direction is rather low, i.e. $Z_\eta \approx 0$. Under those assumptions the CAP can be written as (Heller, 2013, p. 3-122; Holzapfel, 2011, p. 69/94)

$$CAP = -\frac{g\omega_{SP}^2}{V_{A,0} Z_\alpha} = \frac{g}{V_{A,0}} \omega_{SP}^2 T_{\Theta 2} \tag{2-2}$$

where, under the assumptions made, $T_{\Theta 2}$ is the numerator time constant of the transfer function $\Delta\eta$ to Δq. Within the time horizon of the short period motion Z_α and $T_{\Theta 2}$ are normally assumed to be constant for a certain flight condition. While this has been proven in practice as an acceptable assumption it has to be carefully checked for the aircraft system under consideration, especially if an angle of attack feedback is used with a Z_η which is significant.

From (2-2) we can deduct the following:

- The CAP relates short period natural frequency to the short period numerator zero time constant $T_{\Theta 2}$. Together with the damping ratio requirements ζ_{SP} (Figure 12) it therefore defines the allowable relative position of the short period transfer function poles and zero.
- The typical control approach to influence the CAP is to modify the short period natural frequency ω_{SP} according to the flight condition and configuration (cf. Heller, 2013, p. 3-124). The goal is to keep the CAP in the areas allowed by the flying quality specifications and preferably close to constant to ensure a similar aircraft response over the flight envelope.

For a certain trim condition and desired CAP the corresponding natural frequency ω_{SP} for the short period motion can be calculated from (2-2):

$$\omega_{SP} = \sqrt{-CAP \cdot \frac{V_{A,0}}{g} \cdot Z_\alpha} \tag{2-3}$$

Nevertheless, as pointed out by Heller (2013, p. 3-124 & 3-125) and mentioned above, care must be taken when using (2-3) for modern highly augmented aircraft configurations.

Remark 2-1: Extensive pilot in the loop simulations in industry have furthermore shown that the CAP-based ω_{SP} should be upper bounded. Good handling quality results were obtained $\omega_{SP,max} \leq 6.5$ rad/s (cf. Heller, 2013, p. 3-124). This is also the upper bound chosen in this thesis for the nominal ("desired") ω_{SP}. Different values exist for the lower bound. MIL-F-8785C (US DoD, 1996) gives a minimum $\omega_{SP,min,MIL} = 1.0$ rad/s for CAT A flight phases. Nevertheless experience has shown that this leads to a sluggish response. Heller (2013, p. 3-124) suggest $\omega_{SP,min} \geq 1.9$ rad/s based on the above mentioned simulation trails. A third lower bound can be derived from the now widely accepted requirement $n_z/\alpha \geq 2.3$ 1/rad (Brockhaus et al., 2011, p. 463). Plugging this into (2-3) for a target CAP = 1 gives $\omega_{SP,min} \geq 1.5$ rad/s though it should be clear that the latter can normally not be directly influenced by the FCS inner-loop[7]. In other words either the configuration obtains this n_z/α or it does not. For this thesis a $\omega_{SP,min} \geq 1.7$ rad/s has finally been chosen, which lies in the middle of those two approaches.

[7] An exception might be systems with direct lift control.

Figure 12 relates the CAP - ζ_{SP} combinations, for Category A flight phases, to the three different levels of flying qualities as defined by MIL-F-8785C (Table 2). Category A flight phases are "nonterminal Flight Phases that require rapid maneuvering, precision tracking, or precise flight-path control" (US DoD, 1996, p. 2). This includes flight phase typical for fighter aircraft e.g. air-to-air combat, ground attack and formation flying. As it can be readily seen the design goal $CAP = 1$ lies in the middle of the Level 1 region.

The above mentioned design goals of creating a certain CAP - ζ_{SP} combinations is not exclusively academic rather it is the basic longitudinal flying quality design goal for the most advanced fighter aircraft that fly today like the F-22 (NATO RTO, 2000, p. 15) and the Eurofighter Typhoon (Moritz & Osterhuber, 2006, p. 6; Oelker, Osterhuber, & Hanel, 2009, p. 4). It was therefore also chosen for the reference control system developed for this case study. Nevertheless the task of achieving good flying qualities is fairly complex and the flight control system itself gives rise to many secondary effects, e.g. Pilot Induced Oscillations (PIO). Thus it must be mentioned that achieving a certain CAP - ζ_{SP} combination alone does not guarantee good flying qualities. The interested reader is referred to NATO RTO (2000) for an excellent treatment on the best practices of modern flight control system design including the relevant handling/flying quality criteria. A good summary of the latter is also found in Brockhaus et al. (2011, pp. 455-475), Heller (2013), Gibson (1999) and Hodgkinson (1999). Oelker et al. (2009) give an overview over the flying and handling quality criteria applied in the Eurofighter Typhoon program.

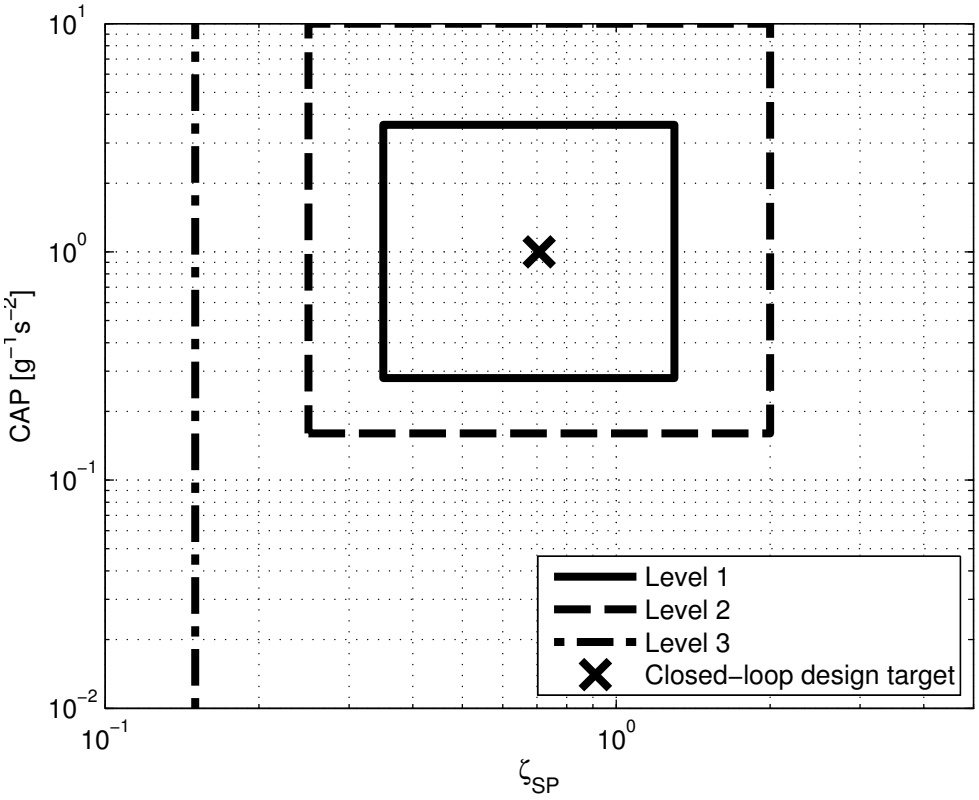

Figure 12 Allowable CAP - ζ_{SP} regions for the short period motion during Category A flight phases (bases on US DoD, 1996, pp. 13-14)

Table 2 Level of flying qualities as defined by MIL-F-8785C (US DoD, 1996, p. 4)

Level of flying qualities	Description
Level 1	"Flying qualities clearly adequate for the mission Flight Phase"
Level 2	"Flying qualities adequate to accomplish the mission Flight Phase, but some increase in pilot workload or degradation in mission effectiveness, or both, exists"
Level 3	"Flying qualities such that the airplane can be controlled safely, but pilot workload is excessive or mission effectiveness is inadequate, or both. Category A Flight Phases can be terminated safely, and Category B and C Flight Phases can be completed."

2.2.3 Redundancy in Current Production Aircraft Flight Control Systems – An example

All of today's large production aircraft mainly rely on hardware based redundancy schemes. Four redundancy structures are common in aircraft flight control systems: the quadruplex, triplex, duo-duplex and duplex arrangements. The interested reader is referred to Moir and Seabridge (2013, pp. 219-226) and Rolf Isermann (2006, pp. 347-354) for general information on those redundancy architectures. An old but, to the author's opinion, rather complete treatment of redundancy structures especially for digital flight control systems is also found in Rice and McCorkle (1979).
Most FCS put into effect a mixture of those structures. This shall be explained at the example of the Eurofighter Typhoon FCS based on the information published by Kaul (1992). The Typhoon is a representative example of a last generation fighter aircraft. In the subsonic flight regime it is highly unstable in the longitudinal axis which means that it is only controllable with the help of the stabilization functions of the FCS. The latter was specified based on the requirements of MIL-F-9490D (US DoD, 1975) which has now been absorbed in AS94900 (SAE, 2007). AS94900 and MIL-F-9490D define so called Operational States (OS) to separate different stages of flight control system degradation due to faults and failures. The major meaning of those states is given in Table 3. AS94900 and MIL-F-9490D furthermore give two definitions which are important for the following discussions:

> Essential FCS functions […] A function is Essential if loss of the function results in an unsafe condition or inability to maintain FCS Operational State III. (SAE, 2007, p. 15)

> Noncritical FCS Functions […] A function is noncritical if loss of the function does not affect flight safety or result in control capability below that required for FCS Operational State III. (SAE, 2007, p. 16)

For more detailed information the interested reader may consult AS94900 (SAE, 2007). The application of the OS from MIL-F-9490D to the Eurofighter Typhoon FCS design lead to the implications summarized in Table 4.
In OS I and II the probability that mission has to be aborted must be smaller than $x \cdot 10^{-3}$ per mission. All essential functions must be intact. A first failure (transition from OS I to OS II) has no effect on essential, and no or just a very limited effect on noncritical functions (e.g. loss of the airbrake functionality). This means that essential functions must be Fail-Operative[8] (FO) and noncritical functions must either

[8] Fail-operative means that a fault or failure has no effect on system functionality

be implemented FO or Fail-Safe[9] (FS) depending on their impact on the mission. The same is true for a second failure (transition from OS II to OS III); however now the mission, and consequently the flight envelope, is reduced to safe cruise, descent, and landing (cf. Table 3). Because of the reduced mission, more noncritical functions become non-mission-relevant and can be lost. It is important to note that after the second failure occurred the recovery from the full flight envelope (e.g. manoeuvring flight) to the more restricted OS III envelope must remain possible. A third failure (transition from OS III to OS IV) may lead to Loss-Of-Control (LOC) and therefore a loss of the aircraft. The probability of LOC must be smaller than $y \cdot 10^{-6}$ per flying hour. For the Typhoon FCS architecture this meant that the essential avionic components (e.g. sensors, data busses, flight control computers, actuator control) had to be implemented in a quadruplex structure. Every Flight Control Computer (FCC) controls its own lane (sensor to actuator) and every FCC is monitoring the other FCCs for faults and failures (cross-monitoring). The actuators of the primary control surfaces are controlled and monitored by all four lanes and powered by two hydraulic circuits. The quadruplex structure ensures that, even after two failures, the essential functions remain available (FO-FO). Non-essential hardware is implemented with less redundancy. The airbrake system, for example, is powered by just one hydraulic circuit, controlled simplex and monitored duplex. It therefore exhibits a FS behaviour. It is interesting to note that duplex monitoring, in this case, is achieved by analytic (software) redundancy. This kind of redundancy will be discussed further in chapter 2.4.6.

The treatment of the Typhoon FCS aimed at giving an example of how redundancy is implemented in current production aircraft. It will form an important basis for the discussion of non-hardware related redundancy approaches in the next chapters. More information of the Eurofighter Typhoon FCS can be found in Kaul (1992). Typical FCS realizations for transport aircraft are described for example in Bartley (2001); Yeh (1996, 1998, 2001) for the Boeing 777 and in Brière, Favre, and Traverse (2000) as well as in Traverse, Lacaze, and Souyris (2004) for the Airbus family.

[9] Fail-safe means that after a fault or failure has occurred the system reverts to a safe state

Table 3 FCS Operational States (extract from SAE, 2007, p. 15)

Operational State	**Major Statement** for details see AS94900 (SAE, 2007, p. 15)
I Normal Operation	"The normal state of FCS performance, safety and reliability."
II Restricted Operation	"The state of less than normal equipment operation or performance, which involves degradation, or failure of only a non-critical portion of the overall FCS. A moderate increase in crew workload and degradation in mission effectiveness may result from a limited selection of normally operating FCS modes available for use; however, the intended mission may be accomplished including aerial refueling and landing at the destination of original intent."
III Minimum Safe Operation	"The state of degraded FCS performance, safety or reliability which permits safe termination of precision tracking or maneuvering tasks, and safe cruise, descent, and landing at the destination of original intent or alternate but where pilot workload is excessive or mission effectiveness is inadequate"
IV Controllable to an Immediate Emergency Landing	"The state of degraded FCS operation at which continued safe flight is not possible; however, sufficient control remains to allow engine restart attempt(s), a controlled descent and immediate emergency landing."
V Controllable to an Evacuable Flight Condition	"The state of degraded FCS operation at which the FCS capability is limited to maneuvers required to reach a flight condition at which crew evacuation may be safely accomplished."

Table 4 Implications of MIL-F-9490D operational states for the Eurofighter Typhoon flight control system (based on Kaul, 1992, p. 1327)

Operational state acc. AS94900/ MIL-F-9490D	**Implication for Eurofighter Typhoon FCS**	**Quantitative requirements Eurofighter Typhoon**
I	Full functionality	Probability that mission has to be aborted must be smaller than $x \cdot 10^{-3}$ per mission.
II	Non-critical functionality reduced	
III	Essential functions sustained	Probability of LOC must be smaller than $y \cdot 10^{-6}$ per flying hour. Failures to considered: e.g. sensors, avionics, actuators, hydraulic and electric power supply
IV	Loss-Of-Control (LOC)	
V		

2.3 Introduction to Fault-Tolerant Control (FTC)

2.3.1 Motivation and Scope of Discussion

The preceding chapter has reviewed typical challenges, design goals, and redundancy setups for contemporary production flight controls systems. This chapter aims at giving a compact *high-level* overview of *some* important fault-tolerant control methods, especially to give the reader a feeling for the difference to conventional FCS. In the last decade FTC has been a very active field of research thus it is not possible, and not the purpose of this text, to discuss the methods in detail or to list all methods available. For more information the reader is referred to the relevant literature.
First of all if we think about how an ideal flight control system would look like, we would find that this would be a fixed structure, fixed gain control system that delivers the desired performance at all possible operating conditions, i.e. dynamic pressures, Mach numbers, angle of attacks, faults. Such a system would render any adaptation or reconfiguration during operation unnecessary, being it a scheduled one (e.g. gain scheduling) or an automatic one (e.g. adaptive control). The system would hence be very reliable as it would be a) less complex and b) would require fewer inputs to work properly (e.g. no gain scheduling variables). This is exactly what passive fault-tolerant control aims for. Unfortunately there is fundamental trade-off between allowable uncertainties and control performance. While appealing in theory passive fault-tolerant control, will most likely not deliver the required performance

to achieve real fault-tolerance. This is the reason why active fault-tolerant control is important.
The following discussion is largely based on the ones in Verhaegen et al. (2010); Alwi, Edwards, and Pin Tan (2011, pp. 1-27); and Zhang and Jiang (2008).

2.3.2 Introduction and Overview

Figure 13 gives an overview of *some* important *fault-tolerant control methods*. In a first step they are broadly classified in active FTC and passive FTC (Eterno, Weiss, Looze, & Willsky, 1985). The former works by detecting a fault and then taking some appropriate control system actions to react on the fault. For the later the fault is treated as model uncertainty in a robust control sense and the control system is designed in a way that the fault lies within the robust stability and acceptable performance limits. Therefore, once a fault occurs, no active actions have to be taken during controller operation; hence this is called passive FTC.

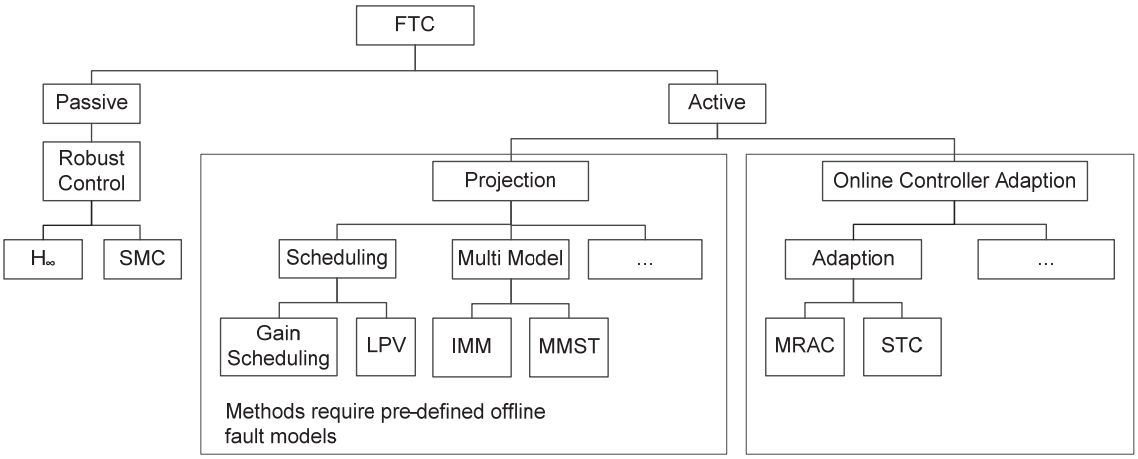

Figure 13 Classification of FTC with some selected methods
(based on Alwi et al., 2011, p. 15)

2.3.3 Concept of Sets

Sets are a useful tool to discuss the different approaches to fault-tolerant control. In Verhaegen et al. (2010, p. 67) the concept of a model set is used to analyse the Multiple Model Switching and Tuning (MMST) approach to FTC. It is extended here in order to support the discussion on most of the FTC methods. To do so the following definitions are required:

Definition 2-1 (Plant Model Set) based on Verhaegen et al. (2010, p. 67)**.** Let $\mathcal{G}$ be a set of N linear models

$$\mathcal{G} : \{G_1, \dots, G_N\} \tag{2-4}$$

that represent all possible damaged and undamaged plant local operating conditions such that

$$G_i : \begin{cases} \dot{x}_i = A_i x_i + B_i u_i \\ y_i = C_i x_i + D_i x_i \end{cases} \tag{2-5}$$

Definition 2-2 (Set of nominal controllers). Let furthermore $\mathcal{C}$ be a set of L controllers

$$\mathcal{C} : \{C_1, \dots, C_L\} \tag{2-6}$$

designed to be stable and to meet the nominal performance requirements when combined with the nominal design model $M_l \in \mathcal{M}$ as defined below.

Definition 2-3 (Set of models that result in stable closed-loop systems). Let $\mathcal{S}_l$ be a set of J models of $\mathcal{G}$, i.e. $\mathcal{G} \subseteq \mathcal{S}_l$,

$$\mathcal{S}_l : \{S_1, \dots, S_J\} \tag{2-7}$$

that create a stable closed-loop system when combined with a controller $C_l \in \mathcal{C}$ in a feedback control system.

Definition 2-4 (Set of nominal design models). Let $\mathcal{M}$ be a set of L models of $\mathcal{S}$, i.e. $\mathcal{G} \subseteq \mathcal{S} \subseteq \mathcal{M}$,

$$\mathcal{M} : \{M_1, \dots, M_L\} \tag{2-8}$$

where M_l is used to design controller $C_l \in \mathcal{C}$.

Definition 2-5 (Plant without fault). Let the linear model $G \in \mathcal{G}$ represent the nominal plant i.e. without fault.

Definition 2-6 (Plant with fault). Let the linear model $G_f \in \mathcal{G}$ represent the plant with fault.

For the following discussion it shall be noted that static stability of the controlled system is a strict requirement for a control system however this does not mean that an acceptable control performance is achieved i.e. the systems fulfils its purpose. For the sake of simplicity the following discussion takes only stability into account however the reader shall keep in mind that there exist more strict acceptable performance requirements however the concept remains the same.

2.3.4 Passive Fault-Tolerant Control (PFTC)

As said above in PFTC a fault is treated like a model uncertainty. As long as the damaged system is within the robustness of the controller no adaptation of the controller gains or structure is necessary.

2.3.4.1 H_∞ - Robust Control

The H_∞ - Robust Control approach to PFTC is graphically displayed in Figure 14. Before the failure occurs the real plant behaviour is represented by model $G \in \mathcal{S}_1$. When the failure occurs the plant transitions from G to $G_f \in \mathcal{S}_1$. Because G, G_f, and the "transition trajectory" lie in $\mathcal{S}_1$ there is no need for any controller adaptation. Unfortunately there is a fundamental trade-off between achievable robustness and achievable performance. This means that if $\mathcal{S}_1$ gets large, e.g. to accommodate significant faults, the controller performance is getting worse which is the reason why fault tolerance based only on robust control theory will most likely not be able to deal with larger faults.

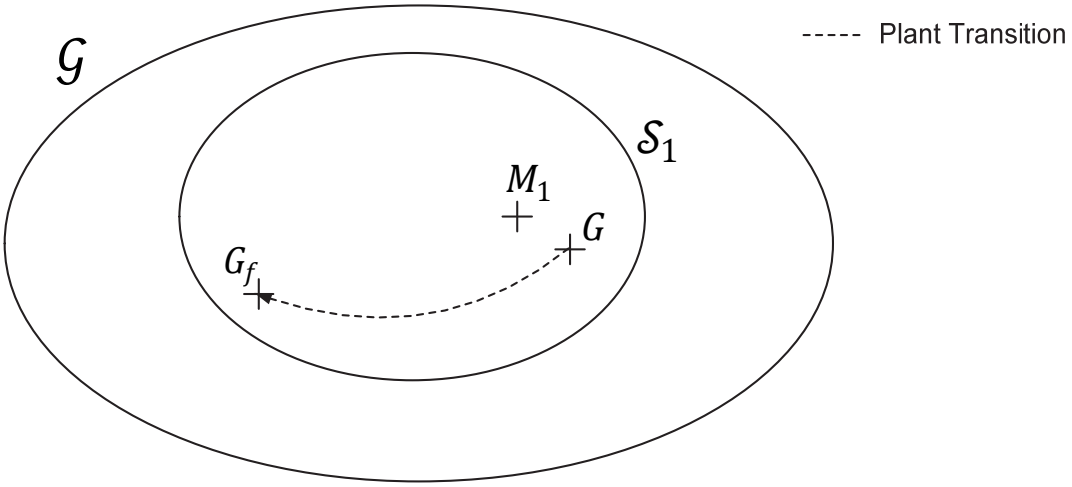

Figure 14 Concept of $\mathcal{H}_\infty$-Robust Control

2.3.4.2 Sliding Mode Control (SMC)

In most of the fault-tolerant control literature SMC is categorized as robust control method. Its approach to robustness however is fundamentally different to what is widely known as robust control theory, especially because it uses a discontinuous switching function.
As Slotine and Li (1990) explain, the basic motivation behind SMC is the fact that a first order system is easier to control than a higher order problem. The idea is therefore to substitute the higher order system by an equivalent first order system, i.e. neglecting the higher order dynamics. For the first order system it can be shown that, in theory, perfect tracking performance can be achieved no matter how large the uncertainties are. This, however, would require the controller to have a very large bandwidth which is a) most of the time not achievable, especially not for mechanical systems, and b) will excite the higher order modes that have been neglected. This practical limitation results in a trade-off between tracking performance and allowable uncertainties. As discussed above the basic idea of any robust control method is to treat system faults as uncertainty. This means that, especially for structural aircraft damage, the uncertainties are large compared to those typically resulting from model imperfection and the required bandwidth can therefore not be achieved. For more details on SMC the reader is referred to Slotine and Li (1990, pp. 276-306).

2.3.5 Active Fault-Tolerant Control (AFTC)

AFTC methods can be categorized into two major groups: projection and online controller redesign/adaptation based methods. The former have in common that they rely on fault models that have been constructed offline. After fault detection the appropriate pre-defined action is taken e.g. a scheduled change of controller gains or the selection of a controller that has been designed for the relevant fault case. Online controller adaptation based methods on the other hand aim at identifying the faulty plant behaviour and designing a controller for this new plant model so that the closed-loop system achieves the control goals.

2.3.5.1 Projection Based Methods

Projection based methods have in common that they rely on pre-defined offline fault models. They are thus not reliably able to handle faults that have not been pre-modelled. However it is quite often the case that it is practically impossible to pre-model all damage scenarios. If, for example due to a mid-air collision, a part of a wing is torn off the air vehicle (cf. F-15 incident, chapter 1.1) it is virtually impossible to foresee and detect all possible wing structure failures, build a plant model, and design a control system in advance for it.

2.3.5.1.1 Scheduling

Scheduling in general refers to a technique where the control systems are adapted in a feed forward manner, that is a change in the system is detected and a control system is activated that has been designed for that case. Because of that, scheduling clearly is a projection-based method that can only reliably deal with faults that have been anticipated during the control system design phase. An important difference to, for example the multi-model based approaches discussed in the next chapter, is that the changes are normally not detected by a change of the dynamic behaviour of the system. In fact, in most of the cases, the fault information comes from conventional hardware redundancy. A faulty angle of attack measurement, detected by sensor hardware redundancy, for example could lead to scheduled reconfiguration of the flight control system to a backup mode that is only based on rate feedback. Fault-tolerant control based on scheduling is the major method to achieve fault tolerance in today's production flight control systems.
Under the category of scheduling fall the special cases of *gain scheduling*, where the controller structure remains unchanged and only the controller gains are adapted. Gain scheduling is also used in nearly all production flight control systems to select the appropriate controller gains for the actual flight condition e.g. dynamic pressure, Mach number, angle of attack, and aircraft configuration.

2.3.5.1.2 Linear Parameter Varying Control (LPV)

LPV systems are a special class of non-linear systems that can be expressed as

$$\begin{aligned} \dot{\boldsymbol{x}} &= \boldsymbol{A}\big(\boldsymbol{\delta}(t)\big)\boldsymbol{x} + \boldsymbol{B}\big(\boldsymbol{\delta}(t)\big)\boldsymbol{u} \\ \boldsymbol{x}(0) &= \boldsymbol{x_0} \end{aligned} \tag{2-9}$$

$$\boldsymbol{y} = \boldsymbol{C}\big(\boldsymbol{\delta}(t)\big)\boldsymbol{x} + \boldsymbol{D}\big(\boldsymbol{\delta}(t)\big)\boldsymbol{u} \tag{2-10}$$

where $\boldsymbol{\delta}(t)$ represents the time-varying parameters. Because the system parameters are no longer constant like for LTI system, LPV systems are non-linear even if the equation structure of (2-9) and (2-10) is linear.
In the "classical" gain scheduling approach, LTI controllers are designed for a grid of operating points. The resulting gains are then interpolated between those operating points based on the measured scheduling variables. This approach implicitly assumes slowly varying scheduling variables, without properly defining what slow in this case means. The difficulty is that, for sufficiently fast varying scheduling variables, neither stability nor performance of the "classical" gain scheduled control system can be guaranteed with LTI theory (J. S. Shamma & Athans, 1992). Inspired by this gain scheduling problem Jeff S. Shamma (1988) introduced the concept of LPV

control design which nowadays allows a systematic theoretical treatment of many aspects of LPV systems. With respect to FTC, LPV control is interesting because also faults can be modelled as system parameter variations and consequently LPV control theory provides tools to design a control system. However, as LPV control belongs to the projection-based methods, it relies on pre-defined offline fault models. It is thus not reliably able to handle faults that have not been pre-modelled. For more information on the subject of LPV systems analysis and control the interested reader is referred to the monograph of Mohammadpour and Scherer (2012) and the recent work of Briat (2015).

2.3.5.1.3 Multi Model (MM) Based Approaches

The basic idea of the multi model based approaches is to construct a plant model for every anticipated failure case, for example based on the set failures identified during a Failure Mode and Effect Analysis (FMEA). For every failure model a controller is designed offline. During operation the models run in parallel to the plant and the output error of each model is monitored. The controller for the model with the smallest output error is activated.

The concept described above is called Multi Model Switching (MMS) because different controllers are virtually switched on and off. This is illustrated in Figure 15. In the failure free case control C_1 designed for model M_1 is activated. When the failure occurs the plant behaviour described by G_f is better modelled by design model M_5 thus controller C_5 is switched on and controller C_1 is switched off. Of course, during the transition from G_f to G_f other controller might be activated, e.g. C_4 for the scenario sketched in Figure 15.

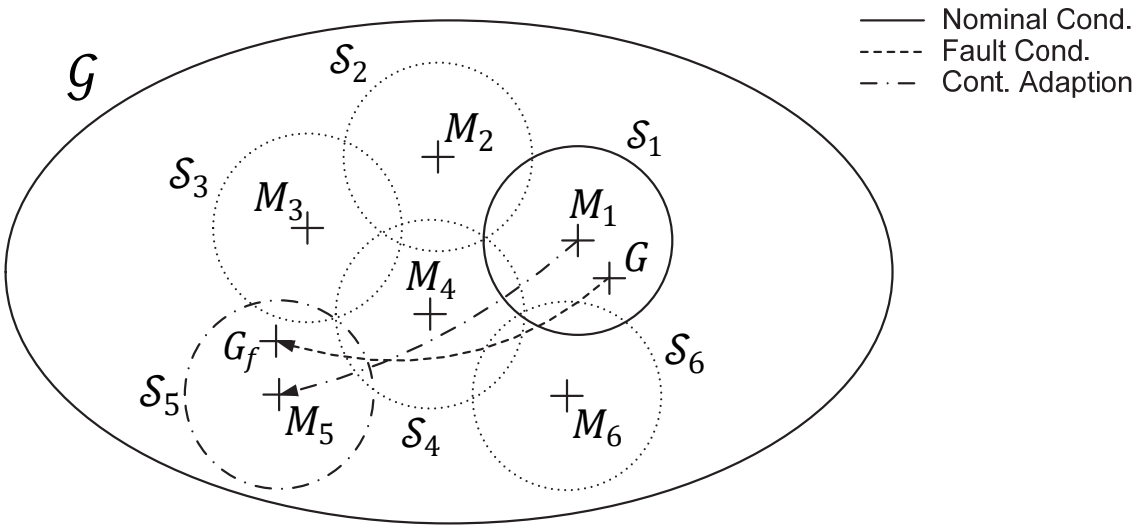

Figure 15 Concept of Multi Model Switching (MMS)

The switching is normally achieved by forming a linear combination of the weighted controller outputs u_{C_i} (Verhaegen et al., 2010, p. 64):

$$u(k) = \sum_{i=1}^{L} \mu_{C_i}(k)\, u_{C_i}(k), \quad \sum_{i=1}^{L} \mu_{C_i}(k) = 1 \tag{2-11}$$

The coefficients μ_{C_i} are determined in a way that the coefficient for the model that is closest to G or G_f has a weighting factor μ_{C_i} close to unity while all other weighting factors are close to zero. This is often implemented by a bank of Kalman filters, each one using one of the models $M_i \in \mathcal{M}$ for the prediction step. From (2-11) it is clear that any unanticipated fault will lead to some kind of linear combination of $u_{C_i}(k)$ that has not been analysed during the design stage. The result might be an unacceptable closed loop performance or even instability.
In many cases the pure MMS approach is extended by adaptive elements. The idea is to perform some kind of adaptive *tuning* of the controller to optimize the closed-loop performance after the controller switching because of the fault occurred. The concept is normally referred to as Multi Model Switching and Tuning (MMST). Strictly speaking, in view of the classification suggested by Figure 13, it is a combination of a projection and online controller redesign based method however it is normally included in the former group because the MMS-part is the primary source of fault tolerance. The advantage of MMST over a pure adaptive approach is that the whole control system reconfiguration tends to be faster. The major disadvantage of MMS and MMST is the fact that they rely on offline pre-computed fault models and therefore

- are unable to reliably handle unanticipated faults and
- lead to high design efforts because for every fault a models and the related controller has to be constructed

A method called Interacting Multiple Models (IMM) seeks to overcome this disadvantage by forming a model M_f of the faulty plant from a convex combination of the design models $M_i \in \mathcal{M}$, i.e.

$$M_f(k) = \sum_{i=1}^{L} \mu_{M_i}(k)\, M_i, \quad \sum_{i=1}^{L} \mu_{M_i}(k) = 1 \tag{2-12}$$

with $\mu_{M_i} \in \mathbb{R} \wedge \mu_{M_i} > 0$ (Verhaegen et al., 2010, p. 68). It becomes clear that IMM is a parameter estimation based method where the weighting coefficients $\mu_{M_i}(k)$ have to be estimated. Therefore it is sometimes also called Multiple Model Adaptive

Estimation (MMAE). The identified model M_f can then be used as estimated plant model to perform the online design of the appropriate controller. The result of this approach to fault-tolerant control is therefore in fact a mixture between multi model and indirect adaptive control. However, as IMM still requires offline pre-designed fault models $M_i \in \mathcal{M}$ it is normally classified as projection based method. As stated by Verhaegen et al. (2010, p. 69) a major disadvantage of IMM is that "it is still an open question how to choose this model set [$\mathcal{M}$] or when the assumption that the failure model can be written as a convex combination of the models in the set, is valid." For more details on multi-model based approaches the reader is referred to Verhaegen et al. (2010, pp. 66-69), on which the discussion above was largely based on, and Alwi et al. (2011, pp. 16-18).

2.3.5.2 Online Controller Adaptation Based Methods

This group of methods has in common that they do not rely on pre-defined offline fault models. Instead the control system is able to detect and identify changes in the systems dynamic behaviour and to redesign the control system online in such a way as to achieve the control goals.

2.3.5.2.1 Model Reference Adaptive Control (MRAC)

For the MRAC approaches the output y of the closed-loop system is compared to the output of a reference model y_m, which describes the desired closed-loop system performance. The goal is to adapt the controller gains in such a *way as to minimize the output* e. The adaptation is driven by the output error signal itself. In contrast to fixed gain control systems, where the feedback signal is multiplied by a constant feedback gain, it is now multiplied by another signal. Therefore the control system is necessarily non-linear as the superposition principle does no longer hold (cf. Smith, 2003, pp. 96-97). The principle control structure is shown in Figure 16.

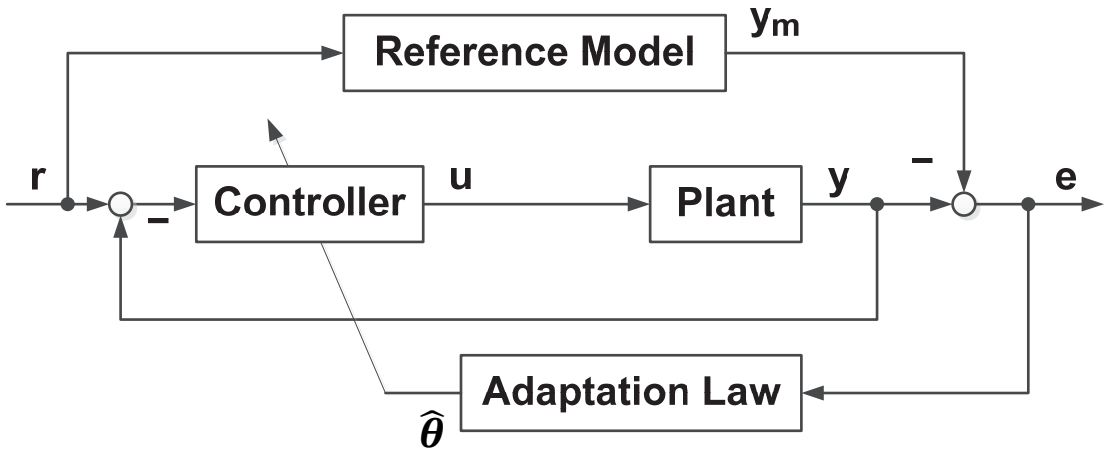

Figure 16 Model Reference Adaptive Control (based on Slotine & Li, 1990, p. 315)

2.3.5.2.2 Self-Tuning Controller (STC)

To discuss the STC approach it is worth reviewing the two major steps of classical offline controller design. Those are a) creation of a model for the *uncontrolled* plant and b) computation of a controller so that controller plus plant model meet the control requirements. The indirect STC methods use the same approach but conduct the two steps online, i.e. during system operation. The resulting architecture is shown in Figure 17. An on-line parameter estimation/identification algorithm is used to create a plant model $\widehat{\boldsymbol{\theta}}$. The latter is then used to calculate a controller, appropriate to meet the control requirements. Like for the MRAC approach the feedback gains are no longer constant, thus also the STC approach leads to a non-linear control system.
The advantages of the STC in comparison to the MRAC concept are a

- better physical interpretation of the plant changes because the plant model $\widehat{\boldsymbol{\theta}}$ is explicitly calculated and
- greater flexibility in the system design because, at least in theory, the identification/estimation algorithm can be chooses independently form the adaptation algorithm

In return a control system based on the STC principle tends to be more complex and stability and performance is generally more difficult to guarantee.
On-line parameter estimation in itself is a vast research topic (cf. e.g. Jategaonkar, 2006; Klein & Morelli, 2006; Tischler & Remple, 2012). One of the major difficulties is to ensure that the on-line estimated parameters always converge to their true values with the major questions of estimating time-varying parameters and data information content or persistence of excitation (Klein & Morelli, 2006, pp. 285-286; D. G. Ward & Monaco, 2005, p. 66-67). Obviously, if they do not, neither stability nor performance of the control system can be ensured.
Because of their inherent non-linearity all adaptation-based approaches have the drawback that the well-established linear control theory cannot be used for their design. While there has been significant progress with respect to non-linear control theory in recent years, certification experience remains limited. Besides that adaptive control promises to be the most powerful FTC approach, because, especially in comparison to robust control, it offers the possibility to ensure control system performance even with large faults. This was for example impressively demonstrated in Jourdan et al. (2010) where control of a subscale F-18 model is maintained even after a major part of the wing was lost. In comparison to active projection based FTC methods they have the advantage of being able to deal with faults that have not been pre-modelled.
The approach of this work, which aims at combining a conventional and fault-tolerant control system and switch to FTC only if the conventional control system is

no longer able to deliver an acceptable closed loop performance, perfectly harmonizes with adaptive FTC, especially the MRAC approach. As we will see later on, the fault detection algorithm, also builds on a reference model of the desired closed-loop performance. As explained in chapter 1.2, the combined approach has, to the author's opinion, some significant advantages with respect to economic considerations and will help to make certification of active, e.g. adaptive, FTC easier. It therefore addresses the biggest drawback of adaptive FTC with respect to its practical implementation in production aircraft flight control systems. For a good introduction to adaptive control the interested reader is referred to Slotine and Li (1990, pp. 311 ff.).

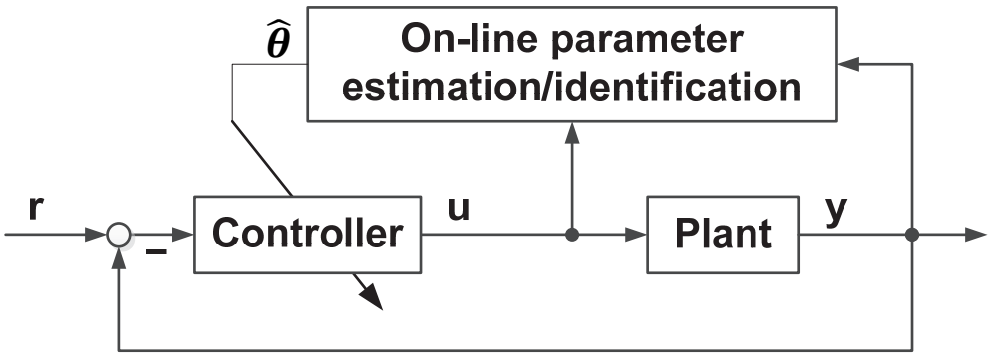

Figure 17 Self-Tuning Controller (based on Slotine & Li, 1990, p. 320)

2.4 Introduction to Fault Detection and Diagnosis (FDD)

2.4.1 Motivation and Scope of Discussion

The last chapter gave an overview of some important FTC methods. This chapter will give an introduction to Fault Detection and Diagnosis (FDD) in dynamic systems and therefore to the heart of this work. As explained before the central focus of this thesis is the Fault Detection (FD) algorithm to activate a fault-tolerant flight control system in case the conventional flight control system is no longer able to deliver the appropriate performance. The approach chosen for fault detection in this thesis is the so-called *model or analytic redundancy based approach*. The discussion of this chapter aims at giving the reader a high-level introduction to the field off FDD in order to allow integrating the former into the bigger picture of FDD. Chapter 3 will then discuss the details of the theoretical studies conducted for the fault detection problem of this work.

2.4.2 Introduction and Overview

The process of Fault Detection and Diagnosis (FDD) consists of three major steps:

- Fault Detection
- Fault Isolation
- Fault Identification (sometimes also referred to as fault analysis)

The terminology in the field of FDD is still not fully harmonized. However a now widely accepted set of definitions was developed by the Technical Committee of the IFAC Symposium on Fault Detection, Supervision and Safety for Technical Process (SAFEPROCESS). Those definitions, published in R. Isermann and Ballé (1997, p. 710), will be used throughout this text:

> Fault detection:
> Determination of the faults present in a system and the time of detection.
>
> Fault isolation:
> Determination of the kind, location and time of detection of a fault. Follows fault detection.
>
> Fault identification:
> Determination of the size and time-variant behaviour of a fault. Follows fault isolation.

Fault diagnosis:
Determination of the kind, size, location and time of detection of a fault. Follows fault detection. Includes fault isolation and identification.

In some literature FDD is sometimes also referred to as Fault Detection and Isolation (FDI) or Fault Detection Isolation and Analysis (FDIA).
Ding (2013, p. 5) suggests classifying FDD into four groups: hardware redundancy, plausibility test, software/analytical redundancy, and signal processing schemes (Figure 18). They will be discussed in more detail in the following chapters.

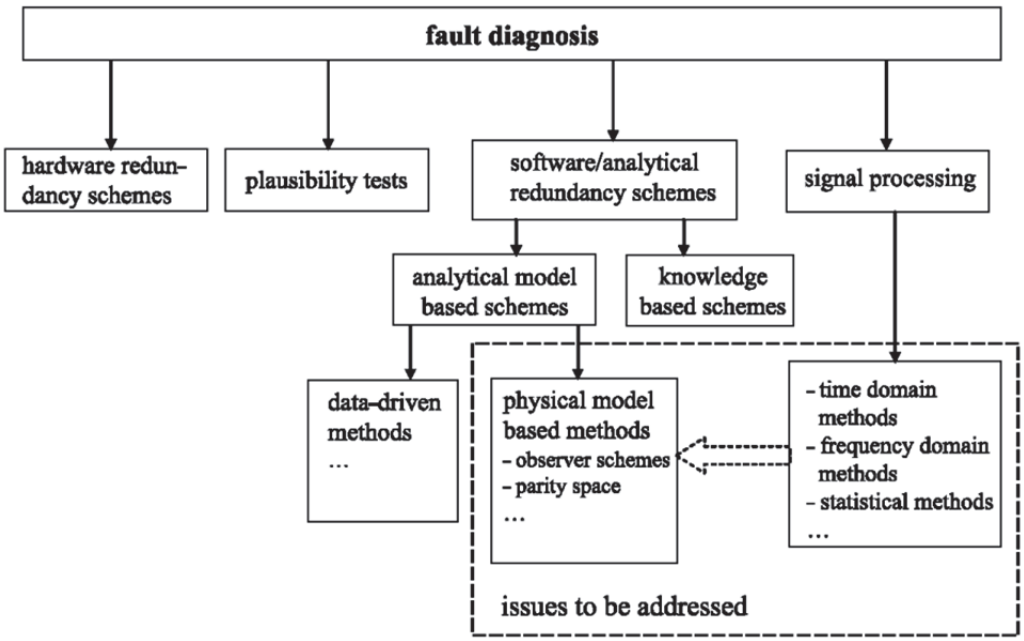

Figure 18 Classification of FDD methods (Ding, 2013, p. 5)

2.4.3 Hardware Redundancy Scheme

The basic principle of hardware-based FDD is shown in Figure 19. Two components work in parallel and are fed by the same input. The output of both components is compared. If the result, the so-called residual, is close to zero[10] the system is declared fault-free. If it deviates strongly from zero a fault is detected (Ding, 2013, p. 4). In the duplex setup shown in Figure 19 a fault can be detected but not isolated i.e. it is not possible to determine which of the two components is faulty. Fault iso-

[10] Because of component tolerances the residual will most of the time not be exactly zero.

lation can only be achieved by introducing more redundant components i.e. a triplex, quadruplex or dual-duplex setup (majority voting, cf. chapter 2.2.3) or by taking the results of component build in tests into account. The latter is normally not done for essential equipment (cf. Kaul, 1992, p. 1323). As discussed in chapter 2.2.3, hardware redundancy based FDD is currently the most widely used form of FDD for aerospace systems.

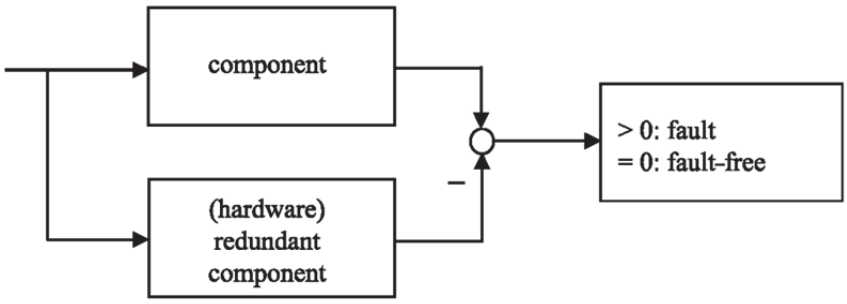

Figure 19 Hardware redundancy scheme (Ding, 2013, p. 5)

2.4.4 Signal Processing Scheme

The signal processing scheme, as shown in Figure 20, aims at extracting features from the output signal of a system that are characteristic (symptoms) for a certain fault (Ding, 2013, p. 5). A simple example could be the use of a high pass filter to monitor the output of an actuator for unwanted high-frequency oscillations. In a fault-free case the output of this high-pass filter should be close to zero. In a fault case high frequency oscillations will show up. The symptom can be further analysed by time domain, frequency domain, or statistical methods (symptom analysis). Application of the signal processing scheme is normally only suitable for simple processes and well defined, known faults.

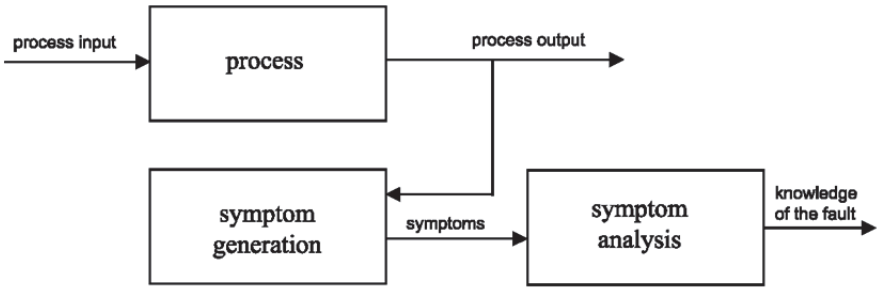

Figure 20 Signal processing based scheme (Ding, 2013, p. 6)

2.4.5 Plausibility Test Scheme

The plausibility test scheme (Figure 21) relies on checking if a process is compliant to the underlying physical laws (Ding, 2013, p. 5). If one of the latter is violated a fault is declared. Application of the plausibility test scheme is normally only suitable for simple processes.

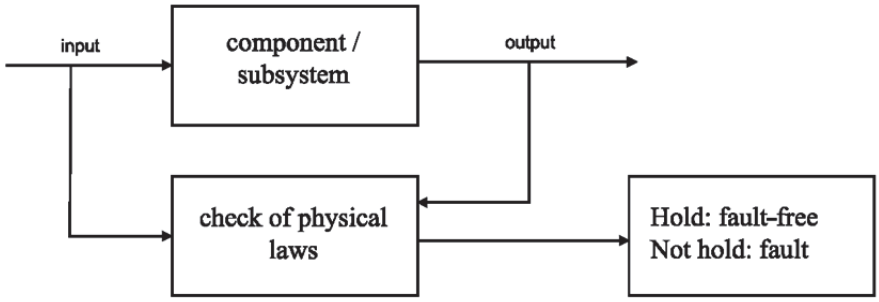

Figure 21 Plausibility test scheme (Ding, 2013, p. 6)

2.4.6 Model-based Scheme or Software Redundancy

As motivating example we shall reconsider the duplex hardware redundancy setup of Figure 19. In this scheme the hardware component must be duplicated to detect a fault. This increasing number of components leads to a significant increase in mass, costs, and maintenance requirements. The idea of the model-based or software redundancy scheme is to replace hardware by a suitable model of the process to avoid duplication of hardware components just for FDD purposes. A second aspect is that for some components it is not at all possible to provide hardware redundancy. Structural airframe damage, for example, can, for obvious reasons, normally not be covered by hardware redundancy because that would require a backup airframe.

The basic idea of the model-based scheme is shown in Figure 22. The output of the process (measurement) is compared to the output of a process model. The resulting signal is called residual and the associated task is called *residual generation*.

The residual is used to detect and analyse a fault. This act is referred to as *residual evaluation*. If the process model would be a *perfect representation* of the real process without faults, than the residual is zero if no fault is present and non-zero if a fault occurred. Unfortunately, in a practical application, the model is always just an approximation of the real process, because of model uncertainties and unknown (not measurable) inputs. In fact nearly all the research on model-based FDD deals with the question how to create a FDD system that minimizes incorrect fault diagnosis in view of the above-discussed fact. The model-based fault detection scheme has the

advantage of being capable of dealing with unknown, not pre-modelled faults, as well as complex processes. It is furthermore more easily integrateable into the hardware redundancy scheme due to its structural similarity, i.e. a hardware component is replaced by its software model.

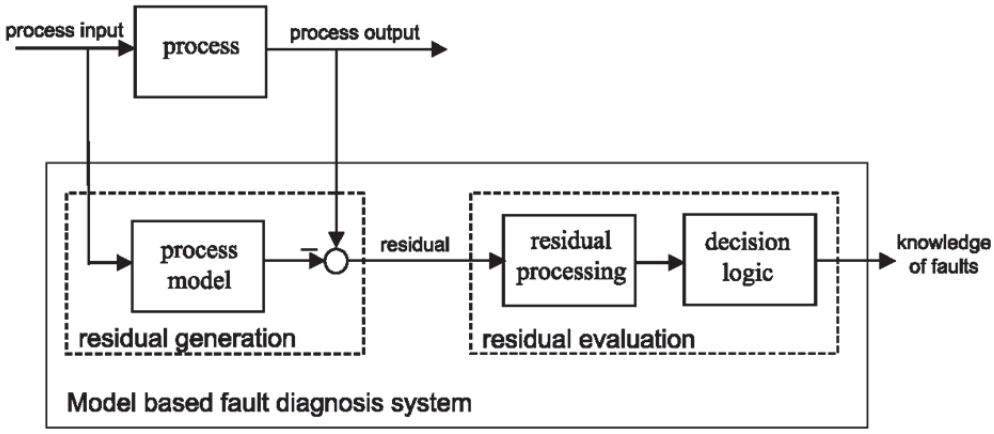

Figure 22 Model-based fault diagnosis scheme (Ding, 2013, p. 7)

2.5 Summary

The preceding chapter gave an overview of typical primary design goals for flight control systems in general, as well as the most important FTC and FDD methods.
Chapter 2.2 discussed one of the most important flying quality parameters for the longitudinal aircraft motion, i.e. the Control Anticipation Parameter (CAP). Because of its importance the CAP forms the basis of the fault detection algorithm proposed in this text (chapter 3.5). The considerations made are therefore very important for the remainder of this work.
In chapter 2.3 it has been shown that FTC can be broadly categorized in passive and active FTC. The latter can be further split into projection-based methods, which rely on an offline pre-defined failure model, and adaptation-based methods that adapt the controller during system operation based on the output error. In contrast to the former, the latter have the advantage of not requiring offline pre-designed failure models. They can thus account for failures which cannot be pre-modelled, e.g. severe structural airframe damage. While appealing in theory passive fault-tolerant control will most likely not deliver the required performance to achieve real fault-tolerance. This is the reason why *active* fault-tolerant control methods are worth investigating. The approach of this work, which aims at combining a CFCS and AFCS, and switch to the latter only if the former is no longer able to deliver an ac-

ceptable closed loop performance, perfectly harmonizes with adaptive FTC, especially the MRAC approach. As we will see later on, the fault detection algorithm, also builds on a reference model of the desired closed-loop performance. The combined approach has, to the author's opinion, some significant advantages with respect to economic considerations and will help to make certification of AFTC easier (cf. chapter 1.2). It therefore addresses the biggest drawback of active FTC with respect to its practical implementation in production aircraft flight control systems.
Chapter 2.4 gave a brief overview of contemporary approaches to FDD. The most widespread method for production aircraft is the hardware redundancy scheme. A high level of hardware redundancy is certainly not desirable because of weight, cost, and maintenance constraints but has historically been the most straight forward solution. Model-based or software redundancy aims at replacing hardware, only used for FDD purposes, by a software model of that component. In comparison to other software based FDD approaches, namely the signal processing and plausibility test scheme, it has the advantage of being capable of dealing with unknown, i.e. not pre-modelled faults, as well as complex processes. It is therefore the FDD approach selected for this work.
The following chapter will initially discuss contemporary model-based FDD methods, as far as relevant for this text, and finally describe the fault detection system for the aircraft longitudinal axis proposed in this work.

3 Theoretical Study on Model-Based Fault Detection

3.1 Motivation and Scope of Discussion

The fault detection system for the aircraft longitudinal axis proposed in this work, which is finally described in chapter 3.5 builds on the model-based fault detection approach. Chapter 3 thus forms the heart of this thesis. It describes the theoretical considerations made that finally lead to the proposed fault detection system architecture.

The whole research on model-based fault detection focuses on minimizing the False Alarm Rate (FAR) and the Missed Detection Rate (MDR). As mentioned before, because of model uncertainties and unknown (not measurable) inputs, the model is always just an approximation of the real process. For a reliable FD those uncertainties and unknown inputs must therefore be accounted for. They can be deterministic or stochastic in nature. Chapter 3.2 will discuss how to model technical systems as dynamic systems with unknown inputs, model uncertainties, and faults. The contemporary approach on residual generation, as far as relevant for this text, is described in chapter 3.3. State of the art residual evaluation is covered in chapter 3.4. Both, residual generation and evaluation will be treated in a stochastic and deterministic context, leading finally to an integrated approach that combines both of it. As mentioned above chapter 3.5 finally introduces the fault detection architecture chosen for this work including the research contributions by the author.

Special emphasis is placed on the residual evaluation part. As explained in chapter 1.3 the approach of this work is to take the relatively simple desired closed loop dynamics derived from the flying quality specifications as a reference model for fault detection. As the model is simple it does not cover all real world effects. Thus, also in a fault free case, the residual will not be zero. It follows that more emphasis has to be put on calculating a proper fault detection threshold for the residual with a *guaranteed FAR*, i.e. on residual evaluation. In contrast, the majority of classical work on fault detection focuses on residual generation, i.e. on creating a residual signal that is as close as possible to zero in the fault-free case. Unfortunately this leads to more and more complex models for fault detection. The disadvantages of such complex models are to the author's opinion mainly twofold:

1. A complex model normally needs more measurement inputs. With an increasing number of measurements the reliability of the system will be reduced as more measurements must be accurate and available for the system to work correctly. Especially for a damaged aircraft this is not a very robust starting point for proper fault detection. The fault detection system proposed in chapter 3.5 in contrast uses only angular accelerations and rates that nor-

mally come from inertial sensors that are located, relatively well protected, deep inside the airframe.

2. Using a complex higher order dynamic model as reference for fault detection when the goal of the closed-loop system is to achieve a simple low order type response poses the problem of deciding which high order response is acceptable. There is simply no basis for proper judgement. As explained in chapter 2.2.2 the typical design goal for nearly all modern flight control systems is to achieve a classical aircraft response beside the unacceptable natural dynamic behaviour of the airframe, e.g. due to stealth or static instability. Classically acceptable flying quality specifications are given as low order system response with a certain allowable parameter range, e.g. CAP, natural frequency and damping ratio ranges. The idea of this text is thus to use this low order flying quality model, including its allowable parameter range, as a reference model for fault detection. It will be shown that this allowable parameter range can be naturally modelled as reference model uncertainties.

To the author's opinion the described approach finally leads to a very clear situation. The reference model defines what closed-loop system response we nominally try to achieve plus the acceptable parameter variations. As well as important the parameters and their variations are directly interpretable in a flying quality context and can be directly compared to the relevant specifications. We acknowledge, because this is simply the truth, that even during fault-free operation we will not achieve this nominal response, due to e.g. unknown inputs (turbulence), build tolerance, and higher order dynamics. The residual reflects this situation and will thus not be zero even in the fault free case. Instead we focus on establishing a reasonable threshold with a *guaranteed* False Alarm Rate (FAR) that takes into account model uncertainties and unknown inputs. When the closed-loop system performance becomes unacceptable the residual signal reaches the threshold and we have to switch to a fault-tolerant flight control system.
The view of the author that not enough focus is placed on the residual evaluation part of FDD is also shared by others. Ding (2013, p. 14) for example states that:

> Another misunderstanding of the observer-based FDI schemes is concerning the role of the observer. Often, the observer-based FDI system design is understood as the observer design and the FDI system performance is evaluated by the observer performance. This leads to an over-weighted research focus on the observer-based residual generation and less interest in studying the residual evaluation problems.

Ding (2013, p. 17) furthermore highlights that:

> Despite of the fact that an FDI system consists of a residual generator, a residual evaluator together with a threshold and a decision maker, in the observer-based FDI framework, studies on the residual evaluation and threshold computation have only been occasionally published. There exist two major residual evaluation strategies. The statistic testing is one of them, which is well established in the framework of statistical methods. Another one is the so-called norm-based residual evaluation.

Contribution 3-1: This work will emphasize *residual evaluation* and applies and extents *the latest residual evaluation techniques* (a combination of norm-base and statistical methods) to the problem on hand which is a fault-detection system to activate an active fault-tolerant flight control system, when the conventional certified flight control system is no longer able to deliver an acceptable closed-loop performance. To the author's knowledge this application and the related extensions are new. The work furthermore adds research results to the, as highlighted by Ding (see above), very sparsely investigated research area of *residual evaluation*.

3.2 Linear Models for Technical Systems

The discussions of this chapter are largely based on Ding (2013, p. 22-29).

3.2.1 Nominal Deterministic Linear System

The two system representations used throughout this text are the state space and the transfer function representation.
For the continuous-time linear system without modelling uncertainties, faults, measurement and process noise, herein called nominal system, the state space representation is given by

$$\begin{aligned} \dot{\boldsymbol{x}}(t) &= \boldsymbol{A}\boldsymbol{x}(t) + \boldsymbol{B}\boldsymbol{u}(t) \\ \boldsymbol{x}(0) &= \boldsymbol{x_0} \end{aligned} \tag{3-1}$$

$$\boldsymbol{y}(t) = \boldsymbol{C}\boldsymbol{x}(t) + \boldsymbol{D}\boldsymbol{u}(t) \tag{3-2}$$

where $\boldsymbol{x} \in \mathbb{R}^n$ is called state vector with its initial conditions $\boldsymbol{x_0}$, $\boldsymbol{u} \in \mathbb{R}^{k_u}$ is called input vector and $\boldsymbol{y} \in \mathbb{R}^m$ is called output vector. For the sake of an easier presentation the variable $\boldsymbol{t}$ will be omitted as long as this does not risk causing confusion. For the discrete-time case (3-1) and (3-2) are transformed into

$$\begin{aligned} \boldsymbol{x}(k+1) &= \boldsymbol{A}\boldsymbol{x}(k) + \boldsymbol{B}\boldsymbol{u}(k) \\ \boldsymbol{x}(0) &= \boldsymbol{x_0} \end{aligned} \tag{3-3}$$

$$\boldsymbol{y}(k) = \boldsymbol{C}\boldsymbol{x}(k) + \boldsymbol{D}\boldsymbol{u}(k) \tag{3-4}$$

As contemporary signal processing is done with digital computers, the remainder of this text will largely focus on the discrete-time case.
The second representation used is the transfer function form. It is a pure input-output description of the system in the frequency domain. The system output is given by

$$\boldsymbol{y}(s) = \boldsymbol{G}_{yu}(s)\boldsymbol{u}(s) \tag{3-5}$$

$$\boldsymbol{y}(z) = \boldsymbol{G}_{yu}(z)\boldsymbol{u}(z) \tag{3-6}$$

where $\boldsymbol{G}_{yu}(s), \boldsymbol{G}_{yu}(z) \in \mathcal{LH}_{\infty}^{mxk_u}$ is the matrix of the corresponding transfer functions while s and z represent the continuous and discrete time frequency domain operators. $\boldsymbol{G}_{yu}$ can be obtained from (3-1) and (3-2) by

$$\boldsymbol{G_{yu}(s) = C(sI - A)^{-1}B + D} \tag{3-7}$$

for the continuous time case and by (3-3) and (3-4)

$$\boldsymbol{G_{yu}(z) = C(zI - A)^{-1}B + D} \tag{3-8}$$

for the discrete time case (cf. eg. The MathWorks Inc., 2017b, p. 1-11539).

3.2.2 Nominal Linear System with Unknown Stochastic and Deterministic Inputs

To model unknown deterministic inputs, as well as stochastic process and measurement noise the discrete deterministic state space model can be extended to

$$\begin{aligned} &\boldsymbol{x}(k+1) = \boldsymbol{Ax}(k) + \boldsymbol{Bu}(k) + \boldsymbol{E_d d}(k) + \boldsymbol{E}_{\nu_P}\boldsymbol{\nu}_P\,(k) \\ &\boldsymbol{x}(0) = \boldsymbol{x_0} \end{aligned} \tag{3-9}$$

$$\boldsymbol{y}(k) = \boldsymbol{Cx}(k) + \boldsymbol{Du}(k) + \boldsymbol{F_d d}(k) + \boldsymbol{F}_{\nu_M}\boldsymbol{\nu}_M\,(k) \tag{3-10}$$

where $\boldsymbol{\nu_P} \in \mathbb{R}^{k_{\nu_P}}$ is called process and $\boldsymbol{\nu_M} \in \mathbb{R}^{k_{\nu_M}}$ measurement noise. Throughout this text $\boldsymbol{\nu_P}$ and $\boldsymbol{\nu_M}$ will be modelled as zero mean, Gaussian white noise process, i.e. $\boldsymbol{\nu_P} \sim \mathcal{N}\left(\boldsymbol{0}, \boldsymbol{\Sigma}_{\nu_P}\right)$ and $\boldsymbol{\nu_M} \sim \mathcal{N}\left(\boldsymbol{0}, \boldsymbol{\Sigma}_{\nu_M}\right)$. Unknown deterministic inputs are represented by the vector $\boldsymbol{d} \in \mathbb{R}^{k_d}$ which influences the states $\boldsymbol{x}$ and outputs $\boldsymbol{y}$ by the corresponding matrices $\boldsymbol{E_d} \in \mathbb{R}^{nxk_d}$ and $\boldsymbol{F_d} \in \mathbb{R}^{mxk_d}$.
In contrast to normal system input $\boldsymbol{u}$, $\boldsymbol{\nu}$ and $\boldsymbol{d}$ are normally not known. Most often this is due to fact that, under practical considerations, they are not measureable. Consequently they are called unknown inputs. An important aircraft related example for unknown stochastic inputs are atmospheric turbulences.

3.2.3 Linear System with Unknown Stochastic and Deterministic Inputs and Model Uncertainty

A real system, even without faults and unknown inputs, will never exactly behave like the modelled system. This is due to the fact that the model parameters are only known with certain accuracy and that not all physical aspects are contained in the model. Those model uncertainties are included into (3-9) and (3-10) by introducing uncertainty matrices $\boldsymbol{\Delta A} \in \mathbb{R}^{nxn}$, $\boldsymbol{\Delta B} \in \mathbb{R}^{nxk_u}$, $\boldsymbol{\Delta C} \in \mathbb{R}^{mxn}$, $\boldsymbol{\Delta D} \in \mathbb{R}^{mxk_u}$, $\boldsymbol{\Delta E_d} \in \mathbb{R}^{nxk_d}$ and $\boldsymbol{\Delta F_d} \in \mathbb{R}^{mxk_d}$ which add to the respective nominal system matrices.

$$\begin{aligned}&\boldsymbol{x}(k+1)\\&\quad=(\boldsymbol{A}+\Delta\boldsymbol{A})\boldsymbol{x}(k)+(\boldsymbol{B}+\Delta\boldsymbol{B})\boldsymbol{u}(k)+(\boldsymbol{E_d}+\Delta\boldsymbol{E_d})\boldsymbol{d}(k)\\&\quad+\boldsymbol{E}_{\nu_P}\boldsymbol{\nu}_P\,(k)\\&\boldsymbol{x}(0)=\boldsymbol{x_0}\end{aligned}\tag{3-11}$$

$$\begin{aligned}&\boldsymbol{y}(k)\\&\quad=(\boldsymbol{C}+\Delta\boldsymbol{C})\boldsymbol{x}(k)+(\boldsymbol{D}+\Delta\boldsymbol{D})\boldsymbol{u}(k)+(\boldsymbol{F_d}+\Delta\boldsymbol{F_d})\boldsymbol{d}(k)\\&\quad+\boldsymbol{F}_{\nu_M}\boldsymbol{\nu}_M\,(k)\end{aligned}\tag{3-12}$$

If required matrices $\Delta\boldsymbol{E}_{\nu_P} \in \mathbb{R}^{nxk_{\nu_P}}$ and $\Delta\boldsymbol{F}_{\nu_M} \in \mathbb{R}^{mxk_{\nu_M}}$ could be defined in a similar way however this is not common because for practical applications it is often hard to do a quantitative judgment concerning those uncertainties.
Different ways exists how the uncertainties given by $\boldsymbol{\Delta A, \Delta B}$ $\boldsymbol{\Delta C}$, $\boldsymbol{\Delta D}$, $\boldsymbol{\Delta E_d}$ and $\boldsymbol{\Delta F_d}$ are modelled themselves. To this end the most common approaches are the norm-bounded, polytopic, and stochastic ones (cf. Ding, 2013, pp. 26-27).
In the case of aircraft model uncertainties are pervasive. They come for example from

- uncertainty in the mass model due to build tolerances and limited knowledge of the true fuel state
- uncertainty in the aerodynamic model due to build tolerances and changing environmental conditions
- the fact that the model was created using calculations and/or a laboratory setup e.g. an aerodynamic model deduced from testing of a subscale aircraft model in a wind tunnel
- higher order dynamics not modelled e.g. structural modes
- the use of linear models for non-linear processes

3.2.4 Linear System with Unknown Stochastic and Deterministic Inputs Subject to Faults

Two groups of faults must be distinguished: so called additive and multiplicative faults. The differences and similarities are discussed in the following chapters.

3.2.4.1 Additive Faults

Additive faults can be represented as system inputs. To model additive faults the discrete LTI system given by (3-9) and (3-10) is extended to

$$\begin{aligned} \boldsymbol{x}(k+1) &= \boldsymbol{A}\boldsymbol{x}(k) + \boldsymbol{B}\boldsymbol{u}(k) + \boldsymbol{E_d}\boldsymbol{d}(k) + \boldsymbol{E}_{\nu_P}\boldsymbol{\nu}_P\,(k) + \boldsymbol{E_f}\boldsymbol{f}(k) \\ \boldsymbol{x}(0) &= \boldsymbol{x_0} \end{aligned} \tag{3-13}$$

$$\boldsymbol{y}(k) = \boldsymbol{C}\boldsymbol{x}(k) + \boldsymbol{D}\boldsymbol{u}(k) + \boldsymbol{F_d}\boldsymbol{d}(k) + \boldsymbol{F}_{\nu_M}\boldsymbol{\nu}_M\,(k) + \boldsymbol{F_f}\boldsymbol{f}(k) \tag{3-14}$$

where vector $\boldsymbol{f} \in \mathbb{R}^{k_f}$ is the fault vector. It influences the states $\boldsymbol{x}$ and outputs $\boldsymbol{y}$ by matrices $\boldsymbol{E_f} \in \mathbb{R}^{nxk_f}$ and $\boldsymbol{F_f} \in \mathbb{R}^{mxk_f}$ respectively**.**

An important point to realise is that additive faults do not affect the stability of the system as they do not influence matrix $\boldsymbol{A}$. However the reader may keep in mind that for practical application $\boldsymbol{f}$ could be a hidden i.e. unknown or unmodelled function of the states $\boldsymbol{x}$**.**

3.2.4.2 Multiplicative Faults

Multiplicative or parametric faults affect the system matrices $\boldsymbol{A}$**,** $\boldsymbol{B}$**,** $\boldsymbol{C}$ and $\boldsymbol{D}$. The faults are modelled as fault matrices $\boldsymbol{A_f} \in \mathbb{R}^{nxn}$ **,** $\boldsymbol{B_f} \in \mathbb{R}^{nxk_u}$**,** $\boldsymbol{C_f} \in \mathbb{R}^{mxn}$ and $\boldsymbol{D_f} \in \mathbb{R}^{mxk_u}$ that add to the respective nominal system matrices. Introducing those matrices in (3-9) and (3-10) leads to

$$\begin{aligned} &\boldsymbol{x}(k+1) \\ &\quad = \big(\boldsymbol{A} + \boldsymbol{A_f}\big)\boldsymbol{x}(k) + \big(\boldsymbol{B} + \boldsymbol{B_f}\big)\boldsymbol{u}(k) + \boldsymbol{E_d}\boldsymbol{d}(k) + \boldsymbol{E}_{\nu_P}\boldsymbol{\nu}_P\,(k) \\ &\boldsymbol{x}(0) = \boldsymbol{x_0} \end{aligned} \tag{3-15}$$

$$\begin{aligned} &\boldsymbol{y}(k) \\ &\quad = \big(\boldsymbol{C} + \boldsymbol{C_f}\big)\boldsymbol{x}(k) + \big(\boldsymbol{D} + \boldsymbol{D_f}\big)\boldsymbol{u}(k) + \boldsymbol{F_d}\boldsymbol{d}(k) + \boldsymbol{F}_{\nu_M}\boldsymbol{\nu}_M\,(k) \end{aligned} \tag{3-16}$$

From (3-15) it is clear that $\boldsymbol{A_f}$ has a direct effect on the system proper motion and stability.

3.3 Contemporary Residual Generation

As mentioned in chapter 2.4.6, the fundamental idea of model-based redundancy is that, if the model is a perfect representation of the real fault-free process, the difference $\boldsymbol{r}(s)$ (now in the frequency domain) between the real process output $\boldsymbol{y}(s)$ and model output $\hat{\boldsymbol{y}}(s)$, i.e.

$$\boldsymbol{r}(s) = \boldsymbol{y}(s) - \hat{\boldsymbol{y}}(s) \tag{3-17}$$

shall be zero in a fault free case and unequal to zero in the fault case. $\boldsymbol{r}(s)$ is called the residual and the process of calculating $\boldsymbol{r}(s)$ is called *residual generation*.
Unfortunately, in a practical sense, the model can only be an approximation of the real process because model uncertainties and unknown (immeasurable) inputs cannot be avoided i.e. the model is no perfect representation of the real process. Furthermore differences in the initial states will influence the result. Let's assume the real process is LTI, and described by

$$\begin{aligned} &\boldsymbol{y}(s) \\ &\quad = [\boldsymbol{C}(s\boldsymbol{I} - \boldsymbol{A})^{-1}\boldsymbol{B} + \boldsymbol{D}] \cdot \boldsymbol{u}(s) + \boldsymbol{C}(s\boldsymbol{I} - \boldsymbol{A})^{-1}\boldsymbol{x}(0) + \boldsymbol{\Delta y}(s) \\ &\quad = \boldsymbol{G}_{\boldsymbol{yu}}(s) \cdot \boldsymbol{u}(s) + \boldsymbol{C}(s\boldsymbol{I} - \boldsymbol{A})^{-1}\boldsymbol{x}(0) + \boldsymbol{\Delta y}(s) \end{aligned} \tag{3-18}$$

where the term $\boldsymbol{C}(s\boldsymbol{I} - \boldsymbol{A})^{-1}\boldsymbol{x}(0)$ represents the influence of the initial states and $\boldsymbol{\Delta y}(s)$ the practically inevitable output because of model uncertainty and unknown inputs. The model-based estimate of $\boldsymbol{y}(s)$ can be expressed as

$$\hat{\boldsymbol{y}}(s) = [\boldsymbol{C}(s\boldsymbol{I} - \boldsymbol{A})^{-1}\boldsymbol{B} + \boldsymbol{D}] \cdot \boldsymbol{u}(s) = \boldsymbol{G}_{\boldsymbol{yu}}(s) \cdot \boldsymbol{u}(s) \tag{3-19}$$

The design goals for a *perfect* residual generator, which cannot necessarily be achieved in a practical application, can be summarized as (Ding, 2013, p. 73)

Design Goal 3-1:

$$\boldsymbol{r}(s) = \boldsymbol{y}(s) - \hat{\boldsymbol{y}}(s) = 0 \text{ for all } \boldsymbol{u}(s) \tag{3-20}$$

Rationale: In a fault-free case the output of the model shall be equivalent to the output of the process for all possible inputs $\boldsymbol{u}(s)$.

Design Goal 3-2:

$$\lim_{t\to\infty}\left(\boldsymbol{y}(t)-\hat{\boldsymbol{y}}(t)\right)=\boldsymbol{0} \text{ for all } \boldsymbol{x}(0) \tag{3-21}$$

Rationale: In a fault-free case, no matter what the initial states $\boldsymbol{x}(0)$ are, the residual $\boldsymbol{r}(t)=\boldsymbol{y}(t)-\hat{\boldsymbol{y}}(t)$ shall converge to zero with time, i. e. $\hat{\boldsymbol{y}}(t)$ must be an *unbiased estimate* of $\boldsymbol{y}(t)$.

Design Goal 3-3:

The convergence rate must be arbitrarily assignable. (3-22)

Rationale: The convergence rate must be assignable to make sure that it is sufficient for the application under consideration

Design Goal 3-4:

The influence of $\boldsymbol{\Delta y}(s)$ should be as far as possible supressed. (3-23)

Rationale: In a practical sense the model can only be an approximation of the real process because model uncertainties and unknown inputs that lead to $\boldsymbol{\Delta y}(s)$ cannot be avoided. Of course the influence of $\boldsymbol{\Delta y}(s)$ should be *as far as possible* supressed, so that $\boldsymbol{r}(s)$ is close to zero in a fault-free case. We will see however that there is a case-by case trade–off between model complexity and quality of suppression. If we allow a higher $\boldsymbol{\Delta y}(s)$ we have to adapt our threshold accordingly to keep the same FAR. Threshold calculation performs part of the process of residual evaluation which is discussed in detail in chapter 3.4. In general, in a practical application, $\boldsymbol{\Delta y}(s)$ cannot be supressed completely therefore a threshold (residual evaluation) is always required.

The discussion of chapter 3.3 are largely based on Ding (2013, pp. 72-74).

3.3.1 Deterministic Open-Loop Scheme

The easiest approach to analytic redundancy is a model-based parallel computation of the monitored measurement (Ding, 2013, p. 72) as graphically shown in Figure 23. Substituting (3-18) and (3-19) in (3-17) results in

$$\boldsymbol{r}(s) = \boldsymbol{C}(s\boldsymbol{I} - \boldsymbol{A})^{-1}\boldsymbol{x}(0) + \boldsymbol{\Delta y}(s) \tag{3-24}$$

It is obvious that Design Goal 3-2 to Design Goal 3-4 are not fulfilled. The reason is the open-loop or feed forward computation of $\boldsymbol{r}(s)$.

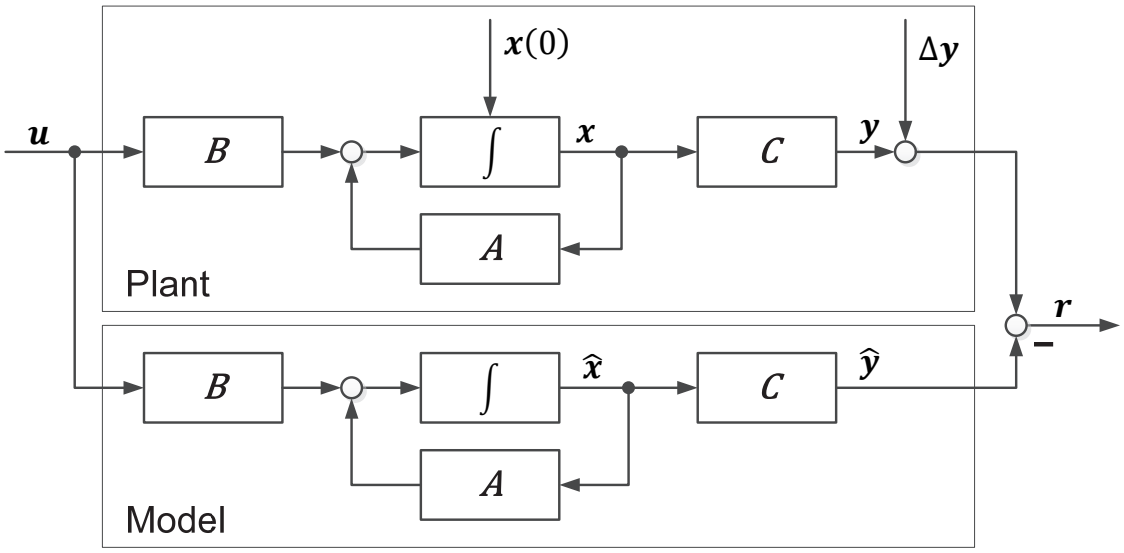

Figure 23 Residual Generation - Open-loop scheme ($D = 0$)

3.3.2 Deterministic Observer-Based Scheme

The disadvantages of the open loop system can be overcome by introducing a feedback term in (3-19):

$$\hat{\boldsymbol{y}}(s) = \boldsymbol{G}_{\boldsymbol{yu}}(s) \cdot \boldsymbol{u}(s) + \boldsymbol{L}(s)\big(\boldsymbol{y}(s) - \hat{\boldsymbol{y}}(s)\big) \tag{3-25}$$

With the help of coprime factorization it can be shown (Ding, 2013, p. 73) that $\boldsymbol{L}(s)$ must be selected as

$$\boldsymbol{L}(s) = \boldsymbol{C}(s\boldsymbol{I} - \boldsymbol{A})^{-1}\boldsymbol{L} \tag{3-26}$$

with $\boldsymbol{L}$ being a user definable feedback gain matrix.

Substituting (3-26) in (3-25) results in

$$\hat{\boldsymbol{y}}(s) = \boldsymbol{G_{yu}}(s) \cdot \boldsymbol{u}(s) + \boldsymbol{C}(s\boldsymbol{I} - \boldsymbol{A})^{-1}\boldsymbol{L}\big(\boldsymbol{y}(s) - \hat{\boldsymbol{y}}(s)\big) \tag{3-27}$$

Furthermore, substituting (3-18) and (3-27) in (3-17), gives

$$\begin{aligned} \boldsymbol{r}(s) &= \boldsymbol{C}(s\boldsymbol{I} - \boldsymbol{A} + \boldsymbol{LC})^{-1}\boldsymbol{x}(0) \\ &+(\boldsymbol{I} - \boldsymbol{C}(s\boldsymbol{I} - \boldsymbol{A} + \boldsymbol{LC})^{-1}\boldsymbol{L})\boldsymbol{\Delta y}(s) \end{aligned} \tag{3-28}$$

Thus, by a suitable selection of $\boldsymbol{L}$, Design Goal 3-1 to Design Goal 3-4 can be achieved given that the pair $(\boldsymbol{C}, \boldsymbol{A})$ is observable. It is furthermore possible to show (Ding, 2013, p. 74) that $\hat{\boldsymbol{y}}(s)$ can be expressed as

$$\begin{aligned} &\hat{\boldsymbol{y}}(s) \\ &\quad = [\boldsymbol{D} + \boldsymbol{C}(s\boldsymbol{I} - \boldsymbol{A} + \boldsymbol{LC})^{-1}(\boldsymbol{B} - \boldsymbol{LD})]\boldsymbol{u}(s) \\ &\quad + \boldsymbol{C}(s\boldsymbol{I} - \boldsymbol{A} + \boldsymbol{LC})^{-1}\boldsymbol{L}\boldsymbol{y}(s) \end{aligned} \tag{3-29}$$

Writing (3-29) in the continuous state space form gives

$$\dot{\hat{\boldsymbol{x}}} = \boldsymbol{A}\hat{\boldsymbol{x}} + \boldsymbol{B}\boldsymbol{u} - \boldsymbol{L}(\boldsymbol{y} - \boldsymbol{C}\hat{\boldsymbol{x}} - \boldsymbol{D}\boldsymbol{u}) \tag{3-30}$$

$$\hat{\boldsymbol{y}} = \boldsymbol{C}\hat{\boldsymbol{x}} + \boldsymbol{D}\boldsymbol{u} \tag{3-31}$$

Or in discrete form

$$\hat{\boldsymbol{x}}(k+1) = \boldsymbol{A}\hat{\boldsymbol{x}}(k) + \boldsymbol{B}\boldsymbol{u}(k) - \boldsymbol{L}\big(\boldsymbol{y}(k) - \boldsymbol{C}\hat{\boldsymbol{x}}(k) - \boldsymbol{D}\boldsymbol{u}(k)\big) \tag{3-32}$$

$$\hat{\boldsymbol{y}}(k) = \boldsymbol{C}\hat{\boldsymbol{x}}(k) + \boldsymbol{D}\boldsymbol{u}(k) \tag{3-33}$$

This is the Luenberger or state observer, well-known from modern control theory (cf. e.g. Müller, 1996, p. 65). The corresponding block diagram is given in Figure 24. The utilization of the observer however is different for control and FDD problems. In control design emphasis is placed on reconstructing the states of the system to enable full state feedback control. In contrast to that FDD problems require the reconstruction of the outputs of a system in a way that Design Goal 3-1 to Design Goal 3-4 are achieved. The state observer provides one widely used, numerical solution to the residual generation problem, but it is not the only one (Ding, 2013, pp. 74-75). The considerations up to this point covered deterministic problems. The next chapter will discuss the extension to stochastic systems.

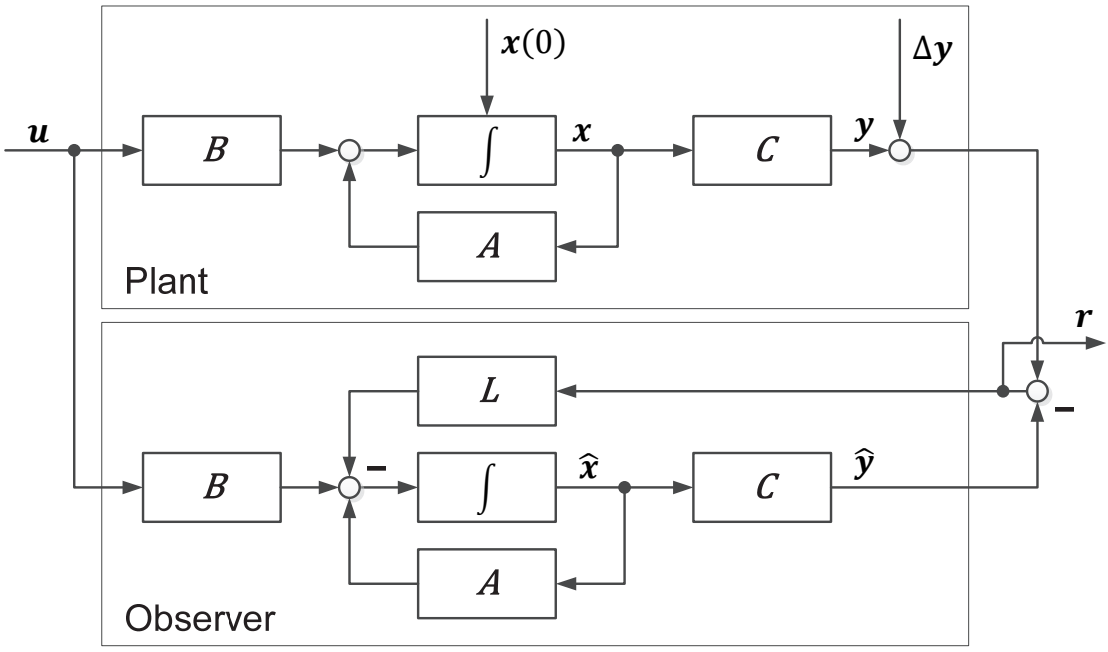

Figure 24 Residual Generation – Observer-based scheme ($D = 0$)
(based on Müller, 1996, p. 65)

3.3.3 Stochastic Observer-Based Scheme – The Kalman filter

The Kalman filter is in structure similar to the deterministic observer as shown in Figure 24. However, in contrast to the latter, the Kalman filter takes into account uncertainty in the measurement and the dynamic model. Those uncertainties are modelled as *additive* zero mean Gaussian *white* noise processes which renders the deterministic observer problem into a stochastic one. For systems subject to process noise $\boldsymbol{\nu}_P \sim \mathcal{N}\left(\mathbf{0}, \boldsymbol{\Sigma}_{\nu_P}\right)$ and measurement noise $\boldsymbol{\nu}_M \sim \mathcal{N}\left(\mathbf{0}, \boldsymbol{\Sigma}_{\nu_M}\right)$, the classical application of the Kalman filter is thus

- Maximum likelihood estimation of the states not measured (e.g. to enable full state feedback control)
- Maximum likelihood estimation of the system output (e.g. to improve the accuracy compared to the measured system output)

Especially the last point led to the great practical success of the Kalman filter. However, for the FDD problem of this text, we are interested in a residual signal that indicates how far the measured system output deviates from the model output. As it will be discussed below this forms an integral part of the Kalman filter and is also known as *innovation process*.

The discrete Kalman filter algorithm consists of two parts, the so-called prediction and correction step. The prediction step is given by

$$\hat{\boldsymbol{x}}(k|k-1) = \boldsymbol{A}\hat{\boldsymbol{x}}(k-1|k-1) + \boldsymbol{B}\boldsymbol{u}(k-1) \tag{3-34}$$

$$\hat{\boldsymbol{y}}(k|k-1) = \boldsymbol{C}\hat{\boldsymbol{x}}(k|k-1) + \boldsymbol{D}\boldsymbol{u}(k-1) \tag{3-35}$$

$$\boldsymbol{P}(k|k-1) = \boldsymbol{A}\boldsymbol{P}(k-1|k-1)\boldsymbol{A}^T + \boldsymbol{E}_{\nu_P}\boldsymbol{\Sigma}_{\nu_P}(k-1)\boldsymbol{\Sigma}_{\nu_P}^T \tag{3-36}$$

and the correction step by

$$\boldsymbol{S}(k) = \boldsymbol{C}\boldsymbol{P}(k|k-1)\boldsymbol{C}^T + \boldsymbol{\Sigma}_{\nu_M}(k) \tag{3-37}$$

$$\boldsymbol{L}(k) = \boldsymbol{P}(k|k-1)\boldsymbol{C}^T\boldsymbol{S}(k)^{-1} \tag{3-38}$$

$$\boldsymbol{P}(k|k) = \boldsymbol{P}(k|k-1) - \boldsymbol{L}(k)\boldsymbol{C}\boldsymbol{P}(k|k-1) \tag{3-39}$$

$$\hat{\boldsymbol{x}}(k|k) = \hat{\boldsymbol{x}}(k|k-1) + \boldsymbol{L}(k)\big(\boldsymbol{y}(k) - \hat{\boldsymbol{y}}(k|k-1)\big) \tag{3-40}$$

Substitution of (3-34) in (3-40) gives

$$\begin{aligned}\hat{\boldsymbol{x}}(k|k) &= \boldsymbol{A}\hat{\boldsymbol{x}}(k-1|k-1) + \boldsymbol{B}\boldsymbol{u}(k-1) \\ &+ \boldsymbol{L}(k)\big(\boldsymbol{y}(k) - \hat{\boldsymbol{y}}(k|k-1)\big)\end{aligned} \tag{3-41}$$

With the notational change $(k|k) \triangleq (k+1)$ and $(k-1) \triangleq (k)$ the equitations (3-41) and (3-35) become

$$\hat{\boldsymbol{x}}(k+1) = \boldsymbol{A}\hat{\boldsymbol{x}}(k) + \boldsymbol{B}\boldsymbol{u}(k) + \boldsymbol{L}(k)\big(\boldsymbol{y}(k) - \hat{\boldsymbol{y}}(k)\big) \tag{3-42}$$

$$\hat{\boldsymbol{y}}(k) = \boldsymbol{C}\hat{\boldsymbol{x}}(k) + \boldsymbol{D}\boldsymbol{u}(k) \tag{3-43}$$

Using (3-43), (3-42) can thus be re-written as

$$\hat{\boldsymbol{x}}(k+1) = \boldsymbol{A}\hat{\boldsymbol{x}}(k) + \boldsymbol{B}\boldsymbol{u}(k) + \boldsymbol{L}(k)\big(\boldsymbol{y}(k) - \boldsymbol{C}\hat{\boldsymbol{x}}(k) - \boldsymbol{D}\boldsymbol{u}(k)\big) \tag{3-44}$$

Comparison of (3-44) to (3-32) confirms that the Kalman filter is similar in structure to the Luenberger observer however, in the non-steady state version, the Kalman filter gain is time varying. Furthermore the Kalman gain calculation according (3-36) to (3-38) is based on statistic reasoning while the gain choice of the Luenberger ob-

server is arbitrary. This means that the Kalman filter provides an optimal solution for a linear system subject to measurement or process noise, as defined by (3-9) and (3-10), in the form that it "is the only observer that results in an independent sequence of residuals, namely the innovations." (Basseville & Nikiforov, 1993, p. 214). For stochastic stationary processes, i.e. $\boldsymbol{\Sigma}_{\boldsymbol{\nu}_M}, \boldsymbol{\Sigma}_{\boldsymbol{\nu}_P} \sim const$, the Kalman filter gain converges to a constant value that can be calculated by solution of the Riccati equation (cf. e.g. Ding, 2013, p. 179):

$$\boldsymbol{P} = \boldsymbol{APA}^T - \boldsymbol{L}\left(\boldsymbol{CPC}^T + \boldsymbol{\Sigma}_{\nu_M}\right)\boldsymbol{L}^T + \boldsymbol{E}_{\nu_P}\boldsymbol{\Sigma}_{\nu_P}\boldsymbol{E}_{\nu_P}^T \tag{3-45}$$

3.3.4 Dynamics of the Observer-Based Residual Signal without Model Uncertainties

We consider a full state observer, e.g. a steady state Kalman filter, given by

$$\hat{\boldsymbol{x}}(k+1) = \boldsymbol{A}\hat{\boldsymbol{x}}(k) + \boldsymbol{Bu}(k) + \boldsymbol{L}\left(\boldsymbol{y}(k) - \hat{\boldsymbol{y}}(k)\right) \tag{3-46}$$

$$\hat{\boldsymbol{y}}(k) = \boldsymbol{C}\hat{\boldsymbol{x}}(k) + \boldsymbol{Du}(k) \tag{3-47}$$

and the process model with unknown stochastic and deterministic inputs subject to faults, i.e. (3-13) and (3-14):

$$\begin{aligned} &\boldsymbol{x}(k+1) = \boldsymbol{Ax}(k) + \boldsymbol{Bu}(k) + \boldsymbol{E}_d\boldsymbol{d}(k) + \boldsymbol{E}_{\nu_P}\boldsymbol{\nu}_P\,(k) + \boldsymbol{E}_f\boldsymbol{f}(k) \\ &\boldsymbol{x}(0) = \boldsymbol{x_0} \end{aligned} \tag{3-48}$$

$$\boldsymbol{y}(k) = \boldsymbol{Cx}(k) + \boldsymbol{Du}(k) + \boldsymbol{F}_d\boldsymbol{d}(k) + \boldsymbol{F}_{\nu_M}\boldsymbol{\nu}_M\,(k) + \boldsymbol{F}_f\boldsymbol{f}(k) \tag{3-49}$$

By introducing the state estimation error

$$\boldsymbol{e}(k) = \boldsymbol{x}(k) - \hat{\boldsymbol{x}}(k) \tag{3-50}$$

it follows that

$$\boldsymbol{e}(k+1) = \boldsymbol{x}(k+1) - \hat{\boldsymbol{x}}(k+1) \tag{3-51}$$

and finally by substituting (3-46) to (3-49) into (3-51)

$$\begin{aligned} &\boldsymbol{e}(k+1) \\ &\quad = (\boldsymbol{A} - \boldsymbol{LC})\boldsymbol{e}(k) + (\boldsymbol{E}_d - \boldsymbol{LF}_d)\boldsymbol{d}(k) + \boldsymbol{E}_{\nu_P}\boldsymbol{\nu}_P\,(k) \\ &\quad + \boldsymbol{LF}_{\nu_M}\boldsymbol{\nu}_M\,(k) + \left(\boldsymbol{E}_f - \boldsymbol{LF}_f\right)\boldsymbol{f}(k) \end{aligned} \tag{3-52}$$

Furthermore by using the definition of the residual according to (3-17)

$$\boldsymbol{r}(k) = \boldsymbol{y}(k) - \hat{\boldsymbol{y}}(k) \tag{3-53}$$

and by inserting (3-47) and (3-49) it follows that

$$\boldsymbol{r}(k) = \boldsymbol{C}\boldsymbol{e}(k) + \boldsymbol{F}_d\boldsymbol{d}(k) + \boldsymbol{F}_{v_M}\boldsymbol{v}_M\,(k) + \boldsymbol{F}_f\boldsymbol{f}(k) \tag{3-54}$$

The dynamics of the residual are thus given by the following state space system

$$\begin{aligned}\boldsymbol{e}(k+1) &= (\boldsymbol{A} - \boldsymbol{L}\boldsymbol{C})\boldsymbol{e}(k) + (\boldsymbol{E}_d - \boldsymbol{L}\boldsymbol{F}_d)\boldsymbol{d}(k) + \boldsymbol{E}_{v_P}\boldsymbol{v}_P\,(k) \\ &\quad + \boldsymbol{L}\boldsymbol{F}_{v_M}\boldsymbol{v}_M\,(k) + \left(\boldsymbol{E}_f - \boldsymbol{L}\boldsymbol{F}_f\right)\boldsymbol{f}(k)\end{aligned} \tag{3-55}$$

$$\boldsymbol{r}(k) = \boldsymbol{C}\boldsymbol{e}(k) + \boldsymbol{F}_d\boldsymbol{d}(k) + \boldsymbol{F}_{v_M}\boldsymbol{v}_M\,(k) + \boldsymbol{F}_f\boldsymbol{f}(k) \tag{3-56}$$

Using (3-55) and (3-56) and the fact that $\boldsymbol{v}_P \sim \mathcal{N}\left(\boldsymbol{0}, \boldsymbol{\Sigma}_{v_P}\right)$ and $\boldsymbol{v}_M \sim \mathcal{N}\left(\boldsymbol{0}, \boldsymbol{\Sigma}_{v_M}\right)$, i.e $\boldsymbol{v}_P$ and $\boldsymbol{v}_M$ are *zero mean*, the mean $\bar{\boldsymbol{e}}$ and $\bar{\boldsymbol{r}}$ in steady state are given by

$$\begin{aligned}\bar{\boldsymbol{e}}(k+1) &= (\boldsymbol{A} - \boldsymbol{L}\boldsymbol{C})\bar{\boldsymbol{e}}(k) + (\boldsymbol{E}_d - \boldsymbol{L}\boldsymbol{F}_d)\boldsymbol{d}(k) + \left(\boldsymbol{E}_f - \boldsymbol{L}\boldsymbol{F}_f\right)\boldsymbol{f}(k)\end{aligned} \tag{3-57}$$

$$\bar{\boldsymbol{r}}(k) = \boldsymbol{C}\bar{\boldsymbol{e}}(k) + \boldsymbol{F}_d\boldsymbol{d}(k) + \boldsymbol{F}_f\boldsymbol{f}(k) \tag{3-58}$$

To separate the influence of $\boldsymbol{d}(k)$ and $\boldsymbol{f}(k)$ on the residual we can split $\bar{\boldsymbol{r}}(k)$ into

$$\bar{\boldsymbol{r}}(k) = \bar{\boldsymbol{r}}_d(k) + \bar{\boldsymbol{r}}_f(k) \tag{3-59}$$

It follows from (3-6), (3-8), (3-57) and (3-58) that

$$\begin{aligned}\boldsymbol{r}_d(z) &= \left[\boldsymbol{C}[z\boldsymbol{I} - (\boldsymbol{A} - \boldsymbol{L}\boldsymbol{C})]^{-1}(\boldsymbol{E}_d - \boldsymbol{L}\boldsymbol{F}_d) + \boldsymbol{F}_d\right]\boldsymbol{d}(z) \\ &= \boldsymbol{G}_{rd}\boldsymbol{d}(z)\end{aligned} \tag{3-60}$$

$$\begin{aligned}\boldsymbol{r}_f(z) &= \left[\boldsymbol{C}[z\boldsymbol{I} - (\boldsymbol{A} - \boldsymbol{L}\boldsymbol{C})]^{-1}\left(\boldsymbol{E}_f - \boldsymbol{L}\boldsymbol{F}_f\right) + \boldsymbol{F}_f\right]\boldsymbol{f}(z) \\ &= \boldsymbol{G}_{rf}\boldsymbol{d}(z)\end{aligned} \tag{3-61}$$

In the fault-free case, i.e. $\boldsymbol{f} = \boldsymbol{0}$, it is therefore obvious that $\bar{\boldsymbol{r}}(k) = \bar{\boldsymbol{r}}_d(k)$.

This is a very important result, because, as we will show in chapter 3.4.2, it means that, without model uncertainties, the energy of the residual signal in the fault free case is bounded by

$$\|\boldsymbol{r}_d\|_2 \leq \|[z\boldsymbol{I} - (\boldsymbol{A} - \boldsymbol{LC})]^{-1}(\boldsymbol{E}_d - \boldsymbol{LF}_d) + \boldsymbol{F}_d\|_\infty \|\boldsymbol{d}\|_2 \tag{3-62}$$

It shall be noted here that the considerations made above hold true for a Luenberger observer as well as a steady state Kalman filter because, as discussed in chapter 3.3.2 and 3.3.3, both are similar in structure and only differ in the way the gain $\boldsymbol{L}$ is calculated. However, as the problem of this text is a stochastic one, it is reasonable to use the Kalman filter approach for the calculation of $\boldsymbol{L}$. This chapter followed in large parts Ding (2013, pp. 340-341).

3.3.5 Dynamics of the Observer-Based Residual Signal with Model Uncertainties and Unknown Inputs

To consider just additive disturbance inputs is unfortunately not sufficient. As discussed before the model is always just an approximation of the real process dynamics. Especially for this work, in which it was decided to use a relatively simple reference model, it is imperative to take into account model uncertainties.
In contrast to Ding (2013, pp. 292-293) we want to approach this problem slightly differently. First of all, for our case we also have to consider stochastic unknown inputs. Secondly, to keep all inputs separately, to the author's opinion hides clarity of what we are doing. For the residual dynamics it is important to distinguish between known and unknown inputs. Therefore we will group all inputs in a known input vector $\boldsymbol{u_k}$ and an unknown input vector $\boldsymbol{u}_u$. In doing so we get a general system model for all model uncertainties and unknown inputs (cf. chapter 3.2.3).
The system model with model uncertainties and unknown inputs was introduced in chapter 3.2.3. We know group and generalize it in the above mentioned way

$$\begin{aligned}\boldsymbol{x}(k+1) \\ = (\boldsymbol{A} + \Delta\boldsymbol{A})\boldsymbol{x}(k) + (\boldsymbol{B}_k + \Delta\boldsymbol{B}_k)\boldsymbol{u}_k(k) + (\boldsymbol{B}_u + \Delta\boldsymbol{B}_u)\boldsymbol{u}_u(k)\end{aligned} \tag{3-63}$$

$$\begin{aligned}\boldsymbol{y}(k) \\ = (\boldsymbol{C} + \Delta\boldsymbol{C})\boldsymbol{x}(k) + (\boldsymbol{D}_k + \Delta\boldsymbol{D}_k)\boldsymbol{u}_k(k) + (\boldsymbol{D}_u + \Delta\boldsymbol{D}_u)\boldsymbol{u}_u(k)\end{aligned} \tag{3-64}$$

With

$$\boldsymbol{u}_k = \boldsymbol{u} \qquad \boldsymbol{u}_u = \begin{bmatrix} \boldsymbol{d} \\ \boldsymbol{f} \\ \boldsymbol{\nu}_P \\ \boldsymbol{\nu}_M \end{bmatrix} \quad \boldsymbol{x}(0) = \boldsymbol{x}_0$$

The model for the full state observer, i.e. (3-46) and (3-47), remains unchanged. By introducing the state estimation error

$$\boldsymbol{e}(k) = \boldsymbol{x}(k) - \hat{\boldsymbol{x}}(k) \tag{3-65}$$

it follows again that

$$\boldsymbol{e}(k+1) = \boldsymbol{x}(k+1) - \hat{\boldsymbol{x}}(k+1) \tag{3-66}$$

and finally by substituting (3-47) and (3-64) in (3-46) and the result as well as (3-63) into (3-66)

$$\begin{aligned} &\boldsymbol{e}(k+1) \\ &\quad = (\boldsymbol{A} - \boldsymbol{LC})\boldsymbol{e}(k) + (\Delta\boldsymbol{A} - \boldsymbol{L}\Delta\boldsymbol{C})\boldsymbol{x}(k) + (\Delta\boldsymbol{B}_k - \boldsymbol{L}\Delta\boldsymbol{D}_k)\boldsymbol{u}_k(k) \\ &\quad + [\boldsymbol{B}_u + \Delta\boldsymbol{B}_u - \boldsymbol{L}(\boldsymbol{D}_u + \Delta\boldsymbol{D}_u)]\boldsymbol{u}_u(k) \end{aligned} \tag{3-67}$$

Furthermore by using the definition of the residual according to (3-17)

$$\boldsymbol{r}(k) = \boldsymbol{y}(k) - \hat{\boldsymbol{y}}(k) \tag{3-68}$$

and by inserting (3-47) and (3-64) we get

$$\boldsymbol{r}(k) = \boldsymbol{Ce}(k) + \Delta\boldsymbol{Cx}(k) + \Delta\boldsymbol{D}_k\boldsymbol{u}_k(k) + (\boldsymbol{D}_u + \Delta\boldsymbol{D}_u)\boldsymbol{u}_u(k) \tag{3-69}$$

Finally we want to add a residual post filter $\boldsymbol{R}(z)$, that will be required later on. Thus (3-69) becomes

$$\begin{aligned} &\boldsymbol{r}(z) \\ &\quad = \boldsymbol{R}(z)[\boldsymbol{Ce}(k) + \Delta\boldsymbol{Cx}(k) + \Delta\boldsymbol{D}_k\boldsymbol{u}_k(k) \\ &\quad + (\boldsymbol{D}_u + \Delta\boldsymbol{D}_u)\boldsymbol{u}_u(k)] \end{aligned} \tag{3-70}$$

By using the state space realization of $\boldsymbol{R}(z)$ with matrices $\boldsymbol{A}_{PF}, \boldsymbol{B}_{PF}, \boldsymbol{C}_{PF}, \boldsymbol{D}_{PF}$ the dynamics of the residual for a system with model uncertainties can thus be expressed as the following state space system

$$\boldsymbol{x}_r(k+1) = \boldsymbol{A}_r \boldsymbol{x}_r(k) + \boldsymbol{B}_{r,k}\boldsymbol{u}_{r,k}(k) + \boldsymbol{B}_{r,u}\boldsymbol{u}_{r,u}(k) \tag{3-71}$$

$$\boldsymbol{r}(k) = \boldsymbol{C}_r \boldsymbol{x}_r(k) + \boldsymbol{D}_{r,k}\boldsymbol{u}_{r,k}(k) + \boldsymbol{D}_{r,u}\boldsymbol{u}_{r,u}(k) \tag{3-72}$$

with

$$\boldsymbol{x}_r = \begin{bmatrix} \boldsymbol{x} \\ \boldsymbol{e} \\ \boldsymbol{x}_{PF} \end{bmatrix} \qquad \boldsymbol{x}_r(0) = \begin{bmatrix} \boldsymbol{x}_0 \\ \boldsymbol{e}_0 \\ \boldsymbol{x}_{PF,0} \end{bmatrix}$$

$$\boldsymbol{u}_{r,k} = \boldsymbol{u} \qquad \boldsymbol{u}_{r,u} = \begin{bmatrix} \boldsymbol{d} \\ \boldsymbol{f} \\ \boldsymbol{\nu}_P \\ \boldsymbol{\nu}_M \end{bmatrix} \text{ with } \boldsymbol{\nu}_P \sim \mathcal{N}\left(\boldsymbol{0}, \boldsymbol{\Sigma}_{\nu_P}\right), \boldsymbol{\nu}_M \sim \mathcal{N}\left(\boldsymbol{0}, \boldsymbol{\Sigma}_{\nu_M}\right)$$

$$\boldsymbol{A}_r = \begin{bmatrix} \boldsymbol{A} + \Delta\boldsymbol{A} & \boldsymbol{0} & \boldsymbol{0} \\ \Delta\boldsymbol{A} - \boldsymbol{L}\Delta\boldsymbol{C} & \boldsymbol{A} - \boldsymbol{L}\boldsymbol{C} & \boldsymbol{0} \\ \boldsymbol{B}_{PF}\Delta\boldsymbol{C} & \boldsymbol{B}_{PF}\boldsymbol{C} & \boldsymbol{A}_{PF} \end{bmatrix}$$

$$\boldsymbol{B}_{r,k} = \begin{bmatrix} \boldsymbol{B}_k + \Delta\boldsymbol{B}_k \\ \Delta\boldsymbol{B}_k - \boldsymbol{L}\Delta\boldsymbol{D}_k \\ \boldsymbol{B}_{PF}\Delta\boldsymbol{D}_k \end{bmatrix} \qquad \boldsymbol{B}_{r,u} = \begin{bmatrix} \boldsymbol{B}_u + \Delta\boldsymbol{B}_u \\ (\boldsymbol{B}_u + \Delta\boldsymbol{B}_u) - \boldsymbol{L}(\boldsymbol{D}_u + \Delta\boldsymbol{D}_u) \\ \boldsymbol{B}_{PF}(\boldsymbol{D}_u + \Delta\boldsymbol{D}_u) \end{bmatrix}$$

$$\boldsymbol{C}_r = [\boldsymbol{D}_{PF}\boldsymbol{\Delta C} \quad \boldsymbol{D}_{PF}\boldsymbol{C} \quad \boldsymbol{C}_{PF}]$$

$$\boldsymbol{D}_{r,k} = \boldsymbol{D}_{PF}\Delta\boldsymbol{D}_k \qquad \boldsymbol{D}_{r,u} = \boldsymbol{D}_{PF}(\boldsymbol{D}_u + \Delta\boldsymbol{D}_u)$$

3.3.6 Summary

Chapter 3.3 started with a discussion of different residual generation schemes, namely the open loop, the deterministic observer-based, and the stochastic observer-based scheme (Kalman filter). It was discussed that, although the most simple approach, the open-loop scheme does not fulfil the important design goals of supressing process input signals and the process initial conditions in the residual signal. To overcome these shortfalls the concept was therefore extended by a feedback

term leading to the observer-based scheme and to the full state or Luenberger observer.
Unfortunately, in case of aircraft, we have to take into account stochastic process noise (e.g. atmospheric turbulence) and measurement noise from our sensors. The introduction of both finally led to the stochastic observer known as Kalman filter. Luenberger observer and Kalman filter are similar in structure and just differ in the way the feedback gain is implemented. The feedback gain calculated by the Kalman filter can be time varying and represents an optimal solution to the stochastic observer problem with additive zero mean, white process and measurement noise. For stochastic stationary processes the Kalman gain converges to a constant value, leading to the steady state Kalman filter with constant gain. As it will be discussed in chapter 3.5.3.1, the Kalman filter was selected as residual generator for this work, as it perfectly fits our aircraft problem with process (atmospheric turbulence) and measurement noise (sensors).
Chapter 3.3.4 was dedicated to derive the residual dynamics for a system with unknown inputs and no model uncertainties. Chapter 3.3.5 finally extended the residual dynamics to the case of model uncertainties and unknown inputs. The next chapter will deal with contemporary residual evaluation, i.e. the calculation of a threshold for the residual signal which triggers a fault detection alarm. To calculate this threshold it is of outmost importance to understand the dynamics of the residual signal especially the influence of unknown inputs (disturbances) and model uncertainties.

3.4 Contemporary Residual Evaluation

3.4.1 Motivation and Scope of Discussion

The basic idea of residual evaluation for fault detection, is that an evaluation feature J of the residual r is compared against a threshold J_{th}. If the evaluation feature is larger than the threshold a fault is detected. In other words the task of fault detection is in fact the task of finding an appropriate threshold J_{th} or as explained by Ding (2013, p. 291) "the tolerant limit of disturbances and model uncertainties under fault-free operation conditions", i.e.

$$J_{th} = \sup_{f=0,d,\Delta} J \tag{3-73}$$

Typical evaluation features are the peak value J_{peak}, the trend J_{trend}, the RMS value J_{RMS} and the signal energy J_2 (i.e. the signal 2-norm). In order for the fault detection system to work properly the following influences must be considered when computing the threshold (Ding, 2013, p. 291):

- Deterministic model uncertainties and unknown inputs with their respective bounds
- Stochastic model uncertainties and/or unknown inputs with their respective bounds
- The dynamics of the residual, i.e. the dynamics of the process plus observer (cf. chapter 3.3.4 and 3.3.5)

The following chapters will discuss the details of how the above-mentioned aspects are taken into account.

3.4.2 Deterministic Residual Evaluation Based on Signal and Systems Norms

3.4.2.1 Norms of LTI Systems

3.4.2.1.1 Important Properties of Norms

Signal and system norms have become an integral part of control system engineering especially in the field of robust control. As discussed, for example in Müller (1996, p. 101), a norm is used to express the "size" of a multidimensional signal by a real number. Within this work norms will be used in the context of residual signal evaluation, to compare a norm of the residual signal to a threshold.

The important properties of norms are:

$$\|\boldsymbol{u}\| \geq 0 \tag{3-74}$$

$$\|\boldsymbol{u}\| = 0 \;\Leftrightarrow\; \boldsymbol{u} = \boldsymbol{0} \tag{3-75}$$

$$\|a\boldsymbol{u}\| = |a|\|\boldsymbol{u}\| \quad \forall\, a \in \mathbb{R} \tag{3-76}$$

$$\|\boldsymbol{u} + \boldsymbol{v}\| \leq \|\boldsymbol{u}\| + \|\boldsymbol{v}\| \tag{3-77}$$

with $\boldsymbol{u} \in \mathbb{R}^{k_u}$ and $\boldsymbol{v} \in \mathbb{R}^{k_v}$.

3.4.2.1.2 Signal Norms

The signal norms used within this text are the L_2-Norm and the RMS-Norm. The discrete time L_2-Norm is defined as

$$\|\boldsymbol{u}\|_{2,def} = \sqrt{\sum_{k=0}^{\infty} \boldsymbol{u}^T(k)\boldsymbol{u}(k)} \tag{3-78}$$

and the Root Mean Square (RMS) -Norm as

$$\|\boldsymbol{u}\|_{RMS,def} = \sqrt{\frac{1}{k}\sum_{k=0}^{\infty} \boldsymbol{u}^T(k)\boldsymbol{u}(k)} = \frac{1}{\sqrt{k}}\|\boldsymbol{u}\|_{2,def} \tag{3-79}$$

For a practical application it is undesirable to calculate the L_2-Norm over a steadily increasing number of samples. Instead it is common practice to just take into account a certain time interval/window, i.e. a limited number of samples N, i.e.

$$\|\boldsymbol{u}\|_2 = \sqrt{\sum_{k=1}^{N} \boldsymbol{u}^T(k)\boldsymbol{u}(k)} \tag{3-80}$$

The L_2-Norm can be interpreted as energy of the signal (cf. Ding, 2013, pp. 165).

In practice it is often more interesting to evaluate average value of the signal energy which is the RMS- norm.

$$\|\boldsymbol{u}\|_{RMS} = \sqrt{\frac{1}{N_{RMS}} \sum_{k=1}^{N_{RMS}} \boldsymbol{u}^T(k)\boldsymbol{u}(k)} = \frac{1}{\sqrt{N_{RMS}}} \|\boldsymbol{u}\|_2 \tag{3-81}$$

If the maximum value instead of the energy is of interest, the so called Peak- or L_∞-Norm is used

$$\|\boldsymbol{u}\|_\infty = \max_{1 \le k \le N} \sqrt{\boldsymbol{u}^T(k)\boldsymbol{u}(k)} \tag{3-82}$$

3.4.2.1.3 LTI System Norms

Analog to signal norms it is possible to define norms for systems. The input-output relation of a LTI system can be described by the relation (cf. chapter 3.2.1)

$$\boldsymbol{y}(p) = \boldsymbol{G}(p)\boldsymbol{u}(p) \tag{3-83}$$

Where $\boldsymbol{p}$ stands for the continuous and discrete time frequency domain operators $\boldsymbol{s}$ and $\boldsymbol{z}$ respectively. We will omit both for the rest of this chapter to simplify notation. The operator $\boldsymbol{G}$ maps the input vector $\boldsymbol{u}$ to the output vector $\boldsymbol{y}$. The operator norm is an induced norm defined by the relation of an output to an input norm

$$\|\boldsymbol{G}\| = \sup_{\boldsymbol{u} \neq 0} \frac{\|\boldsymbol{y}\|}{\|\boldsymbol{u}\|} = \sup_{\boldsymbol{u} \neq 0} \frac{\|\boldsymbol{G}\boldsymbol{u}\|}{\|\boldsymbol{u}\|} \tag{3-84}$$

Within this text the L_2-Norm or RMS-Norm induced H_∞-Norm is used

$$\|\boldsymbol{G}\|_\infty = \sup_{\boldsymbol{u} \neq 0} \frac{\|\boldsymbol{y}\|_2}{\|\boldsymbol{u}\|_2} = \sup_{\boldsymbol{u} \neq 0} \frac{\|\boldsymbol{y}\|_{RMS}}{\|\boldsymbol{u}\|_{RMS}} = \sup_p \sigma_{max}\big(\boldsymbol{G}(p)\big) \tag{3-85}$$

where $\sigma_{max}(\boldsymbol{G})$ refers to the maximum singular value of $\boldsymbol{G}$. From engineering point of view it can be interpreted as the "maximum gain" of $\boldsymbol{G}$.

Remark 3-1: In this context it is important to understand that, in the MIMO case, maximum system gain $\|\boldsymbol{G}\|_\infty$ is only achieved for a specific input direction *and* frequency (Boyd & Lall, 2014, p. 15-21; Brockhaus et al., 2011, p. 556). The maximum input direction is obtained by the Singular Value Decomposition (SVD) of

$\boldsymbol{G}(p_{\|\boldsymbol{G}\|_\infty})$ where $p_{\|\boldsymbol{G}\|_\infty}$ is the frequency that corresponds to the maximum gain (cf. (3-85)). From the SVD it follows that

$$\boldsymbol{G}(p_{\|\boldsymbol{G}\|_\infty}) = \boldsymbol{U}\boldsymbol{\Sigma}\boldsymbol{V}^{\boldsymbol{T}} \tag{3-86}$$

where the diagonal matrix $\boldsymbol{\Sigma}$ contains the singular values on its diagonal in descending order, the column vector $\boldsymbol{v}_i$ of $\boldsymbol{V}$ the corresponding input and the column vectors $\boldsymbol{u}_i$ of $\boldsymbol{U}$ the corresponding output directions. The maximum gain $\sigma_{max} = \sigma_1$ is thus achieved for input direction $\boldsymbol{v}_1$ (cf. e.g. Boyd & Lall, 2014, pp. 15-25 to 15-31).

For more information on norms for signal and systems the interested reader is referred to e.g. Müller (1996).

3.4.2.2 Norm-Based Threshold Computation for LTI Systems Subject to Unknown Deterministic Inputs (Disturbances)

Eq. (3-85) relates the energy of an *arbitrary* input signal to the maximum energy of the output signal. This property is of great importance for the deterministic, i.e. norm-based residual evaluation. For the threshold computation we assume an unknown but energy bounded input signal $\boldsymbol{d}$ (e.g. disturbances) and are interested in the resulting energy bound (threshold) for the residual $\boldsymbol{r}$ (i.e. output signal). The solution to this problem follows directly from (3-85)

$$J_{th,RMS} = \sup_{\boldsymbol{f}=\boldsymbol{0},\boldsymbol{d}\neq\boldsymbol{0}} \|\boldsymbol{r}_d\|_{RMS} = \|\boldsymbol{G}_{rd}\|_\infty \|\boldsymbol{d}\|_{RMS} \tag{3-87}$$

where $\boldsymbol{G}_{rd}$ is the transfer matrix from input $\boldsymbol{d}$ to output $\boldsymbol{r}$. Of course, the same principle applies for the L_2-Norm

$$J_{th,2} = \sup_{\boldsymbol{f}=\boldsymbol{0},\boldsymbol{d}\neq\boldsymbol{0}} \|\boldsymbol{r}_d\|_2 = \|\boldsymbol{G}_{rd}\|_\infty \|\boldsymbol{d}\|_2 \tag{3-88}$$

The transfer matrix $\boldsymbol{G}_{rd}$ follows from the dynamics of the residual signal (3-60) and was derived in chapter 3.3.4 in its discrete time form as

$$\boldsymbol{G}_{rd}(z) = [\boldsymbol{C}[z\boldsymbol{I} - (\boldsymbol{A} - \boldsymbol{L}\boldsymbol{C})]^{-1}(\boldsymbol{E}_d - \boldsymbol{L}\boldsymbol{F}_d) + \boldsymbol{F}_d] \tag{3-89}$$

The fault decision rules follow as

$$d_{\|\boldsymbol{r}\|_{RMS}}(\boldsymbol{r}) = \begin{cases} 0 & if\ \|\boldsymbol{r}_d\|_{RMS} \leq J_{th,RMS} \Rightarrow nofault \\ 1 & if\ \|\boldsymbol{r}_d\|_{RMS} > J_{th,RMS} \Rightarrow fault \end{cases} \tag{3-90}$$

and

$$d_{\|\boldsymbol{r}\|_2}(\boldsymbol{r}) = \begin{cases} 0 & if\ \|\boldsymbol{r}_d\|_2 \leq J_{th,2} \Rightarrow nofault \\ 1 & if\ \|\boldsymbol{r}_d\|_2 > J_{th,2} \Rightarrow fault \end{cases} \tag{3-91}$$

For the sake of completeness it shall be mentioned here that there exist other than signal energy based thresholds in practice. Thresholds based, for example, on the signals peak value and not the energy are also common (Ding, 2013, pp. 293-295). In principal system theory gives rise to many possible approaches (cf. Müller, 1996, p. 113).

3.4.2.3 Norm-based Threshold Computation for LPV Systems Subject to Unknown Deterministic Inputs (Disturbances) and Time-Varying Polytopic Model Uncertainties

We now extend the norm-based residual evaluation scheme to include polytopic model uncertainties. The reason for the name is due to fact that they can be defined as polytope in the parameter space. It is important to realize that we now want to discuss time-varying model uncertainties. In other words we do not know the parameters *and* the parameters are changing with time. This problem leads to a so-called Linear Parameter Varying (LPV) system that can be expressed as

$$\begin{gathered} \dot{\boldsymbol{x}} = \boldsymbol{A}\big(\boldsymbol{\delta}(t)\big)\boldsymbol{x} + \boldsymbol{B}\big(\boldsymbol{\delta}(t)\big)\boldsymbol{u} \\ \boldsymbol{x}(0) = \boldsymbol{x}_0 \end{gathered} \tag{3-92}$$

$$\boldsymbol{y} = \boldsymbol{C}\big(\boldsymbol{\delta}(t)\big)\boldsymbol{x} + \boldsymbol{D}\big(\boldsymbol{\delta}(t)\big)\boldsymbol{u} \tag{3-93}$$

where $\boldsymbol{\delta}(t)$ represents the time-varying parameter vector.

3.4.2.3.1 Lyapunov and Quadratic Stability

Due to the structural similarity of LPV systems with LTI systems one might be tempted to apply the stability and performance results of the control theory for LTI systems also to the LPV system (3-92). However as for example Slotine and Li (1990, p. 114) show it is very simple to create an autonomous LPV system like

$$\dot{\boldsymbol{x}} = \boldsymbol{A}\big(\boldsymbol{\delta}(t)\big)\boldsymbol{x} = \begin{bmatrix} -1 & e^{2t} \\ 0 & -1 \end{bmatrix} \begin{bmatrix} x_1 \\ x_1 \end{bmatrix} \tag{3-94}$$

that has negative eigenvalues, i.e. should be stable according to LTI theory, but is not stable as the upper right element of $\boldsymbol{A}\big(\boldsymbol{\delta}(t)\big)$ increases exponentially with time.
One of the consequences of the non-applicability of LTI theory for residual evaluation is the fact, that calculating $\|\boldsymbol{r}_d\|_2$ according (3-88) is no longer possible for LPV systems as the transfer function based H_∞-Norm is only defined for LTI systems. Therefore we have to look for a way to calculate the worst case system gain of a LPV system. Fortunately there is some help in form of *Lyapunov's direct method*. Laypunov's underlying idea is nicely summarized by Slotine and Li (1990, p. 57):

> The basic philosophy of Lyapunov's direct method is the mathematical extension of a fundamental physical observation: if the total *energy* of a mechanical (or electrical) system is continuously dissipated, then the system*, whether linear or nonlinear*, must eventually settle down to an equilibrium point. Thus, we may conclude the stability of a system by examining the variation of a single scalar function.

This simple idea leads to several powerful stability analysis and control design methods for linear and non-linear systems including the Linear Matrix Inequality (LMI) approach. The above-mentioned concept can be expressed in a more strict form by the following definition (based on Slotine & Li, 1990, p. 61):

Definition 3-1 (Lyapunov Function) If a function $\boldsymbol{V(x)}$ is positive definite and has continuous partial derivatives, and if its time derivative along any state trajectory of system (3-92) is negative semi-definite, i.e., $\dot{\boldsymbol{V}}(\boldsymbol{x}) \leq \boldsymbol{0}$, then $\boldsymbol{V(x)}$ is said to be a Lyapunov function for the system (3-92).

Lyapunov's theorem for global (asymptotic) stability furthermore states (based on Slotine & Li, 1990, p. 65):

Theorem 3-1 (Global Asymptotic Stability) Assume that there exists a scalar function $\boldsymbol{V(x)}$, with continuous first order derivatives such that

- $V(\boldsymbol{x}) > 0$
- $\dot{V}(\boldsymbol{x}) < 0$
- $V(\boldsymbol{x}) \to \infty$ as $\|\boldsymbol{x}\| \to \infty$ (i.e. $V(\boldsymbol{x})$ is radially unbounded)

then the equilibrium at the origin is globally asymptotically stable.

Remark 3-2: For LTI systems asymptotic stability is always global and implies exponential stability (cf. Slotine & Li, 1990, p.52).

For LTI and LPV systems, we can say that

$$V(\boldsymbol{x}) = \boldsymbol{x}^T \boldsymbol{P} \boldsymbol{x} > \boldsymbol{0} \tag{3-95}$$

$$\Rightarrow \boldsymbol{P} > 0 \tag{3-96}$$

Furthermore by differentiating (3-95) and substituting (3-92) we get ($\boldsymbol{\delta(t)}$ will be omitted for simplicity)

$$\dot{V}(\boldsymbol{x}) = \dot{\boldsymbol{x}}^T \boldsymbol{P} \boldsymbol{x} + \boldsymbol{x}^T \boldsymbol{P} \dot{\boldsymbol{x}} = (\boldsymbol{A}\boldsymbol{x})^T \boldsymbol{P} \boldsymbol{x} + \boldsymbol{x}^T \boldsymbol{P} (\boldsymbol{A}\boldsymbol{x}) = \boldsymbol{x}^T (\boldsymbol{A}^T \boldsymbol{P} + \boldsymbol{P}\boldsymbol{A}) \boldsymbol{x} < 0 \tag{3-97}$$

$$\Rightarrow \boldsymbol{A}^T \boldsymbol{P} + \boldsymbol{P}\boldsymbol{A} < 0 \tag{3-98}$$

Eq. (3-98) is the so-called *Lyapunov equation*. (3-96) and (3-98) yield a set of inequalities that can be expressed as LMI:

$$\begin{bmatrix} -\boldsymbol{P} & 0 \\ 0 & \boldsymbol{A}^T(\boldsymbol{\delta}(t))\boldsymbol{P} + \boldsymbol{P}\boldsymbol{A}(\boldsymbol{\delta}(t)) \end{bmatrix} < 0 \tag{3-99}$$

If a system fulfils (3-99) it is also said to be *quadratically stable*, as stability analysis is based on the quadratic Lyapunov function $\boldsymbol{V(x)}$. Furthermore, if a system is quadratically stable, it means that it is stable for *arbitrary fast time-varying parameters* (cf. Scherer & Weiland, 2016, p. 7/25). This is a very powerful result, however, as a

consequence, the quadratic stability test can be overly conservative for systems with slowly varying parameters. This will be discussed further in chapter 3.5.4.3.

3.4.2.3.2 Polytopic Model Uncertainty

We have not yet specified the set $\mathcal{D}$ of possible parameters $\boldsymbol{\delta}$. While (3-99) remains valid no matter how it looks like it becomes practically infeasible to find a solution for $\boldsymbol{P}$ if we do not impose certain limitations on set $\mathcal{D}$. A common simplification is to assume that the system matrices $\boldsymbol{A}(\boldsymbol{\delta})$, $\boldsymbol{B}(\boldsymbol{\delta})$, $\boldsymbol{C}(\boldsymbol{\delta})$, $\boldsymbol{D}(\boldsymbol{\delta})$, … are affine in $\boldsymbol{\delta}$ and that the parameters variations are contained in a convex polytope in parameter space, i.e. $\boldsymbol{\mathcal{D}} = co\{\delta_1, \dots, \delta_N\}$ (Scherer & Weiland, 2015, p. 5/25).
For affine systems the system matrices can be expressed in the form (Gu, Petkov, & Konstantinov, 2013, p. 223)

$$\boldsymbol{A}(\boldsymbol{\delta}) = \boldsymbol{A}_0 + \delta_1\boldsymbol{A}_1 + \delta_2\boldsymbol{A}_2 + \cdots + \delta_N\boldsymbol{A}_N \tag{3-100}$$

$$\boldsymbol{B}(\boldsymbol{\delta}) = \boldsymbol{B}_0 + \delta_1\boldsymbol{B}_1 + \delta_2\boldsymbol{B}_2 + \cdots + \delta_N\boldsymbol{B}_N \tag{3-101}$$

$$\boldsymbol{C}(\boldsymbol{\delta}) = \boldsymbol{C}_0 + \delta_1\boldsymbol{C}_1 + \delta_2\boldsymbol{C}_2 + \cdots + \delta_N\boldsymbol{C}_N \tag{3-102}$$

$$\boldsymbol{D}(\boldsymbol{\delta}) = \boldsymbol{D}_0 + \delta_1\boldsymbol{D}_1 + \delta_2\boldsymbol{D}_2 + \cdots + \delta_N\boldsymbol{D}_N \tag{3-103}$$

A typical parameter polytope is shown in Figure 25 for two parameters. The polytopic model uncertainty is fully defined by the systems that correspond to the parameter combination of the corners of the polytope, i.e. $\Pi_{1,\dots,4}$ in the case of two parameters.

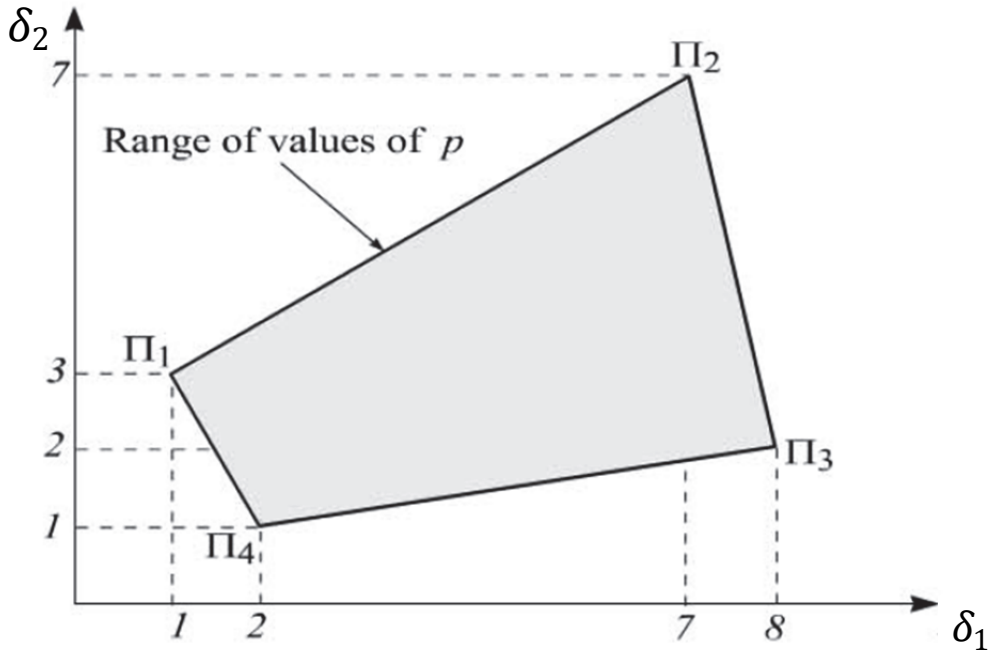

Figure 25 Parameter polytope in parameter space for two parameters (based on Gu et al., 2013, p. 227)

The concept of polytopic model uncertainty perfectly fits our needs of this text. For aircraft the *desired* closed loop performance derived from the flying quality specifications like MIL-STD-1797A (US DoD, 2004) is normally expressed as low-order linear dynamic systems (cf. chapter 2.2.2). For this work here we restrict ourselves to the longitudinal short period motion. In this case the desired closed-loop performance can be defined as linear second order system, thus the parameter space is two-dimensional. This will be discussed in detail in chapter 3.5.4.3.

3.4.2.3.3 LMI-Based Bound on the Energy Gain

Quadratic stability in itself does not yet help us for our residual evaluation problem, but it implies another result, that is a bound on the worst case system gain for the LPV system, comparable to the H_∞-Norm for LTI systems (Scherer & Weiland, 2016, pp. 61/79-62/79). The LMI-based calculation for a discrete residual system as given for example with (3-71) and (3-72) is described in Ding (2013, pp. 300-301). While the approach is appealing from a theoretical point of view, it has finally not been implemented for the fault detection system of this thesis. As for quadratic stability the results are *very conservative*, i.e. the gains and therefore the fault detection thresholds become very large. Furthermore we do not want to allow arbitrarily fast parameter variations in the fault-free case as they constitute a dynamic in themselves. As a result the author found that there is no practical use for the aircraft fault detection problem of this text. This aspect will be discussed further in chap-

ter 3.5.4.3.1. Nevertheless the idea of polytopic model uncertainty has been adopted, thus the discussions of chapter 3.4.2.3 remain important herein.

3.4.3 Stochastic Residual Evaluation

3.4.3.1 Statistical Hypothesis Testing

We consider the simple statistical model

$$y = \theta + \nu \tag{3-104}$$

with output $y \in \mathbb{R}$, a constant $\theta \in \mathbb{R}$ and noise $\nu \sim \mathbb{N}(0, \sigma^2)$. Our goal is finding a threshold J_{th} to decide if $\theta = \theta_0$ or $\theta = \theta_1$. The null hypothesis $\boldsymbol{H}_0$ and alternative hypothesis $\boldsymbol{H}_1$ can thus be defined as

$$\begin{aligned} \boldsymbol{H}_0 &: \quad \theta = \theta_0 \\ \boldsymbol{H}_1 &: \quad \theta = \theta_1 \end{aligned} \tag{3-105}$$

We have obtained N samples (observations) of signal y, i.e. the random variable $\boldsymbol{Y} = [y, y_1, \dots, y_N]^T$. A sample y_i is also called realisation of $\boldsymbol{Y}$. The sample mean

$$E(\boldsymbol{Y}) = \bar{y} = \frac{1}{N}\sum_{i=1}^{N} y_i \tag{3-106}$$

will serve as a testing statistic. We furthermore specify our decision rule $d(\boldsymbol{Y})$ as

$$d_{\bar{y}}(\boldsymbol{Y}) = d = \begin{cases} 0 & if \ \ |\bar{y}| \le J_{th}; \quad \boldsymbol{H}_0 \ is \ chosen \\ 1 & if \ \ |\bar{y}| > J_{th}; \quad \boldsymbol{H}_1 is \ chosen \end{cases} \tag{3-107}$$

where J_{th} is the threshold we have to calculate. We now get the probability for a Type I fault, i.e. deciding for $\boldsymbol{H}_1$ if $\boldsymbol{H}_0$ is true, as

$$p(|\bar{y}| > J_{th} | \theta = \theta_0) = \alpha_0(d) \tag{3-108}$$

Analogously we can define the probability of a Type II fault, i.e. deciding for $\boldsymbol{H}_0$ if $\boldsymbol{H}_1$ is true, as

$$p(|\bar{y}| \le J_{th} | \theta = \theta_1) = \alpha_1(d) \tag{3-109}$$

In a statistical context $\alpha_0(d)$ is called *size* or *level of significance of test* d, while $\beta(d) = 1 - \alpha_1(d)$ is referred to as *power of test* d. $\alpha_0(d)$ and $\alpha_1(d)$ will be determined by the user for the respective application (Tartakovsky, Nikiforov, & Basseville, 2015, p. 90). Table 5 relates the failure probabilities to the outcome of the hypothesis test as well as to the failure notations used in statistics and FDD.

Table 5 Outcome of a two hypothesis test with related probabilities/statistics and FDD failure notations

	$\boldsymbol{H_0}$ is true i.e. no fault occurred	$\boldsymbol{H_1}$ is true i.e. a fault occurred
Hypothesis test d decides for $\boldsymbol{H_0}$ (no fault occurred)	Correct decision Probability: $1 - \alpha_0(d)$	Wrong decision *Type II failure* (MDR) Probability[11]: $\alpha_1(d)$
Hypothesis test d decides for $\boldsymbol{H_1}$ (a fault occurred)	Wrong decision *Type I failure* (FAR) Probability: $\alpha_0(d)$ (size, level of significance of test d)	Correct decision Probability: $\beta(d) = 1 - \alpha_1(d)$ (power of test d)

In the context of fault detection the probability of a *Type I* failure, i.e. deciding for $\boldsymbol{H_1}$ (a fault occurred) if $\boldsymbol{H_0}$ (no fault occurred) is true, will be referred to as *False Alarm rate (FAR)*. On the other hand the probability of deciding for $\boldsymbol{H_1}$ if $\boldsymbol{H_0}$ is true, i.e. conducting a *Type II* failure, is known as *Missed Detection Rate (MDR)*. In the FDD case y will be the fault detection signal i.e. the residual r, with $|\bar{r}|$ being small for the fault-free case and large if a fault occurred, that is $\theta_0 \ll \theta_1$ (cf. chapter 3).
For more details on the topic of this chapter the interested reader may consult Tartakovsky et al. (2015) and Ding (2013) on which this discussion is based on.

3.4.3.1.1 Likelihood Ratio – Simple Hypothesis Testing

If θ_0 and θ_1 are known we speak about *simple hypothesis testing*. Based on model (3-104) and hypothesis (3-105) we define the log Likelihood Ratio (LR) $s(y_i)$ for sample y_i as

$$s(y_i) = ln\frac{p_{\theta_1}(y_i)}{p_{\theta_0}(y_i)} \tag{3-110}$$

[11] The probability of a Type II failure is sometimes also referred to as β instead of α_1 (cf. e.g. Tschirk, 2014, p. 67). However here the convention as for example in Tartakovsky et al. (2015) has been adopted.

Because $\nu \sim \mathbb{N}(0, \sigma^2)$ it follows that

$$p_\theta(y_i) = \frac{1}{\sqrt{2\pi}\sigma} e^{-\frac{(y_i-\theta)^2}{2\sigma^2}} \tag{3-111}$$

and therefore

$$\begin{aligned} s(y_i) &= \ln \frac{p_{\theta_1}(y_i)}{p_{\theta_0}(y_i)} = \ln \frac{e^{-\frac{(y_i-\theta_1)^2}{2\sigma^2}}}{e^{-\frac{(y_i-\theta_0)^2}{2\sigma^2}}} = -\frac{(y_i-\theta_1)^2}{2\sigma^2} + \frac{(y_i-\theta_0)^2}{2\sigma^2} \\ &= \frac{1}{2\sigma^2}[(y_i-\theta_0)^2 - (y_i-\theta_1)^2] \end{aligned} \tag{3-112}$$

For N samples we get

$$\begin{aligned} S(\boldsymbol{Y}) &= \sum_{i=1}^{N} s(y_i) = \frac{1}{2\sigma^2} \sum_{i=1}^{N} [(y_i-\theta_0)^2 - (y_i-\theta_1)^2] \\ &= \frac{\theta_1-\theta_0}{\sigma^2} \sum_{i=1}^{N} \left(y_i - \frac{\theta_1+\theta_0}{2} \right) \end{aligned} \tag{3-113}$$

Therefore, for a fixed sample size N, the decision rule becomes

$$d_{LR}(\boldsymbol{Y}) = \begin{cases} 0 & if\ S(\boldsymbol{Y}) \le J_{th}; \quad \boldsymbol{H}_0\ is\ chosen \\ 1 & if\ S(\boldsymbol{Y}) > J_{th}; \quad \boldsymbol{H}_1\ is\ chosen \end{cases} \tag{3-114}$$

A test of two simple hypotheses based on the LR is referred to as Most Powerful Test (MP) as it minimizes the probability α_1 of a Type II failure for an allowable maximum probability α_0 of a Type I failure. This is a direct consequence of the Neyman-Pearson lemma (Neyman & Pearson, 1933) which shows that an optimal most powerful test must be based on the LR (Basseville & Nikiforov, 1993, pp. 111-112; Tartakovsky et al., 2015, p. 91). The LR test for two simple scalar hypotheses is therefore often also called Neyman-Pearson test. In FDD words the likelihood ratio based test d_{LR} is optimal in the sense that it minimizes the MDR for a given FAR, which is a very powerful result for designing a fault detection system (McDonough & Whalen, 1995, p. 187).

3.4.3.1.2 Generalized Likelihood Ratio (GLR) – Composite Hypothesis Testing

In some practical fault detection application, $\boldsymbol{\theta_1}$ is unknown and must therefore be estimated. This case is called *composite hypothesis testing* problem and we have to use the Generalized (log) Likelihood Ratio (GLR) method. The GLR replaces $\boldsymbol{\theta_1}$ by its Maximum Likelihood (ML) estimate $\hat{\boldsymbol{\theta}}_1$. In this sense we effectively obtain an estimate of the log likelihood ratio (Basseville & Nikiforov, 1993, p. 47; Tartakovsky et al., 2015, p.111)

$$\hat{S}(\boldsymbol{Y}) = ln \frac{\sup\limits_{\theta_1} p_{\theta_1}(\boldsymbol{Y})}{p_{\theta_0}(\boldsymbol{Y})} \tag{3-115}$$

The decision rule for the GLR becomes

$$\hat{d}_{GLR}(\boldsymbol{Y}) = \begin{cases} 0 & if\ \hat{S}(\boldsymbol{Y}) \leq J_{th}; \quad \boldsymbol{H_0}\ is\ chosen \\ 1 & if\ \hat{S}(\boldsymbol{Y}) > J_{th}; \quad \boldsymbol{H_1}\ is\ chosen \end{cases} \tag{3-116}$$

The precise optimality conditions of test $\hat{d}_{GLR}(\boldsymbol{Y})$ are not known (Tartakovsky et al., 2015, p. 111) but it can be seen as a kind of suboptimal solution because the unkown $\boldsymbol{\theta_1}$ is replaced by its ML estimate $\hat{\boldsymbol{\theta}}_1$ (Ding, 2013, p. 326).
As shown in Ding (2013, pp. 319-320), for the practically relevant case that $\boldsymbol{\theta_0 = 0}$ and $\boldsymbol{\theta_1}$ is unknown, using (3-113) we get

$$\begin{aligned} \hat{S}_{\theta_0=0}(\boldsymbol{Y}) &= \sup_{\theta_1} \frac{1}{2\sigma^2} \sum_{i=1}^{N} [(y_i)^2 - (y_i - \theta_1)^2] \\ &= \frac{1}{2\sigma^2} \left[\frac{1}{N} \left(\sum_{i=1}^{N} y_i \right)^2 - N(\theta_1 - \bar{y})^2 \right] \end{aligned} \tag{3-117}$$

where $\bar{y}$ is the arithmetic mean according (3-106). From (3-117) it is obvious that

$$\hat{\theta}_1 = \arg\sup_{\theta_1} \hat{S}_{\theta_0=0}(\boldsymbol{Y}) = \bar{y} \tag{3-118}$$

Substituting (3-118) and afterwards (3-106) back into (3-117) results in

$$\hat{S}_{\theta_0=0}(\boldsymbol{Y}) = \frac{1}{2\sigma^2} \frac{1}{N} \left(\sum_{i=1}^{N} y_i \right)^2 = \frac{N}{2\sigma^2} (\bar{y})^2 \tag{3-119}$$

This leads to the following conclusions (Ding, 2013, p. 320):

- The ML estimate of θ_1 is the arithmetic mean $\bar{y}$
- Eq. (3-119) shows that the GLR is always non-negative
- As $\bar{y}$ is normally distributed with zero mean it follows from (3-119) that $\hat{S}_{\theta_0=0}(\boldsymbol{Y})$ is central χ^2-distributed with degree of freedom one (cf. Basseville & Nikiforov, 1993, pp. 70-71; Klein & Morelli, 2006, p. 447; Koch, 1999, pp. 126-127)

3.4.3.1.3 Vector-Valued Generalized Likelihood Ratio (GLR)

The considerations made above for scalars can be extended to the multidimensional case (cf. Ding, 2013, pp. 320-322). The vector model is given by

$$\boldsymbol{y} = \boldsymbol{\theta} + \boldsymbol{\nu} \tag{3-120}$$

with output $\boldsymbol{y} \in \mathbb{R}^m$, a constant $\boldsymbol{\theta} \in \mathbb{R}^m$ and noise $\boldsymbol{\nu} \sim \mathbb{N}(\mathbf{0}, \boldsymbol{\Sigma})$. The multivariate Gaussian probability density is given by

$$p_{\boldsymbol{\theta},\boldsymbol{\Sigma}}(\boldsymbol{y}_i) = \frac{1}{\sqrt{(2\pi)^n \det(\boldsymbol{\Sigma})}} e^{-\frac{1}{2}(\boldsymbol{y}_i-\boldsymbol{\theta})^T\boldsymbol{\Sigma}^{-1}(\boldsymbol{y}_i-\boldsymbol{\theta})} \tag{3-121}$$

Following the approach of (3-112), the multivariate log LR becomes

$$s(\boldsymbol{y}_i) = \frac{1}{2}[(\boldsymbol{y}_i - \boldsymbol{\theta}_0)^T\boldsymbol{\Sigma}^{-1}(\boldsymbol{y}_i - \boldsymbol{\theta}_0) - (\boldsymbol{y}_i - \boldsymbol{\theta}_1)^T\boldsymbol{\Sigma}^{-1}(\boldsymbol{y}_i - \boldsymbol{\theta}_1)] \tag{3-122}$$

Again for the case that $\boldsymbol{\theta}_0 = \mathbf{0}$ and $\boldsymbol{\theta}_1$ is unknown, using (3-131) we get the GLR by

$$\begin{aligned}\hat{S}_{\boldsymbol{\theta}_0=\mathbf{0}}(\boldsymbol{Y}) &= \sup_{\boldsymbol{\theta}_1} \frac{1}{2}\left[\sum_{i=1}^{N} \boldsymbol{y}_i^T\boldsymbol{\Sigma}^{-1}\boldsymbol{y}_i - \sum_{i=1}^{N}(\boldsymbol{y}_i - \boldsymbol{\theta}_1)^T\boldsymbol{\Sigma}^{-1}(\boldsymbol{y}_i - \boldsymbol{\theta}_1)\right] \\ &= \sup_{\boldsymbol{\theta}_1} \frac{1}{2}[N\bar{\boldsymbol{y}}^T\boldsymbol{\Sigma}^{-1}\bar{\boldsymbol{y}} - N(\bar{\boldsymbol{y}} - \boldsymbol{\theta}_1)^T\boldsymbol{\Sigma}^{-1}(\bar{\boldsymbol{y}} - \boldsymbol{\theta}_1)]\end{aligned} \tag{3-123}$$

with vector mean

$$E(\boldsymbol{Y}) = \bar{\boldsymbol{y}} = \frac{1}{N}\sum_{i=1}^{N} \mathbf{y}_i \tag{3-124}$$

and $\overline{\boldsymbol{y}} \sim \mathbb{N}(\mathbf{0}, \boldsymbol{\Sigma}/N)$ (e.g. Klein & Morelli, 2006, p. 446). As for (3-123) it is obvious that

$$\widehat{\boldsymbol{\theta}}_1 = \arg\sup_{\boldsymbol{\theta}_1} \hat{S}_{\boldsymbol{\theta}_0=\mathbf{0}}(\boldsymbol{Y}) = \overline{\boldsymbol{y}} \tag{3-125}$$

Substituting (3-125) and afterwards (3-124) back into (3-123) results in

$$\hat{S}_{\boldsymbol{\theta}_0=\mathbf{0}}(\boldsymbol{Y}) = \frac{N}{2}\overline{\boldsymbol{y}}^T\boldsymbol{\Sigma}^{-1}\overline{\boldsymbol{y}} \tag{3-126}$$

As from (3-126) it is clear that $\hat{S}_{\boldsymbol{\theta}_0=\mathbf{0}}(\boldsymbol{Y})$ is the sum of squares of m zero mean normal distributed random variables it follows that $\hat{S}_{\boldsymbol{\theta}_0=\mathbf{0}}(\boldsymbol{Y})$ is central χ^2-distributed with m degree of freedoms (cf. e.g. DasGupta, 2011, pp. 210-211)

3.4.3.2 Threshold Computation for Stochastic Unknown Inputs (Disturbances)

In a fault detection application the testing statistic is calculated online, based on obtained residual signal samples, and compared against a threshold J_{th}. In this text the GLR will be used for the purpose of composite hypothesis testing. The above considerations give rise to the following algorithm to calculate the threshold J_{th} given a fixed false alarm rate and the following hypothesises

$$\boldsymbol{H}_0 = \{\theta\colon\ \theta = 0\} \text{ and } \boldsymbol{H}_1 = \{\theta\colon\ \theta \neq 0\} \tag{3-127}$$

From (3-116) and (3-119) it follows for the scalar case that

$$\hat{d}_{GLR}(\boldsymbol{Y}) = \begin{cases} 0 & if\ \hat{S}_{\theta_0=0}(\boldsymbol{Y}) \leq J_{th};\quad \boldsymbol{H}_0\ is\ chosen\ \Rightarrow nofault \\ 1 & if\ \hat{S}_{\theta_0=0}(\boldsymbol{Y}) > J_{th};\quad \boldsymbol{H}_1\ is\ chosen \Rightarrow fault \end{cases} \tag{3-128}$$

and from (3-116) and (3-119) for the vector case that

$$\hat{d}_{GLR}(\boldsymbol{Y}) = \begin{cases} 0 & if\ \hat{S}_{\boldsymbol{\theta}_0=\mathbf{0}}(\boldsymbol{Y}) \leq J_{th};\quad \boldsymbol{H}_0\ is\ chosen\ \Rightarrow nofault \\ 1 & if\ \hat{S}_{\boldsymbol{\theta}_0=\mathbf{0}}(\boldsymbol{Y}) > J_{th};\quad \boldsymbol{H}_1\ is\ chosen \Rightarrow fault \end{cases} \tag{3-129}$$

If $\boldsymbol{Y} \sim \mathbb{N}(\boldsymbol{0}, \boldsymbol{\Sigma})$, it follows that $\overline{\boldsymbol{y}} \sim \mathbb{N}(\boldsymbol{0}, \boldsymbol{\Sigma}/\mathrm{N})$ (e.g. Klein & Morelli, 2006, p. 446) and therefore that $\hat{S}_{\boldsymbol{\theta}_0=\boldsymbol{0}}(\boldsymbol{Y}) = \frac{N}{2}\overline{\boldsymbol{y}}^T\boldsymbol{\Sigma}^{-1}\overline{\boldsymbol{y}}$ is *central* χ^2-distributed with m degrees of freedom.
In the more general case, which will become relevant in chapter 3.4.4, where $\boldsymbol{Y} \sim \mathbb{N}(\boldsymbol{\mu}, \boldsymbol{\Sigma})$, it follows that $\overline{\boldsymbol{y}} \sim \mathbb{N}(\boldsymbol{\mu}, \boldsymbol{\Sigma}/\mathrm{N})$ and therefore that $\hat{S}_{\boldsymbol{\theta}_0=\boldsymbol{0}}(\boldsymbol{Y}) = \frac{N}{2}\overline{\boldsymbol{y}}^T\boldsymbol{\Sigma}^{-1}\overline{\boldsymbol{y}}$ is *non-central* $\chi^2_m(\lambda)$-distributed with m degrees of freedom and non-centrality parameter

$$\lambda = \boldsymbol{\mu}^T\boldsymbol{\Sigma}^{-1}\boldsymbol{\mu} \tag{3-130}$$

(Basseville & Nikiforov, 1993, pp. 70-71; Koch, 1999, pp. 126-127; Tartakovsky et al., 2015, p. 108). As a result we have to solve

$$p(\chi > \chi_{\alpha_0}) = \alpha_0 \tag{3-131}$$

where α_0 is the significance level or in a fault detection context the FAR (cf. chapter 3.4.3) for χ_{α_0}. The threshold is then obtained by

$$J_{th} = \frac{\chi_{\alpha_0}}{2} \tag{3-132}$$

3.4.4 Integration of Norm-Based and Stochastic Threshold Computation for Deterministic and Stochastic Unknown Inputs (Disturbances)

$\|\boldsymbol{r}_d\|_2$ according (3-62) gives an energy bound for the residual signal for an *arbitrary* unknown input signal with known energy bound $\|\boldsymbol{d}\|_2$. Selecting the threshold

$$J_{th,2} = \sup_{\boldsymbol{f}=\boldsymbol{0},\boldsymbol{d}\neq\boldsymbol{0}} \|\boldsymbol{r}\|_2 = \|\boldsymbol{G}_{rd}\|_\infty \|\boldsymbol{d}\|_2 = \|\boldsymbol{r}_d\|_2 \tag{3-133}$$

therefore solves the fault detection problem for *deterministic unknown inputs with known energy bound* (cf. chapter 3.4.2.2), but does not take into account any *stochastic unknown inputs*. However, we can easily recast the statistic fault detection problem (3-127), which aims on detecting a change in the mean of the residual signal into a problem that tries to decide, in the presence of noise, if the energy of the residual signal measured is higher than the energy of the residual signal due to unknown deterministic disturbances, i.e. $\|\boldsymbol{r}\|_2 > \|\boldsymbol{r}_d\|_2$.

In this case the hypotheses become

$$\boldsymbol{H}_0 = \{\boldsymbol{\theta}: \|\boldsymbol{\theta}\| = 0\} \text{ and } \boldsymbol{H}_1 = \{\boldsymbol{\theta}: \|\boldsymbol{\theta}\| \geq \|\boldsymbol{r}_d\|_2\} \tag{3-134}$$

Using (3-80) we can rewrite (3-134) into

$$\boldsymbol{H}_0 = \{\boldsymbol{\theta}: \boldsymbol{\theta}^T\boldsymbol{\theta} = 0\} \text{ and } \boldsymbol{H}_1 = \{\boldsymbol{\theta}: \boldsymbol{\theta}^T\boldsymbol{\theta} \geq \|\boldsymbol{r}_d\|_2^2\} \tag{3-135}$$

It follows that the test statistics becomes

$$\hat{S}_{\|\boldsymbol{\theta_0}\|=0}(\boldsymbol{R}) = \frac{N}{2}\bar{\boldsymbol{r}}^T{\boldsymbol{\Sigma}_{\boldsymbol{r}}}^{-1}\bar{\boldsymbol{r}} \tag{3-136}$$

with vector mean

$$E(\boldsymbol{R}) = \bar{\boldsymbol{r}} = \frac{1}{N}\sum_{i=1}^{N}\mathbf{r}_i \tag{3-137}$$

However now, as $\bar{\boldsymbol{r}} \sim \mathbb{N}(\boldsymbol{r}_d, \boldsymbol{\Sigma}_r/\mathrm{N})$ in the boundary case, it follows with the considerations made in chapter 3.4.3.2, that $\hat{S}_{\|\boldsymbol{\theta_0}\|=0}(\boldsymbol{R})$ is *non-central* $\chi_m^2(\lambda)$-distributed with m degrees of freedom and non-centrality parameter

$$\lambda = \boldsymbol{r}_d^T{\boldsymbol{\Sigma}_r}^{-\mathbf{1}}\boldsymbol{r}_d \tag{3-138}$$

3.5 The Fault Detection System Proposed in this Thesis and Related Research Contributions

3.5.1 Introduction to the Fault-Detection System Proposed in this Thesis

Figure 26 schematically illustrates the fault detection system proposed in this thesis in combination with the closed-loop plant.

The closed-loop plant consists of the open-loop plant and the Conventional Flight Control System (CFCS). For the purpose of this text a simplified CFCS with proportional feed-forward and feedback control was modelled as q_{cmd}-system. This was a choice for this work, which has the goal of proving principal feasibility of the proposed FD system. The suggested FD system architecture itself can be easily adapted to different more complex closed-loop plant setups. The plant is subject to process noise $\boldsymbol{\nu_P}$ from atmospheric turbulence as well as measurement noise $\boldsymbol{\nu_M}$ from the sensors. The details of the plant will be discussed in chapter 3.5.2.

The model-based FD system is built from a residual generation and a residual evaluation part. The former is based on a Kalman filter as residual generator, a band-pass residual post filter to supress low frequency effects and high frequency noise, as well as a variance scaling filter. The latter ensures the right stochastical properties of the residual signal for the integrated deterministic/stochastic fault detection. Chapter 3.5.4 will discuss the details of residual generation.

The residual evaluation part consists of a recursive sliding window RMS generator to obtain $\|q_{cmd}\|^2_{RMS}$ and $\|\boldsymbol{r}\|^2_{RMS}$, a deterministic adaptive threshold, a stochastic threshold and finally a decision maker that raises the Fault Bit if a fault has been detected. The details of the different systems will be discussed in chapter 3.5.4.

With respect to the signals required by the FD system we can readily see that those are only the command input q_{cmd}, the pitch rate q, and the pitch acceleration $\dot{q}$ measurements. Thus the FD system is *compliant with* the requirements to minimize the amount of measurements necessary (Requirement 1-4, p. 11) and not to use angle of attack measurements for fault detection (Requirement 1-5, p. 11). It is furthermore easily retrofitable, because the interface to the existing aircraft flight control system is limited to the three measurements mentioned above and therefore also *compliant* to Requirement 1-2 (p. 11).

The idea of combining a conventional FCS with an active fault-tolerant one has only been very sparsely investigated in the past. Furthermore earlier work did either not focus on the required switching logic (Wohletz et al., 2000) or selected an approach where the fault-tolerant flight control system always works in parallel to the conventional one (for example D. G. Ward & Monaco, 2005). The latter inhibits a clear segregation of both systems (cf. chapter 1.4).

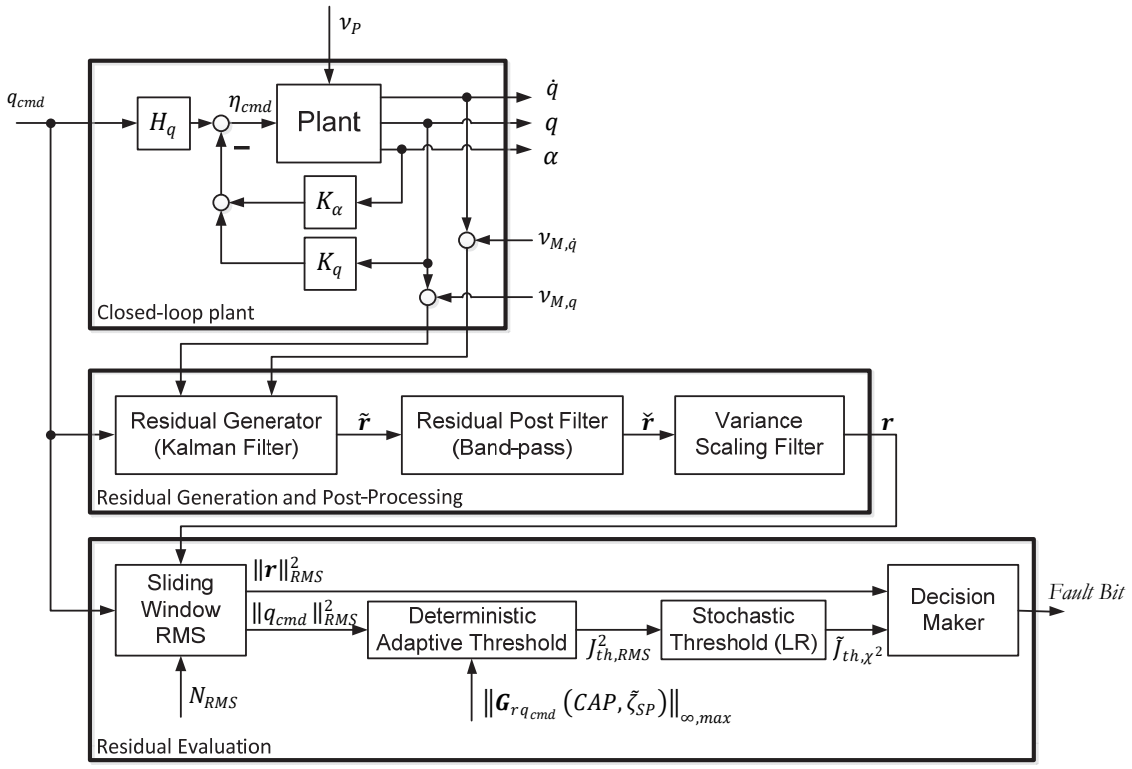

Figure 26 Schematic of the fault detection system proposed in this thesis

As for Wohletz et al. (2000) the approach chosen in this work is to activate the active fault-tolerant control system only in case that the certified conventional flight control system delivers an unacceptable closed-loop performance. Such an approach would potentially allow keeping the Active fault-tolerant FCS (AFCS) largely outside certification scope. This will help to avoid/limit problems that may arise from the immature certification experience with respect to AFCS. Furthermore it will allow to *augment* the existing certified and proven CFCS of existing aircrafts instead of replacing them entirely, thus leading to significantly reduced costs and development risks. Such a setup of course warrants reliable means to detect a CFCS problem that is severe enough so that it warrants switching to the AFCS. To the author's knowledge, the following aspects constitute the new research contributions of this thesis *to the area of aircraft fault detection*:

Contribution 3-2: The idea of combining a CFCS with an AFCS, albeit not completely new, has only been very sparsely investigated in the past and none of the work known to the author (cf. chapter 1.4) treat the problem of how to define a useable switching logic/threshold beyond mentioning its existence. This thesis focusses especially on the switching, i.e. fault detection, algorithm. The above mentioned reasoning chain implies that the possibility that the fault-tolerant flight control system is *inadvertently activated* must be very remote, i.e. the False Alarm Rate

(FAR) must be very low. To judge the possibility for inadvertent activation, the FAR must be quantifiable by a number. This work *uses a strict, state of the art FAR-based design approach,* as suggested by Ding (2013), and applies it to the aircraft fault detection problem on hand. This strict FAR-based design approach is, to the author's knowledge, new in the context of aircraft fault detection

Contribution 3-3: The classical approach to model-based FDD, which builds the heart of the algorithm used in this text, is to detect changes in the dynamic behaviour of the plant. Herein a different approach is chosen that aims at detecting changes in the combination of plant and controller, i.e. in the systems closed-loop behaviour. Keeping in mind that the control system design goal is to achieve a certain closed-loop performance led the author to the corollary that the deviation from the desired close-loop behaviour must be the primary measure for fault detection. To say it in other words: The pilot of a fly-by-wire aircraft does not care about the dynamic behaviour of the plant he cares about the dynamic behaviour of the closed-loop system because that is what is visible to him when he pilots the aircraft. Therefore the closed-loop behaviour will decide if he is able to safely pilot the aircraft and consequently an unacceptable deviation of the actual closed-loop behaviour to the desired closed-loop behaviour must be detected. A comparable approach was chosen before also by Wohletz et al. (1999) however the mechanization of the reference model, which describes the desired performance, was different. Wohletz, et al. decided to use a Low-order Equivalent System (LOES) model with online estimated parameters. While at a first glance this seems to be very appealing it gives rise to the problem of how to certify this online estimation system. To the author's knowledge this is not possible with the theory at hand (cf. chapter 1.4). However if the reference model is unreliable the fault-tolerant control system might be activated when no significant fault exists simply because the reference model is wrong. As of today, certification of the system suggested by Wohletz, et al., if at all possible, seems therefore unrealistic because the correct function of the system cannot be proven by theory or a reasonable amount of empirical testing. Furthermore their strategy aims at generating an error signal that is very close to zero when no fault is present and to use a very tight threshold on that signal to detect a failure. While, at the expense of a very high work effort, a fault signal close to zero might be achievable in theory it becomes very hard in practice due to unknown, i.e. immeasurable, inputs like turbulence. Most important the work mentioned above also does not describe how to obtain a the threshold. The author suggests to model the acceptable closed-loop performance, directly derived from the respective flying qualities standards, as deterministic model uncertainties of reference model used for fault detection. The approach, which will be discussed in detail in chapter 3.5.4.3.1, to use the flying quality standard derived CAP-ζ_{SP} combination to define a ω_{SP}-ζ_{SP} parameter polytope of

acceptable reference model uncertainties and consequently derive the norm-based residual threshold based on this reference model was developed by the author and is, to the author's knowledge, new. *This approach furthermore gives a direct interpretation of what we tried to achieve in terms of operational performance, where we are with the real system with respect to this goal, and if we are still inside the acceptable performance boundaries. Thus it enables a readily interpretable, clear picture where we are with respect to the design goal.* Last but not least the dynamics we try to achieve in terms of closed-loop performance is most often much less complex than the dynamics of the uncontrolled plant. As explained above and in chapter 2.2.2 in case of the aircraft longitudinal motion the closed-loop design goal can be expressed by a simple second (short period) or fourth order (short period & phugoid) system, while the underlying plant can be of much higher order, when taking into account secondary effects.

Contribution 3-4: The FD system proposed in this thesis is to author opinion, very flexible to adapt to different practical demands. Adaptations are easily done by just changing the range of acceptable *closed-loop* natural frequencies and damping ratios. Most important, those two parameters can be readily interpreted in physical and flying quality context and they allow a direct comparison with the flying quality standards MIL-F-8785C (US DoD, 1996) and MIL-STD-1797B[12] (US DoD, 2012). To the author's opinion this is a significant practical advantage and furthermore gives the aerospace engineer a direct understanding what the effect of the parameter changes are.

The aforementioned approach required several extensions of the combined stochastic/norm-based fault detection method for deterministic and stochastic unknown *inputs*, as suggested by Ding (2013, pp. 339-345), to the much more complex case of deterministic/stochastic unknown inputs and *deterministic model uncertainties*. The extensions suggested by the author will be discussed within the following chapters.

3.5.2 Closed-loop Plant

3.5.2.1 Open-loop Plant - Aircraft Linearized Longitudinal Motion Model

As mentioned above, in the context of this text, the linear state space model of the plant is used to calculate the required controller gains for a certain trim condition. For the state equation we have (cf. Holzapfel, 2011, p. 28/12)

$$\dot{\boldsymbol{x}} = \boldsymbol{A}\boldsymbol{x} + \boldsymbol{B}\boldsymbol{u} \tag{3-139}$$

[12] Restricted distribution, therefore information from MIL-F-8785C is used within this text.

with

$$\boldsymbol{A} = \begin{bmatrix} \frac{Z_q \cdot M_{\dot\alpha} + M_{\dot\alpha} + M_q - M_q \cdot Z_{\dot\alpha}}{1 - Z_{\dot\alpha}} & M_\alpha - \frac{M_{\dot\alpha} \cdot Z_\alpha}{Z_{\dot\alpha} - 1} & M_V - \frac{M_{\dot\alpha} \cdot Z_V}{Z_{\dot\alpha} - 1} & \frac{g}{V_0} \sin\gamma_0 \frac{M_{\dot\alpha}}{Z_{\dot\alpha} - 1} & M_h - \frac{M_{\dot\alpha} \cdot Z_h}{Z_{\dot\alpha} - 1} & 0 \\ \frac{Z_q + 1}{1 - Z_{\dot\alpha}} & \frac{-Z_\alpha}{Z_{\dot\alpha} - 1} & \frac{-Z_V}{Z_{\dot\alpha} - 1} & \frac{g}{V_0} \sin\gamma_0 \frac{M_{\dot\alpha}}{Z_{\dot\alpha} - 1} & \frac{-Z_h}{Z_{\dot\alpha} - 1} & 0 \\ \frac{Z_q \cdot X_{\dot\alpha} + X_{\dot\alpha} + X_q - X_q \cdot Z_{\dot\alpha}}{1 - Z_{\dot\alpha}} & X_\alpha - \frac{X_{\dot\alpha} \cdot Z_\alpha}{Z_{\dot\alpha} - 1} & X_V - \frac{X_{\dot\alpha} \cdot Z_V}{Z_{\dot\alpha} - 1} & \frac{g}{V_0} \sin\gamma_0 \frac{X_{\dot\alpha}}{Z_{\dot\alpha} - 1} - g\cos\gamma_0 & X_h - \frac{X_{\dot\alpha} \cdot Z_h}{Z_{\dot\alpha} - 1} & 0 \\ \frac{Z_{\dot\alpha} + Z_q}{Z_{\dot\alpha} - 1} & \frac{Z_\alpha}{Z_{\dot\alpha} - 1} & \frac{Z_V}{Z_{\dot\alpha} - 1} & \frac{g}{V_0} \sin\gamma_0 \frac{X_{\dot\alpha}}{1 - Z_{\dot\alpha}} & \frac{Z_h}{Z_{\dot\alpha} - 1} & 0 \\ 0 & 0 & \sin\gamma_0 & V_0 \cos\gamma_0 & 0 & 0 \\ 0 & 0 & \cos\gamma_0 & -V_0 \sin\gamma_0 & 0 & 0 \end{bmatrix}$$

$$\boldsymbol{B} = \begin{bmatrix} M_\eta - \frac{M_{\dot\alpha} \cdot Z_\eta}{Z_{\dot\alpha} - 1} & M_{\delta_T} - \frac{M_{\dot\alpha} \cdot Z_{\delta_T}}{Z_{\dot\alpha} - 1} \\ \frac{Z_\eta}{1 - Z_{\dot\alpha}} & \frac{Z_{\delta_T}}{1 - Z_{\dot\alpha}} \\ X_\eta - \frac{X_{\dot\alpha} \cdot Z_\eta}{Z_{\dot\alpha} - 1} & X_{\delta_T} - \frac{X_{\dot\alpha} \cdot Z_{\delta_T}}{Z_{\dot\alpha} - 1} \\ \frac{Z_\eta}{Z_{\dot\alpha} - 1} & \frac{Z_{\delta_T}}{Z_{\dot\alpha} - 1} \\ 0 & 0 \\ 0 & 0 \end{bmatrix} \qquad \boldsymbol{x} = \begin{bmatrix} \Delta q_K \\ \Delta \alpha_K \\ \Delta V_K \\ \Delta \gamma \\ \Delta h \\ \Delta x \end{bmatrix} \qquad \boldsymbol{u} = \begin{bmatrix} \Delta\eta \\ \Delta\delta_T \end{bmatrix}$$

3.5.2.1.1 Simplified Linearized Longitudinal Motion Model

The effect of altitude variation around the trim condition can be considered small, therefore it is a common simplification, which is also used herein, to sume $\mathrm{M_h} = Z_h = X_h = 0$ and in consequence to remove the state h from the state space model. Furthermore the position x is independent of all other states and can therefore also be removed (Holzapfel, 2011, p. 45/12). The matrices $\boldsymbol{A}$, $\boldsymbol{B}$ and state vector $\boldsymbol{x}$ then simplify to

$$\dot{\boldsymbol{x}} = \boldsymbol{A}\boldsymbol{x} + \boldsymbol{B}\boldsymbol{u} \tag{3-140}$$

with

$$\boldsymbol{A} = \begin{bmatrix} \frac{Z_q \cdot M_{\dot\alpha} + M_{\dot\alpha} + M_q - M_q \cdot Z_{\dot\alpha}}{1 - Z_{\dot\alpha}} & M_\alpha - \frac{M_{\dot\alpha} \cdot Z_\alpha}{Z_{\dot\alpha} - 1} & M_V - \frac{M_{\dot\alpha} \cdot Z_V}{Z_{\dot\alpha} - 1} & \frac{g}{V_0} \sin\gamma_0 \frac{M_{\dot\alpha}}{Z_{\dot\alpha} - 1} \\ \frac{Z_q + 1}{1 - Z_{\dot\alpha}} & \frac{Z_\alpha}{Z_{\dot\alpha} - 1} & \frac{-Z_V}{Z_{\dot\alpha} - 1} & \frac{g}{V_0} \sin\gamma_0 \frac{M_{\dot\alpha}}{Z_{\dot\alpha} - 1} \\ \frac{Z_q \cdot X_{\dot\alpha} + X_{\dot\alpha} + X_q - X_q \cdot Z_{\dot\alpha}}{1 - Z_{\dot\alpha}} & X_\alpha - \frac{X_{\dot\alpha} \cdot Z_\alpha}{Z_{\dot\alpha} - 1} & X_V - \frac{X_{\dot\alpha} \cdot Z_V}{Z_{\dot\alpha} - 1} & \frac{g}{V_0} \sin\gamma_0 \frac{X_{\dot\alpha}}{Z_{\dot\alpha} - 1} - g\cos\gamma_0 \\ \frac{Z_{\dot\alpha} + Z_q}{Z_{\dot\alpha} - 1} & \frac{Z_\alpha}{Z_{\dot\alpha} - 1} & \frac{Z_V}{Z_{\dot\alpha} - 1} & \frac{g}{V_0} \sin\gamma_0 \frac{X_{\dot\alpha}}{1 - Z_{\dot\alpha}} \end{bmatrix}$$

$$\boldsymbol{B} = \begin{bmatrix} M_\eta - \frac{M_{\dot\alpha} \cdot Z_\eta}{Z_{\dot\alpha} - 1} & M_{\delta t} - \frac{M_{\dot\alpha} \cdot Z_{\delta_T}}{Z_{\dot\alpha} - 1} \\ \frac{Z_\eta}{1 - Z_{\dot\alpha}} & \frac{Z_{\delta_T}}{1 - Z_{\dot\alpha}} \\ X_\eta - \frac{X_{\dot\alpha} \cdot Z_\eta}{Z_{\dot\alpha} - 1} & X_{\delta_T} - \frac{X_{\dot\alpha} \cdot Z_{\delta_T}}{Z_{\dot\alpha} - 1} \\ \frac{Z_\eta}{Z_{\dot\alpha} - 1} & \frac{Z_{\delta\delta_T}}{Z_{\dot\alpha} - 1} \end{bmatrix} \qquad \boldsymbol{x} = \begin{bmatrix} \Delta q_K \\ \Delta \alpha_K \\ \Delta V_K \\ \Delta \gamma \end{bmatrix} \qquad \boldsymbol{u} = \begin{bmatrix} \Delta \eta \\ \Delta \delta_T \end{bmatrix}$$

3.5.2.1.2 Linear Longitudinal Short Period Approximation

It is common practice during FCS inner-loop control law design (cf. e.g. Osterhuber, Hanel, & Hammon, 2004,p. 3) and general studies on short period handling qualities (Gibson, 1999, p. 23; Heller, 2013, p. 3-89) to further simplify (3-140) by splitting the state space model in a phugoid approximation, dominated by states V_K and γ and short period approximation, dominated by states q_K and α_K. To arrive at the short period approximations the following assumptions are made (Holzapfel, 2011, p. 45/12 & 14/94):

- $\Delta V_K = 0$, i.e. $V_K = V_{K,0} = \text{const.}$
- $\Delta \gamma_K = 0$, i.e. $\gamma_K = \gamma_{K,0} = \text{const.}$
- $\Delta \delta_T = 0$, i.e. $\delta_T = \delta_{T,0} = \text{const.}$
- The effect of the angle of attack derivative $\dot\alpha$ is small for conventional aircraft configurations, i.e. $X_{\dot\alpha} = Z_{\dot\alpha} = M_{\dot\alpha} = 0$

The resulting state space model is then given by

$$\begin{aligned} \dot{\boldsymbol{x}}_{SP,OL} &= \boldsymbol{A}_{SP,OL}\boldsymbol{x}_{SP,OL} + \boldsymbol{B}_{SP,OL}\eta \\ \boldsymbol{y}_{SP,OL} &= \boldsymbol{C}_{SP,OL}\boldsymbol{x}_{SP,OL} + \boldsymbol{D}_{SP,OL}\eta \end{aligned} \tag{3-141}$$

with

$$\boldsymbol{A}_{SP,OL} = \begin{bmatrix} M_q & M_\alpha \\ Z_q + 1 & Z_\alpha \end{bmatrix} \quad \boldsymbol{B}_{SP,OL} = \begin{bmatrix} M_\eta \\ Z_\eta \end{bmatrix} \qquad \boldsymbol{x}_{SP,OL} = \begin{bmatrix} q_K \\ \alpha_K \end{bmatrix}$$

$$\boldsymbol{C}_{SP,OL} = \begin{bmatrix} 1 & 0 \\ \boldsymbol{A}_{SP}(1,:) \end{bmatrix} \qquad \boldsymbol{D}_{SP,OL} = \begin{bmatrix} 0 \\ \boldsymbol{B}_{SP}(1,:) \end{bmatrix} \qquad \boldsymbol{y}_{SP,OL} = \begin{bmatrix} q_K \\ \dot q_K \end{bmatrix}$$

The output equation potentially needs some further explanation. For our fault detection purposes we want to use the pitch rate q_K and pitch acceleration $\dot q_K$. The

latter provides the quickest reaction on a fault and therefore helps with respect to a small fault detection delay. As $\dot{q}_K$ is not a state but a state derivative we have to "reconstruct" it in the output equation. From the state space model (3-141) it should be clear that

$$\dot{q}_K = \boldsymbol{A}_{SP,OL}(1,:)\boldsymbol{x}_{SP,OL} + \boldsymbol{B}_{SP,OL}(1,:)\eta \tag{3-142}$$

where $(1,:)$ denotes all columns of the first row. That is how we got the above shown matrices $\boldsymbol{C}_{SP,OL}$ and $\boldsymbol{D}_{SP,OL}$.

Remark 3-3: Several authors also assume $Z_q = 0$. This assumption is potentially acceptable for aircraft *without* a q-feedback control, but for aircraft including the latter Z_q should *not* be omitted because it is normally significant due to the feedback term $K_q Z_\eta$.

Remark 3-4: The simulation case study of this thesis uses the linear short period approximation (3-141) because the fault detection system, in its current status, aims at detecting unacceptable deviations for the short period flying qualities (dynamics). To supress lower frequency dynamics (e.g. phugoid motion and steady state deviations) as well as higher frequency dynamics/noise, the residual $\boldsymbol{r}$ is filtered through a band-pass filter (Chapter 3.5.3.2). The short period model is deemed sufficient by the author to demonstrate principle *feasibility* of the fault detection approach suggested in this thesis. The assumption that the band-pass filter mentioned is sufficient has to be *verified* at some point. To use only the short period approximation is also a common simplification used during FCS inner-loop control law design (cf. e.g. Osterhuber et al., 2004, p. 3) and general studies on short period handling qualities (cf. Gibson, 1999, p. 23). In general the longitudinal short period motion is of much higher importance for the flying qualities of an aircraft than the phugoid motion (cf. e.g. Hodgkinson, 1999) though the latter shall not be forgotten.

3.5.2.2 Flight Control System

3.5.2.2.1 Closed-Loop Plant without Actuator Dynamics

For the purpose of this thesis a basic state feedback control system with pitch rate q_K and angle of attack α_K feedback and gain

$$\boldsymbol{K} = [K_q \quad K_\alpha] \tag{3-143}$$

has been used. In addition a feed-forward gain H_q was introduced to ensure that the closed-loop system steady state gain for output q_K is equal one, i.e. a q_{cmd} = 1 rad/s leads to a stedy state output $q_{K,\infty}$ = 1 rad/s. The setup is schemati-

cally shown in Figure 26. Based on (3-141) we get for the state equation of the closed-loop system

$$\begin{aligned} \dot{\boldsymbol{x}}_{SP,CL} &= \boldsymbol{A}_{SP,CL}\boldsymbol{x}_{SP,CL} + \boldsymbol{B}_{SP,CL}q_{cmd} \\ \boldsymbol{y}_{SP,CL} &= \boldsymbol{C}_{SP,CL}\boldsymbol{x}_{SP,CL} + \boldsymbol{D}_{SP,CL}q_{cmd} \end{aligned} \tag{3-144}$$

and with $\boldsymbol{A}_{SP,CL} = \boldsymbol{A}_{SP,OL} - \boldsymbol{B}_{SP,OL}\boldsymbol{K}$

$$\boldsymbol{A}_{SP,CL} = \begin{bmatrix} M_{q,OL} - K_q M_\eta & M_{\alpha,OL} - K_\alpha M_\eta \\ 1 + Z_{q,OL} - K_q Z_\eta & Z_{\alpha,OL} - K_\alpha Z_\eta \end{bmatrix} \qquad \boldsymbol{B}_{SP,CL} = \begin{bmatrix} H_q M_\eta \\ H_q Z_\eta \end{bmatrix}$$

$$\boldsymbol{C}_{SP,CL} = \begin{bmatrix} 1 & 0 \\ \boldsymbol{A}_{SP,CL}(1,:) \end{bmatrix} \qquad \boldsymbol{D}_{SP,CL} = \begin{bmatrix} 0 \\ \boldsymbol{B}_{SP,CL}(1,:) \end{bmatrix}$$

$$\boldsymbol{x}_{SP,CL} = \begin{bmatrix} q_K \\ \alpha_K \end{bmatrix} \qquad \boldsymbol{y}_{SP,CL} = \begin{bmatrix} q_K \\ \dot{q}_K \end{bmatrix}$$

3.5.2.2.2 Closed-Loop Plant with Actuator Dynamics

For the practical relevant failure case discussed in chapter 4.3.4, where the closed-loop aircraft becomes unstable, the actuator dynamics have been modelled, because without doing this the results would be less meaningful. This fault detection system setup is discussed in chapter 4.3.4.2.3 to prevent confusion at this point.

3.5.3 Residual Generation and Post-processing

3.5.3.1 Residual Generator

3.5.3.1.1 Kalman Filter Extension for Colored Process Noise

In case of aircraft the assumption of chapter 3.3.3 that the process noise is white, i.e. $\nu_P \sim \mathcal{N}(0, \Sigma_{\nu_P})$ or power spectral density $\Phi_{\nu_P\nu_P}(s) = \Sigma_{\nu_P}$, is normally not a good one. Typical aircraft process noise comes from turbulence or gusts that are modelled as stochastic processes. Naturally atmospheric turbulence is mainly concentrated on lower frequencies thus the power spectral density $\Phi_{\nu_P\nu_P}(s)$ is not flat and therefore by definition not *white* but *colored*. The most widely used stochastic turbulence model for flight dynamics, which is also accepted by the military specifications (SAE, 2007, pp. 27-29; US DoD, 2004, p. 678), is Dryden (1961). Turbulence is one of the major disturbances for aircraft and must therefore be properly accounted for (cf. Brockhaus et al., 2011, p. 18).

Many important statistical concepts and their applications, e.g. the Kalman filter, are based on the assumption of white process noise. Therefore the question arises how colored noise can be implemented.

Contribution 3-5: The colored process noise extension of the Kalman filter is to the author's knowledge not covered by contemporary FDD literature, e.g. Ding (2013). In the residual generation context it was introduced by the author to handle the problem of colored aircraft atmospheric turbulence. The theory is based on the respective known Kalman filter state observer colored noise extensions given for example in Lewis, Xie, and Popa (2007, p. 124-127).

As shown for example in Maybeck (1979), the spectral factorisation theorem yields that for any $\left|\Phi_{\nu_P\nu_P}(s)\right| \neq 0$ there exists a square, rational and asymptotically stable factor $\Phi_{\nu_P\nu_{P,L}}(s)$ such that

$$\Phi_{\nu_P\nu_P}(s) = \Phi_{\nu_P\nu_{P,L}}(s)\Phi_{\nu_P\nu_{P,R}}(s) \tag{3-145}$$

holds true, i.e. $\Phi_{\nu_P\nu_{P,L}}(s)$ contains all poles and zeros on the left hand plane and $\Phi_{\nu_P\nu_{P,R}}$ all on the right hand plane. This means that $\Phi_{\nu_P\nu_{P,L}}(s)$ is stable and minimum phase while $\Phi_{\nu_P\nu_{P,R}}(s)$ is not. Because of the symmetry to the coordinate axes we furthermore get the relation

$$\Phi_{\nu_P\nu_{P,R}}(s) = \Phi_{\nu_P\nu_{P,L}}(-s) \tag{3-146}$$

With a similar approach we can define for a white noise process $\Phi_{\nu_N\nu_N}(s) = \Sigma_{\nu_P}$, that

$$\begin{aligned}\Phi_{\nu_N\nu_N}(s) &= \Phi_{\nu_N\nu_{N,L}}(s)\Phi_{\nu_N\nu_{N,R}}(s) = \Phi_{\nu_N\nu_{N,L}}(s)\Phi_{\nu_N\nu_{N,L}}(-s) \\ &= \sqrt{\Sigma_{\nu_P}}\sqrt{\Sigma_{\nu_P}}\end{aligned} \tag{3-147}$$

We remember the goal is to find a system that transfers $\Phi_{\nu_N\nu_N}(s)$ to $\Phi_{\nu_P\nu_P}(s)$, i.e. white to colored noise. We therefor define

$$\Phi_{\nu_P\nu_{P,L}}(-s) = G(s)G(-s)\Phi_{\nu_N\nu_{N,L}}(s)\Phi_{\nu_N\nu_{N,L}}(-s) \tag{3-148}$$

For the stable, minimum phase system we thus get

$$G_{\nu_P\nu_N}(s) = \frac{\Phi_{\nu_P\nu_{P,L}}(s)}{\Phi_{\nu_N\nu_{N,L}}(s)} \tag{3-149}$$

This means that, if the LTI system defined by $G_{\nu_P\nu_N}(s)$ is driven by white noise with power spectral density $\Phi_{\nu_N\nu_N}(s)$, the output of $G_{\nu_P\nu_N}(s)$ is colored noise with power spectral density $\Phi_{\nu_P\nu_P}(s)$.
Relation (3-149) can be further simplified by choosing $\Phi_{\nu_N\nu_N}(s) = 1$ because with (3-147) it follows that in this case $\Phi_{\nu_N\nu_N,L}(s) = 1$ and therefore

$$G_{\nu_P\nu_N}(s) = \Phi_{\nu_P\nu_P,L}(s) \tag{3-150}$$

The situation is illustrated in Figure 27. $G_{\nu_P\nu_N}(s)$ is also called *noise* or *spectrum shaping filter*.

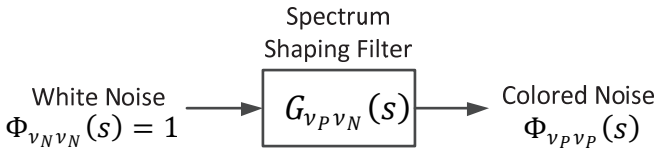

Figure 27 Spectrum shaping filter (based on Lewis et al., 2007, p. 124)

Taking the Dryden form vertical wind gust power spectral density $\Phi_{w_W}(\omega)$ given in MIL-STD-1797A (US DoD, 2004, p. 678) and published by Yeager (1998, p. 36)

$$\Phi_{w_W}(\Omega) = \sigma_{w_W}^2 \frac{2L_{w_W}}{\pi} \frac{1 + 12\left(L_{w_W}\Omega\right)^2}{\left[1 + 4\left(L_{w_W}\Omega\right)^2\right]^2} \tag{3-151}$$

where Ω is the frequency, L_{w_W} is the turbulence scale length and $\sigma_{w_W}^2$ the turbulence variance or turbulence intensity. With the relations $\Omega = \omega/V_K$, $\Phi(\Omega) = V_K\Phi(\omega)$ and period $T_{w_W} = L_{w_W}/V_k$ (cf. Brockhaus et al., 2011, p. 194) we get

$$\Phi_{w_W}(\omega) = \sigma_{w_W}^2 \frac{2T_{w_W}}{\pi} \frac{1 + 12\left(T_{w_W}\omega\right)^2}{\left[1 + 4\left(T_{w_W}\omega\right)^2\right]^2} \tag{3-152}$$

With $\mathrm{s} = \mathrm{j}\omega$ it follows that $\omega^2 = -s^2$ and therefore

$$\Phi_{w_W}(\mathrm{s}) = \sigma_{w_W}^2 \frac{2T_{w_W}}{\pi} \frac{1 - 12\left(T_{w_W}\mathrm{s}\right)^2}{\left[1 - 4\left(T_{w_W}\mathrm{s}\right)^2\right]^2} \tag{3-153}$$

(3-154) can now be factorised

$$\begin{aligned}&\Phi_{w_W}(\mathrm{s}) = \\ &= \left[\sqrt{\sigma_{w_W}^2 \frac{2T_{w_W}}{\pi}} \frac{1+\sqrt{12}T_{w_W}\mathrm{s}}{\left(1+\sqrt{4}T_{w_W}\mathrm{s}\right)^2}\right]\left[\sqrt{\sigma_{w_W}^2 \frac{2T_{w_W}}{\pi}} \frac{1-\sqrt{12}T_{w_W}\mathrm{s}}{\left(1-\sqrt{4}T_{w_W}\mathrm{s}\right)^2}\right] \\ &= \Phi_{w_W,L}(\mathrm{s})\Phi_{w_W,R}(\mathrm{s})\end{aligned} \tag{3-154}$$

Using (3-150) we get the noise filter transfer function, for the filter driven by white noise $\mathcal{N}(0,1)$

$$\begin{aligned}G_{\nu_P\nu_N,w_W}(s) &= \sqrt{\sigma_{w_W}^2 \frac{2T_{w_W}}{\pi}} \frac{1+\sqrt{12}T_{w_W}\mathrm{s}}{\left(1+\sqrt{4}T_{w_W}\mathrm{s}\right)^2} \\ &= \sigma_{w_W}\sqrt{\frac{2T_{w_W}}{\pi}} \frac{1+2\sqrt{3}T_{w_W}\mathrm{s}}{\left(1+2T_{w_W}\mathrm{s}\right)^2}\end{aligned} \tag{3-155}$$

(3-155) is also used by the "Dryden Wind Turbulence Model (Continuous) Block" of the Simulink's Aerospace Blockset (The MathWorks Inc., 2014, p. 4-266). MIL-F-8785C (US DoD, 1996, p. 47) and MIL-STD-1797A (US DoD, 2004, p. 678) define σ_{w_W} as function of altitude. Herein the medium/high altitude model is used which is valid above an altitude of 2000 ft and assumes isotropic turbulence. σ_{w_W} is found from the graph shown in Figure 28 for three different turbulence severity levels, i.e. light, moderate, and severe. As apparent the severity level also defines the probability of exceedance. The turbulence scale length is given as L_{w_W} = 1750 ft.
The vertical wind velocity w_W induces the wind angle of attack α_W via

$$\alpha_W = \frac{w_W}{V_A} \tag{3-156}$$

Remark 3-5: Because in our case $\gamma_K = 0$ it follows that $(w_W^G)_0^0 = (w_W^G)_K^0$.

Remark 3-6: q_W has not been taken into account in this thesis because for the F-16 used in the simulation case study because for a conventional fighter type aircraft like the F-16 used in the simulation case study it is not significant acc. MIL-STD-1797A (US DoD, 2004, p. 680).

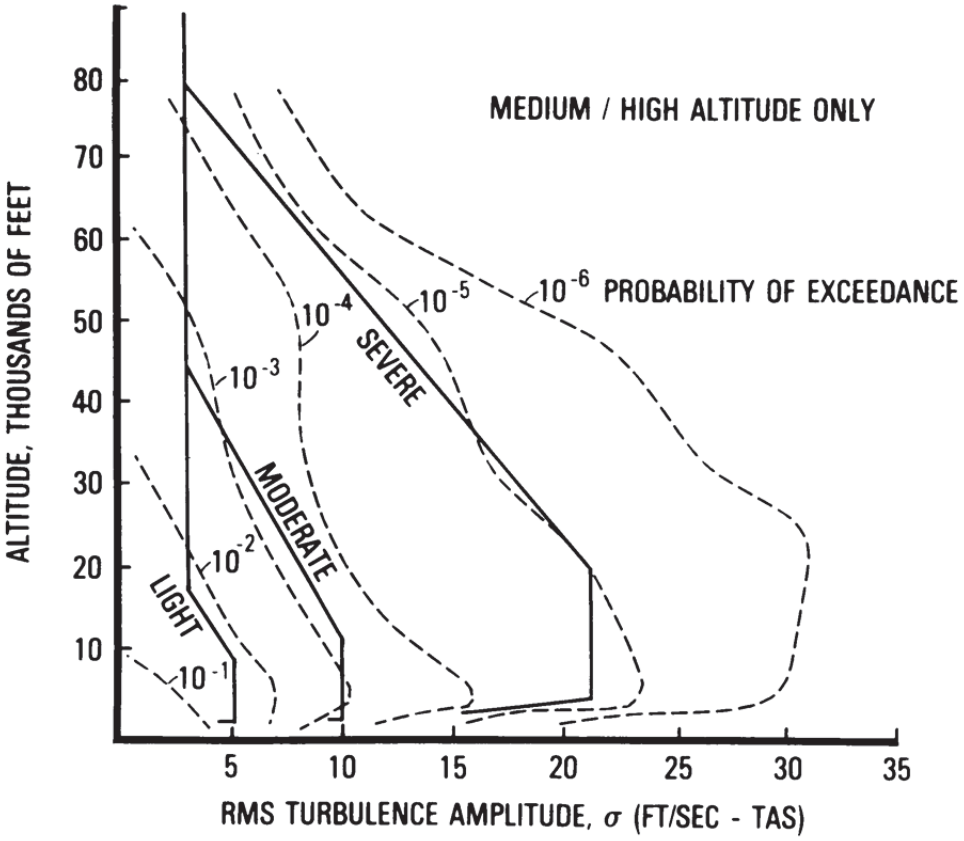

Figure 28 Turbulence severity and exceedance probability (US DoD, 2004, p. 673) retrieved from Wikipedia (2016)

Transfer function (3-155) and (3-156) can be expressed in observable canonical form

$$\begin{aligned} \dot{\boldsymbol{x}}_W &= \boldsymbol{A}_W \boldsymbol{x}_W + \boldsymbol{B}_W \nu_P \\ \alpha_W &= \boldsymbol{C}_W \boldsymbol{x}_W \end{aligned} \tag{3-157}$$

with

$$\boldsymbol{A}_W = \begin{bmatrix} 0 & -\frac{1}{T_{w_W}^2} \\ 1 & -\frac{2}{T_{w_W}} \end{bmatrix} \qquad \boldsymbol{B}_W = \begin{bmatrix} \frac{\sigma_{w_W}\sqrt{\frac{T_{w_W}}{\pi}}}{T_{w_W}^2 V_A} \\ \frac{\sigma_{w_W}\sqrt{3}\sqrt{\frac{T_{w_W}}{\pi}}}{T_{w_W} V_A} \end{bmatrix}$$

$$\boldsymbol{C}_W = [0 \quad 1] \qquad \boldsymbol{x}_W = \begin{bmatrix} x_{W,1} \\ \alpha_W \end{bmatrix} \qquad \boldsymbol{x}_W(0) = \boldsymbol{x}_{W,0}$$

The wind angle of attack α_W is therefore the 2nd state of the wind process.

3.5.3.1.2 Combined Wind Closed-Loop Aircraft Model

We are now in a position to setup the combined *wind* and *closed-loop aircraft short period* system. The state space model of the process, in our case the aircraft short period (index SP), can be augmented by the state space model of the wind process (index W), i.e. the turbulence spectrum shaping filter. The latter couples on the $\dot{q}_K$ and $\dot{\alpha}_K$ of the aircraft process via the open-loop $-M_{\alpha,OL}$ and $-Z_{,OL\alpha}$ respectively (Brockhaus et al., 2011, p. 276). At the same time we want to add the measurement noise input $\boldsymbol{\nu}_M$ and separate unknown (matrix index u) and known inputs (matrix index k). The latter is desirable due to the reasons described in chapter 3.3.5.

Combining (3-144) and (3-157) the state space model for the combined *wind* and *closed-loop aircraft short period* system becomes

$$\begin{aligned}\dot{\boldsymbol{x}}_{W,SP,CL} &= \boldsymbol{A}_{W,SP,CL}\boldsymbol{x}_{W,SP,CL} + \boldsymbol{B}_{W,SP,CL,k}q_{cmd} + \boldsymbol{B}_{W,SP,CL,u}\boldsymbol{\nu}_{W,SP,CL} \\ \boldsymbol{y}_{W,SP,CL} &= \boldsymbol{C}_{W,SP,CL}\boldsymbol{x}_{W,SP,CL} + \boldsymbol{D}_{W,SP,CL,k}q_{cmd} + \boldsymbol{D}_{W,SP,CL,u}\boldsymbol{\nu}_{W,SP,CL}\end{aligned} \tag{3-158}$$

with

$$\boldsymbol{A}_{W,SP,CL} = \begin{bmatrix} & \boldsymbol{A}_W & & 0 & 0 \\ & & & 0 & 0 \\ 0 & -M_{\alpha,OL} & & \boldsymbol{A}_{SP,CL} & \\ 0 & -Z_{\alpha,OL} & & & \end{bmatrix}$$

$$\boldsymbol{B}_{W,SP,CL,k} = \begin{bmatrix} 0 \\ 0 \\ \boldsymbol{B}_{SP,CL} \end{bmatrix} \qquad \boldsymbol{B}_{W,SP,CL,u} = \begin{bmatrix} \boldsymbol{B}_W & 0 & 0 \\ & 0 & 0 \\ 0 & 0 & 0 \\ 0 & 0 & 0 \end{bmatrix}$$

$$\boldsymbol{C}_{W,SP,CL} = \begin{bmatrix} 0 & 0 & 1 & 0 \\ \boldsymbol{A}_{W,SP,CL}(3,:) \end{bmatrix}$$

$$\boldsymbol{D}_{W,SP,CL,k} = \begin{bmatrix} 0 \\ \boldsymbol{B}_{W,SP,CL,k}(3,:) \end{bmatrix} \qquad \boldsymbol{D}_{W,SP,CL,u} = \begin{bmatrix} 0 & 1 & 0 \\ 0 & 0 & 1 \end{bmatrix}$$

$$\boldsymbol{x}_{W,SP,CL} = \begin{bmatrix} \boldsymbol{x}_W \\ \boldsymbol{x}_{SP,CL} \end{bmatrix} = \begin{bmatrix} x_{W,1} \\ \alpha_W \\ q_K \\ \alpha_K \end{bmatrix} \qquad \boldsymbol{x}(0) = \begin{bmatrix} \boldsymbol{x}_{W,0} \\ \boldsymbol{x}_{SP,CL,0} \end{bmatrix} \qquad \boldsymbol{y}_{W,SP,CL} = \begin{bmatrix} q_K \\ \dot{q}_K \end{bmatrix}$$

$$\boldsymbol{\nu}_{W,SP,CL} = \begin{bmatrix} \nu_P \\ \nu_{M,q} \\ \nu_{M,\dot{q}} \end{bmatrix} \text{ with } \nu_P \sim \mathcal{N}\left(0, \Sigma_{\nu_P}\right), \nu_{M,q} \sim \mathcal{N}\left(0, \Sigma_{\nu_{M,q}}\right), \nu_{M,\dot{q}} \sim \mathcal{N}\left(0, \Sigma_{\nu_{M,\dot{q}}}\right)$$

The augmented state space model of aircraft short period motion and noise shaping filter has a white noise input $\boldsymbol{\nu}_{W,SP,CL}$ and can therefore be treated by normal Kalman filter methods. Of course the Kalman filter has to estimate the states of the shaping filter because they are not measurable under normal practical conditions.

Remark 3-7: α_W couples with *negative* M_α and *negative* Z_α on $\dot{q}_K$ and $\dot{\alpha}_K$ of the aircraft process because of the definition of a positive wind angle of attack α_W. We recall that (cf. e.g. Brockhaus et al., 2011, pp. 64-66)

$$\vec{\boldsymbol{V}}_A^G = \vec{\boldsymbol{V}}_K^G - \vec{\boldsymbol{V}}_W^G \tag{3-159}$$

and therefore, for the longitudinal motion of this case study, i.e. $\Phi = 0$

$$\alpha_A = \alpha_K - \alpha_W \tag{3-160}$$

This means that for a *down draft,* w_W and α_W are positive therefore reducing α_A.

3.5.3.1.3 Residual Generator (Kalman filter)

The Kalman filter has been introduced in chapter 3.3.3. Comparison of (3-44) to (3-32) confirms that the Kalman filter is similar in structure to the Luenberger observer (Figure 24) however, in the non-steady state version, the Kalman filter gain is time varying. The Kalman filter gain calculation takes into account stochastic unknown inputs in the form of measurement noise $\boldsymbol{\nu}_M \sim \mathcal{N}\left(\mathbf{0}, \boldsymbol{\Sigma}_{\nu_M}\right)$ and process noise $\boldsymbol{\nu}_P \sim \mathcal{N}\left(\mathbf{0}, \boldsymbol{\Sigma}_{\nu_P}\right)$ thus is based on statistic reasoning while the gain choice of the Luenberger observer is arbitrary. This means that the Kalman filter provides an optimal solution for a linear system subject to measurement and process noise in the form that it "is the only observer that results in an independent sequence of residuals, namely the innovations." (Basseville & Nikiforov, 1993, p. 214). By inspection of (3-158) it thus becomes clear that the Kalman filter is the optimal solution to our residual generation problem.

For stochastic stationary processes, i.e. $\boldsymbol{\Sigma}_{\nu_M}, \boldsymbol{\Sigma}_{\nu_P} \sim const$, the Kalman filter gain converges to a constant value. This Kalman filter variant with constant gain $\boldsymbol{L}$ is known as *steady-state Kalman filter*. It is the approach chosen for this work. For us a time-invariant gain $\boldsymbol{L}$ is very important, because the latter is an integral part of the residual dynamics used for residual evaluation (cf. chapter 3.5.4.3.1.2). While a time-

varying gain $\boldsymbol{L}$ at first glance might look helpful for stochastic residual evaluation it is unfavourable for the deterministic part of the integrated deterministic/stochastic fault detection. This is due to fact for time-varying gain $\boldsymbol{L}$ we have to consider a fast varying parameter in the residual dynamics which leads to high deterministic thresholds as will be discussed in chapter 3.5.4.3.1.3. The downside of the steady-state Kalman filter approach is that we have to assume the worst-case variances $\boldsymbol{\Sigma}_{\nu_M}$ and $\boldsymbol{\Sigma}_{\nu_P}$ for the calculation of $\boldsymbol{L}$ and the stochastic residual evaluation. However we will show in chapter 4.3.4 that even with this approach a good fault detection performance can be obtained.
The variance $\boldsymbol{\Sigma}_{\nu_M}$ is obtained from the sensor used, in our case the sensors to measure q_K and $\dot{q}_K$. The process noise variance is equal one ($\Sigma_{\nu_P} = 1$). The scaling to the correct variance $\sigma_{w_W}^2$ is done in the atmospheric turbulence model (spectral filter) as described in chapter 3.5.3.1.1.
(3-158) is a good structure for calculating the residual dynamics (chapter 3.5.4.3.1.2). For the Kalman gain calculation we have to rearrange (3-158) slightly by separating the process and measurement noise inputs.

$$\begin{aligned}\dot{\boldsymbol{x}}_{W,SP,CL} &= \boldsymbol{A}_{W,SP,CL}\boldsymbol{x}_{W,SP,CL} + \boldsymbol{B}_{W,SP,CL,k}q_{cmd} + \boldsymbol{B}_{W,SP,CL,\nu_P}\nu_P \\ \boldsymbol{y}_{W,SP,CL} &= \boldsymbol{C}_{W,SP,CL}\boldsymbol{x}_{W,SP,CL} + \boldsymbol{D}_{W,SP,CL,k}q_{cmd} + \boldsymbol{I}\boldsymbol{\nu}_M\end{aligned} \tag{3-161}$$

with

$$\boldsymbol{B}_{W,SP,CL,\nu_P} = \begin{bmatrix}\boldsymbol{B}_W \\ 0 \\ 0\end{bmatrix} \qquad \nu_P \sim \mathcal{N}\left(0, \Sigma_{\nu_P}\right)$$

$$\boldsymbol{\nu}_M = \begin{bmatrix}\nu_{M,q} \\ \nu_{M,\dot{q}}\end{bmatrix} \text{ with } \nu_{M,q} \sim \mathcal{N}\left(0, \Sigma_{\nu_{M,q}}\right),\ \nu_{M,\dot{q}} \sim \mathcal{N}\left(0, \Sigma_{\nu_{M,\dot{q}}}\right)$$

Thus the process noise covariance matrix is obtained by

$$\boldsymbol{\Sigma}_{\nu_P} = \boldsymbol{B}_{W,SP,CL,\nu_P}\Sigma_{\nu_p}\boldsymbol{B}_{W,SP,CL,\nu_P}^T \tag{3-162}$$

while the measurement noise covariance becomes

$$\boldsymbol{\Sigma}_{\nu_M} = \begin{bmatrix}\Sigma_{\nu_{M,q}} & 0 \\ 0 & \Sigma_{\nu_{M,\dot{q}}}\end{bmatrix} \tag{3-163}$$

For the steady state discrete time filter the gain can now be calculated by solving the Riccati equation for example using the function *dare* (The MathWorks Inc., 2017a, p. 2-183)

$$\begin{aligned}&\overline{\boldsymbol{A}}_{W,SP,CL}\overline{\boldsymbol{P}}\overline{\boldsymbol{A}}_{W,SP,CL}^{T}-\overline{\boldsymbol{P}}-\left(\overline{\boldsymbol{A}}_{W,SP,CL}\overline{\boldsymbol{P}}\overline{\boldsymbol{C}}_{W,SP,CL}^{T}\right)\\&\quad\cdot\left(\overline{\boldsymbol{C}}_{W,SP,CL}\overline{\boldsymbol{P}}\overline{\boldsymbol{C}}_{W,SP,CL}^{T}+\overline{\boldsymbol{\Sigma}}_{\nu_M}\right)^{-1}\left(\overline{\boldsymbol{C}}_{W,SP,CL}\overline{\boldsymbol{P}}\overline{\boldsymbol{A}}_{W,SP,CL}^{T}\right)+\overline{\boldsymbol{\Sigma}}_{\nu_P}\\&\quad=\boldsymbol{0}\end{aligned}\tag{3-164}$$

for $\overline{\boldsymbol{P}}$ and then the gain $\overline{\boldsymbol{L}}$ by

$$\overline{\boldsymbol{L}}=\left[\left(\overline{\boldsymbol{C}}_{W,SP,CL}\overline{\boldsymbol{P}}\overline{\boldsymbol{C}}_{W,SP,CL}^{T}+\overline{\boldsymbol{\Sigma}}_{\nu_M}\right)^{-1}\overline{\boldsymbol{C}}_{W,SP,CL}\overline{\boldsymbol{P}}\overline{\boldsymbol{A}}_{W,SP,CL}^{T}\right]^{T}\tag{3-165}$$

The dash on top marks the discrete time matrices. The system matrices are obtained by converting (3-161) into a discrete time system by standard system theory methods (cf. e.g. The MathWorks Inc., 2017a, p. 2-87). The residual dynamics will be introduced in chapter 3.5.4.3.1.2.

Remark 3-8: From system theory we know that the matrix $\boldsymbol{C}$ and $\boldsymbol{D}$ remain unaffected by the conversion from a continuous to a discrete time system, i.e. $=\overline{\boldsymbol{C}}$ $\boldsymbol{D}=\overline{\boldsymbol{D}}$, nevertheless to prevent confusion and possible traps the author clearly marks all matrices accordingly.

3.5.3.2 Residual Post Filter

Especially in view of a practical application a residual band-pass post filter has been added, to supress lower frequency dynamics (e.g. phugoid motion and steady state deviations) as well as higher frequency dynamics/noise (Remark 3-4, p. 99). Nevertheless the assumption that the band-pass filter mentioned is sufficient for a practical application has to be *verified* at some point.
The filter was obtained by a series connection of a DT1 high-pass and PT1 low-pass, i.e.

$$\boldsymbol{G}_{\check{r}\tilde{r}}(s)=\left[\frac{\frac{s}{\left(\frac{1}{\omega_{HP,q}}+1\right)\left(\frac{1}{\omega_{LP,q}}+1\right)}}{\frac{s}{\left(\frac{1}{\omega_{HP,\dot{q}}}+1\right)\left(\frac{1}{\omega_{LP,\dot{q}}}+1\right)}}\right]\tag{3-166}$$

(3-166) can be converted into a state space system and discrete time by standard system theoretical methods (cf. e.g. The MathWorks Inc., 2017a, p. 2-87 & 2-978).

The result is the discrete state space system

$$(\overline{\boldsymbol{A}}_{PF}, \overline{\boldsymbol{B}}_{PF}, \overline{\boldsymbol{C}}_{PF}, \overline{\boldsymbol{D}}_{PF}) \tag{3-167}$$

with $\overline{\boldsymbol{A}}_{PF} \in \mathbb{R}^{4x4}$, $\overline{\boldsymbol{B}}_{PF} \in \mathbb{R}^{4x2}$, $\overline{\boldsymbol{C}}_{PF} \in \mathbb{R}^{2x4}$, and $\overline{\boldsymbol{D}}_{PF} \in \mathbb{R}^{2x2}$ as well as output

$$\check{\boldsymbol{r}}(k) = \begin{bmatrix} \check{r}_q(k) \\ \check{r}_{\dot{q}}(k) \end{bmatrix}$$

and input

$$\tilde{\boldsymbol{r}}(k) = \begin{bmatrix} \tilde{r}_q(k) \\ \tilde{r}_{\dot{q}}(k) \end{bmatrix}$$

The transmission gain of the filter has been adjusted to achieve $\boldsymbol{K}_{PF} = [1 \quad 1]^T$ in the middle of the pass band.

3.5.3.3 Variance Scaling Filter

A peculiarity of the chi-square distribution, used for the stochastic FD threshold (Chapter 3.5.4.4), is that it assumes a unit variance for all of the m squared random variables. In our case the consequence is that we first of all have to ensure

$$Cov\big(\boldsymbol{r}(k)\big) = \boldsymbol{I} \tag{3-168}$$

This means that there is no cross-correlation between the elements of $\boldsymbol{r}(k)$ and all elements have *unit variance*. For the residual $\check{\boldsymbol{r}} \sim \mathcal{N}(\boldsymbol{\mu}_{\check{r}}, \overline{\boldsymbol{\Sigma}}_{\check{r}})$ we can achieve this goal by the use of a filter matrix $\overline{\boldsymbol{V}} \in \mathbb{R}^{2x2}$. The filter can be calculated by

$$\overline{\boldsymbol{V}} = \overline{\boldsymbol{\Sigma}}_{\check{r}}^{-\frac{\boldsymbol{1}}{\boldsymbol{2}}} \tag{3-169}$$

For discrete-time systems we can determine $\overline{\boldsymbol{\Sigma}}_{\check{r}}$ by solving the discrete Lyapunov equation (see e.g. The MathWorks Inc., 2017a, p. 2-153), for example using the function *dlyap* (The MathWorks Inc., 2017a, p. 2-195),

$$\overline{\boldsymbol{A}}_{r,\mathcal{V}_i} \overline{\boldsymbol{Q}} \overline{\boldsymbol{A}}_{r,\mathcal{V}_i}^{\boldsymbol{T}} - \overline{\boldsymbol{Q}} + \overline{\boldsymbol{B}}_{r,u,\mathcal{V}_i} \overline{\boldsymbol{\Sigma}}_{\boldsymbol{\nu}_{W,SP,CL}} \overline{\boldsymbol{B}}_{r,u,\mathcal{V}_i}^{\boldsymbol{T}} = \boldsymbol{0} \tag{3-170}$$

for the state-covariance $\overline{\boldsymbol{Q}}$ then calculating the output covariance $\overline{\boldsymbol{\Sigma}}_{\check{r},\mathcal{V}_i}$ by

$$\overline{\boldsymbol{\Sigma}}_{\check{r},\mathcal{V}_i} = \overline{\boldsymbol{C}}_{r,\mathcal{V}_i}\overline{\boldsymbol{Q}}\overline{\boldsymbol{C}}^{\boldsymbol{T}}_{r,\mathcal{V}_i} + \overline{\boldsymbol{D}}_{r,u,\mathcal{V}_i}\overline{\boldsymbol{\Sigma}}_{\boldsymbol{\nu}_{W,SP,CL}}\overline{\boldsymbol{D}}^{\boldsymbol{T}}_{r,u,\mathcal{V}_i} \tag{3-171}$$

The system matrices $r, \mathcal{V}_i$ are obtained from the residual dynamics (3-219) and (3-220) which will be introduced in chapter 3.5.4.3.1.2. The filtered residual $\boldsymbol{r}$

$$\boldsymbol{r}(k) = \overline{\boldsymbol{V}}_{r,\mathcal{V}_i}\check{\boldsymbol{r}}(k) \tag{3-172}$$

will then be uncorrelated and the elements have unit variance, i.e. $Cov\big(\boldsymbol{r}(k)\big) = \boldsymbol{I}$. As explained in chapter 3.4.4, such a filter is also used in the integrated norm-based/stochastic fault detection approach suggested by Ding (2013) *for deterministic unknown inputs* $\boldsymbol{d}$. As those inputs are *additive,* $\overline{\boldsymbol{\Sigma}}_{\check{\boldsymbol{r}}}$, and therefore the filter $\overline{\boldsymbol{V}}$, do not change because of $\boldsymbol{d}$**.** However in our case we have to deal with *deterministic model uncertainties*, thus $\overline{\boldsymbol{\Sigma}}_{\check{\boldsymbol{r}}}$ and the filter $\overline{\boldsymbol{V}}$ are influenced. As a consequence the approach suggested by Ding (2013) had to be modified by the author. As this aspect has to be debated together with the stochastic residual evaluation, the discussion is postponed to chapter 3.5.4.4.1.

3.5.4 Residual Evaluation

3.5.4.1 Important Relationships

We want to recall some relationships from chapter 3.4 that are extensively used through-out this chapter.

3.5.4.1.1 Signal Norms

For a general signal $\boldsymbol{u}$, according (3-78), the $\mathcal{L}_2$-norm or signal energy for an unlimited observation window is defined as

$$\|\boldsymbol{u}\|_{2,def} = \sqrt{\sum_{k=0}^{\infty} \boldsymbol{u}^T(k)\boldsymbol{u}(k)} \tag{3-173}$$

In the same manner we define according (3-80)

$$\|\boldsymbol{u}\|_2 = \sqrt{\sum_{k=1}^{N} \boldsymbol{u}^T(k)\boldsymbol{u}(k)} \tag{3-174}$$

for a limited observation window. The related RMS-signals (3-79) and (3-81) are also commonly used

$$\|\boldsymbol{u}\|_{RMS,def} = \sqrt{\frac{1}{N_{RMS}} \sum_{k=1}^{\infty} \boldsymbol{u}^T(k)\boldsymbol{u}(k)} = \frac{1}{\sqrt{N_{RMS}}} \|\boldsymbol{u}\|_{2,def} \tag{3-175}$$

$$\|\boldsymbol{u}\|_{RMS} = \sqrt{\frac{1}{N_{RMS}} \sum_{k=1}^{N_{RMS}} \boldsymbol{u}^T(k)\boldsymbol{u}(k)} = \frac{1}{\sqrt{N_{RMS}}} \|\boldsymbol{u}\|_2 \tag{3-176}$$

3.5.4.1.2 System Norms

Within this text the $\mathcal{L}_2$-Norm or RMS-Norm induced H_∞-Norm is used as introduced with (3-85)

$$\|\boldsymbol{G}\|_\infty = \sup_{\boldsymbol{u}\neq 0} \frac{\|\boldsymbol{y}\|_2}{\|\boldsymbol{u}\|_2} = \sup_{\boldsymbol{u}\neq 0} \frac{\|\boldsymbol{y}\|_{RMS}}{\|\boldsymbol{u}\|_{RMS}} = \sup_z \sigma_{max}\big(\boldsymbol{G}(z)\big) \tag{3-177}$$

where $\sigma_{max}(\boldsymbol{G})$ refers to the maximum singular value of $\boldsymbol{G}$. From engineering point of view it can be interpreted as the "maximum gain" of $\boldsymbol{G}$ for an LTI system.

3.5.4.1.3 Deterministic Threshold

From (3-177) we can define a deterministic threshold (cf. chapter 3.4.2.2) for an output signal $\boldsymbol{y}$ as

$$\begin{aligned} J_{th,2} &= \sup\|\boldsymbol{y}\|_2 = \left\|\boldsymbol{G}_{yu}\right\|_\infty \|\boldsymbol{u}\|_2 = \sqrt{N_{RMS}} \cdot \sup\|\boldsymbol{y}\|_{RMS} \\ &= \sqrt{N_{RMS}} \cdot \left\|\boldsymbol{G}_{yu}\right\|_\infty \|\boldsymbol{u}\|_{RMS} \end{aligned} \tag{3-178}$$

and likewise

$$\begin{aligned} J_{th,RMS} &= \sup\|\boldsymbol{y}\|_{RMS} = \left\|\boldsymbol{G}_{yu}\right\|_\infty \|\boldsymbol{u}\|_{RMS} = \frac{J_{th,2}}{\sqrt{N_{RMS}}} \\ &= \frac{\left\|\boldsymbol{G}_{yu}\right\|_\infty \|\boldsymbol{u}\|_2}{\sqrt{N_{RMS}}} \end{aligned} \tag{3-179}$$

3.5.4.2 Recursive Sliding Window RMS

Remark 3-9: Without loss of generality, from this point onward, we will use the squared norms as this is the form as this is the form that is required for integrated stochastic/deterministic fault detection system as it will be explained in chapter 3.5.4.4

The sliding window RMS algorithm used in this text utilizes a fixed window length N_{RMS} . From (3-174) it follows for a general signal $\boldsymbol{u}$

$$\|\boldsymbol{u}\|_2^2(k) = \sum_{n=k-N_{rms}+1}^{k} \boldsymbol{u}^T(n)\boldsymbol{u}(n) \tag{3-180}$$

This can be implemented recursively as

$$\|\boldsymbol{u}\|_2^2(k) = \|\boldsymbol{u}\|_2^2(k-1) + \boldsymbol{u}^T(k)\boldsymbol{u}(k) \\ -\boldsymbol{u}^T(k-N_{rms}+1)\boldsymbol{u}(k-N_{rms}+1) \tag{3-181}$$

For the RMS-signal we get with (3-176)

$$\|\boldsymbol{u}\|_{RMS}^2(k) = \frac{\|\boldsymbol{u}\|_2^2(k)}{N_{RMS}} \tag{3-182}$$

For this text we need two RMS-Signals. The first one is the residual RMS-value $\|\boldsymbol{r}\|_{RMS}^2$, the second one is the input RMS-signal, which in our case is $\|q_{cmd}\|_{RMS}^2$. Both are calculated according (3-181) and (3-182).

3.5.4.3 Deterministic Adaptive Threshold

3.5.4.3.1 Norm-based Threshold Computation for Systems Subject to Time-Invariant Polytopic Model Uncertainties

For aircraft the *desired* closed loop performance derived from the flying quality specifications like MIL-F-8785C (US DoD, 1996, p. 14) and MIL-STD-1797A (US DoD, 2004) is normally expressed as low-order linear dynamic systems (cf. chapter 2.2.2). For this work here we restrict ourselves to the longitudinal short period motion. In this case the desired closed-loop performance can be defined as linear second order system, thus the parameter space is two-dimensional.
As discussed in chapter 2.2.2, MIL-F-8785C (US DoD, 1996, p. 14) defines allowable CAP - ζ_{SP} combinations (cf. e.g. Figure 12, p. 35) and relates them to the three different levels of flying qualities (Table 2, p. 35). For a certain flight condition the allowable CAP area for a certain flying quality level can be, with the aid of (2-3), transformed into an allowable range of ω_{SP}. *Therefore, and this is of central importance to this work, the requirements for e.g. Level 1 flying qualities for the short period motion can be converted into a set of allowable values for* ω_{SP} *and* ζ_{SP}. The short period motion for a desired flying quality level can thus be explained as second-order system where the parameters damping ratio ζ_{SP} and natural frequency ω_{SP} shall stay within a certain polytope in parameter space. They can therefore be modelled as polytopic model uncertainties (cf. chapter 3.4.2.3.2).
The approach to use the flying quality derived CAP-ζ_{SP} combination to define a ω_{SP}-ζ_{SP} parameter polytope of acceptable model uncertainties and consequently derive the norm-based residual threshold based on this reference model was developed by the author and is, to the author's knowledge, new (cf. Contribution 3-3, p. 95)

3.5.4.3.1.1 Polytopic Parameterization of the Reference Model with Model Uncertainties

The overall goal of this chapter is to *parameterize the closed-loop plant dynamics as function of our model uncertainties* ω_{SP} and ζ_{SP} while at the same time *keeping a physically meaningful state space representation*. The former is required to establish the residual dynamics in chapter 3.5.4.3.1.2. The latter might initially look complicated but it finally enables a clear picture how ω_{SP} and ζ_{SP} affect the dynamics of the closed-loop plant.
As introductory example we want to define our second order short period reference model in observable canonical form, because this leads to cleaner system matrices. Later on we will choose a different state space realization that keeps physical meaningful states.
The system matrices $\boldsymbol{A}$ and $\boldsymbol{B}$ of a general PT2 element can be expressed as

$$\boldsymbol{A} = \begin{bmatrix} 0 & -\omega^2 \\ 1 & -2\zeta\omega \end{bmatrix} \tag{3-183}$$

and

$$\boldsymbol{B} = \begin{bmatrix} K_p\omega^2 \\ 0 \end{bmatrix} \tag{3-184}$$

where K_p is the proportional gain. By defining the two parameters

$$\boldsymbol{\delta} = \begin{bmatrix} \delta_1 \\ \delta_2 \end{bmatrix} = \begin{bmatrix} \zeta_{SP}\omega_{SP} \\ \omega_{SP}^2 \end{bmatrix} \tag{3-185}$$

this can be rendered into an affine problem with

$$\boldsymbol{A}(\boldsymbol{\delta}) = \begin{bmatrix} 0 & 0 \\ 1 & 0 \end{bmatrix} + \delta_1 \begin{bmatrix} 0 & 0 \\ 0 & -2 \end{bmatrix} + \delta_2 \begin{bmatrix} 0 & -1 \\ 0 & 0 \end{bmatrix} \tag{3-186}$$

$$\boldsymbol{B}(\boldsymbol{\delta}) = \begin{bmatrix} 0 \\ 0 \end{bmatrix} + \delta_1 \begin{bmatrix} 0 \\ 0 \end{bmatrix} + \delta_2 \begin{bmatrix} K_p \\ 0 \end{bmatrix} \tag{3-187}$$

Therefore ω_{SP} and ζ_{SP} fully define the allowable parameter space of δ_1 and δ_2.

While (3-186) and (3-187) are affine they are not polytopic as shown in Figure 29. Because of the definition of the parameters in (3-185), δ_2 depends quadratically on δ_1, thus the parameter space on the "left" and "right" side is bounded by a parabola instead of a straight line. Furthermore the "left" bound is not convex, therefore violating one of the underlying assumptions of polytopic systems.

Contribution 3-6: To overcome this problem, the author has chosen the approximated parameter polytope shown in Figure 29. In terms of the problem on hand, i.e. the aircraft longitudinal short period motion, this would mean that the set of allowable values for the damping ratio ζ_{SP} is slightly reduced. However it is ensured that the approximation stays in the area of the desired level of flying qualities, i.e. on the "safe side". To the author's knowledge using such an approach in the context of a flying quality model is also new.

Taking the example of Figure 29 it was assumed the allowable CAP for the actual flight conditions leads to an allowable ω_{SP} range between ω_{SP} = 2 rad/s and ω_{SP}= 4 rad/s, with a nominal, i.e. desired, $\omega_{SP,nom}$ = 3 rad/s. Furthermore, for Level 1 flying qualities, in Category A flight phases, MIL-F-8785C allows ζ_{SP} to vary between $\zeta_{SP} = 0.35$ and $\zeta_{SP} = 1.3$. The nominal damping ratio was selected as $\zeta_{SP,nom}$ = 0.707. We can now clearly see that the parameter polytope approximation chosen by the author ensures that ω_{SP} and ζ_{SP} remain inside the area for Level 1 flying qualities for this flight condition.

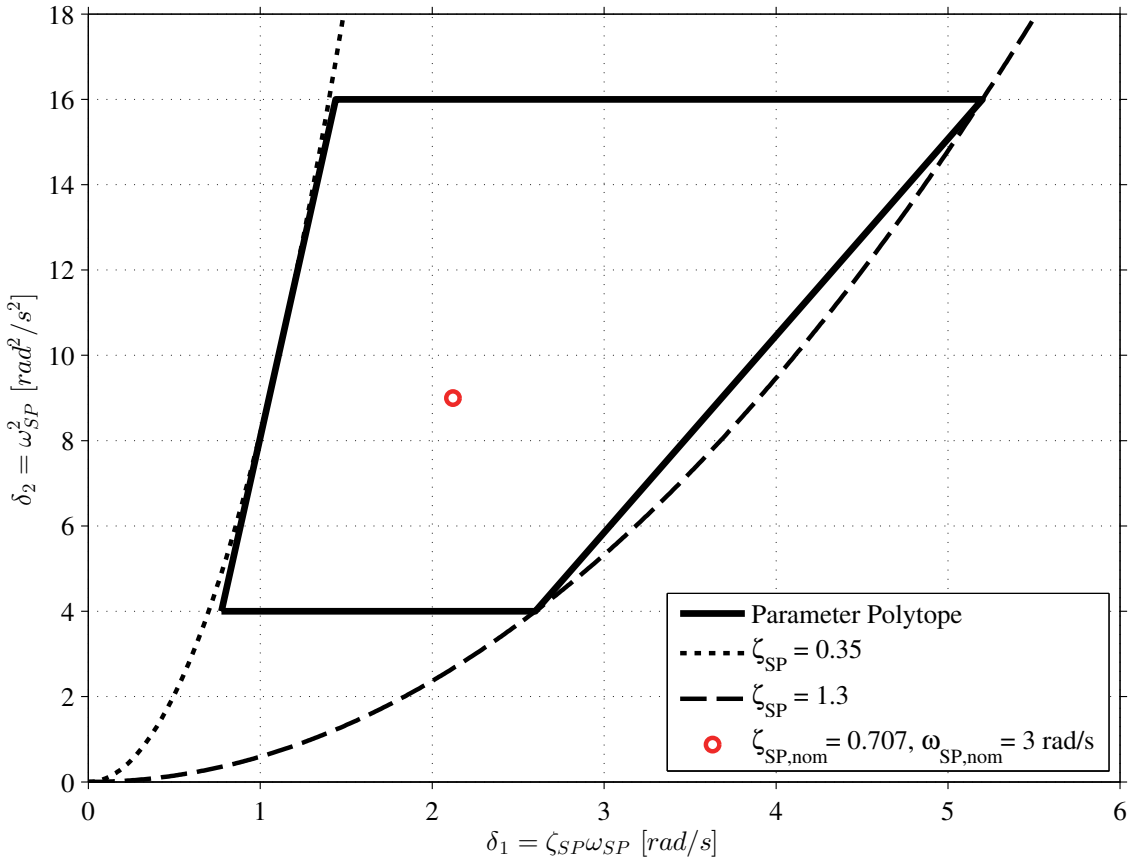

Figure 29 Example of acceptable short period parameter space with selected parameter polytope and nominal system

As said above the observable canonical form gives clear system matrices but leads to states without direct physical meaning. Furthermore above we have omitted the transmission zero that it is also important in a flying qualities context. We therefore want to see how we can parameterize the matrix $\boldsymbol{A}_{SP,OL}$ of the physical short period state space model (3-141) in terms of $\boldsymbol{\delta}$.

For the time being we assume $\boldsymbol{C}_{SP,OL} = \boldsymbol{I}$ and $\boldsymbol{D}_{SP,OL} = \boldsymbol{0}$. Therefore we get

$$\begin{aligned} \dot{\boldsymbol{x}}_{SP,OL} &= \boldsymbol{A}_{SP,OL}\boldsymbol{x}_{SP,OL} + \boldsymbol{B}_{SP,OL}\eta \\ \boldsymbol{y}_{SP,OL} &= \boldsymbol{x}_{SP,OL} \end{aligned} \tag{3-188}$$

with

$$\boldsymbol{A}_{SP,OL} = \begin{bmatrix} M_q & M_\alpha \\ Z_q + 1 & Z_\alpha \end{bmatrix} \quad \boldsymbol{B}_{SP,OL} = \begin{bmatrix} M_\eta \\ Z_\eta \end{bmatrix} \qquad \boldsymbol{C}_{SP} = \boldsymbol{I} \qquad \boldsymbol{D}_{SP} = \boldsymbol{0}$$
$$\boldsymbol{x}_{SP,OL} = \begin{bmatrix} q_K \\ \alpha_K \end{bmatrix}$$

This problem can be most easily approached in the frequency domain. By the aid of (3-7) we transform (3-188) in the transfer matrix

$$\boldsymbol{G}_{SP,OL}(s) = \begin{bmatrix} \dfrac{M_\eta s + M_\alpha Z_\eta - M_\eta Z_\alpha}{N(s)} \\ \dfrac{Z_\eta s + M_\eta + M_\eta Z_q - M_q Z_\eta}{N(s)} \end{bmatrix} \tag{3-189}$$

With the common nominator

$$N_{SP,OL}(s) = s^2 + \left(-M_q - Z_\alpha\right)s + \left(-M_\alpha - M_\alpha Z_q + M_q Z_\alpha\right) \tag{3-190}$$

From system theory we know that the numerator of a T2 element is

$$N_{T2}(s) = s^2 + 2\zeta\omega s + \omega^2 \tag{3-191}$$

Therefore by inspection of (3-190) we get

$$\omega_{SP}^2 = -M_\alpha - M_\alpha Z_q + M_q Z_\alpha = -M_\alpha\left(1 + Z_q\right) + M_q Z_\alpha \tag{3-192}$$

$$\zeta_{SP}\omega_{SP} = \frac{-M_q - Z_\alpha}{2} \tag{3-193}$$

$$M_q = -2\zeta_{SP}\omega_{SP} - Z_\alpha \tag{3-194}$$

$$\begin{aligned} M_\alpha &= -\frac{\omega_{SP}^2 - M_q Z_\alpha}{(1+Z_q)} = \frac{-\omega_{SP}^2}{(1+Z_q)} + \frac{(-2\zeta_{SP}\omega_{SP} - Z_\alpha)Z_\alpha}{(1+Z_q)} \\ &= \frac{-\omega_{SP}^2}{(1+Z_q)} + \frac{-2\zeta_{SP}\omega_{SP}Z_\alpha}{(1+Z_q)} + \frac{-Z_\alpha^2}{(1+Z_q)} \end{aligned} \tag{3-195}$$

With (3-194) and (3-195), the matrix $\boldsymbol{A}_{SP,OL}$ of (3-141) can be written as

$$\boldsymbol{A}_{SP,OL} = \begin{bmatrix} -2\zeta_{SP}\omega_{SP} - Z_\alpha & -\frac{\omega_{SP}^2 - (-2\zeta_{SP}\omega_{SP} - Z_\alpha)Z_\alpha}{(1+Z_q)} \\ Z_q + 1 & Z_\alpha \end{bmatrix} \tag{3-196}$$

Furthermore $\boldsymbol{A}_{SP,OL}$ can be parameterized as

$$\boldsymbol{A}_{SP,OL}(\boldsymbol{\delta}) = \boldsymbol{A}_{SP,OL,0} + \delta_1 \boldsymbol{A}_{SP,OL,1} + \delta_2 \boldsymbol{A}_{SP,OL,2} \tag{3-197}$$

with

$$\boldsymbol{A}_{SP,OL,0} = \begin{bmatrix} -Z_\alpha & \frac{-Z_\alpha^2}{(1+Z_q)} \\ Z_q + 1 & Z_\alpha \end{bmatrix} \qquad \boldsymbol{A}_{SP,OL,1} = \begin{bmatrix} -2 & \frac{-2Z_\alpha}{(1+Z_q)} \\ 0 & 0 \end{bmatrix}$$

$$\boldsymbol{A}_{SP,OL,2} = \begin{bmatrix} 0 & \frac{-1}{(1+Z_q)} \\ 0 & 0 \end{bmatrix}$$

For our purpose (3-197) is not yet sufficient. As explained in chapter 2.2 for modern statically unstable aircraft designs we can only achieve the desired short period characteristics, i.e. ω_{SP} and ζ_{SP}, with the aid of a FCS. Even without considering the additional influence of certain FCS elements, e.g. actuator dynamics, time delays, (3-196) will look differently for an open-loop unstable aircraft with feedback control than for an open-loop stable aircraft, even if both achieve the same ω_{SP} and ζ_{SP}.

The closed-loop aircraft short period system is given by (3-144). We furthermore define

$$M_{q,CL} = M_{q,OL} - K_q M_\eta \tag{3-198}$$

$$M_{\alpha,CL} = M_{\alpha,OL} - K_\alpha M_\eta \tag{3-199}$$

$$Z_{\alpha,CL} = Z_{\alpha,OL} - K_\alpha Z_\eta \tag{3-200}$$

$$Z_{q,CL} = Z_{q,OL} - K_q Z_\eta \tag{3-201}$$

Our goal is that $M_{q,CL}$ and $M_{\alpha,CL}$ follow (3-194) and (3-195). Thus we have

$$M_{q,CL} = -2\zeta_{SP}\omega_{SP} - Z_{\alpha,CL} \tag{3-202}$$

$$M_{\alpha,CL} = -\frac{\omega_{SP}^2 - M_{q,CL}Z_{\alpha,CL}}{\left(1 + Z_{q,CL}\right)} \tag{3-203}$$

It follows that (3-197) becomes

$$\boldsymbol{A}_{SP,CL}(\boldsymbol{\delta}) = \boldsymbol{A}_{SP,CL,0} + \delta_1 \boldsymbol{A}_{SP,CL,1} + \delta_2 \boldsymbol{A}_{SP,CL,2} \tag{3-204}$$

with

$$\boldsymbol{A}_{SP,CL,0} = \begin{bmatrix} -Z_{\alpha,CL} & \frac{-Z_{\alpha,CL}^2}{\left(1 + Z_{q,CL}\right)} \\ Z_{q,CL} + 1 & Z_{\alpha,CL} \end{bmatrix} = \begin{bmatrix} -\left(Z_{\alpha,OL} - K_\alpha Z_\eta\right) & \frac{-\left(Z_{\alpha,OL} - K_\alpha Z_\eta\right)^2}{Z_{q,OL} - K_q Z_\eta + 1} \\ Z_{q,OL} - K_q Z_\eta + 1 & Z_{\alpha,OL} - K_\alpha Z_\eta \end{bmatrix}$$

$$\boldsymbol{A}_{SP,CL,1} = \begin{bmatrix} -2 & \frac{-2Z_{\alpha,CL}}{\left(1 + Z_{q,CL}\right)} \\ 0 & 0 \end{bmatrix} = \begin{bmatrix} -2 & \frac{-2\left(Z_{\alpha,OL} - K_\alpha Z_\eta\right)}{Z_{q,OL} - K_q Z_\eta + 1} \\ 0 & 0 \end{bmatrix}$$

$$\boldsymbol{A}_{SP,CL,2} = \begin{bmatrix} 0 & \frac{-1}{\left(1 + Z_{q,CL}\right)} \\ 0 & 0 \end{bmatrix} = \begin{bmatrix} 0 & \frac{-1}{Z_{q,OL} - K_q Z_\eta + 1} \\ 0 & 0 \end{bmatrix}$$

In a last step we want to see how we can parameterize the combined *wind* and *closed-loop aircraft short period* system (3-158) in terms of $\boldsymbol{\delta}$. This system is required to establish the residual dynamics as function of the polytopic model uncertainties. The im-

portant point to consider here is that the wind system couples with the aircraft short period system via the *open-loop* $M_{\alpha,OL}$ and $Z_{\alpha,OL}$ and *not* the *closed-loop* $M_{\alpha,CL}$ and $Z_{\alpha,CL}$ (cf. Brockhaus et al., 2011, p. 827).

Let us start with substituting (3-202) in (3-203)

$$\begin{aligned} M_{\alpha,CL} &= -\frac{\omega_{SP}^2 - \left(-2\zeta_{SP}\omega_{SP} - Z_{\alpha,CL}\right)Z_{\alpha,CL}}{\left(1 + Z_{q,CL}\right)} \\ &= -\frac{\omega_{SP}^2}{\left(1 + Z_{q,CL}\right)} + \frac{2\zeta_{SP}\omega_{SP}Z_{\alpha,CL}}{\left(1 + Z_{q,CL}\right)} + \frac{Z_{\alpha,CL}^2}{\left(1 + Z_{q,CL}\right)} \end{aligned} \tag{3-205}$$

Now we substitute (3-200) and (3-201)

$$\begin{aligned} M_{\alpha,CL} &= -\frac{\omega_{SP}^2}{\left(1 + Z_{q,OL} - K_q Z_\eta\right)} \\ &+ \frac{2\zeta_{SP}\omega_{SP}\left(Z_{\alpha,OL} - K_\alpha Z_\eta\right)}{\left(1 + Z_{q,OL} - K_q Z_\eta\right)} + \frac{\left(Z_{\alpha,OL} - K_\alpha Z_\eta\right)^2}{\left(1 + Z_{q,OL} - K_q Z_\eta\right)} \end{aligned} \tag{3-206}$$

Finally, with (3-199), we have

$$\begin{aligned} M_{\alpha,OL} &= M_{\alpha,CL} + K_\alpha M_\eta \\ &= -\frac{\omega_{SP}^2}{\left(1 + Z_{q,OL} - K_q Z_\eta\right)} + \frac{2\zeta_{SP}\omega_{SP}\left(Z_{\alpha,OL} - K_\alpha Z_\eta\right)}{\left(1 + Z_{q,OL} - K_q Z_\eta\right)} \\ &+ \frac{\left(Z_{\alpha,OL} - K_\alpha Z_\eta\right)^2}{\left(1 + Z_{q,OL} - K_q Z_\eta\right)} + K_\alpha M_\eta \end{aligned} \tag{3-207}$$

From (3-158) we get

$$\boldsymbol{A}_{W,SP,CL} = \begin{bmatrix} & \boldsymbol{A}_W & 0 & 0 \\ & & 0 & 0 \\ 0 & -M_{\alpha,OL} & & \\ 0 & -Z_{\alpha,OL} & \boldsymbol{A}_{SP,CL} & \end{bmatrix}$$

which can be parameterized as affine matrix

$$\boldsymbol{A}_{W,SP,CL}(\boldsymbol{\delta}) = \boldsymbol{A}_{W,SP,CL,0} + \delta_1 \boldsymbol{A}_{W,SP,CL1} + \delta_2 \boldsymbol{A}_{W,SP,CL,2} \tag{3-208}$$

with

$$\boldsymbol{A}_{W,SP,CL,0} = \begin{bmatrix} \boldsymbol{A}_W & \begin{matrix} 0 & 0 \\ 0 & 0 \end{matrix} \\ \begin{matrix} 0 \\ 0 \end{matrix} & \begin{matrix} \dfrac{\left(Z_{\alpha,OL} - K_\alpha Z_\eta\right)^2}{\left(1 + Z_{q,OL} - K_q Z_\eta\right)} - K_\alpha M_\eta \\ -Z_{\alpha,OL} \end{matrix} & \boldsymbol{A}_{SP,CL,0} \end{bmatrix}$$

$$\boldsymbol{A}_{W,SP,CL,1} = \begin{bmatrix} \begin{matrix} 0 & 0 \\ 0 & 0 \end{matrix} & \begin{matrix} 0 & 0 \\ 0 & 0 \end{matrix} \\ \begin{matrix} 0 \\ 0 \end{matrix} & \begin{matrix} \dfrac{2\left(Z_{\alpha,OL} - K_\alpha Z_\eta\right)}{\left(1 + Z_{q,OL} - K_q Z_\eta\right)} \\ 0 \end{matrix} & \boldsymbol{A}_{SP,CL,1} \end{bmatrix}$$

$$\boldsymbol{A}_{W,SP,CL,2} = \begin{bmatrix} \begin{matrix} 0 & 0 \\ 0 & 0 \end{matrix} & \begin{matrix} 0 & 0 \\ 0 & 0 \end{matrix} \\ \begin{matrix} 0 \\ 0 \end{matrix} & \begin{matrix} \dfrac{1}{\left(1 + Z_{q,OL} - K_q Z_\eta\right)} \\ 0 \end{matrix} & \boldsymbol{A}_{SP,CL,2} \end{bmatrix}$$

From (3-158) we know that the matrix $\boldsymbol{C}_{W,SP,CL}$ depends on the matrix $\boldsymbol{A}_{W,SP,CL}$ because we require the state derivative $\dot{\boldsymbol{q}}_K$ in the output equation. We had

$$\boldsymbol{C}_{W,SP,CL} = \begin{bmatrix} 0 & 0 & 1 & 0 \\ \boldsymbol{A}_{W,SP,CL}(3,:) \end{bmatrix}$$

Thus it immediately follows that we can say

$$\boldsymbol{C}_{W,SP,CL}(\boldsymbol{\delta}) = \boldsymbol{C}_{W,SP,CL,0} + \delta_1 \boldsymbol{C}_{W,SP,CL,k,1} + \delta_2 \boldsymbol{C}_{W,SP,CL,2} \qquad (3\text{-}209)$$

with

$$\boldsymbol{C}_{W,SP,CL,0} = \begin{bmatrix} 0 & 0 & 1 & 0 \\ \boldsymbol{A}_{W,SP,CL,0}(3,:) \end{bmatrix} \qquad \boldsymbol{C}_{W,SP,CL,1} = \begin{bmatrix} 0 & 0 & 0 & 0 \\ \boldsymbol{A}_{W,SP,CL,1}(3,:) \end{bmatrix}$$

$$\boldsymbol{C}_{W,SP,CL,2} = \begin{bmatrix} 0 & 0 & 0 & 0 \\ \boldsymbol{A}_{W,SP,CL,2}(3,:) \end{bmatrix}$$

The matrices $\boldsymbol{B}_{W,SP,CL,k}$, $\boldsymbol{B}_{W,SP,CL,u}$, $\boldsymbol{D}_{W,SP,CL,k}$, and $\boldsymbol{D}_{W,SP,CL,u}$ according (3-158) do not depend on ζ_{SP} and ω_{SP}.We are now in a position to attack our final goal of setting up the residual dynamics as function of the parameters ω_{SP} and ζ_{SP}.

3.5.4.3.1.2 Residual Dynamics

In the last chapter we have parameterized system W, SP, CL as function of $\boldsymbol{\delta}$, i.e. ω_{SP} and ζ_{SP}. We found that the $\boldsymbol{\delta}$-dependend matrices are $\boldsymbol{A}_{W,SP,CL}$ (3-208) and $\boldsymbol{C}_{W,SP,CL}$ (3-209). The nominal system is given by (3-158). Using (3-185) we can calculate the parameter $\boldsymbol{\delta}_{\mathcal{V}_i}$ for vertex $\mathcal{V}_i$ of our four vertices, i.e. $i = \{1,2,3,4\}$.

$$\boldsymbol{\delta}_{\mathcal{V}_i} = \begin{bmatrix} \delta_{\mathcal{V}_i} \\ \delta_{\mathcal{V}_i} \end{bmatrix} = \begin{bmatrix} \tilde{\zeta}_{SP,\mathcal{V}_i}\omega_{SP,\mathcal{V}_i} \\ \omega^2_{SP,\mathcal{V}_i} \end{bmatrix} \tag{3-210}$$

where $\tilde{\zeta}_{SP,\mathcal{V}_i}$ denotes the damping ratio of the polytope approximation as explained at the beginning of chapter 3.5.4.3.1.1. Now using (3-208) we get

$$\boldsymbol{A}_{W,SP,CL,\mathcal{V}_i}(\boldsymbol{\delta}_{nom}) = \boldsymbol{A}_{W,SP,CL,0} + \delta_{1,\mathcal{V}_i}\boldsymbol{A}_{W,SP,CL1} + \delta_{2,\mathcal{V}_i}\boldsymbol{A}_{W,SP,CL,2} \tag{3-211}$$

and with (3-209)

$$\boldsymbol{C}_{W,SP,CL,\mathcal{V}_i}(\boldsymbol{\delta}) = \boldsymbol{C}_{W,SP,CL,0} + \delta_{1,\mathcal{V}_i}\boldsymbol{C}_{W,SP,CL,1} + \delta_{2,\mathcal{V}_i}\boldsymbol{C}_{W,SP,CL,2} \tag{3-212}$$

Thus for every vertex we get a state space system

$$\left(\boldsymbol{A}_{W,SP,CL,\mathcal{V}_i},\ [\boldsymbol{B}_{W,SP,CL,k} \quad \boldsymbol{B}_{W,SP,CL,u}],\ \boldsymbol{C}_{W,SP,CL,\mathcal{V}_i},\ [\boldsymbol{D}_{W,SP,CL,k} \quad \boldsymbol{D}_{W,SP,CL,u}]\right)_{W,SP,CL,\mathcal{V}_i}$$

We convert those four systems as well as the nominal system (3-158)

$$\left(\boldsymbol{A}_{W,SP,CL},\ [\boldsymbol{B}_{W,SP,CL,k} \quad \boldsymbol{B}_{W,SP,CL,u}],\ \boldsymbol{C}_{W,SP,CL},\ [\boldsymbol{D}_{W,SP,CL,k} \quad \boldsymbol{D}_{W,SP,CL,u}]\right)_{W,SP,CL}$$

into a discrete time system by standard system theory methods (cf. e.g. The MathWorks Inc., 2017a, p. 2-87).

Using the resulting *discrete time* matrices (marked by a dash on top) we get

$$\Delta\overline{\boldsymbol{A}}_{W,SP,CL,\mathcal{V}_i} = \overline{\boldsymbol{A}}_{W,SP,CL,\mathcal{V}_i} - \overline{\boldsymbol{A}}_{W,SP,CL} \tag{3-213}$$

$$\Delta\overline{\boldsymbol{B}}_{W,SP,CL,k,\mathcal{V}_i} = \overline{\boldsymbol{B}}_{W,SP,CL,k,\mathcal{V}_i} - \overline{\boldsymbol{B}}_{W,SP,CL,k} \tag{3-214}$$

$$\Delta\overline{\boldsymbol{B}}_{W,SP,CL,u,\mathcal{V}_i} = \overline{\boldsymbol{B}}_{W,SP,CL,u,\mathcal{V}_i} - \overline{\boldsymbol{B}}_{W,SP,CL,u} \tag{3-215}$$

$$\Delta\overline{\boldsymbol{C}}_{W,SP,CL,\mathcal{V}_i} = \overline{\boldsymbol{C}}_{W,SP,CL,\mathcal{V}_i} - \overline{\boldsymbol{C}}_{W,SP,CL} \tag{3-216}$$

$$\Delta\overline{\boldsymbol{D}}_{W,SP,CL,k,\mathcal{V}_i} = \overline{\boldsymbol{D}}_{W,SP,CL,k,\mathcal{V}_i} - \overline{\boldsymbol{D}}_{W,SP,CL,k} \tag{3-217}$$

$$\Delta\overline{\boldsymbol{D}}_{W,SP,CL,u,\mathcal{V}_i} = \overline{\boldsymbol{D}}_{W,SP,CL,u,\mathcal{V}_i} - \overline{\boldsymbol{D}}_{W,SP,CL,u} \tag{3-218}$$

The residual dynamics for the residual subject to stochastic and deterministic unknown inputs as well as model uncertainties has been derived in chapter 3.3.5. For the calculation of the maximum gain, which will be discussed in the next chapter, we need to consider the boundary case with no faults present, i.e. $\boldsymbol{f} = \boldsymbol{0}$. Furthermore in our case, we do not have deterministic unknown inputs and therefore also $\boldsymbol{d} = \boldsymbol{0}$. Finally we also have to include the variance scaling filter (matrix) $\overline{\boldsymbol{V}}_{r,\mathcal{V}_i}$ according (3-169) into the output equation. Using (3-71), (3-72), and (3-169) we get

$$\begin{aligned}\boldsymbol{x}_{r,\mathcal{V}_i}(k+1) &\\ = \boldsymbol{A}_{r,\mathcal{V}_i}\boldsymbol{x}_{r,\mathcal{V}_i}(k) &+ \boldsymbol{B}_{r,k,\mathcal{V}_i}q_{cmd}(k) + \boldsymbol{B}_{r,u,\mathcal{V}_i}\boldsymbol{\nu}_{W,SP,CL}(k)\end{aligned} \tag{3-219}$$

$$\begin{aligned}\boldsymbol{r}_{\mathcal{V}_i}(k) &\\ = \overline{\boldsymbol{V}}_{r,\mathcal{V}_i}\big[\boldsymbol{C}_{r,\mathcal{V}_i}\boldsymbol{x}_{r,\mathcal{V}_i}(k) &+ \boldsymbol{D}_{r,k,\mathcal{V}_i}q_{cmd}(k) + \boldsymbol{D}_{r,u,\mathcal{V}_i}\boldsymbol{\nu}_{W,SP,CL}(k)\big]\end{aligned} \tag{3-220}$$

with

$$\boldsymbol{A}_{r,\mathcal{V}_i} = \begin{bmatrix} \overline{\boldsymbol{A}}_{W,SP,CL} + \Delta\overline{\boldsymbol{A}}_{W,SP,CL,\mathcal{V}_i} & \boldsymbol{0} & \boldsymbol{0} \\ \Delta\overline{\boldsymbol{A}}_{W,SP,CL,\mathcal{V}_i} - \boldsymbol{L}\Delta\overline{\boldsymbol{C}}_{W,SP,CL,\mathcal{V}_i} & \overline{\boldsymbol{A}}_{W,SP,CL} - \boldsymbol{L}\overline{\boldsymbol{C}}_{W,SP,CL} & \boldsymbol{0} \\ \overline{\boldsymbol{B}}_{PF}\Delta\overline{\boldsymbol{C}}_{W,SP,CL,\mathcal{V}_i} & \overline{\boldsymbol{B}}_{PF}\overline{\boldsymbol{C}}_{W,SP,CL} & \overline{\boldsymbol{A}}_{PF} \end{bmatrix}$$

$$\boldsymbol{B}_{r,k,\mathcal{V}_i} = \begin{bmatrix} \overline{\boldsymbol{B}}_{W,SP,CL,k} + \Delta\overline{\boldsymbol{B}}_{W,SP,CL,k,\mathcal{V}_i} \\ \Delta\overline{\boldsymbol{B}}_{W,SP,CL,k,\mathcal{V}_i} - \boldsymbol{L}\Delta\overline{\boldsymbol{D}}_{W,SP,CL,k,\mathcal{V}_i} \\ \boldsymbol{B}_{PF}\Delta\overline{\boldsymbol{D}}_{W,SP,CL,k,\mathcal{V}_i} \end{bmatrix}$$

$$\boldsymbol{B}_{r,u,\mathcal{V}_i} = \begin{bmatrix} \overline{\boldsymbol{B}}_{W,SP,CL,u} + \Delta\overline{\boldsymbol{B}}_{W,SP,CL,u,\mathcal{V}_i} \\ \left(\overline{\boldsymbol{B}}_{W,SP,CL,u} + \Delta\overline{\boldsymbol{B}}_{W,SP,CL,u,\mathcal{V}_i}\right) - \boldsymbol{L}\left(\overline{\boldsymbol{D}}_{W,SP,CL,u} + \Delta\overline{\boldsymbol{D}}_{W,SP,CL,u,\mathcal{V}_i}\right) \\ \boldsymbol{B}_{PF}\left(\overline{\boldsymbol{D}}_{W,SP,CL,u} + \Delta\overline{\boldsymbol{D}}_{W,SP,CL,u,\mathcal{V}_i}\right) \end{bmatrix}$$

$$\boldsymbol{C}_r = \begin{bmatrix} \overline{\boldsymbol{D}}_{PF}\Delta\overline{\boldsymbol{C}}_{W,SP,CL,\mathcal{V}_i} & \overline{\boldsymbol{D}}_{PF}\overline{\boldsymbol{C}}_{W,SP,CL} & \overline{\boldsymbol{C}}_{PF} \end{bmatrix}$$

$$\boldsymbol{D}_{r,k,\mathcal{V}_i} = \overline{\boldsymbol{D}}_{PF}\Delta\overline{\boldsymbol{D}}_{W,SP,CL,k,\mathcal{V}_i} \qquad \boldsymbol{D}_{r,u,\mathcal{V}_i} = \overline{\boldsymbol{D}}_{PF}\left(\overline{\boldsymbol{D}}_{W,SP,CL,u} + \Delta\overline{\boldsymbol{D}}_{W,SP,CL,u,\mathcal{V}_i}\right)$$

$$\boldsymbol{x}_{r,\mathcal{V}_i} = \begin{bmatrix} \boldsymbol{x}_{W,SP,CL} \\ \boldsymbol{e} \\ \boldsymbol{x}_{PF} \end{bmatrix} \qquad \boldsymbol{x}_{r,\mathcal{V}_i}(0) = \begin{bmatrix} \boldsymbol{x}_{W,SP,CL,0} \\ \boldsymbol{e}_0 \\ \boldsymbol{x}_{PF,0} \end{bmatrix} \qquad \boldsymbol{r}_{\mathcal{V}_i} = \begin{bmatrix} r_q \\ r_{\dot{q}} \end{bmatrix}$$

$$\boldsymbol{\nu}_{W,SP,CL} = \begin{bmatrix} \nu_P \\ \nu_{M,q} \\ \nu_{M,\dot{q}} \end{bmatrix} \text{ with } \nu_P \sim \mathcal{N}\left(0, \Sigma_{\nu_P}\right), \nu_{M,q} \sim \mathcal{N}\left(0, \Sigma_{\nu_{M,q}}\right), \nu_{M,\dot{q}} \sim \mathcal{N}\left(0, \Sigma_{\nu_{M,\dot{q}}}\right)$$

In chapter 3.5.3.3 we used the variance matrix $\boldsymbol{\Sigma}_{\boldsymbol{\nu}_{W,SP,CL}}$ which is obtained by

$$\boldsymbol{\Sigma}_{\boldsymbol{\nu}_{W,SP,CL}} = \begin{bmatrix} \Sigma_{\nu_P} & 0 & 0 \\ 0 & \Sigma_{\nu_{M,q}} & 0 \\ 0 & 0 & \Sigma_{\nu_{M,\dot{q}}} \end{bmatrix}$$

3.5.4.3.1.3 Deterministic Threshold with Polytopic Model Uncertainties

With (3-219) and (3-220) we have properly defined our residual dynamics with *stochastic unknown inputs* and *deterministic polytopic model uncertainties*. In this chapter we want to discuss how to obtain a bound on the maximum gain of $\boldsymbol{G}_{rq_{cmd}}$ i.e. loosely speaking the "worst-case" gain due to the acceptable deviations from the nominal system (model uncertainties). If the gain $\mathcal{K}_{\boldsymbol{G}_{rq_{cmd}}}$ of all other systems described by the parameter polytope is smaller than $\mathcal{K}_{\boldsymbol{G}_{rq_{cmd}},max}$ we can calculate the deterministic threshold $J^2_{th,RMS}$ by

$$J^2_{th,RMS} = \sup_{\boldsymbol{f}=\boldsymbol{0},\boldsymbol{\Delta}\neq\boldsymbol{0}} \|\boldsymbol{r}\|^2_{RMS} = \mathcal{K}^2_{\boldsymbol{G}_{rq_{cmd}},max} \, \|q_{cmd}\|^2_{RMS} \tag{3-221}$$

There are three possible approaches to this problem. The first on is the *quadratic stability* approach that leads to an upper bound on the worst case gain $\mathcal{K}_{\boldsymbol{G}_{rq_{cmd}},max}$ for *time-varying* LPV systems with *arbitrary fast varying* parameters $\boldsymbol{\delta}$, i.e. $\dot{\boldsymbol{\delta}} \to \infty$ (cf.

chapter 3.4.2.3.3). While this is for sure a powerful theoretical result, in our practical aircraft application we have to consider three things:

- The gains calculated by this approach are *very conservative*, i.e. they become *very large*. Therefore the fault detection performance for all cases where $\dot{\boldsymbol{\delta}} < \infty$ is significantly reduced. Actually the author's experience is that the gains obtained are useless in a practical aircraft fault detection problem.
- Arbitrary fast varying parameters constitute a dynamic in itself, that is for sure not in line with our flying quality requirements of specifications MIL-F-8785C (US DoD, 1996, p. 14) and MIL-STD-1797A (US DoD, 2004).
- At fault (damage) occurrence the parameters are potentially heavily time varying but this is a case we *for sure want to detect*. Treating those time variations as normal parameter variations that occur during normal (fault-free) operations would be contradictory to our fault detection goal.

The approach was initially followed by the author but then discarded due to those three reasons.
The second approach, finally chosen by the author, is to assume uncertain but time-invariant parameters $\boldsymbol{\delta}$, i.e. $\dot{\boldsymbol{\delta}} \cong \mathbf{0}$. This solved the three problems mentioned above. Nevertheless there is an important assumption in using this approach. Clearly in an aircraft context the parameters $\boldsymbol{\delta}$ *slowly vary* under fault-free operations with the flight condition. The assumption made is that the dynamics of these slowly varying parameters $\boldsymbol{\delta}$ is *insignificant*. A similar assumption is made for nearly all gain-scheduled CFCS, i.e. closed-loop aircraft systems, used in production aircraft. Therefore it is reasonable to assume that it is also an acceptable assumption in our case. Nevertheless as for gain scheduled CFCS a strict theoretical treatment would be desirable.
This brings us to the third approach, which, to the author's opinion, should be investigated in a follow on work.

Further Work 3-1: In systems theory the concept of *robust stability* was developed which assumes bounds on the parameter change rates $\dot{\boldsymbol{\delta}}$. It contains the case of *time-invariant* parameters ($\dot{\boldsymbol{\delta}} = \mathbf{0}$) and *arbitrary fast time-varying parameters* ($\dot{\boldsymbol{\delta}} \to \infty$) as special cases (cf. e.g. Scherer & Weiland, 2016, pp. 9/25-13/25) and potentially offers the possibility of a strict theoretical treatment of *slowly varying* parameters $\boldsymbol{\delta}$ under fault-free operations in our fault detection context. Nevertheless to derive bounds on the parameter rates $\dot{\boldsymbol{\delta}}$ for the aircraft under fault-free operation is potentially also not straight forward and requires careful analysis of all fault-free operation conditions.

Finally we come to the goal of this chapter, i.e. how to calculate a deterministic residual threshold for fault detection. The fact that we used an uncertain but time-invariant system allows us to calculate the maximum gain $\mathcal{K}_{\boldsymbol{G}_{rq_{cmd}},max}$ using the H_∞-norm. Remains the question for which system described by the parameter polytope the maximum gain $\left\|\boldsymbol{G}_{rq_{cmd}}\right\|^2_{\infty,max}$ is found. Inspired by the idea of *robust stability,* that contains the approach $\dot{\boldsymbol{\delta}} \cong \mathbf{0}$ as special case, the author deducted that the $\left\|\boldsymbol{G}_{rq_{cmd}}\right\|^2_{\infty,max}$ is found at one of the vertices $\mathcal{V}_i$. While the author is not able to provide a strict theoretical proof it has been verified, for the fault detection system of this text, by simulation in chapter 4.3.2.1.

Further Work 3-2: While it has been verified by simulation in chapter 4.3.2.1, it would be desirable to provide a strict theoretical proof that the maximum gain $\left\|\boldsymbol{G}_{rq_{cmd}}\right\|^2_{\infty,max}$, for the fault detection system of this text, is found at one of the vertices $\mathcal{V}_i$.

For the integrated stochastic/deterministic fault detection we will require $J^2_{th,2}$ and $J^2_{th,RMS}$. Using (3-178) and (3-179) and the considerations made above we get

$$\begin{aligned} J^2_{th,2} &= \sup_{\boldsymbol{f}=\mathbf{0},\boldsymbol{\Delta}\neq\mathbf{0}} \|\boldsymbol{r}\|_2^2 = \left\|\boldsymbol{G}_{rq_{cmd}}\right\|^2_{\infty,max} \|q_{cmd}\|_2^2 \\ &= N_{RMS}\left\|\boldsymbol{G}_{rq_{cmd}}\right\|^2_{\infty,max}\|q_{cmd}\|^2_{RMS} = J^2_{th,RMS}N_{RMS} \end{aligned} \tag{3-222}$$

or likewise

$$\begin{aligned} J^2_{th,RMS} &= \sup_{\boldsymbol{f}=\mathbf{0},\boldsymbol{\Delta}\neq\mathbf{0}} \|\boldsymbol{r}\|^2_{RMS} = \left\|\boldsymbol{G}_{rq_{cmd}}\right\|^2_{\infty,max}\|q_{cmd}\|^2_{RMS} = \frac{J^2_{th,2}}{N_{RMS}} \\ &= \frac{\left\|\boldsymbol{G}_{rq_{cmd}}\right\|^2_{\infty,max}\|q_{cmd}\|_2^2}{N_{RMS}} \end{aligned} \tag{3-223}$$

It is important to remember this relation between $J^2_{th,2}$ and $J^2_{th,RMS}$ because it will be used several times during the rest of this text. The decision rule $\boldsymbol{d}_{FD,det}$ for the deterministic case, i.e. without stochastic unknown inputs, becomes

$$d_{FD,det} = \begin{cases} 0 & if\ \|\boldsymbol{r}\|^2_{RMS} \leq J^2_{th,RMS} \Rightarrow nofault \\ 1 & if\ \|\boldsymbol{r}\|^2_{RMS} > J^2_{th,RMS} \Rightarrow fault \end{cases} \tag{3-224}$$

3.5.4.3.2 Implications of a Limited RMS Observation Window

What we have to keep in mind when using (3-223) and (3-224) is that, they are strictly speaking only correct for $\|q_{cmd}\|^2_{RMS,def}$ and $\|\boldsymbol{r}\|^2_{RMS,def}$ according (3-175), i.e. an *unlimited* observation window. Clearly, from a practical point of view an unlimited observation window is not at all desirable, because

- We have to handle signal values that potentially grow versus ∞
- The *sensitivity to faults is decreasing with time* because only for a q_{cmd} sine input with $\boldsymbol{\omega}_{\|\boldsymbol{G}_{rq_{cmd}}\|_{\infty,\max}}$, $\|\boldsymbol{r}\|^2_{RMS,def}$ will stay close to $J^2_{th,RMS}$.

A common suggestion (cf. e.g. Ding, 2013, p. 166) in order to overcome this problem is to use a limited observation window, i.e. (3-176). While this seems to be a simple solution it is not so simple in practice and none of the texts known to the author discussed the problems arising from a *limited* observation window.
The implication of the limited observation window size is that $\|.\|_2$ and $\|.\|_{RMS}$ with their limited number of samples will behave *significantly* different than $\|.\|_{2,def}$ and $\|.\|_{RMS,def}$. Figure 30 illustrates this difference for a q_{cmd} sine input with $\omega_{\|\boldsymbol{G}_{rq_{cmd}}\|_{\infty,\max}}$. The test conditions have been equivalent to Test Case 3.3 that will be introduced and discussed in detail in chapter 4.3.2.2. $\|\boldsymbol{G}_{rq_{cmd}}\|_{\infty,\max}$ for this flight condition is found at Vertex 3. The first plot shows the sine input q_{cmd} while the second illustrates the resulting $\|q_{cmd}\|^2_{RMS,def}$. Using $\|.\|_{RMS,def}$, (3-223) becomes

$$J^2_{th,RMS,def} = \|\boldsymbol{G}_{rq_{cmd}}\|^2_{\infty,max}\|q_{cmd}\|^2_{RMS,def} \tag{3-225}$$

$J^2_{th,RMS,def}$ (dashed) and $\|\boldsymbol{r}\|^2_{RMS,def}$ (solid) are shown in the third plot. We nicely see how $\|\boldsymbol{r}\|^2_{RMS,def}$ asymptotically approaches $J^2_{th,RMS,def}$ but does not exceed it. In comparison the fourth plot depicts $\|q_{cmd}\|^2_{RMS}$ and the fifth plot $J^2_{th,RMS}$ (dashed) and $\|\boldsymbol{r}\|^2_{RMS}$ (solid). $J^2_{th,RMS}$ has been calculated by (3-223). Two things are obvious. First of all the signals $\|q_{cmd}\|^2_{RMS}$, $J^2_{th,RMS}$, and $\|\boldsymbol{r}\|^2_{RMS}$ are significantly different than $\|q_{cmd}\|^2_{RMS,def}$, $J^2_{th,RMS,def}$, and $\|\boldsymbol{r}\|^2_{RMS,def}$. Second and most important $\|\boldsymbol{r}\|^2_{RMS}$ violates $J^2_{th,RMS}$ instead asymptotically approaching it. As a result we cannot directly use $\|q_{cmd}\|^2_{RMS}$ with (3-223), because this would lead to false alarms when the closed-loop system reaches the boundary of acceptable model uncertainties, i.e. in the case here Vertex 3.
The solution proposed in this text is a signal envelope detector for $\|q_{cmd}\|^2_{RMS}$. It will be introduced in the next chapter.

Contribution 3-7: To the author's knowledge the implications for fault detection of using a limited RMS window size are not discussed in current FDD literature. The aspects discussed are therefore also new.

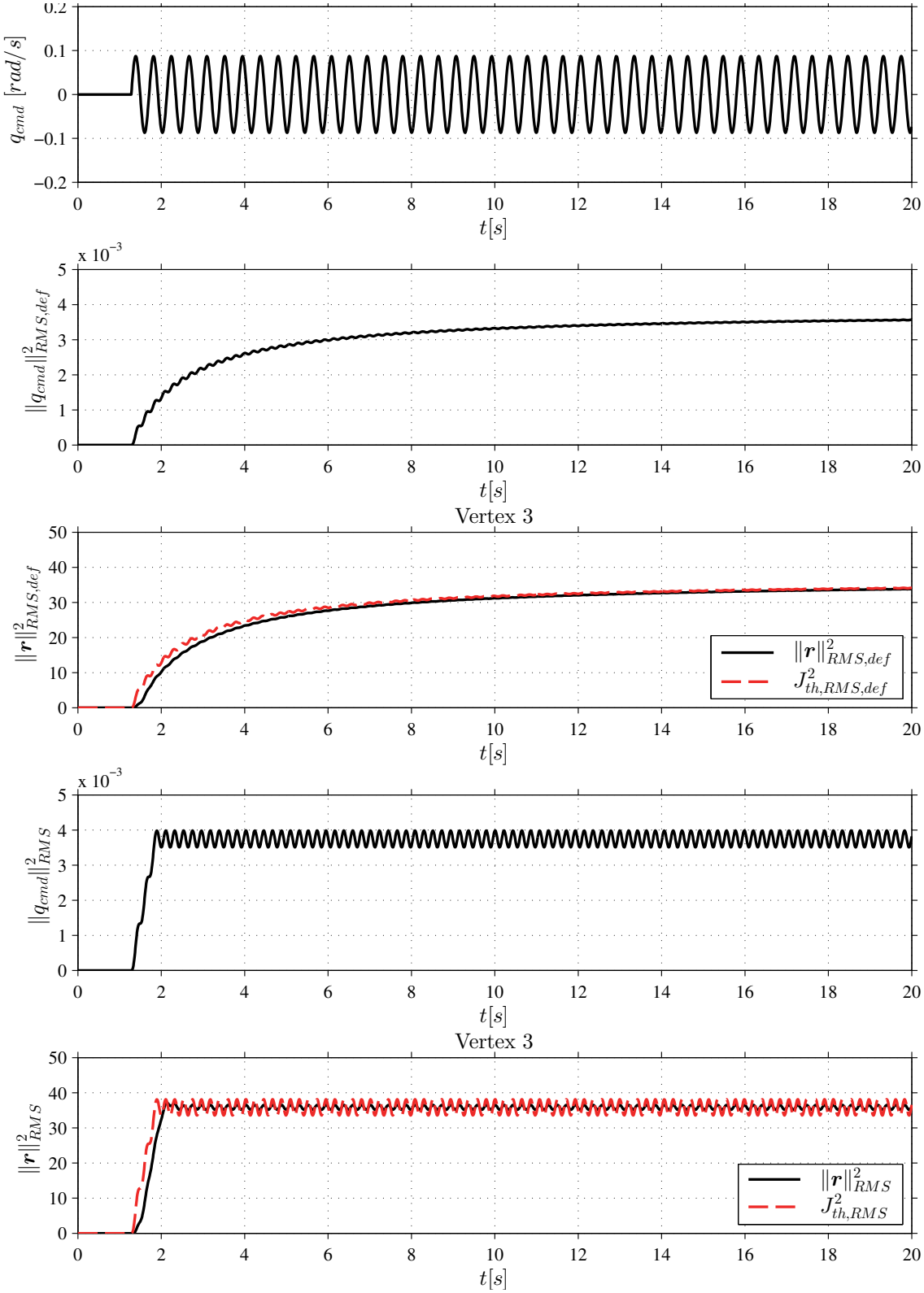

Figure 30 Comparison between different RMS signals (TC 3.3)

3.5.4.3.3 Input Envelope Detector

The above mentioned implications of a limited RMS window size warrant some solution. In electrical engineering so called envelope detectors are used to retrieve the envelope of a signal. Inspired by this approach the author wants to suggest an envelope detector as basis for an adaptive fault detection threshold. While there is already limited research on residual evaluation in general (cf. chapter 3.4.1) there is even less on adaptive thresholds. This is also due to the fact the limited research on residual evaluation in most of the cases focuses on systems subject to *additive unknown inputs* $\boldsymbol{d}$ but *not on model uncertainties*. For the former the authors normally assume a constant bound on $\|\boldsymbol{d}\|^2_{RMS}$. In such a case, there is no need for a threshold generator because $\|\boldsymbol{d}\|^2_{RMS}$ and therefore $J^2_{th,RMS}$ according (3-87) is constant.

For systems subject to model uncertainties the situation is significantly different, because for them the system input $\boldsymbol{u}$, in our case q_{cmd}, clearly affects the residual $\boldsymbol{r}$ and therefore also the threshold. For sure the system input q_{cmd}, i.e. the pilot control input, varies nearly all the time. To use a constant on $\|q_{cmd}\|^2_{RMS}$ is therefore unrealistic, as we would have to use the worst-case $\|q_{cmd}\|^2_{RMS,max}$ for all conditions that can be experienced in practice. This would for example mean that we have to consider the largest control input $q_{cmd,max}$ possible. While we could ensure no false alarms with such an approach it should be clear from (3-223) that for cases where $q_{cmd} \ll q_{cmd,max}$ the threshold $J^2_{th,RMS}$ is much too large, and therefore more or less useless for practical fault detection application. *For our application, i.e. fault detection for aircraft, the use of an adaptive threshold or threshold generator is therefore a requirement.*

The suggestions how to establish such an adaptive threshold are very limited. The author only knows Ding (2013, p. 311) who proposes to use $\|\boldsymbol{u}\|_{RMS}$ with a *limited* observation window, but it has been demonstrated in the last chapter that this alone is not sufficient.

As said above the author wants to suggest a new approach for an adaptive threshold based on $\|\boldsymbol{u}\|^2_{RMS}$ envelope detector modelled as state machine. The latter was modelled in MathWorks'® Stateflow®. The envelope detectors Stateflow® state diagram is shown in Figure 31.

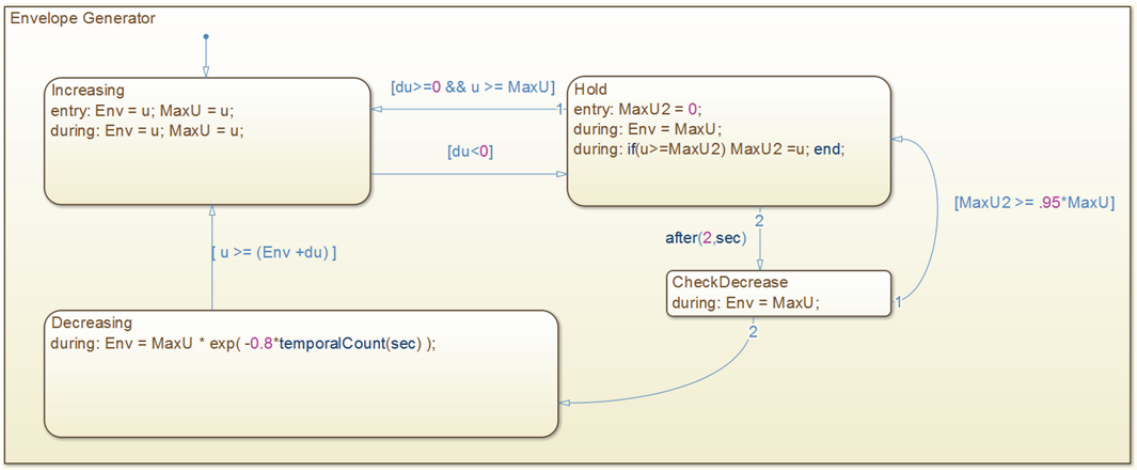

Figure 31 Envelope generator state machine

State Increasing

The system enters the *Increasing* state and remains in this state till signal u is decreasing. While it is in this state the signal envelope Env is equal the signal u. At the same time the maximum signal value, i.e the current u, is stored in the variable $MaxU$. The system remains in the increasing state till the signal decreases, that is the difference between consecutive samples $du < 0$. If this condition is fulfilled the machine enters the *Hold* state.

State Hold

When the system enters the *Hold* state it holds the maximum signal value $MaxU$ as signal envelope, i.e $Env = MaxU$. While it is in the state it stores the maximum signal value u since it is in *Hold* in the variable $MaxU2$. If the signal u starts to increase again while the machine is in the *Hold* state *and* the signal $u \geq MaxU$, then it reverts back in the *Increasing* state. After T_H = 2 sec the machine enters the *CheckDecrease* state.

State CheckDecrease

While in *CheckDecrease* the envelope remains $Env = MaxU$. If the maximum signal value where the machine has been in the *Hold* state $MaxU2$ has decreased less than Tol_H = 5% in comparison to $MaxU$, i.e. $MaxU2 \geq (1 - Tol_H) \cdot MaxU$ the *Hold* state is activated again. If this is not the case then the *Decreasing* state is entered.

State Decrease

When entering the *Decrease* state the envelope decreases exponentially from the maximum signal value $MaxU$, that is $Env = MaxU \cdot e^{-\lambda t}$, with λ = 0.8. The system

remains in *Decrease* till $u \geq Env + du$. If this condition is true, i.e. the signal u increases again and is equal the current envelope Env the machine reverts back the *Increasing* state.

Chapters 4.3.2.2 and 4.3.2.3 will demonstrate that the proposed envelope detector works as desired, i.e. correctly detects the signal envelope $Env = \|q_{cmd,env}\|_{RMS}^2$ for $u = \|q_{cmd}\|_{RMS}^2$. The envelope detector described needs three parameters, that have been empirically be determined for the simulation case study of this thesis, which has the goal of demonstrating principle feasibility of the fault detection system proposed. Those three parameters are the exponential time constant λ, the time in the *Hold* state T_H, and the tolerance Tol_H. Those parameters have been determined for this case study using q_{cmd} sine and step inputs of chapter 4.3.2.2. However chapter 4.3.2.3 will demonstrate that the envelope detector with those parameters also works correctly for arbitrary q_{cmd} inputs.
Using the envelope detector the adaptive deterministic threshold can now be calculated (3-226) by

$$\begin{aligned} J_{th,RMS}^2(k) &= \sup_{\boldsymbol{f=0,\Delta\neq 0}} \|\boldsymbol{r}\|_{RMS}^2 \\ &= \|\boldsymbol{G}_{rq_{cmd}}\|_{\infty,max}^2 \|q_{cmd,env}\|_{RMS}^2(k) \\ &= \frac{J_{th,2}^2(k)}{N_{RMS}} = \frac{\|\boldsymbol{G}_{rq_{cmd}}\|_{\infty,max}^2 \|q_{cmd,env}\|_2^2(k)}{N_{RMS}} \end{aligned} \tag{3-226}$$

Contribution 3-8: The author provides an approach for a signal envelope detector based adaptive fault detection threshold (threshold generator) that overcomes the problems of RMS-signals with limited observation time (cf. chapter 3.5.4.3.2). The threshold generator ensures validity of (3-223) for the case of limited observation times *and* enables a fault detection threshold $J_{th,RMS}^2$ that is small enough to be useful in a practical context. The former will be demonstrated by simulation in chapter 4.3.2.2 and 4.3.2.3, the latter in chapter 4.3.4.

3.5.4.4 Stochastic Threshold for Integrated Stochastic/Deterministic Fault Detection with Deterministic Model Uncertainties

This chapter builds on the theoretical results of chapter 3.4.3 and 3.4.4. From (3-176) it follows that

$$\|\boldsymbol{r}\|_2^2 = N_{RMS}\|\boldsymbol{r}\|_{RMS}^2 = \sum_{k=1}^{N_{RMS}} \boldsymbol{r}^T(k)\boldsymbol{r}(k) \tag{3-227}$$

For the time being we want to consider N_{RMS} = 1, i.e. just one sample, thereby we get

$$\|\boldsymbol{r}(k)\|_2^2 = \boldsymbol{r}^T(k)\boldsymbol{r}(k) \tag{3-228}$$

The chi-square distribution arises from the sum of m squared independent normal distributed random variables. Clearly, in our case, with $\boldsymbol{r}$ being two dimensional,

$$\|\boldsymbol{r}(k)\|_2^2 = r_1(k)^2 + r_2(k)^2 \tag{3-229}$$

Thus if $\boldsymbol{r}(k) \sim \mathcal{N}(\boldsymbol{r}_{det}(k), \mathbf{I})$ and the components r_1 and r_2 are independent, then $\|\boldsymbol{r}(k)\|_2^2$ follows a non-central chi-square distribution with $m_{\chi^2,r(k)}$ = 2 degrees of freedom and non-centrality parameter $\lambda_{\chi^2,r(k)} = \boldsymbol{r}_{det}{}^T(k), \boldsymbol{r}_{det}(k)$, i.e.

$$\|\boldsymbol{r}(k)\|_2^2 \sim \chi_2^2\left(\lambda_{\chi^2,r(k)}\right) \tag{3-230}$$

From now on we want to consider the practical relevant case of N_{RMS} > 1. The sum of N_{RMS}, $\chi_2^2(\lambda)$ distributed random variables $\|\boldsymbol{r}(k)\|_2^2$ also has a chi-square distribution with $m_{\chi^2,RMS} = 2N_{RMS}$ degrees of freedom (cf. e.g. PennState, 2017) and non-centrality parameter

$$\lambda_{\chi^2} = \sum_{k=1}^{N_{RMS}} \boldsymbol{r}_{det}{}^T(k)\, \boldsymbol{r}_{det}(k) = \|\boldsymbol{r}_{det}\|_2^2. \tag{3-231}$$

By inspection of (3-227) it is therefore clear that

$$\|\boldsymbol{r}\|_2^2 = N_{RMS}\|\boldsymbol{r}\|_{RMS}^2 \sim \chi_{2N_{RMS}}^2\left(\lambda_{\chi^2}\right) \tag{3-232}$$

The maximum $\|\boldsymbol{r}_{det}\|_2^2$ possible in a fault-free case we get from (3-222)

$$J_{th,2}^2 = \sup_{\boldsymbol{f}=\boldsymbol{0},\boldsymbol{\Delta}\neq\boldsymbol{0}} \|\boldsymbol{r}_{det}\|_2^2 = \left\|\boldsymbol{G}_{rq_{cmd}}\right\|_{\infty,max}^2 \|q_{cmd}\|_2^2 \tag{3-233}$$

We can therefore write for the non-centrality parameter

$$\lambda_{\chi^2} = J_{th,2}^2 = J_{th,RMS}^2 N_{RMS} \tag{3-234}$$

$$m_{\chi^2,RMS} = 2N_{RMS} \tag{3-235}$$

Thus with (3-232) we finally get

$$\|\boldsymbol{r}\|_{RMS}^2 \sim \frac{\chi_{2N_{RMS}}^2\left(J_{th,RMS}^2 N_{RMS}\right)}{N_{RMS}} \tag{3-236}$$

For $\boldsymbol{r}$ being independent, the integrated stochastic/deterministic fault detection threshold can thereby be calculated by

$$J_{th,\chi^2} = \frac{\text{inv}\,\chi_{2N_{RMS}}^2\left(1 - FAR_{req}, J_{th,RMS}^2 N_{RMS}\right)}{N_{RMS}} \tag{3-237}$$

where $\text{inv}\,\chi_{2N_{RMS}}^2$is the inverse Cumulative Distribution Function (CDF). The fault detection decision rule follows as

$$d_{\chi^2} = \begin{cases} 0 & if\ \|\boldsymbol{r}\|_{RMS}^2 \leq J_{th,\chi^2} \Rightarrow no\ fault \\ 1 & if\ \|\boldsymbol{r}\|_{RMS}^2 > J_{th,\chi^2} \Rightarrow fault \end{cases} \tag{3-238}$$

3.5.4.4.1 Variance Scaling Filter

A peculiarity of the chi-square distribution, used for the stochastic FD threshold is that it assumes a unit variance for all of the m squared random variables. In our case the consequence is that we first of all have to get $Cov\left(\boldsymbol{r}(k)\right) = \boldsymbol{I}$. This means that there is no cross-correlation between the elements of $\boldsymbol{r}(k)$ and all elements have *unit variance*. In chapter 3.5.3.3 we therefore introduced the filter matrix $\overline{\boldsymbol{V}} \in \mathbb{R}^{2x2}$. According (3-172) the filtered residual is obtained by

$$\boldsymbol{r}(k) = \overline{\boldsymbol{V}}_{r,\mathcal{V}_i} \check{\boldsymbol{r}}(k) \tag{3-239}$$

Remark 3-10: At this point it is important to realize the practical influence of $\overline{\boldsymbol{V}}_{r,\mathcal{V}_i}$ on our FD system. On one hand it will influence the deterministic part of the FD system by the residual dynamics (3-220), therfore $\boldsymbol{G}_{rq_{cmd}}$, and thus via (3-179) the deterministic threshold $J^2_{th,RMS}$. On the other hand it enables $Cov(\boldsymbol{r}(k)) = \boldsymbol{I}$ for the stochastic FD part. Both aspects influence J_{th,χ^2} according (3-237). The former via the non-centrality parameter λ_{χ^2}, the latter in providing the correct covariance to use the χ^2 distribution.

As explained in chapter 3.4.4, such a filter is also used in the integrated norm-based/stochastic fault detection approach suggested by Ding (2013) *for deterministic unknown inputs* $\boldsymbol{d}$. As those inputs are *additive,* $\overline{\boldsymbol{\Sigma}}_{\check{\boldsymbol{r}}}$ and therefore the filter $\overline{\boldsymbol{V}}$ do not change because of $\boldsymbol{d}$**.** However in our case we have to deal with *deterministic model uncertainties*, thus $\overline{\boldsymbol{\Sigma}}_{\check{\boldsymbol{r}}}$ and the filter $\overline{\boldsymbol{V}}$ are influenced. As a consequence the approach suggested by Ding (2013) had to be modified by the author.
We recall that the primary goal of this thesis is to ensure that the FD system has to guarantee a FAR equal or lower the required FAR_{req} (Requirement 1-1, p. 11). The simulations performed have shown that, for every flight condition, we can identify a worst-case vertex $\mathcal{V}_{Var,max}$ that generates the highest variance $Var(\boldsymbol{r}_m(k))$ for the residual dynamic systems with model uncertainties contained inside the parameter polytope of acceptable model-uncertainties. By using the filter $\overline{\boldsymbol{V}}_{r,\mathcal{V}_{Var,max}}$, derived for this worst-case system by (3-169), we can ensure that all other systems contained inside the polytope will generate a residual $\boldsymbol{r} \in \mathbb{R}^m$ where the variance of the elements $Var(\boldsymbol{r}_m(k)) \leq 1$. From stochastic theory and (3-237) it should thus be clear that a stochastic threshold J_{th,χ^2}, which is based on the worst-case variance. $Var(\boldsymbol{r}_m(k)) = 1$, ensures $FAR_{J_{th,\chi^2}} \leq FAR_{req}$. In chapter 4.3.3 it will be verified by simulation that the considerations made above are valid. What we cannot ensure with this approach is perfect de-correlation between the elements of $\boldsymbol{r}(k)$, because we can only optimize the filter for $\mathcal{V}_{Var,max}$. However cross-correlation was found to be insignificant.

The approach for selection of filter $\overline{\boldsymbol{V}}$ for the integrated stochastic/deterministic fault detection scenario with *deterministic polytopic model uncertainties* suggested by the author and chosen in this thesis is therefore:

- For every flight condition, identify the vertex $\mathcal{V}_{Var,max}$ with the highest $Var\left(\boldsymbol{r}_m(k)\right)$ (offline)
- Choose the correlation filter $\overline{\boldsymbol{V}}_{r,\mathcal{V}_{Var,max}}$ that belongs to this vertex (offline). This ensures $Var\left(\boldsymbol{r}_m(k)\right) \leq 1$ for all residual dynamic systems inside the parameter polytope of acceptable model-uncertainties.
- Implemented this filter $\overline{\boldsymbol{V}}$ for online processing of the residual $\boldsymbol{r}(k) = \overline{\boldsymbol{V}}_{r,\mathcal{V}_{Var,max}}\check{\boldsymbol{r}}(k)$, which is a simple multiplication of a matrix with a vector.

Contribution 3-9: The suggested approach for the selection of $\overline{\boldsymbol{V}}$ in case of a residual subject to *stochastic unknown inputs* and *deterministic polytopic model uncertainties* is to the author's knowledge new.

Further Work 3-3: In the simulation case study of this thesis we use certain points in the flight envelope as dedicated flight conditions. For sure in a potential implementation in a real system some means have to be found for adaptation of $\overline{\boldsymbol{V}}$ between all flight conditions possible (e.g. like gain scheduling for controller gains). This is an area of further work that has to be addressed for a practical application.

The considerations made above are critical with respect to ensure a $FAR_{J_{th,\chi^2}} \leq FAR_{req}$ (Requirement 1-1, p. 11). The resulting $FAR_{J_{th,\chi^2}}$ with the above presented choice of variance scaling filter $\overline{\boldsymbol{V}}_{r,\mathcal{V}_{Var,max}}$ has thus been verified by simulation in chapter 4.3.3 .

Further Work 3-4: While the above suggested approach makes sense from an engineering judgment point of view, and will also be verified by the simulation case study in chapter 4.3.3, a stringent theoretical understanding and solution would be desirable. This should be tackled in a follow on work.

3.5.4.4.2 Auto-Correlation Because of Residual Post Filter

From the theory of the non-central chi-square distribution (cf. e.g. McDonough & Whalen, 1995, p. 140) we know that in general that mean μ_{χ^2} of the chi-square distributed random variables is

$$\mu_{\chi^2} = \lambda_{\chi^2} + m_{\chi^2} \tag{3-240}$$

and variance Σ_{χ^2}

$$\Sigma_{\chi^2} = 4\lambda_{\chi^2} + 2m_{\chi^2} \tag{3-241}$$

Thus for our case with (3-234) and (3-235) we finally get

$$\mu_{\chi^2,RMS} = m_{\chi^2,RMS} + \lambda_{\chi^2} = N_{RMS}(2 + J_{th,RMS}^2) \tag{3-242}$$

$$\Sigma_{\chi^2,RMS} = 2m_{\chi^2,RMS} + 4\lambda_{\chi^2} = 4N_{RMS}(1 + J_{th,RMS}^2) \tag{3-243}$$

Eq. (3-242) and (3-243) are again only correct for *uncorrelated* random variables. Unfortunately for $N_{RMS} > 1$ the assumption of an *uncorrelated residual* $\boldsymbol{r}$ in our case is no longer a good one, because the residual post-filter (chapter 3.5.3.2) is a dynamic system and therefore it is clear from theory that it introduces auto-correlation. That is $\boldsymbol{r}(k)$ is correlated in time with samples $\boldsymbol{r}(k+n)$. Thus the noise is no longer white (flat PSD) but colored (PSD not flat). For details on autocorrelation the interested reader is referred to e.g. the compact summary of Klein and Morelli (2006pp. 452-453).

The effect of auto-correlation on the variance becomes visible as soon as we sum up residual samples $\boldsymbol{r}(k)$ ... $\boldsymbol{r}(k+n)$. From (3-227) it is clear that this is exactly what we do when we calculate $\|\boldsymbol{r}\|_{RMS}^2$ for $N_{RMS} > 1$. Thus we have to account for the effect of colored noise. The effect of colored noise is that the variance of the signal is increased in comparison to the case where the noise is white. In parameter least-square estimation it is practice to correct the effect of colored noise on the variance by a correction factor (Klein & Morelli, 2006, p. 134-137). Inspired by this idea the author wants to suggest a comparable empiric approach for hypothesis testing using the $\chi_m^2(\lambda)$ normal distribution approximation. The normal approximation becomes necessary because for the $\chi_m^2(\lambda)$-distribution there is a fixed relation between non-centrality parameter λ_{χ^2}, degrees of freedom m_{χ^2}, mean μ_{χ^2} and Var_{χ^2} according (3-240) and (3-241). In other words $\chi_m^2(\lambda)$ is not defined for other μ_{χ^2}-Σ_{χ^2}-combinations but the normal distributions for sure is.

The $\chi_m^2(\lambda)$ normal distribution approximation follows from the central limit theorem and can be found in standard literature. With standard deviation

$$\sigma_{\chi^2} = \sqrt{\Sigma_{\chi^2}} \tag{3-244}$$

it follows that

$$\chi_m^2(\lambda) \cong \mathcal{N}\left(\mu_{\chi^2}, \sqrt{\Sigma_{\chi^2}}\right) \tag{3-245}$$

We define a corrected variance by introduction of a correction factor $\varepsilon_{Var,1}(\lambda_{\chi^2})$:

$$\tilde{\Sigma}_{\chi^2,RMS} = \varepsilon_{Var,1}(\lambda_{\chi^2}) \cdot \Sigma_{\chi^2,RMS} \tag{3-246}$$

In our case, where the test statistic is $\|\boldsymbol{r}\|_{RMS}^2$, the correction factor is calculated by

$$\varepsilon_{Var,1}(\lambda_{\chi^2}) = \frac{\hat{\Sigma}_{\chi^2,RMS}(\lambda_{\chi^2})}{\Sigma_{\chi^2,RMS}(\lambda_{\chi^2})} \tag{3-247}$$

For this work $\hat{\Sigma}_{\chi^2,RMS}(\lambda_{\chi^2})$ has been estimated offline by simulation for five non-centrality parameters in the range of interest in this thesis. The correction factor $\varepsilon_{Var,1}(\lambda_{\chi^2})$ has then been calculated according (3-247). For every flight condition the five correction factor have been stored in a look-up table as supporting points for online interpolation as function of λ_{χ^2} (Table 14, p. 190).

Further Work 3-5: In the simulation case study of this thesis we use certain points in the flight envelope as dedicated flight conditions. For sure in a potential implementation in a real system some means have to be found for adaptation of $\varepsilon_{Var,1}$ between all flight conditions possible, e.g. like gain scheduling for controller gains. Even better would of course be a theoretical solution to the overall correction. This is for sure an area of further work that has to be addressed for a practical application.

Further Work 3-6: A method for calculating $\hat{\Sigma}_{\chi^2,RMS}(\lambda_{\chi^2})$ instead of estimating it from offline simulation would be more "elegant" and therefore desirable.

Unfortunately it was found in simulation that the correction of the variance according (3-246) alone still leads to a $FAR_{J_{th,\chi^2}}$ slightly higher than FAR_{req}. The reason is not fully understood yet and has to be investigated further in a follow on work. It might be related to the normal approximation itself but due to the central limit the-

orem only an insignificant approximation error should be expected as $m_{\chi^2,RMS} = 2N_{RMS} = 120$ is already relative large.
For this thesis the correct $FAR_{\tilde{J}_{th,\chi^2}}$ was obtained by an additional constant correction factor

$$\varepsilon_{Var,2} = 1.35 \tag{3-248}$$

for all λ_{χ^2} and flight conditions. Finally, with calculation of the threshold according

$$\tilde{J}_{th,\chi^2} = \frac{inv\,\mathcal{N}\left(1 - FAR_{req}, \mu_{\chi^2,RMS}, \sqrt{\tilde{\Sigma}_{\chi^2,RMS} \cdot \varepsilon_{Var,2}}\right)}{N_{RMS}} \tag{3-249}$$

the requirement $FAR_{\tilde{J}_{th,\chi^2}} \leq FAR_{req}$ was achieved and therefore Requirement 1-1 (p. 11) fulfilled. As mentioned above this will be demonstrated by simulation in chapter 4.3.3.

Further Work 3-7: The use of $\varepsilon_{Var,2}$ to obtain $FAR_{\tilde{J}_{th,\chi^2}} \leq FAR_{req}$ is for sure not fully satisfactory. *Although we can ensure* $FAR_{\tilde{J}_{th,\chi^2}} \leq FAR_{req}$ by $\varepsilon_{Var,2}$, and therefore fulfil Requirement 1-1 (p. 11), a theoretical solution would be desirable.

Contribution 3-10: The suggested approach of using the $\chi^2_m(\lambda)$ normal distribution approximation and a colored noise corrected variance for fault detection χ^2 hypothesis testing problems is to the author's knowledge also new.

Two alternative approaches to the above discussed shall also be mentioned here. The first one, that was initially used by the author, would be to calculate J_{th,χ^2} based on the variance of $Var(\|\boldsymbol{r}(k)\|_2^2)$ instead of $Var(\|\boldsymbol{r}\|_{RMS}^2)$ because $\|\boldsymbol{r}\|_{RMS}^2$ is an moving average of $\|\boldsymbol{r}(k)\|_2^2$, necessarily $Var(\|\boldsymbol{r}\|_{RMS}^2) \ll Var(\|\boldsymbol{r}(k)\|_2^2)$. In fact for white noise $Var(\|\boldsymbol{r}\|_{RMS}^2)$ would be

$$Var(\|\boldsymbol{r}\|_{RMS}^2) = \frac{Var(\|\boldsymbol{r}(k)\|_2^2).}{N_{RMS}} \tag{3-250}$$

While this approach would not require any correction factor $\varepsilon_{Var,1}$or $\varepsilon_{Var,2}$ it turned out to be very conservative and was therefore finally not implemented. Furthermore it is the author's opinion that the suggested approach of correcting the variance for colored noise is more elegant and in chapter 4.3.4 it will be demonstrated that this approach leads to thresholds $\tilde{J}_{th,\chi^2}$that are not overly conservative and useable in a practical relevant aircraft fault scenarios. Nevertheless the author admits

that there are extensions necessary for a real application (Further Work 3-5) and room for more elegant ways of solving the problem (Further Work 3-6; Further Work 3-7).
The second solution would be *not to use* a residual post filter and therefore obtain a residual without auto-correlation. In this case the threshold could be calculated by the standard $\chi^2_m(\lambda)$ according to (3-237). However for the reasons discussed in chapter 3.5.3.2 this should not be the preferred approach.

3.5.4.5 Decision Maker

The decision maker simply implements the decision rule

$$d_{FD} = \begin{cases} 0 & if\ \|\boldsymbol{r}\|^2_{RMS} \leq \tilde{J}_{th,\chi^2} \Rightarrow nofault \\ 1 & if\ \|\boldsymbol{r}\|^2_{RMS} > \tilde{J}_{th,\chi^2} \Rightarrow fault \end{cases} \tag{3-251}$$

Once a fault has been detected the fault bit d_{FD} is set and hold.

4 Results of Simulation Case Studies

4.1 Simulation Setup

The basic simulation setup follows the setup as introduced in chapter 3.5 and is depicted in Figure 26 (p. 94). The different elements have already been discussed from a theoretical point of view in the subchapters of chapter 3.5. Here we only want to summarize the parameters used for simulation. Deviations to the basic setup, if required, will be described with the relevant chapters discussing the different test cases.

4.1.1 Plant

To achieve the desired CAP- ζ_{SP} combination a control strategy must be chosen. In analysing the control system of today's series production aircraft it becomes quickly apparent that, especially the inner feedback loops are designed using classical linear control theory (see for example Brockhaus et al., 2011, Chapters 19 & 20; Moritz & Osterhuber, 2006). As the reference control system designed for this case study shall be representative for a contemporary system a similar approach has been chosen here. The high level design steps can be summarized as follows

- Trim system at a certain flight condition defined by angle of attack $\alpha_{K,0}$, altitude $h_{A,0}$ and true airspeed $V_{A,0}$
- Linearize non-linear system around trim point
- Calculate feedback gains based on the linear model

Remark 4-1: To cover the full flight envelope in terms of speed, Mach number, altitude, angle of attack range and aircraft configurations it is common practice to calculate the controller gains for a reasonable number of trim conditions and store the results in a look-up table. During controller operation the correct gain for the actual flight condition is then taken from this table which results in a feed-forward type adaptation of the feedback gains, i.e. gain scheduling (Brockhaus et al., 2011, pp. 563-565; Moritz & Osterhuber, 2006). However herein gain scheduling was not implemented for the reference control system as this is not necessary for our purposes of proving principal feasibility of the FD system proposed in this thesis.

4.1.1.1 Open-Loop Plant

The open-loop short period approximation (chapter 3.5.2.1.2) was obtained for the respective flight condition (chapter 4.2) by linearization from the F-16 non-linear simulation model as described in Appendix A. For this case study a centre of gravity position $(x^G)_B = 0{,}4 \cdot \bar{c}$ has been chosen to obtain an open-loop unstable plant

with time to double representative for contemporary fighter aircraft configurations (cf. Appendix A.4 and A.6).

4.1.1.2 Closed-Loop Plant

The feedback gain calculation (chapter 3.5.2.2) for the reference control system was done using the Eigenstructure assignment algorithm *evmin* provided with Srinathkumar (2011a, 2011b). A comparable algorithm has also been chosen for the design of the YF-22 flight control system (NATO RTO, 2000, p. 15). Because only one system input is available, the Eigenstructure algorithm effectively becomes a pole placement algorithm[13]. General information concerning Eigenstructure assignment can be found in (Brockhaus et al., 2011, pp. 543-548).
For the practical relevant failure case discussed in chapter 4.3.4, where the closed-loop aircraft becomes unstable, also the actuator dynamics have been modelled, because without doing this the results would be less meaningful. This fault detection system setup is discussed in chapter 4.3.4.2.3 to prevent confusion at this point.

Remark 4-2: A peculiarity of this simulation case study is the relative simple FCS design utilizing just proportional feedback. Production FCS normally also contain an integrator to ensure stationary guidance accuracy to the pilot command beside disturbance. For a $q_{K,cmd}$-system with such an integrator, the deviation of q_K from $q_{K,cmd}$ due to disturbances α_W would be smaller. However this is not of particular importance for the purpose of our case study here. Therefore the integrator was not included in the simple FCS used herein.

4.1.2 Residual Generation and Post-Processing

4.1.2.1 Residual Generator (Kalman Filter)

The steady state Kalman filter was implemented as discrete time system. The filter gain $\bar{\boldsymbol{L}}$ has been calculated offline for every flight condition as described in chapter 3.5.3.1.3. The Kalman filter structure implemented online is given in Figure 24 (p. 68).

4.1.2.2 Residual Post Filter

The residual post filter was implemented as discrete time system. It has been calculated offline as described in chapter 3.5.3.2 and uses a fixed pass-band $\omega_{PF} = 0.5 \ldots 50$ rad/s for all flight conditions. The pass-band had to be relatively

[13] This is also a common situation for modern flight control systems, realized in practice, because quite often the control input is rather one combined moment demand than specific control surface deflections (NATO RTO, 2000, p. 15).

larger, because due to fact that this is an analog filter implementation, the high and low pass cut-off frequency sharpness is not very good.

4.1.2.3 Variance Scaling Filter

The variance scaling filter $\overline{\boldsymbol{V}}$ has been calculated offline as described in chapter 3.5.3.3. For online implementation the respective filter $\overline{\boldsymbol{V}}_{r,\nu_{Var,max}}$ for every flight condition has then been selected as explained in chapter 3.5.4.4.1.

4.1.3 Residual Evaluation

4.1.3.1 Recursive Sliding Window RMS

The recursive sliding window RMS has been implemented online as discussed in chapter 3.5.4.2 with a fixed window size N_{RMS} = 60 samples for all flight conditions.

4.1.3.2 Deterministic Adaptive Threshold

The $\|q_{cmd}\|^2_{RMS}$ envelope detector has been used to obtain $\left\|q_{cmd,env}\right\|^2_{RMS}$ (chapter 3.5.4.3.3). The adaptive deterministic threshold has then been calculated using (3-226):

$$J^2_{th,RMS}(k) = \left\|\overline{\boldsymbol{G}}_{rq_{cmd}}\right\|^2_{\infty,max}\left\|q_{cmd,env}\right\|^2_{RMS}(k) \tag{4-1}$$

$\left\|\overline{\boldsymbol{G}}_{rq_{cmd}}\right\|^2_{\infty,max}$ has been determined offline for every flight condition as described in chapter 3.5.4.3.1.3.

4.1.3.3 Stochastic Threshold for Integrated Stochastic/Deterministic Fault Detection

The stochastic threshold (chapter 3.5.4.4.2) has been implemented by (3-249):

$$\tilde{J}_{th,\chi^2} = \frac{inv\,\mathcal{N}\left(1 - FAR_{req}, \mu_{\chi^2,RMS}, \sqrt{\tilde{\Sigma}_{\chi^2,RMS}\cdot\varepsilon_{Var,2}}\right)}{N_{RMS}} \tag{4-2}$$

with

$$\lambda_{\chi^2} = J^2_{th,RMS}N_{RMS} \tag{4-3}$$

$$\mu_{\chi^2,RMS} = N_{RMS}(2 + J^2_{th,RMS}) \tag{4-4}$$

$$\tilde{\Sigma}_{\chi^2,RMS} = \varepsilon_{Var,1}(\lambda_{\chi^2})\cdot\Sigma_{\chi^2,RMS} \tag{4-5}$$

$$\Sigma_{\chi^2,RMS} = 4N_{RMS}(1 + J_{th,RMS}^2) \tag{4-6}$$

$\hat{\Sigma}_{\chi^2,RMS}(\lambda_{\chi^2})$ has been estimated offline by simulation for five non-centrality parameters in the range of interest in this thesis. The correction factor $\varepsilon_{Var,1}(\lambda_{\chi^2})$ has then been calculated according (3-247). For every flight condition the five correction factor have been stored in a look-up table for online interpolation as function of λ_{χ^2} (Table 14, p. 190). As discussed in chapter 3.5.4.4.2

$$\varepsilon_{Var,2} = 1.35 \tag{4-7}$$

has been a constant used for all flight conditions. Finally FAR_{req} is a design requirement (Requirement 1-1, p. 11). The different values used will be discussed with the relevant test cases in chapter 4.3.3 and 4.3.4.

Remark 4-3: For the simulation case study the inverse normal distribution (4-2) was calculated online, because it was found that this is computationally not overly expensive. If this should become a problem $\tilde{J}_{th,\chi^2}$ can also be stored in a look-up table as function of $J_{th,RMS}^2$.

4.2 Simulated Flight Conditions

For the simulation case study, four to the author's opinion representative Flight Conditions (FC) have been selected in the F-16 envelope covered by the non-linear simulation model (cf. Appendix A.1). The important key parameters characterizing the FCs are summarized in Table 6. In all cases the aircraft was trimmed for straight and level flight, i.e. $\gamma_{K,0} = 0$. The other assumptions resulting from the use of the linear short period approximation are described in chapter 3.5.1.

4.2.1 Flight Condition 1

FC 1 is representative of a typical landing approach phase with the aircraft at an altitude of 650 m (2132 ft), at a typical approach angle of attack $\alpha_{K,0}$ = 13.0 deg and a true airspeed of $V_{A,0}$ = 76.0 m/s (148 KTAS). The landing gear was in the retracted position, as no aircraft data for landing gear down was available. For comparability to the other flight conditions/test cases the CAP requirements for category A flight phase were kept besides the fact that approach would be category C according to MIL-F-8785C (US DoD, 1996, p. 3). The short period parameters ω_{SP}, ζ_{SP}, and CAP are summarized in Table 7. For FC 1 the resulting CAP for the nominal system is CAP_{nom} = 1.28. The reason that the CAP is slightly higher than one is the lower bound on ω_{SP} as explained in the following remark.

Remark 4-4: The acceptable range of ω_{SP} is first of all derived from $0.28 \leq CAP_{L1} \leq 3.6$ (cf. chapter 2.2.2). Due to the reasons discussed in Remark 2-1 (p. 33) also absolute limits $1.7 \leq \omega_{SP} \leq 7.0$ rad/s have been imposed. Both limitations together result in $\omega_{SP,L1}$. The nominal system was first of all targeted to achieve CAP = 1. A second limitation was imposed for $\omega_{SP,nom}$ to stay 0.5 rad/s away form $\omega_{SP,L1}$. If the nominal system would lie on the boundary given by $\omega_{SP,L1}$ we would not be able to demonstrate what we want to demonstrate, i.e. the impact of deviations from the nominal system. The result of the two limitations for the nominal system is $\omega_{SP,nom}$. The resulting CAP is CAP_{nom}. The allowable damping ratio range, derived from the L1 flying quality requirements (cf. chapter 2.2.2), is $0.35 \leq \zeta_{SP,L1} \leq 1.3$. The damping ratio of the nominal system is $\zeta_{SP,nom}$ = 0.707.

4.2.2 Flight Condition 2

FC 2 was selected as low altitude, high speed case. The aircraft is trimmed at an altitude of 650 m (2132 ft), low $\alpha_{K,0}$= -0.6 deg at a true airspeed of $V_{A,0}$ = 321 m/s (624 KTAS) resulting in a Mach number $Ma_{A,0}$ = 0.95. As the non-linear simulation model available supports only subsonic speeds the choice of a higher Mach number has not been possible for this case study. The short period parameters ω_{SP}, ζ_{SP}, and CAP are summarized in Table 7. For FC 2 the resulting CAP for the nominal

system is CAP_{nom} = 0.60. The reason that the CAP is slightly lower than one, is the upper bound on ω_{SP} as explained in Remark 4-4.

4.2.3 Flight Condition 3

FC 3 simulates the aircraft in a high altitude cruise condition at $h_{A,0}$ = 13700 m (44948 ft) and high subsonic speed ($Ma_{A,0}$ = 0.95). The resulting true airspeed $V_{a,0}$ is 280 m/s (544 KTAS) with $\alpha_{K,0}$= 3.8 deg. For FC 3 the resulting CAP for the nominal system is CAP_{nom} = 1.0.

4.2.4 Flight Condition 4

For FC 4 the F-16 is trimmed at $\alpha_{K,0}$= 20 deg close to its normal operating envelope angle of attack limit, $\alpha_{K,lim}$ = 25.1 deg, at a medium altitude of 5000 m (16404 ft). This altitude has also been chosen because it leads to the highest Dryden medium/high altitude model turbulence standard deviation σ_{w_W}. Together with the low airspeed $V_{A,0}$ = 76.4 m/s (148 KTAS) this results in strong turbulence induced angle of attack variations and requires pronounced elevator deflections η to control the aircraft in pitch. The short period parameters ω_{SP}, ζ_{SP}, and CAP are summarized in Table 7. For FC 4 the resulting CAP for the nominal system is CAP_{nom} = 2.27. The reason that the CAP is higher than one is the lower bound on ω_{SP} as explained in Remark 4-4.

Table 6 Summary of key parameters for simulated flight conditions

FC ID	$h_{A,0}$ [m]	$V_{A,0}$ [m/s]	$V_{EAS,0}$ [m/s]	$Ma_{A,0}$ [-]	$\bar{q}_{A,0}$ [kPa]	$\alpha_{K,0}$ [deg]	η_0 [deg]	$T_{2,OL}$ [s]
1	650	76.0	73.6	0.22	3.32	13.0	4.9	1.26
2	650	321	311	0.95	59.2	-0.6	-0.7	0.40
3	13700	280	123.5	0.95	9.34	3.8	1.2	0.98
4	5000	76.4	59.2	0.24	2.15	20.0	8.6	2.68

Table 7 Summary of short-period parameters for simulated flight conditions

FC ID	CAP_{L1} [-]	$\omega_{SP,lim}$ [rad/s]	$\omega_{SP,L1}$ [rad/s]	$\omega_{SP,nom}$ [rad/s]	CAP_{nom} [-]	$\zeta_{SP,L1}$ [-]	$\zeta_{SP,nom}$ [-]
1	0.28 - 3.6	1.7 – 7.0	1.70 – 3.70	2.20	1.28	0.35 – 1.30	0.707
2			4.45 – 7.00	6.50	0.60		
3			1.70 – 6.10	3.22	1.00		
4			1.70 – 2.77	2.20	2.27		

4.3 Results of Simulation Case Studies

This chapter will discuss the results of the simulation case study concerning the performance of the fault detection system proposed in this thesis. Chapter 4.3.2 describes the results under purely deterministic conditions, i.e. without stochastic unknown inputs, to verify the theoretical results for the deterministic FD part. In the same manner chapter 4.3.3 gives the results with respect to the stochastic FD performance though this also requires some deterministic assumptions. Finally chapter 4.3.4 demonstrates the performance of the fault detection system for a demanding practical relevant failure case where the closed-loop aircraft becomes unstable.

4.3.1 Nominal System Response

4.3.1.1 Test Goal

The goal of this chapter is to introduce the reader to the response of the nominal system with and without turbulence.

4.3.1.2 Introductory Remarks

For the four flight conditions introduced in the last chapter, realistic pitch rate command inputs have been identified. This chapter discusses the *desired* system response without fault conditions. The results for two different levels of simulation model fidelity are presented. First of all the closed-loop short period model *without* actuator dynamics, rate and position limits referred to as "Ideal Act. (PT0)". It will be used later on as reference of what we aim to achieve in terms of short period motion and to verify some theoretical results. Second a closed-loop short period model including the linear 2nd-order actuator dynamics, rate and position limits as presented in Table 16 (p. 196). This model will be called "Realistic Act. (PT2, RL)".
Before starting the discussion of the TCs the author wants to add some introductory notes:

Remark 4-5: The TC ID is a unique number containing the flight condition ID as number after the dot. We will therefore in most cases no longer explicitly refer to the FC as it is implicit in the TC ID.

Remark 4-6: The F-16 production FCS limits the commandable angle of attack $\alpha_{K,lim}$ as function of the normal load factor $(n_z)_K$. The schedule is reproduced in Appendix A.7. For the case study the schedule from the production FCS has been retained, despite the fact, that for $(x^G)_B = 0{,}4 \cdot \bar{c}$, selected for the case study, the aircraft is significantly more unstable than the F-16 production design and has less nose down control power (cf. chapter A.6). We will come back to this peculiarity in the relevant discussions about recovering the system from a fault in which it has become closed-loop unstable.

Remark 4-7: If we refer to a steady state in the following discussion, we mean the steady state of the *linear short period model* used in this simulation case study. Of course in a higher-order linear or non-linear simulation as well as for a real aircraft the changes of flight path angle and airspeed, together with its related system responses e.g. phugoid motion, would manifest itself. The short period model chosen is deemed sufficient by the author to demonstrate principle *feasibility* of the fault detection approach suggested in this thesis. It is also a common simplification used during FCS inner-loop control law design (cf. e.g. Osterhuber et al., 2004,p. 3) and general studies on short period handling qualities (cf. Gibson, 1999, p. 23).

4.3.1.3 Specific Simulation Setup

The test cases used the basic simulation setup as described in chapter 4.1 tough the fault detection part is not required for the content discussed in this paragraph. The model with actuator dynamics will be described in chapter 4.3.4.2.3.

4.3.1.4 Test Condition

The simulation runs have been performed at FC 1-4 using filtered step inputs. The parameters for TC 1.xt are identical to TC 1.x, beside the fact that vertical atmospheric turbulence has now been simulated using the Dryden high/medium altitude model. A "worst-case" turbulence standard deviation $\sigma_{w_W}(h_A)$ for severe turbulence at a probability of exceedance < 10^{-6} has been selected (cf. Figure 28, p. 104).

Remark 4-8: The $q_{K,cmd}$ inputs were modelled as step inputs filtered by a 1st-order low pass filter (T_{LP} = 0.15 s, $k_{P,LP}$ = 1) in order to prevent actuator rate and position limiting (saturation) for regular (pilot) command inputs. Command limiting, potentially in a different form, is also required for real flight control systems (cf. Brockhaus et al., 2011, pp. 820; NATO RTO, 2000, p. 56). Furthermore no pilot can produce a real step input.

4.3.1.5 Test Results and Discussion

4.3.1.5.1 Test Case 1.1 and 1.1t

In TC 1.1 a pitch rate command $q_{K,cmd}$ = 5 deg/s is applied at t = 1 s (Figure 32). The command leads to a desired pitch rate peak $q_{K,max}$ = 11.1 deg/s at t = 1.8 s (cf. CAP, chapter 2.2.2). Without the pitch rate peak the build-up of α_K and therefore $(n_z)_K$ would be to slow, resulting in a flight path response which a pilot would likely call "sluggish" (cf. e.g. Gibson, 1999', p. 42; Heller, 2013, p. 3-134; Holzapfel, 2011, p. 14-65/94). The pitch rate q_K finally settles at the commanded value of 5 deg/s after around 3.5 sec.
The angle of attack α_K increases from the trim value of 13.0 deg to its peak value of 22.0 deg in 3 sec. This is already quite closed to the limit $\alpha_{K,lim}\big((n_z)_K\big)$ = 24.3 deg. The normal load factor $(n_z)_K$ initially shows a small decrease after the pitch rate command was applied at t = 1 s and then reaches its steady state value of 1.7 g at approximately 3 sec. The decrease of $(n_z)_K$ has its roots in the initially negative elevator deflection, that results at first in an overall lift decrease due to Z_η. The effect is not very pronounced in TC 1.1 though visible.
The elevator deflection η shows the typical pitch-up command response for an open-loop unstable plant, requiring an initial negative deflection (nose up) but afterwards a positive (nose down) value in the steady state. For an open-loop stable design the deflection would be negative in the steady state.

Remark 4-9: This positive elevator deflection in the steady state also constitutes the aerodynamic advantage of an open-loop unstable aircraft because the lift generated by the elevator is in the same direction as the lift generated by the wing therefore increasing the maximum possible lift coefficient $\left(C_{Z,max}\right)_A$ of a configuration and reducing the induced drag for a given trim condition (cf. chapter 2.2.1).

In comparison to TC 1.1, the response of TC 1.1t (Figure 33) shows the typical impact of unknown stochastic disturbances, in our case the vertical wind velocity with standard deviation σ_{w_W} = 6.96 m/s that induces the wind angle of attack α_W via (3-156). Under normal practical conditions, α_W cannot be measured and is therefore not known to a FCS. By inspection of (3-160) it is therefore clear that the same is true for the aerodynamic angle of attack α_A. α_W thus constitutes a stochastic unknown input (disturbance) and the FCS can only counteract the aircraft reaction on α_W which shows up in the measureable values q_K and α_K. The reaction on α_W is of course more pronounced for statically unstable designs because M_α of the open-loop plant is positive and all the counteracting moment has to be generated by the FCS via M_η (cf. Brockhaus et al., 2011, p. 827). Because α_W cannot be measured the reaction of the FCS will not occur before the effect of α_W shows up in q_K and α_K.

A stronger reaction of the aircraft on disturbance α_W can therefore not be avoided. The effect is clearly visible in Figure 33. The increase of α_A (because of α_W) from $t \sim 3$ sec to 8 sec leads to a positive pitch rate q_K that is reduced by a counter acting positive elevator deflection η.

Remark 4-10: It should be clear that also the free-stream $\alpha_{K,\infty}$ can not be measured under practical conditions. We normally measure the local angle of attack more (e.g. ADS vanes) or less (e.g. nose boom vanes) close to the airframe and then, using to a greater or lesser extent sophisticated corrections, estimate $\hat{\alpha}_{K,\infty}$.

4.3.1.5.2 Test Case 1.2 and 1.2t

Figure 34 illustrates the system response for TC 1.2 It shows the same characteristics as described for TC 1.1 though the system response in terms of $(n_z)_K$ and $q_{K,max}$ is much more pronounced as expected for a flight condition at low altitude and high speed, i.e. with high dynamic pressure $\bar{q}_A$. The FC and pitch rate command $q_{K,cmd}$ = 14 deg/s were chosen to achieve a normal load factor response, $(n_z)_K$ = 8.5 g, close to the F-16 limit of $(n_{z,lim})_K$ = 9.0 g. Furthermore it is interesting to note the more distinct initial decrease of the normal load factor $(n_z)_K$ due to the, in the beginning, negative η as well as the pronounced limitation $\alpha_{K,lim}((n_z)_K)$ = 16.6 deg of the F-16 production FCS.
TC 1.2t (Figure 35) shows the same characteristic as discussed for the *flight condition* in TC 1.2 and for the *effect of atmospheric turbulence* in TC 1.1t. When compared to the latter, the response to the disturbance α_W in terms of absolute value of q_K and $(n_z)_K$ are of course more significant as to be expected for a flight condition with high dynamic pressure $\bar{q}_A$ = 59.2 kPa and $V_{EAS,0}$ = 311 m/s

4.3.1.5.3 Test Case 1.3 and 1.3t

Also TC 1.3 (Figure 36) and TC 1.3t (Figure 37) show the same principal characteristics as described for TC 1.1/1.1t and TC 1.2/1.2t. Despite the fact that, compared to TC 1.2/1.2t, the Mach number ($Ma_{A,0}$ = 0.95) is the same and $q_{K,cmd}$ = 5 deg/s is much smaller, the angle of attack variations and elevator deflections are much more pronounced. The reason is the much lower dynamic pressure $\bar{q}_A$ = 4.24 kPa manifesting itself also in the much lower $V_{EAS,0}$ = 123.5 m/s.

4.3.1.5.4 Test Case 1.4 and 1.4t

TC 1.4 (Figure 38) has been intended as low speed and high angle of attack scenario. At the given FC a small $q_{K,cmd}$ = 1.4 deg/s already induces an $\alpha_{K,max}$ = 24.8 deg, very close to $\alpha_{K,lim}((n_z)_K)$ = 24.9 deg of the F-16 production FCS. Another pecu-

liarity of this TC is the high elevator trim deflection with η_0 = 8.6 deg. In view of the elevator deflection limit of η_{lim} = 25 deg this leaves limited nose down control power in a possible fault case, to be discussed later, where the aircraft becomes unstable and has to be recovered.
TC 1.4t in Figure 39 shows all the signs of a typical low $V_{EAS,0}$ = 59.2 m/s ($\bar{q}_A$ = 2.15 kPa) flight condition under turbulence with pronounced α_W induced α_A variations but relatively weak absolute aircraft reaction in q_K and $(n_z)_K$. The comparably strong elevator deflections to counter the disturbance are also visible. As for TC 1.1t we see the pitch-up reaction on an increase of α_A due to the unstable open-loop plant. As already said in chapter 4.2, the turbulence standard deviation σ_{w_W} = 9.37 m/s chosen also represents the maximum value for the Dryden medium/ high altitude model over all altitudes (cf. Figure 28, p. 104).

Table 8 summarizes the key response characteristics for all test cases, as discussed in the above paragraphs.

Table 8 Key response characteristics for nominal system
(TC 1.1 - 1.4 & TC 1.1t - 1.4t)

Test Case ID	$q_{K,cmd}$ [deg/s]	$q_{K,max}$ [deg/s]	$\alpha_{K,max}$ [deg]	$(n_{z,max})_K$ [g]
1.1	5	11.1	22.0	1.7
1.2	14	20.5	5.2	8.5
1.3	5	19.4	17.3	3.7
1.4	1.4	5.2	24.8	1.2
1.1t	5	10.7	22.6	1.8
1.2t	14	20.2	5.4	8.9
1.3t	5	18.8	17.4	3.7
1.4t	1.4	4.3	24.9	1.2

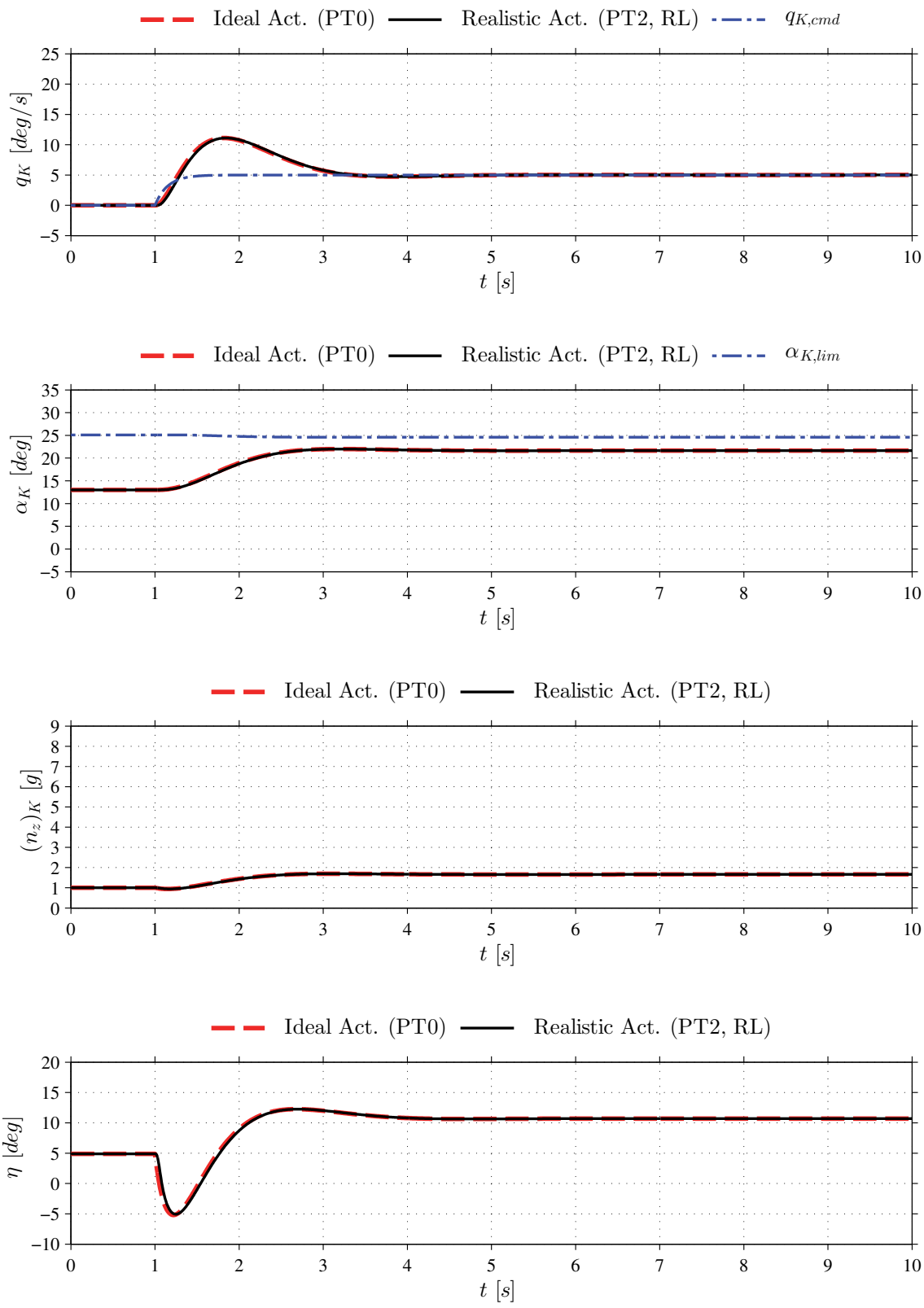

Figure 32 F-16 closed-loop response to a control input $q_{K,cmd}$ = 5 deg/s (TC 1.1)

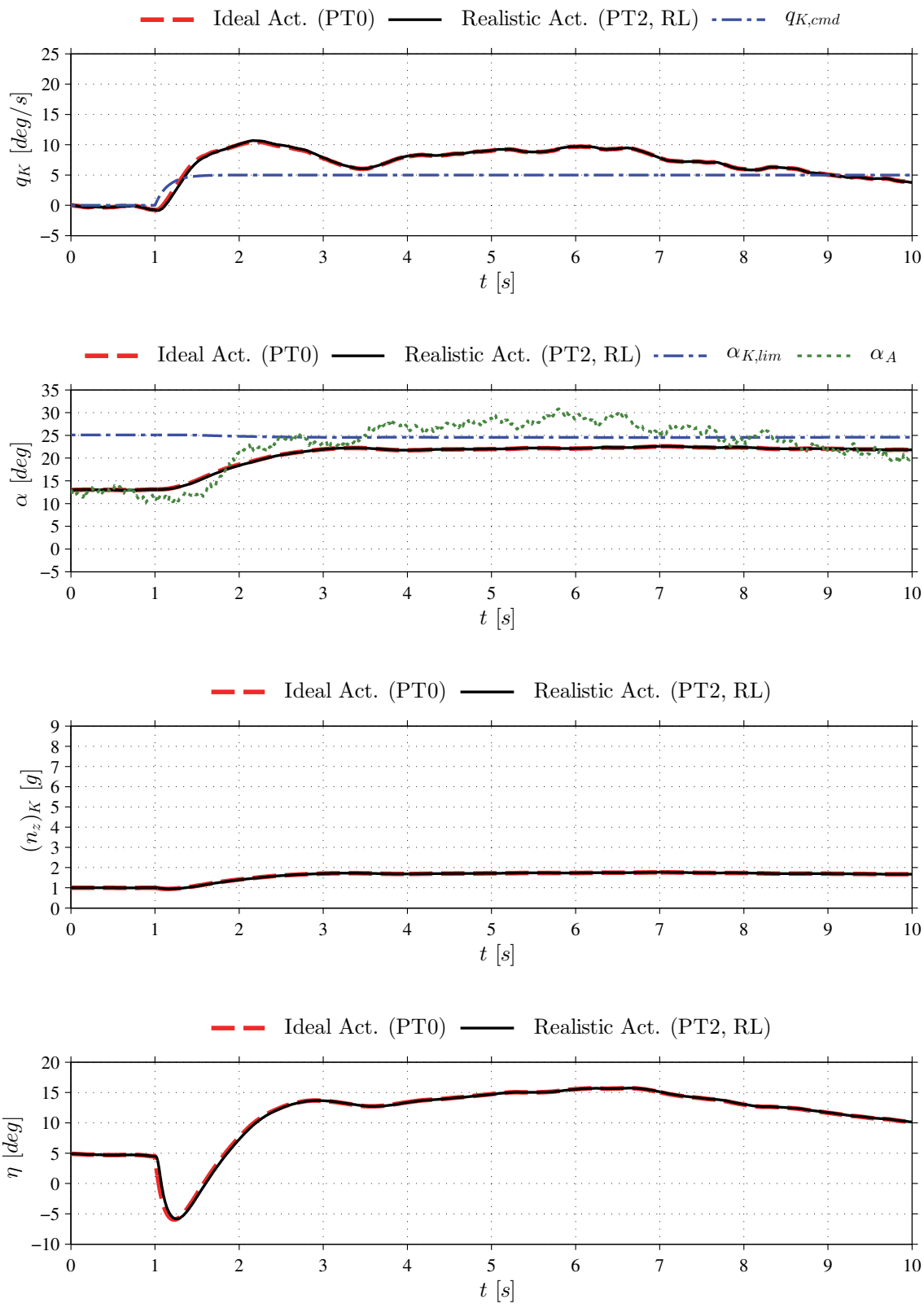

Figure 33 F-16 closed-loop response to a control input $q_{K,cmd}$ = 5 deg/s with atmospheric turbulence (TC 1.1t)

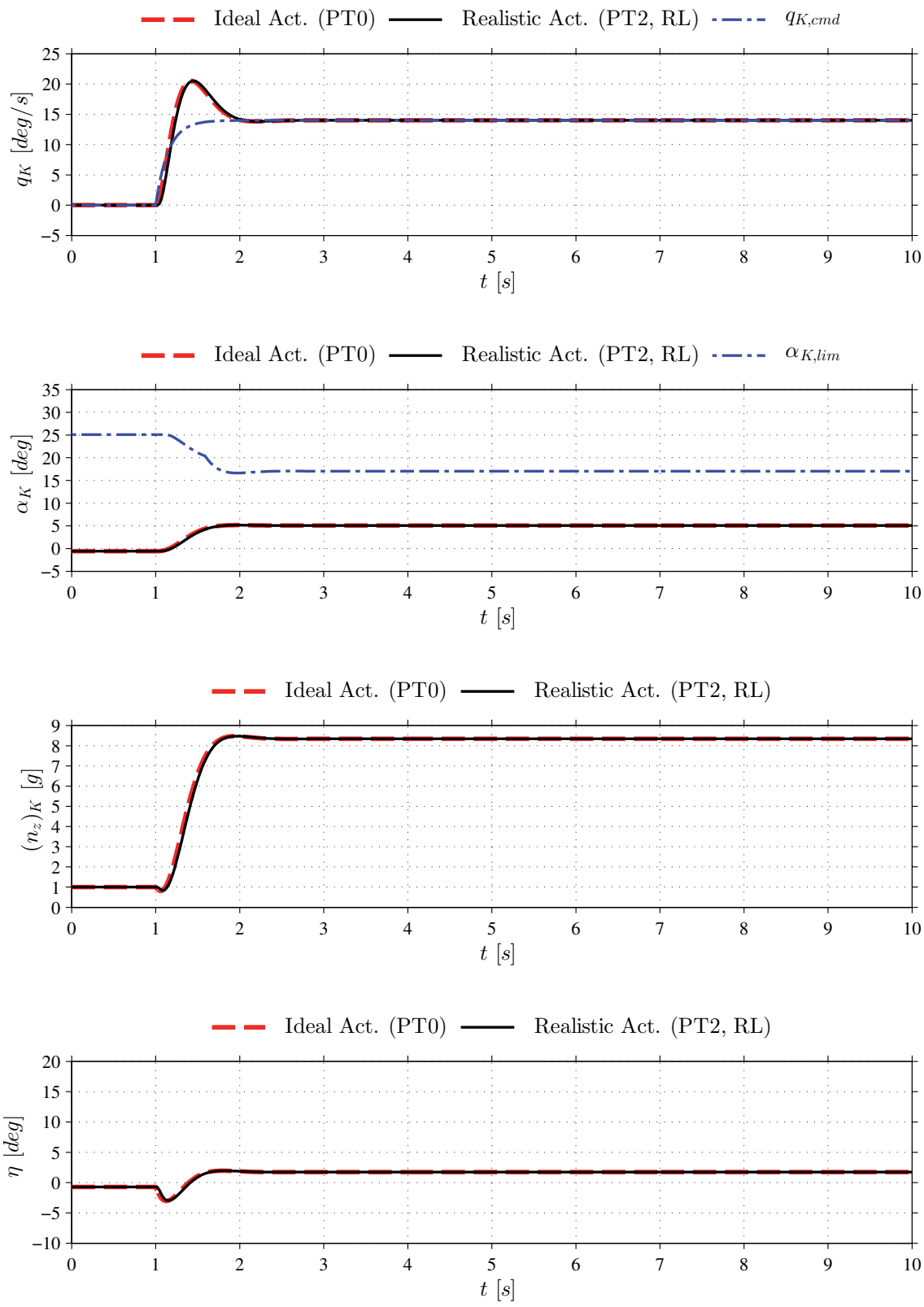

Figure 34 F-16 closed-loop response to a control input $q_{K,cmd}$ = 14 deg/s (TC 1.2)

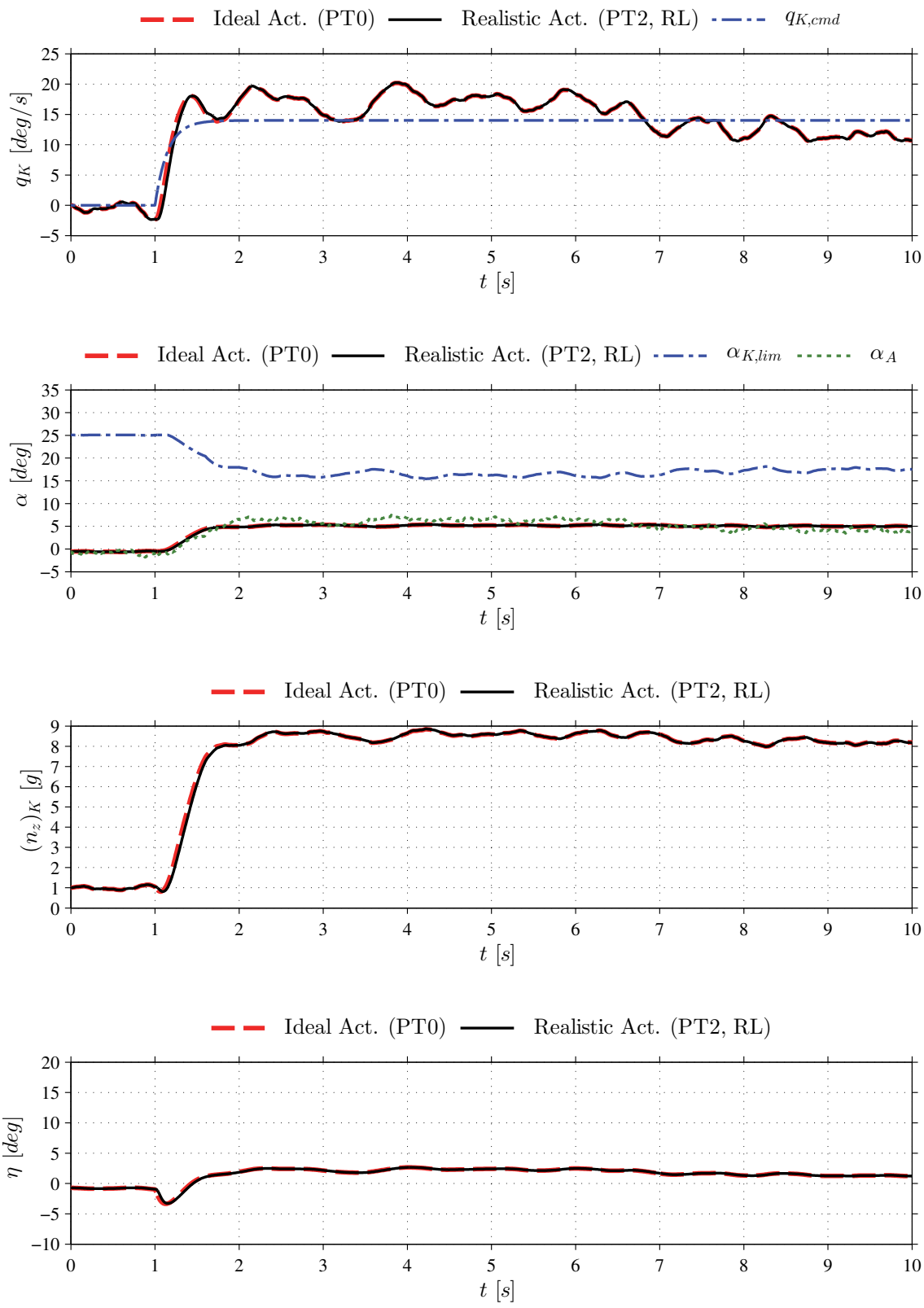

Figure 35 F-16 closed-loop response to a control input $q_{K,cmd}$ = 14 deg/s with atmospheric turbulence (TC 1.2t)

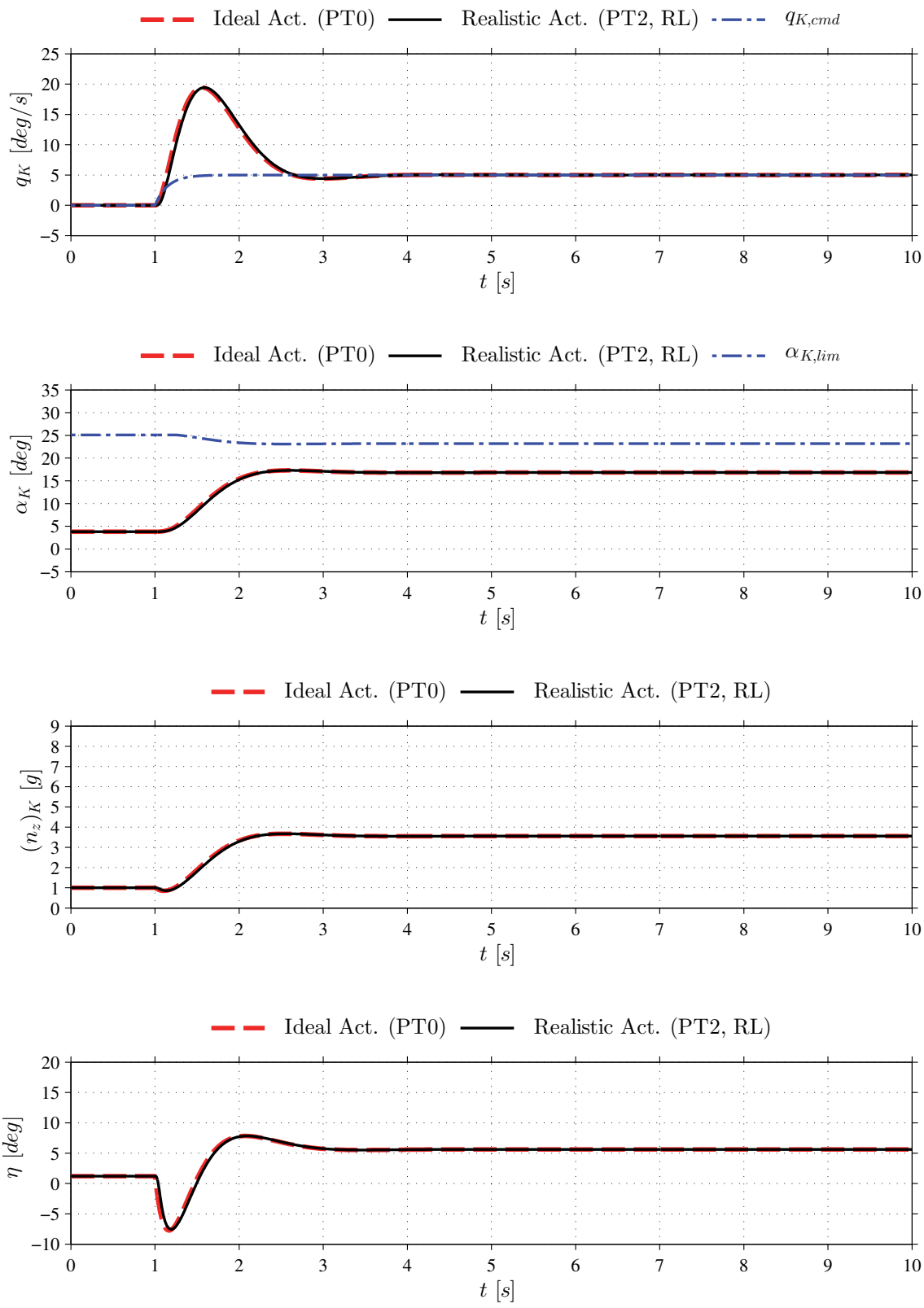

Figure 36 F-16 closed-loop response to a control input $q_{K,cmd}$ = 5 deg/s (TC 1.3)

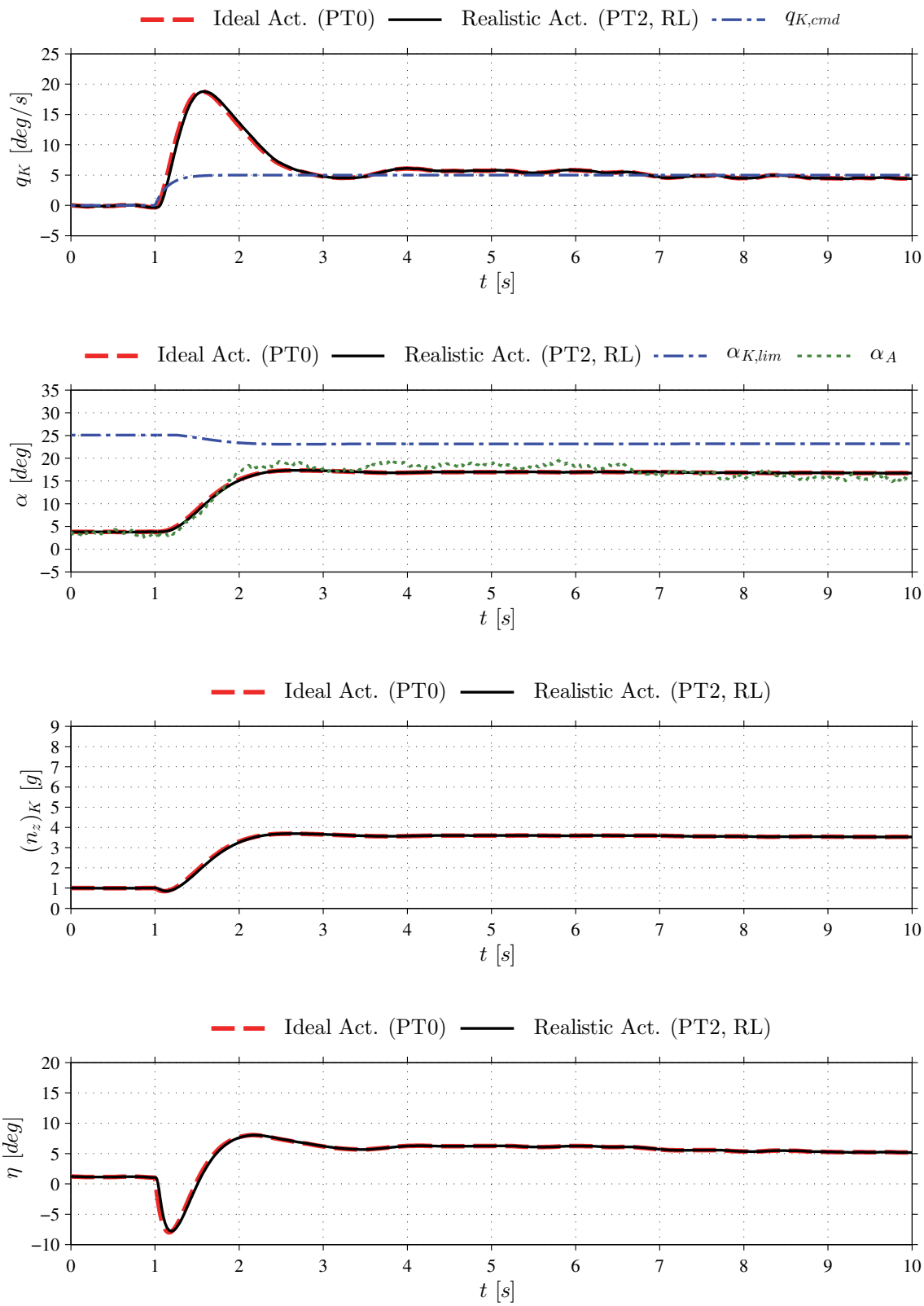

Figure 37 F-16 closed-loop response to a control input $q_{K,cmd}$ = 5 deg/s with atmospheric turbulence (TC 1.3t)

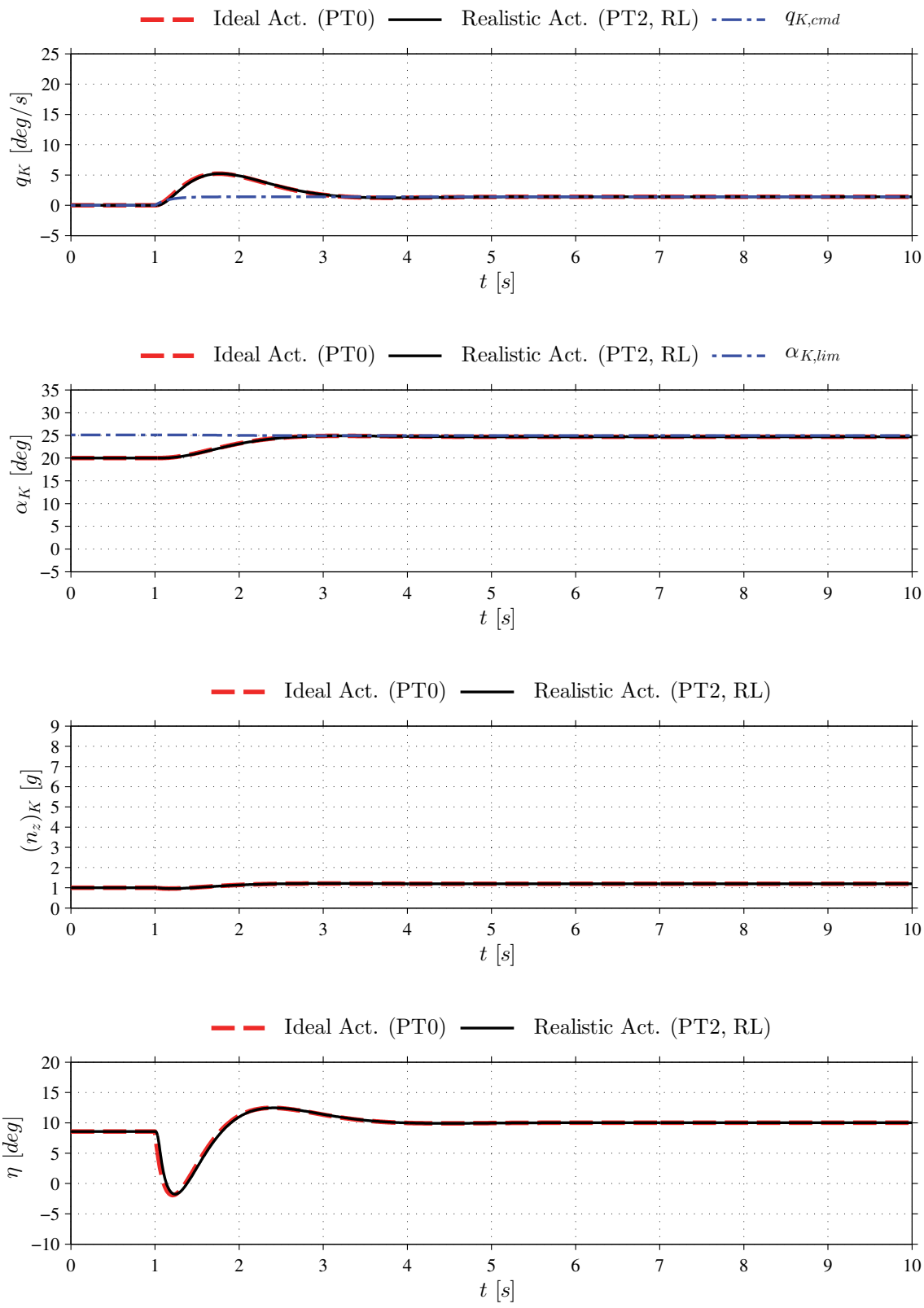

Figure 38 F-16 closed-loop response to a control input $q_{K,cmd}$ = 1.4 deg/s (TC 1.4)

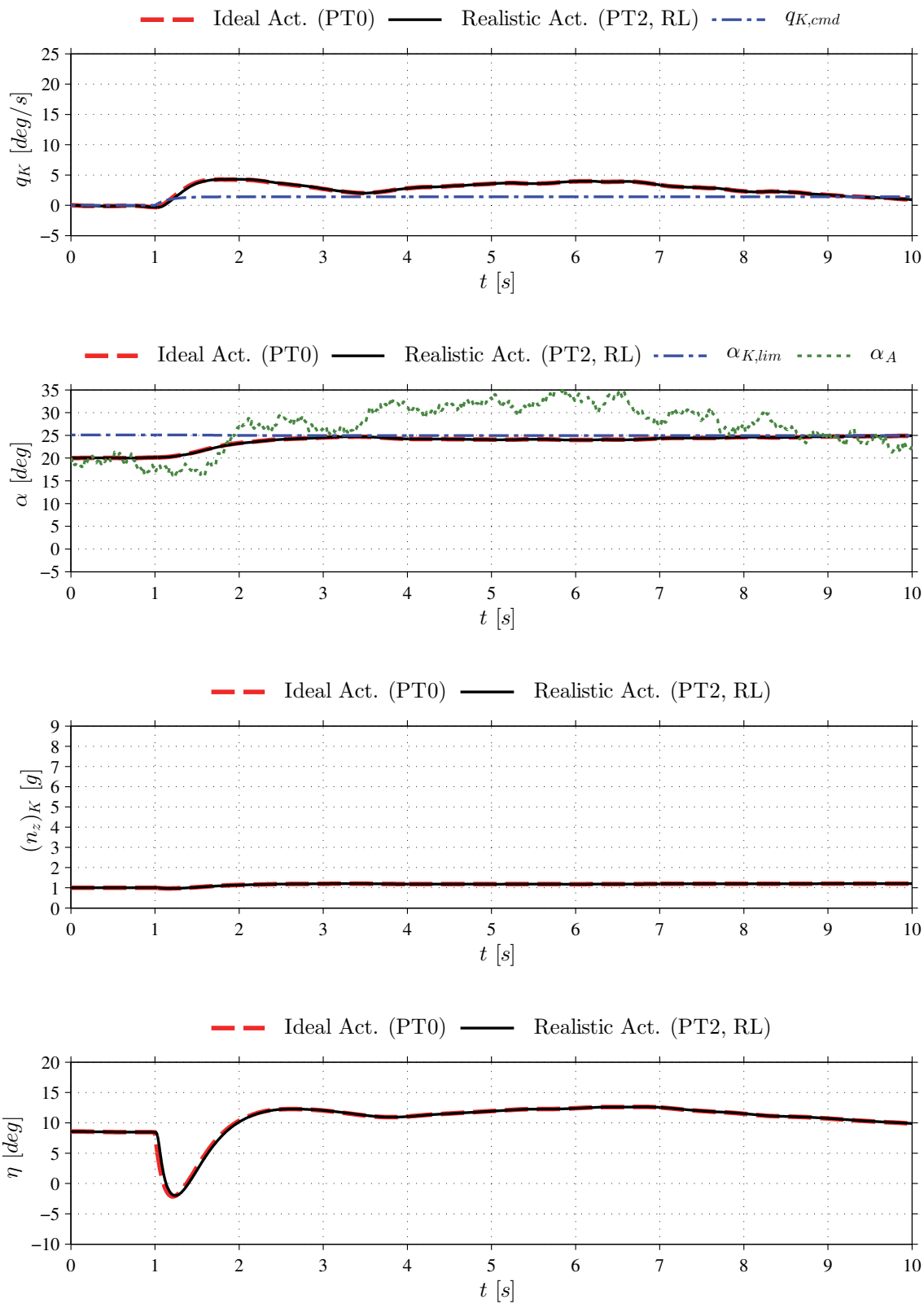

Figure 39 F-16 closed-loop response to a control input $q_{K,cmd}$ = 1.4 deg/s with atmospheric turbulence (TC 1.4t)

4.3.2 Verification of Theoretical Results - Deterministic Fault Detection

The overall goal of this chapter is to verify the theoretical results for the deterministic part (cf. chapter 3.5.4.3) of the fault detection system suggested in this thesis. It is especially intended to demonstrate that no false alarms have to be expected, which is a requirement (Requirement 1-1, p. 11) for the FD system.
In order to increase readability for the remainder of this text we will use the following abbreviations

$$\mathcal{H}_\infty \equiv \left\| \boldsymbol{G}_{rq_{cmd}} \right\|_\infty \tag{4-8}$$

$$\mathcal{H}_{\infty,max} \equiv \left\| \boldsymbol{G}_{rq_{cmd}} \right\|_{\infty,max} \tag{4-9}$$

with related input frequency

$$\omega_{\mathcal{H}_{\infty,max}} \equiv \omega_{\left\| \boldsymbol{G}_{rq_{cmd}} \right\|_{\infty,max}} \tag{4-10}$$

for q_{cmd} sine inputs. Likewise we will call the vertex that leads to $\left\| \boldsymbol{G}_{rq_{cmd}} \right\|_{\infty,max}$

$$\mathcal{V}_{\infty,max} \equiv \mathcal{V}_{\left\| \boldsymbol{G}_{rq_{cmd}} \right\|_{\infty,max}} \tag{4-11}$$

4.3.2.1 Maximum $\mathcal{H}_\infty$-Gain of Residual Dynamic System Derived from the Reference Model with Polytopic Time-Invariant Model Uncertainties

4.3.2.1.1 Test Goal

In chapter 3.5.4.3.1.3 the author claimed that for the residual dynamic system derived from a reference model with time-invariant polytopic model uncertainties as used in this thesis, the maximum gain $\mathcal{H}_{\infty,max}$ is found at one of the four vertices $\mathcal{V}_i$, i.e. all other residual systems described by the model uncertainties inside the parameter polytope have a lower $\mathcal{H}_\infty$. The goal of the simulation case study of this chapter is to verify that this claim is correct.

4.3.2.1.2 Specific Simulation Setup

A Monte Carlo simulation has been conducted in which $\mathcal{H}_\infty$ was calculated for 1000 residual dynamic systems inside the parameter polytope. The residual dynamics are given by (3-219) and (3-220).

4.3.2.1.3 Test Conditions

The simulation runs TC 2.1 – 2.4 have been performed for FC 1-4. The allowable deviation of system response from its nominal values were set to $\omega_{SP,L1}$ and $\tilde{\zeta}_{SP,L1}$ according Table 10. The parameters $\delta_1 = \tilde{\zeta}_{SP}\omega_{SP}$ and $\delta_2 = \omega_{SP}^2$ have been calculated for 1000 randomly selected ζ_{SP}-ω_{SP} parameter combinations, chosen from a uniform random distribution, inside the parameter polytope defined by $\omega_{SP,L1}$ and $\tilde{\zeta}_{SP,L1}$ (cf. chapter 3.5.4.3.1).

Remark 4-11: $\tilde{\zeta}_{SP,L1}$ represents the polytope approximation of $\zeta_{SP,L1}$ as explained in chapter 3.5.4.3.1.1.

4.3.2.1.4 Test Results

Figure 40 to Figure 43 show the results of the Monte Carlo simulation for FC 1 to 4 respectively. Simulation points where

- $\mathcal{H}_\infty < 0.5\,\mathcal{H}_{\infty,max}$ are marked as *green dots*
- $0.5\,\mathcal{H}_{\infty,max} \leq \mathcal{H}_\infty < 0.75\,\mathcal{H}_{\infty,max}$ are marked as *cyan asterisk*
- $0.75\,\mathcal{H}_{\infty,max} \leq \mathcal{H}_\infty < 0.99\,\mathcal{H}_{\infty,max}$ are marked as *orange plus sign*
- $\mathcal{H}_\infty \geq 0.99\,\mathcal{H}_{\infty,max}$ would be marked as *red cross*

As visible form the aforementioned figures, *for none of the FCs* a simulation point has been found where $\mathcal{H}_\infty \geq 0.99\,\mathcal{H}_{\infty,max}$. Table 9 compares the maximum $\mathcal{H}_{\infty,MC}$ found during Monte Carlos simulation with $\mathcal{H}_{\infty,max}$. It is readily visible that $\mathcal{H}_{\infty,MC} < \mathcal{H}_{\infty,max}$. Table 10 summarizes $\mathcal{H}_\infty$ for the vertices $\mathcal{V}_i$. The nominal system is shown as cross-check. Obviously $\mathcal{H}_{\infty,nom}$ must be equal to zero if the calculations have been done correctly.

Remark 4-12: The vertices $\mathcal{V}_i$ are numbered in the clockwise direction starting from the lower left corner of the polytope.

4.3.2.1.5 Discussion of Results with Respect to Test Goal

The simulation verified that, for the conditions tested, no system inside the parameter polytope defined by $\omega_{SP,L1}$ and $\tilde{\zeta}_{SP,L1}$ has a $\mathcal{H}_\infty \geq \mathcal{H}_{\infty,max}$, which confirms that $\mathcal{H}_{\infty,max}$ is found at one of the vertices $\mathcal{V}_i$. This is of great importance for the deterministic part of the FD system proposed in this thesis. From (3-226) we recall that the deterministic fault detection threshold is calculated by

$$J_{th,RMS}^2(k) = \sup_{\boldsymbol{f=0,\Delta\neq 0}} \|\boldsymbol{r}\|_{RMS}^2 = \mathcal{H}_{\infty,max}^2 \left\|q_{cmd,env}\right\|_{RMS}^2(k)$$

If there would be a system inside the parameter polytope for which $\mathcal{H}_\infty \geq \mathcal{H}_{\infty,max}$ a false alarm could thus be raised. For the conditions tested this has *not* been the case.

4.3.2.1.6 Conclusion

For the conditions test it has been verified that the maximum $\mathcal{H}_\infty$ for the residual dynamic system derived from the reference model with time-invariant polytopic model uncertainties is found at one of the system vertices $\mathcal{V}_i$. No system inside the parameter polytope has a higher $\mathcal{H}_\infty$ than $\mathcal{H}_{\infty,max}$, where $\mathcal{H}_{\infty,max}$ is the maximum $\mathcal{H}_\infty$ of all four vertices $\mathcal{V}_i$.

Table 9 Comparison of $\mathcal{H}_{\infty,max}$ against $\mathcal{H}_{\infty,MC}$ from Monte Carlo simulation

FC ID	TC ID	$\mathcal{V}_{\infty,max}$	$\mathcal{H}_{\infty,max}$	$\mathcal{H}_{\infty,MC}$ Monte Carlo	$\frac{\mathcal{H}_{\infty,MC}}{\mathcal{H}_{\infty,max}}$
1	2.1	Vertex 3	27.44	25.60	0.93
2	2.2	Vertex 1	23.15	22.59	0.98
3	2.3	Vertex 3	97.83	93.85	0.96
4	2.4	Vertex 3	93.22	87.14	0.93

Table 10 $\mathcal{H}_\infty$ for all flight conditions and vertices $\mathcal{V}_i$

FC ID	System	$\omega_{SP,L1}$ [rad/s] (Table 7)	$\zeta_{SP,L1}$ [-] (Table 7)	$\tilde{\zeta}_{SP,L1}$ [-]	$\mathcal{H}_\infty$
1	Vertex 1	1.70	0.350	0.400	12.02
	Vertex 2	3.70	0.350	0.361	17.68
	Vertex 3	3.70	1.30	1.30	27.44
	Vertex 4	1.70	1.30	1.30	5.94
	Nominal	2.20	0.707	0.707	0
2	Vertex 1	4.45	0.350	0.363	23.15
	Vertex 2	7.00	0.350	0.356	15.27
	Vertex 3	7.00	1.30	1.30	18.54
	Vertex 4	4.45	1.30	1.30	5.80
	Nominal	6.50	0.707	0.707	0
3	Vertex 1	1.70	0.350	0.527	63.00
	Vertex 2	6.10	0.350	0.367	88.60
	Vertex 3	6.10	1.30	1.30	97.83
	Vertex 4	1.70	1.30	1.30	22.27
	Nominal	3.22	0.707	0.707	0
4	Vertex 1	1.70	0.350	0.366	59.18
	Vertex 2	2.77	0.350	0.356	52.45
	Vertex 3	2.77	1.30	1.30	93.22
	Vertex 4	1.70	1.30	1.30	32.30
	Nominal	2.20	0.707	0.707	0

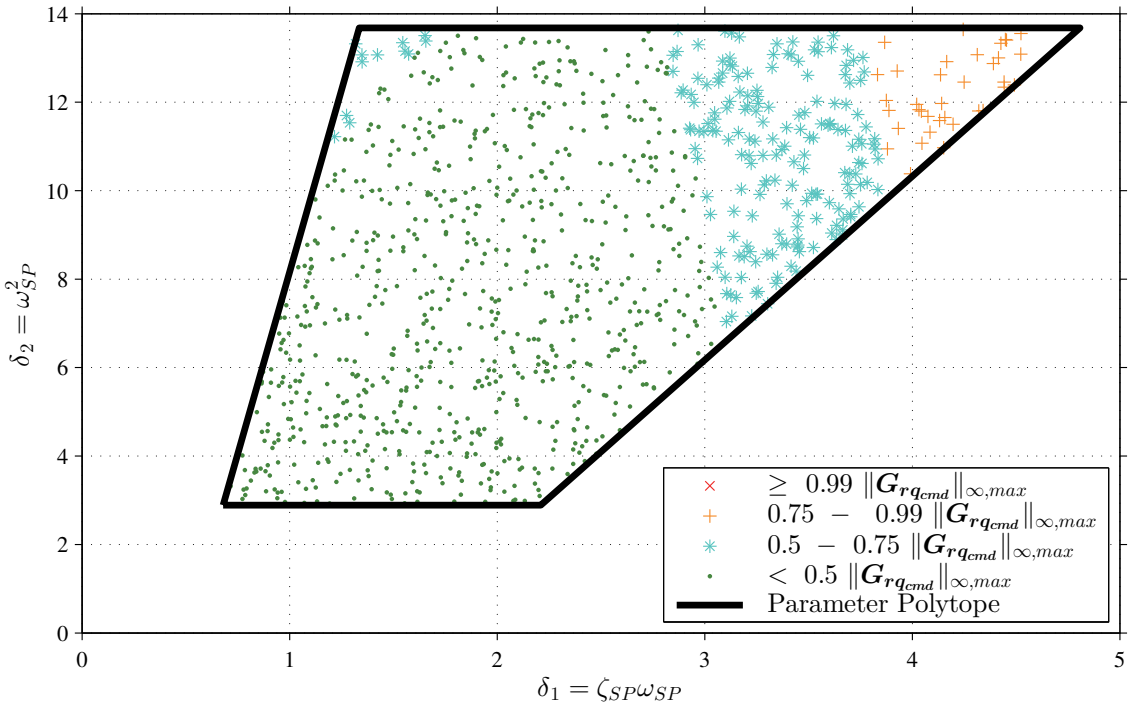

Figure 40 Monte Carlo Simulation $\mathcal{H}_\infty$ at FC 1 (TC 2.1)

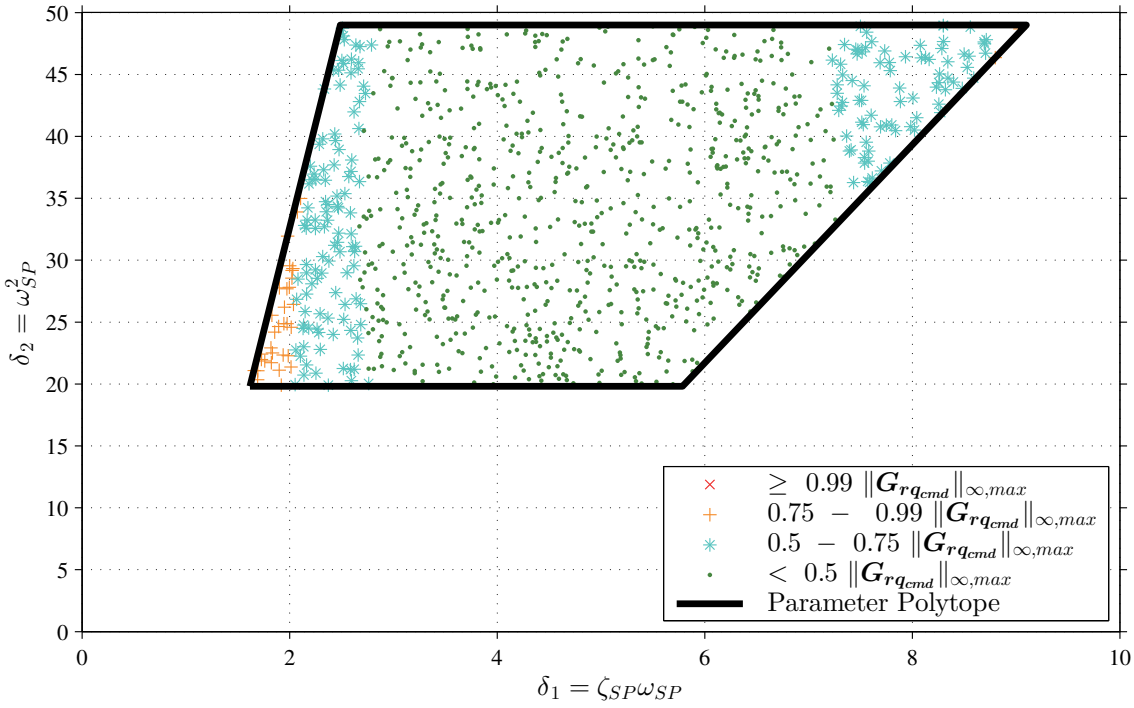

Figure 41 Monte Carlo Simulation $\mathcal{H}_\infty$ at FC 2 (TC 2.2)

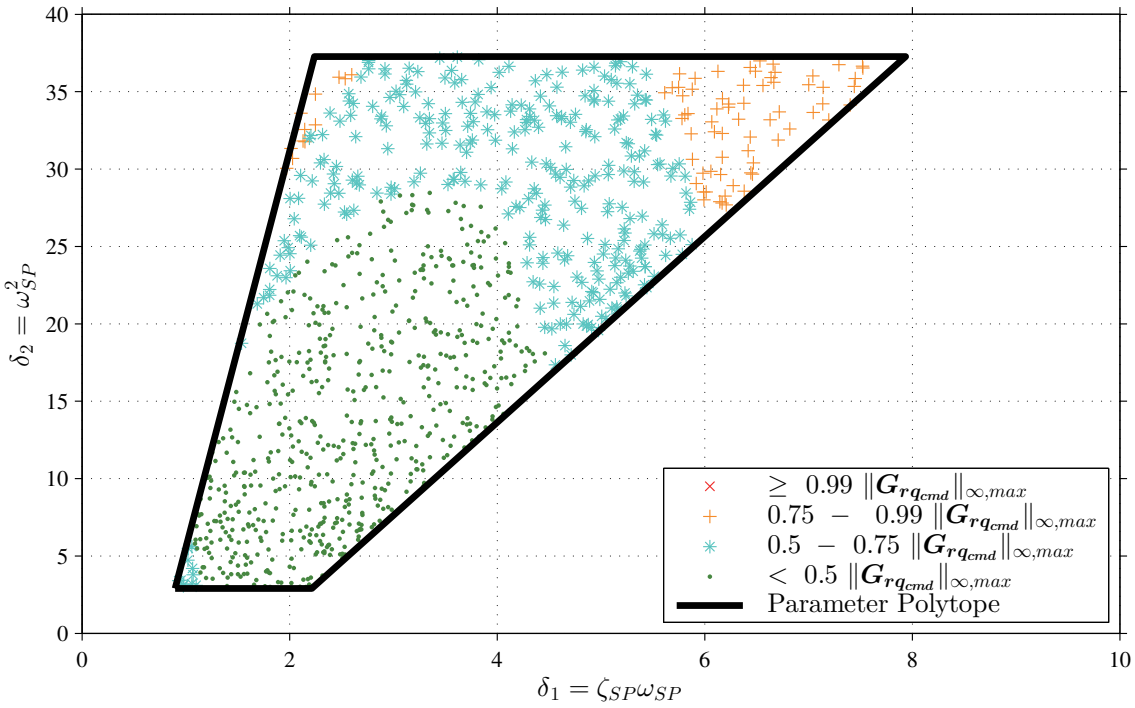

Figure 42 Monte Carlo Simulation $\mathcal{H}_\infty$ at FC 3 (TC 2.3)

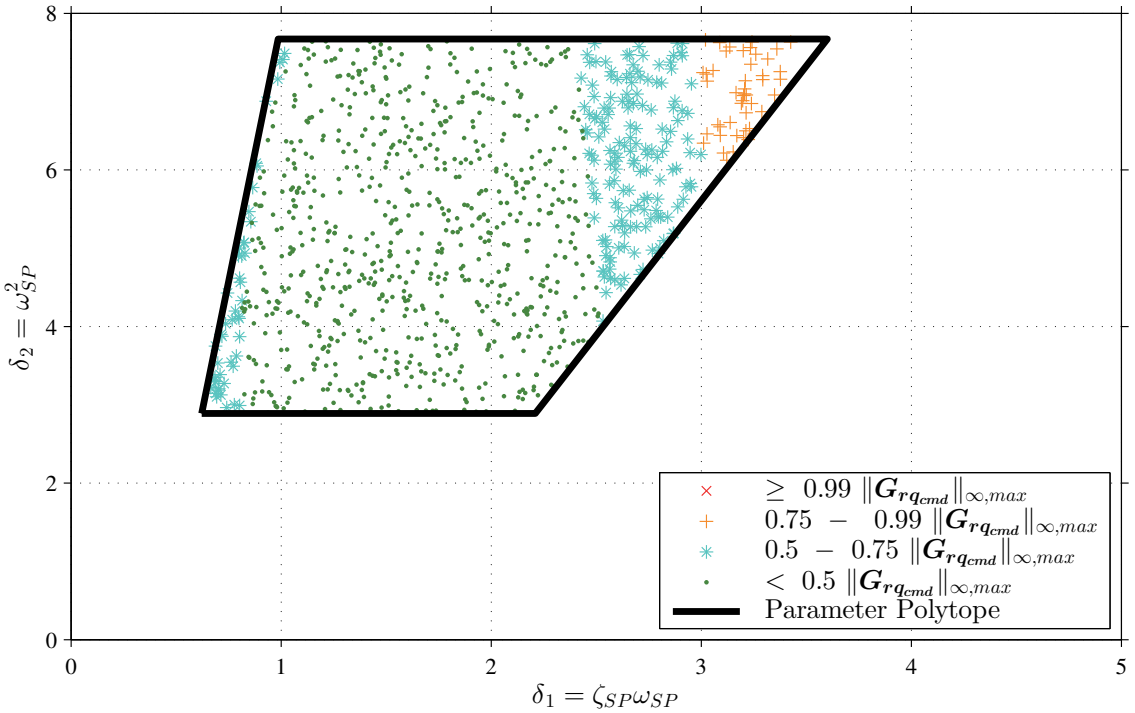

Figure 43 Monte Carlo Simulation $\mathcal{H}_\infty$ at FC 4 (TC 2.4)

4.3.2.2 Boundary Case for Largest Acceptable Model Uncertainties of the Reference Model with Time-Invariant Polytopic Model Uncertainties

4.3.2.2.1 Test Goal

In chapter 4.3.2.1 it has been demonstrated that $\mathcal{H}_{\infty,max}$ is the highest $\mathcal{H}_\infty$ of all systems inside the parameter polytope and that it is found at one of the vertices, namely $\mathcal{V}_{\infty,max}$ (cf. chapter 3.5.4.3.1.3). The goal of the simulation case study of this chapter is to demonstrate that the deterministic threshold $J^2_{th,RMS}$ according (3-226) is reached for the vertex $\mathcal{V}_{\infty,max}$ (cf. Table 9) but not violated (boundary case).

4.3.2.2.2 Test Conditions

The simulation runs have been performed at FC 1-4. The acceptable closed-loop ω_{SP}-ζ_{SP} parameter envelope was set to $\omega_{SP,L1}$ and $\tilde{\zeta}_{SP,L1}$ according Table 10.
Derived from the realistic inputs of chapter 4.3.1 some generic inputs have been defined. Those are sine inputs (TCs 3.x) with angular velocity $\omega_{\mathcal{H}_{\infty,max}}$ for the respective flight condition, and step inputs (TC 4.x). Both sine and step inputs use the same q_{cmd}-amplitudes per flight condition as discussed for TC 1.x. All test case parameters are summarized in Table 19 and Table 20 (p. 225).
In view of a practical application two tolerances have been defined. The first one is a relative tolerance on $\left\|q_{cmd,env}\right\|^2_{RMS}$, in our case a 4% increase, i.e. (3-226) becomes

$$\begin{aligned} J^2_{th,RMS}(k) &= \sup_{\boldsymbol{f=0,\Delta\neq 0}} \|\boldsymbol{r}\|^2_{RMS} \\ &= \mathcal{H}^2_{\infty,max}\left(1.04 \cdot \left\|q_{cmd,env}\right\|^2_{RMS}(k)\right) \end{aligned} \tag{4-12}$$

The second one is a small minimum $\left\|q_{cmd,env}\right\|^2_{RMS,min}$ = 1.1e-4, modelled as dead band. This dead band is absolutely necessary in a practical application because if q_{cmd} = 0, then $\left\|q_{cmd,env}\right\|^2_{RMS}$ = 0 and therefore, according (3-226), $J^2_{th,RMS}$ = 0. This means that an alarm would be triggered even for $\|\boldsymbol{r}\|^2_{RMS}$ = 0. As it will be shown in the next chapter the relative tolerance is hardly visible in all test cases. The same is true for the dead band besides where q_{cmd} is very small (e.g. TC 3.4 and 4.4 with q_{cmd} = 1.4 deg/s). The choice of the two tolerances can be as required for the practical application on hand. As already mentioned in Remark 3-9 (p. 112), the squared values $J^2_{th,RMS}$, $\mathcal{H}^2_{\infty,max}$, and $\left\|q_{cmd,env}\right\|^2_{RMS}$ are used here for comparability with the integrated stochastic/deterministic fault detection discussed later on. For

the latter this is the form required as input for the stochastic FD part (see chapter 3.5.4.4).

4.3.2.2.3 Test Results

Test Case 3.1 and 4.1

Figure 44 shows the results for TC 3.1 (sine input). The first plot illustrates the input side with $\|q_{cmd}\|^2_{RMS}$ (solid) and $\left\|q_{cmd,env}\right\|^2_{RMS}$ (dashed). It is visible that the signal envelope $\left\|q_{cmd,env}\right\|^2_{RMS}$ has been correctly detected. Furthermore we see $\left\|q_{cmd,env}\right\|^2_{RMS}$ is slightly higher than the peaks of $\|q_{cmd}\|^2_{RMS}$. This is the desired effect of the relative tolerance according (4-12).
The lower four plots show the relation between the residual $\|\boldsymbol{r}\|^2_{RMS}$ (solid) and the threshold $J^2_{th,RMS}$ (dashed) for the four vertices $\mathcal{V}_i$, i.e. the closed-loop systems with the maximum acceptable deviation in terms of ω_{SP} and ζ_{SP}. The vertex $\mathcal{V}_{\infty,max}$ for FC 1 is vertex 3. All vertex parameters are summarized in Table 10 (p. 163). Two important results are evident: First, as shown in the third plot, the residual indeed reaches the threshold for this Vertex but does not violate it. This is the expected and desired result. Second for all other vertices, besides Vertex 3, the residual $\|\boldsymbol{r}\|^2_{RMS}$ is much smaller than the threshold $J^2_{th,RMS}$. This will be discussed further in chapter 4.3.2.2.4.
Figure 45 illustrates the results for TC 4.1 (step inputs). The first plot again shows the input side with $\|q_{cmd}\|^2_{RMS}$ (solid) and $\left\|q_{cmd,env}\right\|^2_{RMS}$ (dashed). The same remarks a given above for TC 3.1 remain valid.
The lower four plots depict the relation between the residual $\|\boldsymbol{r}\|^2_{RMS}$ (solid) and the threshold $J^2_{th,RMS}$ (dashed). The important result here is that, for all vertices also for step inputs the threshold is *not* violated. From theory it should be clear that the $\mathcal{H}_{\infty,max}$ in general is only reached for a sine input with angular velocity $\omega_{\mathcal{H}_{\infty,max}}$, i.e. TC 3.1. This has also been verified here.

Remark 4-13: If the author says that $\mathcal{H}_\infty$ is only reached for a sine input with angular velocity $\omega_{\mathcal{H}_{\infty,max}}$, this is only true for the scalar input system discussed here. For MIMO systems also the input direction, defined by the input vector, is important.

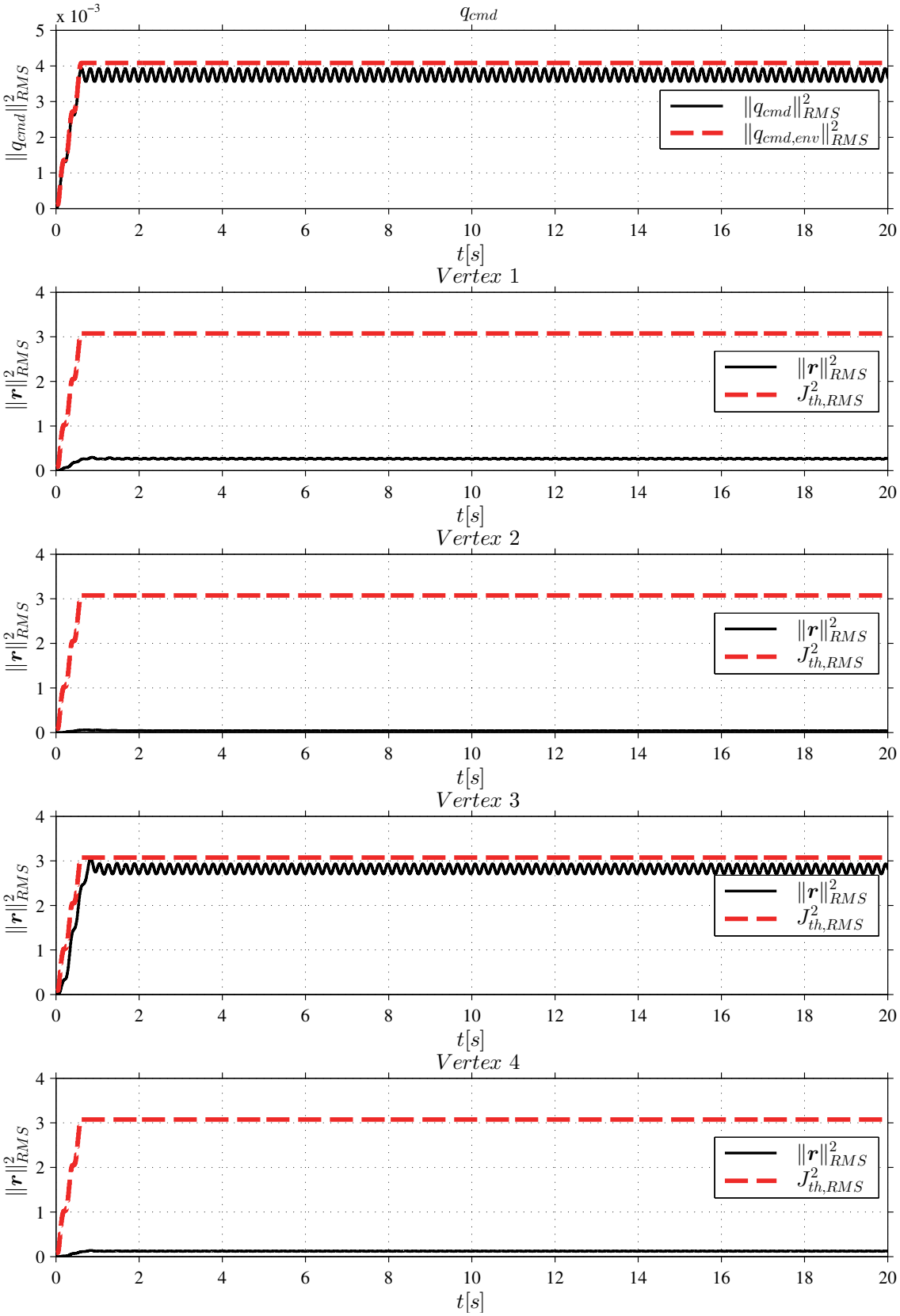

Figure 44 Comparison between residual and threshold at FC 1 (TC 3.1)

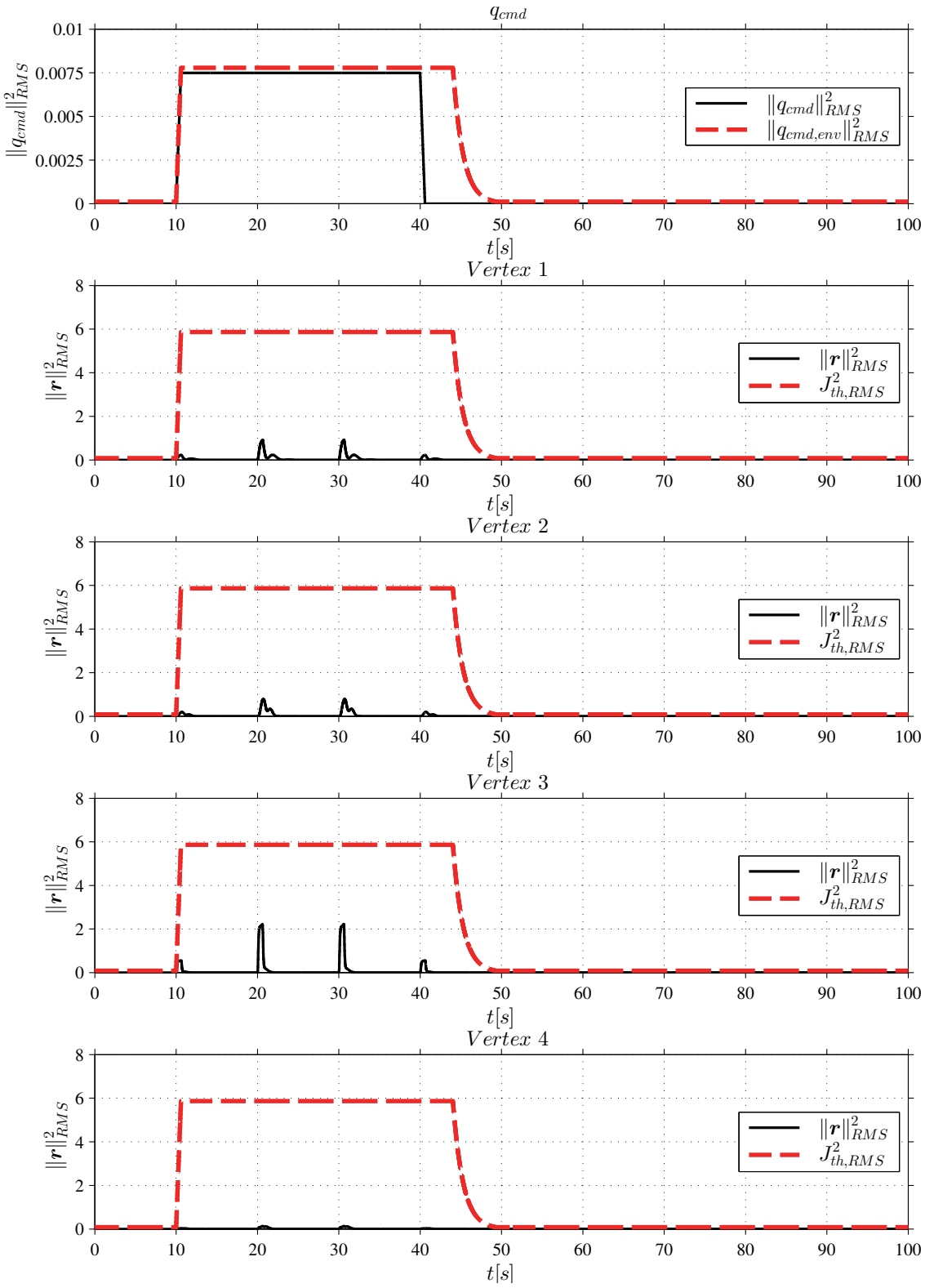

Figure 45 Comparison between residual and threshold at FC 1 (TC 4.1)

Test Case 3.2 and 4.2

Figure 46 and Figure 47 show the results for TC 3.2 (sine input) and TC 4.2 (step input) at FC 2. The same remarks a given above for TC 3.1 and 4.1 remain valid.
The vertex $\mathcal{V}_{\infty,max}$ for FC 2 is Vertex 1 (cf. Table 10). As depicted in the second plot of Figure 46, the residual $\|\boldsymbol{r}\|^2_{RMS}$ (solid) indeed reaches the threshold $J^2_{th,RMS}$ (dashed) for $\mathcal{V}_{\infty,max}$ but does *not* violate it. For the other vertices the residual is much smaller. Figure 47 demonstrates that also for step inputs the threshold is *not* violated.

Test Case 3.3 and 4.3

Figure 48 and Figure 49 show the results for TC 3.3 (sine input) and TC 4.3 (step input) at FC 3. The same remarks a given above for TC 3.1 and 4.1 remain valid.
The vertex $\mathcal{V}_{\infty,max}$ for FC 3 is Vertex 3 (cf. Table 10). As depicted in the fourth plot of Figure 48, the residual $\|\boldsymbol{r}\|^2_{RMS}$ (solid) indeed reaches the threshold $J^2_{th,RMS}$ (dashed) for $\mathcal{V}_{\infty,max}$ but does *not* violate it. For the other vertices the residual is much smaller. Figure 49 demonstrates that also for step inputs the threshold is *not* violated.

Test Case 3.4 and 4.4

Figure 50 and Figure 51 show the results for TC 3.4 (sine input) and TC 4.4 (step input) at FC 4. The remarks, given above for TC 3.1 and 4.1, remain valid.
The vertex $\mathcal{V}_{\infty,max}$ for FC 4 is Vertex 3 (cf. Table 10). As depicted in the fourth plot of Figure 48, the residual $\|\boldsymbol{r}\|^2_{RMS}$ (solid) indeed reaches the threshold $J^2_{th,RMS}$ (dashed) $\mathcal{V}_{\infty,max}$ but does *not* violate it. For the other vertices the residual is much smaller. Figure 49 demonstrates that, for all vertices, also for step inputs the threshold is *not* violated.
As mentioned in chapter 4.3.2.2.2 for small q_{cmd}, as in TC 3.4 and 4.4, the $\left\|q_{cmd,env}\right\|^2_{RMS,min}$ dead band of 1.1e-4 and its effect on the threshold $J^2_{th,RMS}$ is visible (Figure 50 and Figure 51). It is clear that the dead band could have been made much smaller for this simulation case study, as long as $\left\|q_{cmd,env}\right\|^2_{RMS,min} > 0$
The choice $\left\|q_{cmd,env}\right\|^2_{RMS,min}$ = 1.1e-4 was arbitrary.

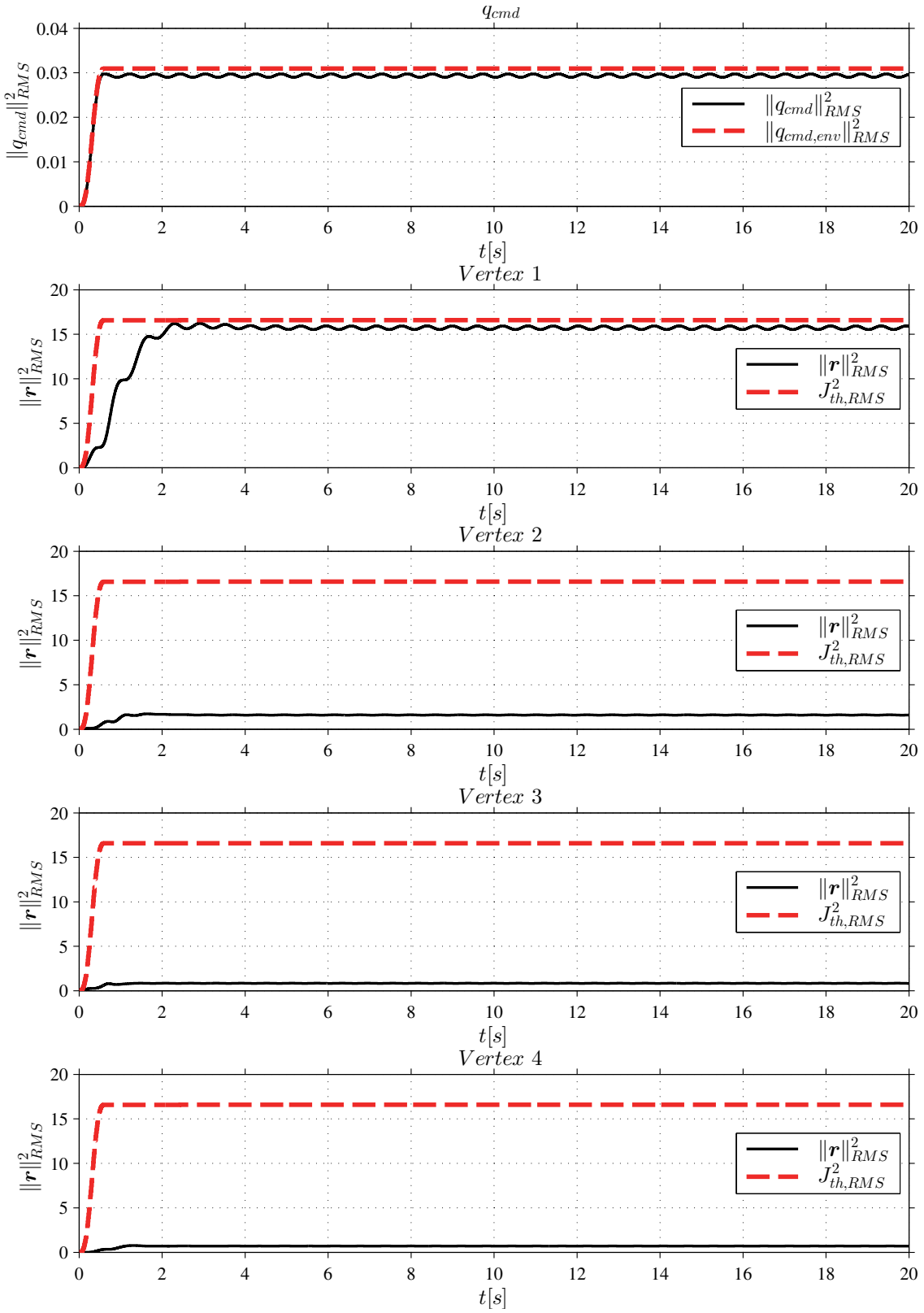

Figure 46 Comparison between residual and threshold at FC 2 (TC 3.2)

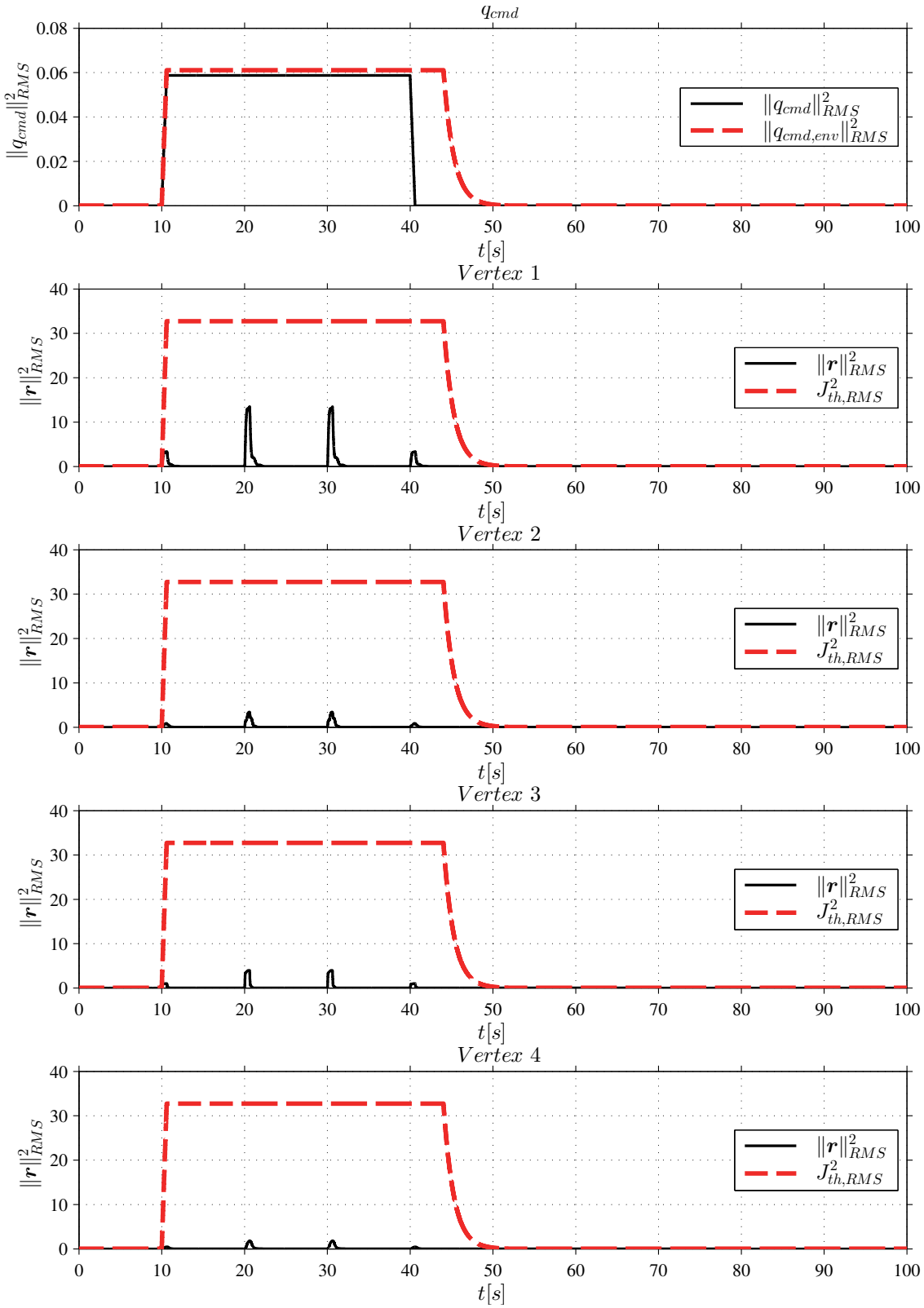

Figure 47 Comparison between residual and threshold at FC 2 (TC 4.2)

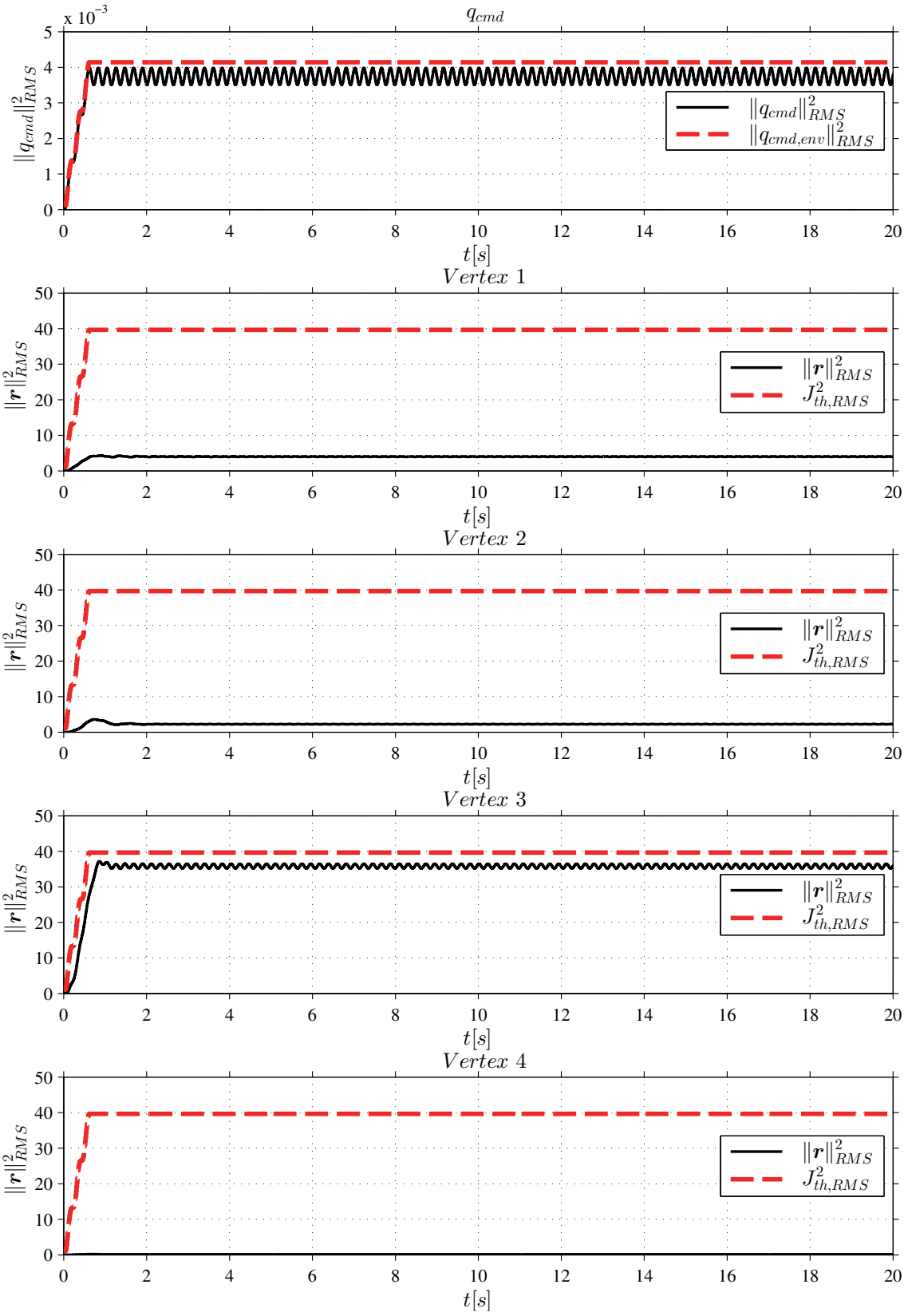

Figure 48 Comparison between residual and threshold at FC 3 (TC 3.3)

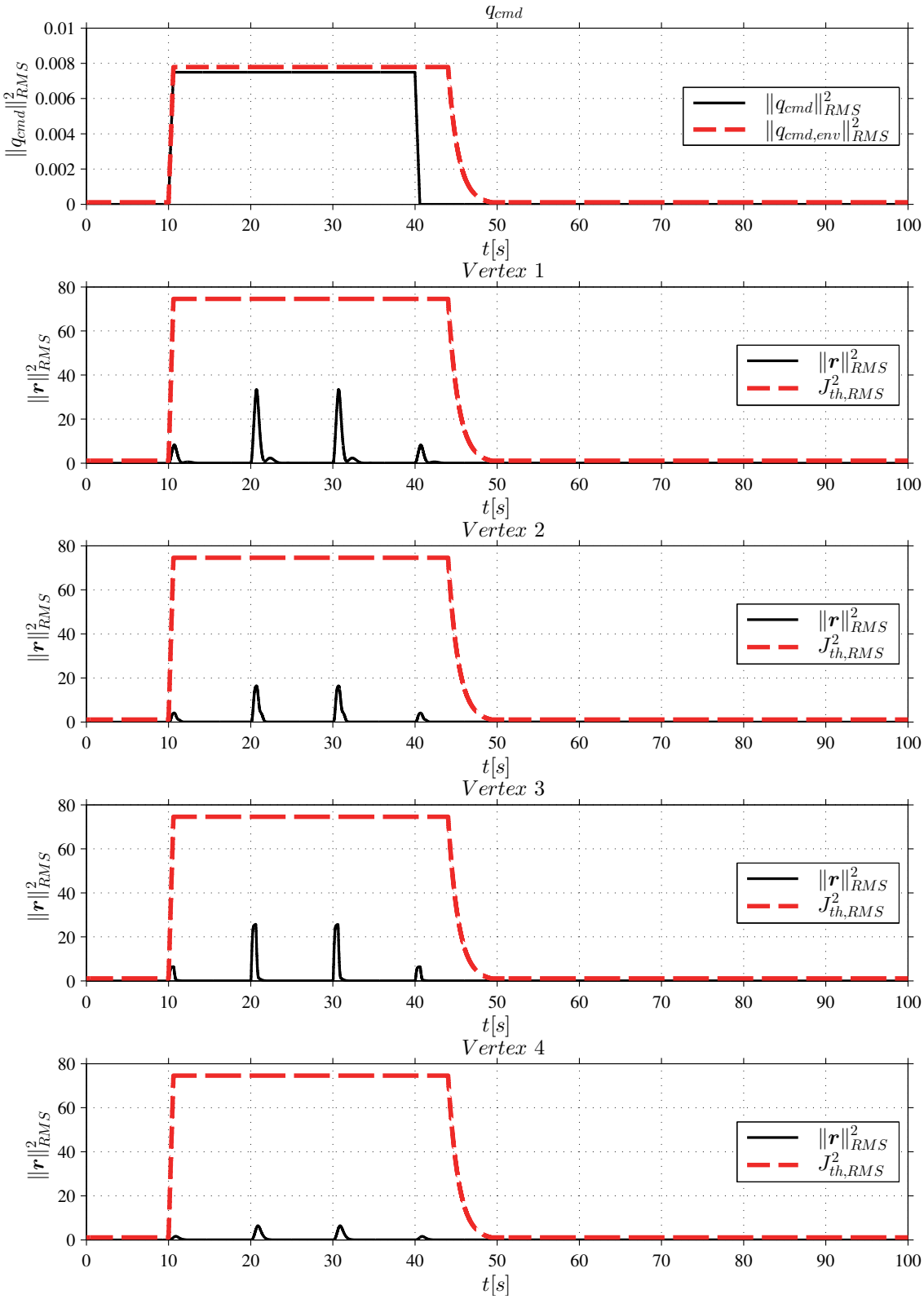

Figure 49 Comparison between residual and threshold at FC 3 (TC 4.3)

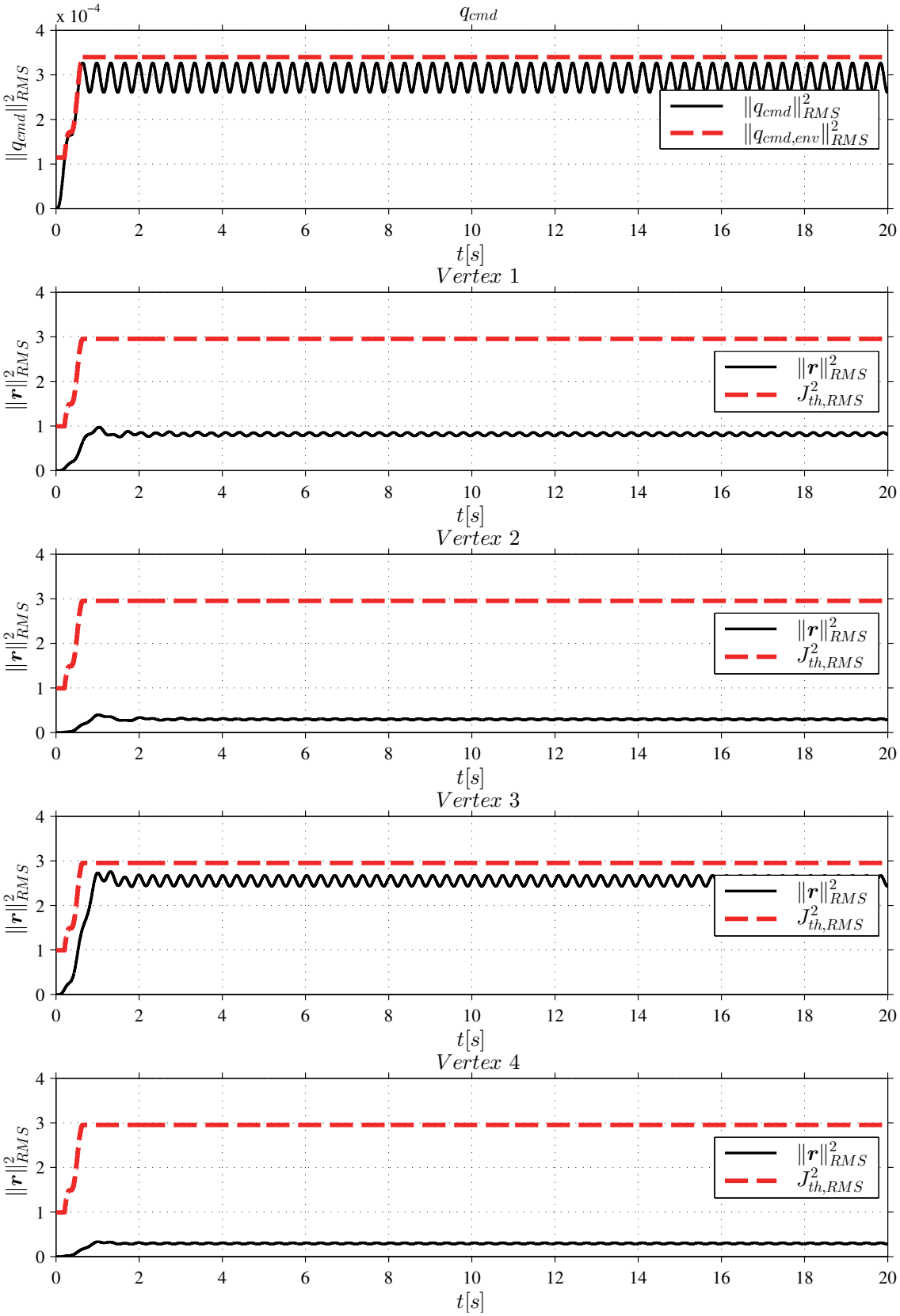

Figure 50 Comparison between residual and threshold at FC 4 (TC 3.4)

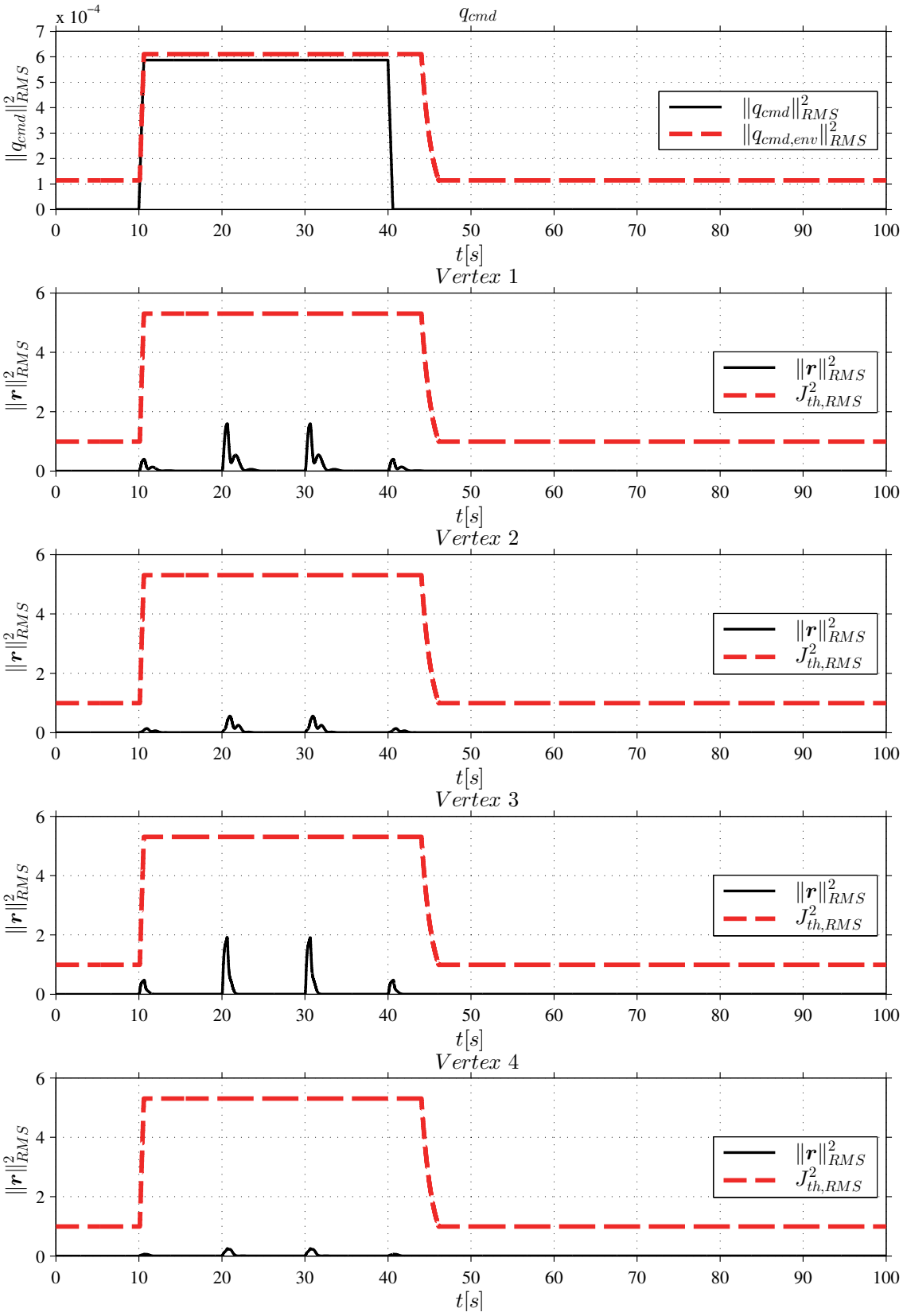

Figure 51 Comparison between residual and threshold at FC 4 (TC 4.4)

4.3.2.2.4 Discussion of Results With Respect to Test Goal

For the representative conditions tested it has been demonstrated that the residual $\|\boldsymbol{r}\|_{RMS}^2$, for a q_{cmd} sine input with $\omega_{\mathcal{H}_{\infty,max}}$, indeed reaches but does *not* violate the threshold $J_{th,RMS}^2$ for the vertex $\mathcal{V}_{\infty,max}$. Furthermore it has been shown that also for q_{cmd} step inputs $J_{th,RMS}^2$ is not exceeded. Therefore *no* false alarm will be raised as long as the closed-loop system stays inside the parameter polytope of acceptable ω_{SP} and ζ_{SP} parameter deviations, in this chapter defined by $\omega_{SP,L1}$ and $\tilde{\zeta}_{SP,L1}$ according Table 10. This are the expected and desired results. The considerations made in chapter 3.5.4.3 have thus been verified. This assumes that $\mathcal{H}_{\infty,max}$ has been correctly determined, which was verified in chapter 4.3.2.1.
It has also been shown that for all vertices, besides the vertex $\mathcal{V}_{\infty,max}$ the residual $\|\boldsymbol{r}\|_{RMS}^2$ is smaller than the threshold $J_{th,RMS}^2$. The same observation can be made for step inputs. The implication of this is that, with the proposed FD system of this thesis, we can detect a fault where the closed-loop system is *for sure* outside the parameter polytope of acceptable ω_{SP} and ζ_{SP} parameter deviations, i.e. *we can guarantee no false alarms*. This is very important in order to make sure that the AFCS is not activated while the CFCS is still able to deliver an acceptable performance. On the other hand we *cannot* ensure that we detect every fault where the CFCS closed-loop system is outside the parameter polytope of acceptable ω_{SP} and ζ_{SP} parameter deviations, i.e. *there will be missed detections*. We recall that the primary goal of this thesis was to design a FD system that ensures a False Alarm Rate (FAR). Thus we are complainant in this regard; nevertheless there is some room for improvement with regard to improve the Missed Detection Rate (MDR) here.
A possible solution and area of further work can be to use four residuals, one for every vertex. In this case we could "turn around" the residual evaluation and detect those cases where one or more of the four residuals is close to zero.
Besides all that it will be demonstrated in chapter 4.3.4 that *the FD system of this work is also well capable of detecting significant faults*.

4.3.2.2.5 Conclusion

For the conditions tested, it has been verified that the residual $\|\boldsymbol{r}\|_{RMS}^2$ only exceeds the threshold $J_{th,RMS}^2$ if the CFCS closed-loop system is for sure outside the parameter polytope of acceptable ω_{SP} and ζ_{SP} parameter deviations. This assumes that $\mathcal{H}_{\infty,max}$ has been correctly determined, which was verified in chapter 4.3.2.1.

4.3.2.3 Envelope Generator

4.3.2.3.1 Test Goal

In chapter 4.3.2.2 it was demonstrated that the deterministic threshold $J_{th,RMS}^2$ according to (4-12) is reached for the vertex $\mathcal{V}_{\infty,max}$ (cf. Table 9) but not violated (boundary case). In this regard it has also been verified that the envelope detector as introduced in chapter 3.5.4.3.3 works for sine and step inputs for the conditions tested. In this chapter the author wants to demonstrate that the envelope detector also functions correctly for complicated q_{cmd} inputs.

4.3.2.3.2 Test Conditions

Besides for the q_{cmd} input, the test conditions are identical to the ones described in chapter 4.3.2.2.2. For this chapter the former is constructed as

$$q_{cmd}\,(t) = \breve{q}_{cmd} \cdot [u_1(t) \cdot u_2(t) \cdot u_3(t)] \tag{4-13}$$

Figure 52 exemplarily shows the resulting signal and the different components for TC 5.2. The first plot displays $q_{cmd}\,(t)$. The sine wave component

$$u_1(t) = \sin\left(\omega_{\mathcal{H}_{\infty,max}} \cdot t\right) \tag{4-14}$$

is depicted in the second subplot. It is, together with $\breve{q}_{cmd}$, the only component that is flight condition dependent because of $\omega_{\mathcal{H}_{\infty,max}}$. $u_2(t)$ is a uniform distributed random number, in the range [-1,1] with a sample time of 2 sec (third plot). Finally $u_3(t)$ is a combination of step and ramp input as shown in the fourth plot. The flight condition dependent parameters $\breve{q}_{cmd}$ and $\omega_{\mathcal{H}_{\infty,max}}$ are given in Table 11.

4.3.2.3.3 Test Results

The test results for TC 5.1 to 5.4 are depicted in Figure 53 to Figure 56 respectively. The first plot shows the command input q_{cmd} as discussed in the last chapter. The second plot illustrates $\|q_{cmd}\|_{RMS}^2$ (solid) and the input signal envelope $\left\|q_{cmd,env}\right\|_{RMS}^2$ (dashed) with tolerance and dead band as explained in chapter 4.3.2.2.2. $\|\boldsymbol{r}\|_{RMS}^2$ (solid) and $J_{th,RMS}^2$ (dashed) are displayed in the fourth plot. The fifth plot indicates the fault bit, which would be 1 if $\|\boldsymbol{r}\|_{RMS}^2 \geq J_{th,RMS}^2$.

4.3.2.3.4 Discussion of Test Result with Respect To Test Goal

It can be readily seen that for *none* of the TCs we have $\|\boldsymbol{r}\|_{RMS}^2 \geq J_{th,RMS}^2$. Therefore no fault has been detected which is the intended result.

4.3.2.3.5 Conclusion

For the conditions tested it has been demonstrated that even for complicated inputs q_{cmd} the envelope detector works correctly. Thus no false alarms due to incorrect envelope detection by the envelope detector have to be expected, which is the intended result.

Table 11 Parameters of input signal for envelope detector verification

TC ID	$\check{q}_{cmd}$ [deg/s]	$\omega_{\mathcal{H}_\infty,max}$ [rad/s]
5.1	5	15.0
5.2	14	5.2
5.3	5	14.7
5.4	1.4	9.3

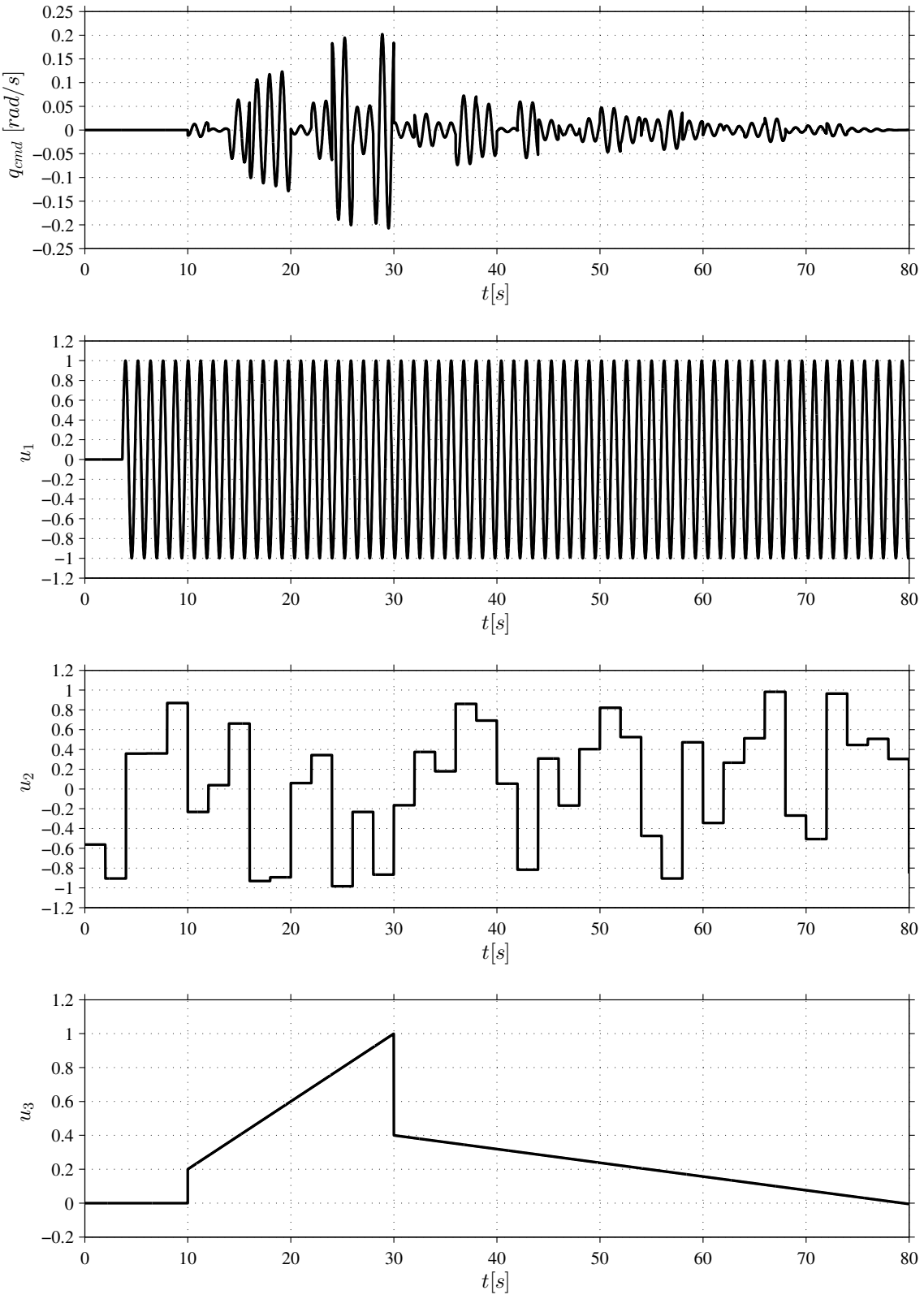

Figure 52 Input signal for envelope detector verification (TC 5.2)

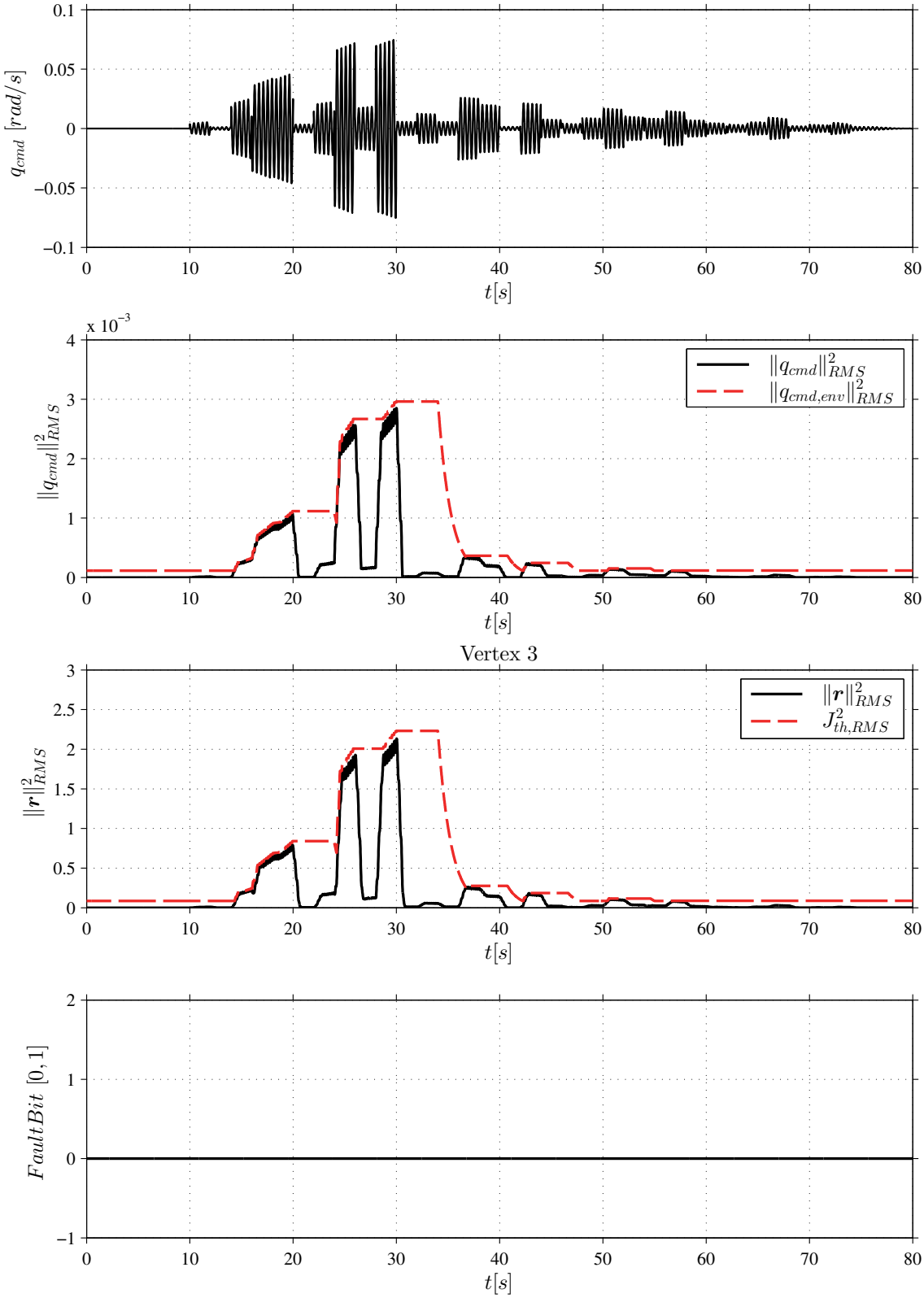

Figure 53 Results for envelope detector verification (TC 5.1)

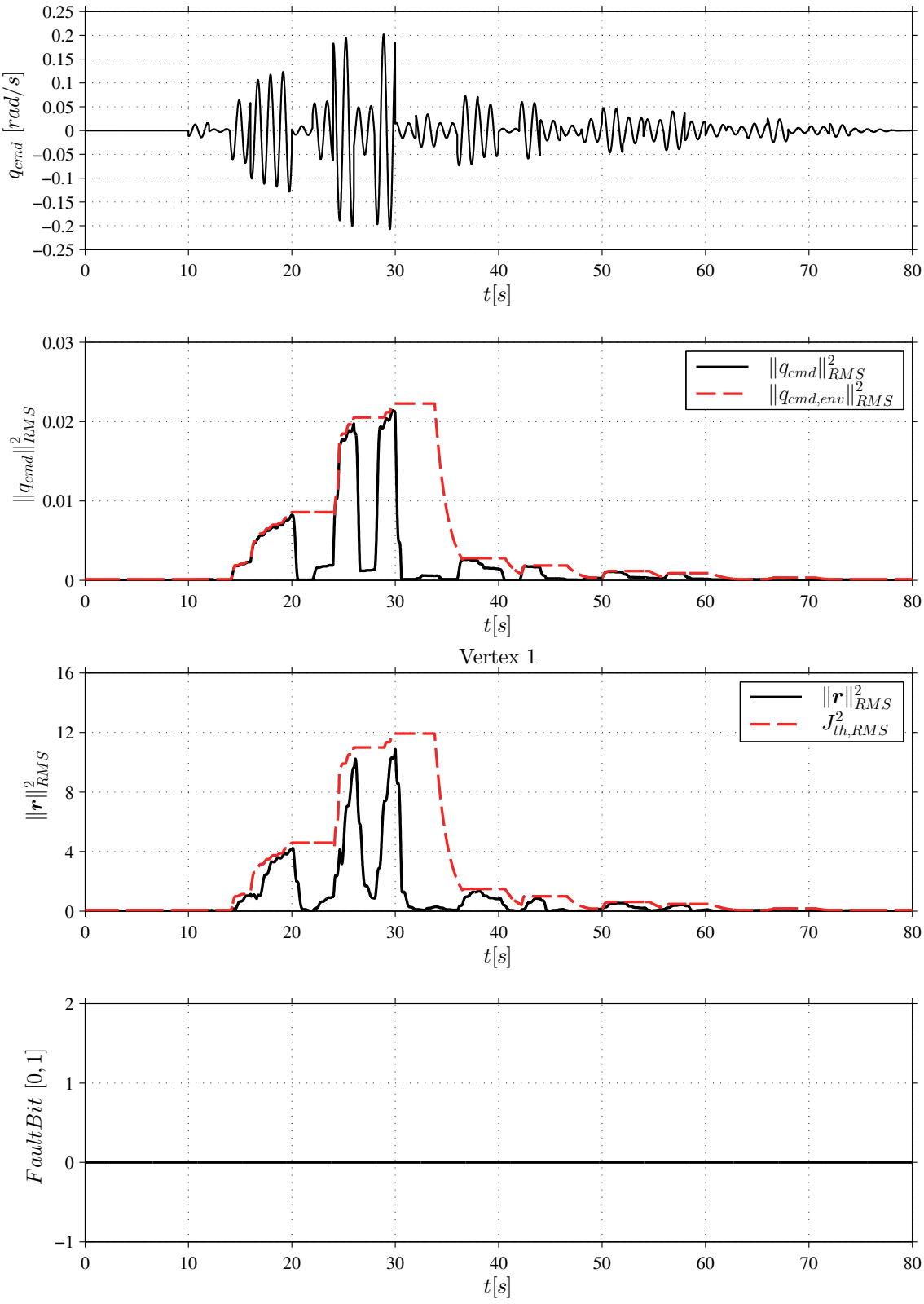

Figure 54 Results for envelope detector verification (TC 5.2)

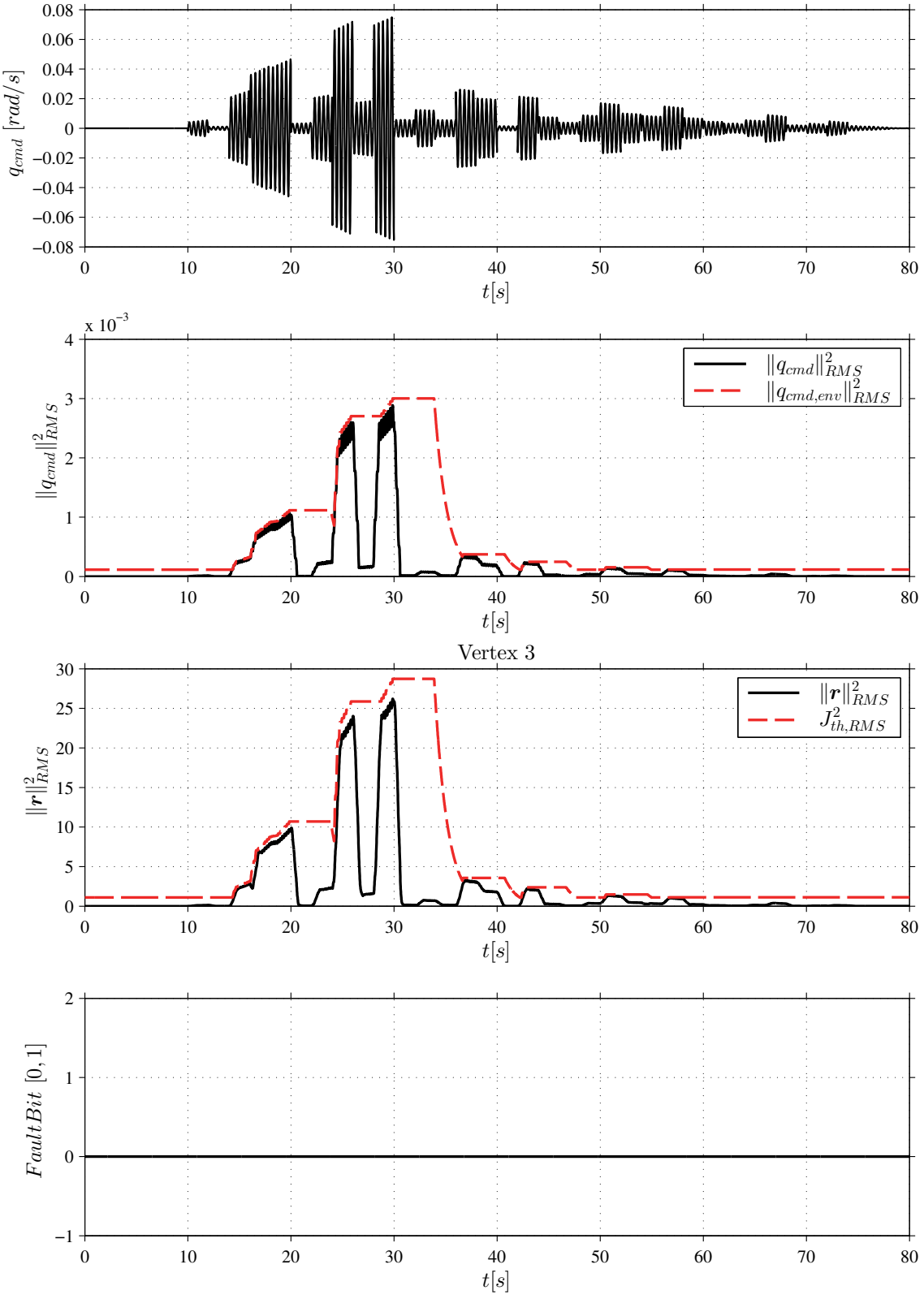

Figure 55 Results for envelope detector verification (TC 5.3)

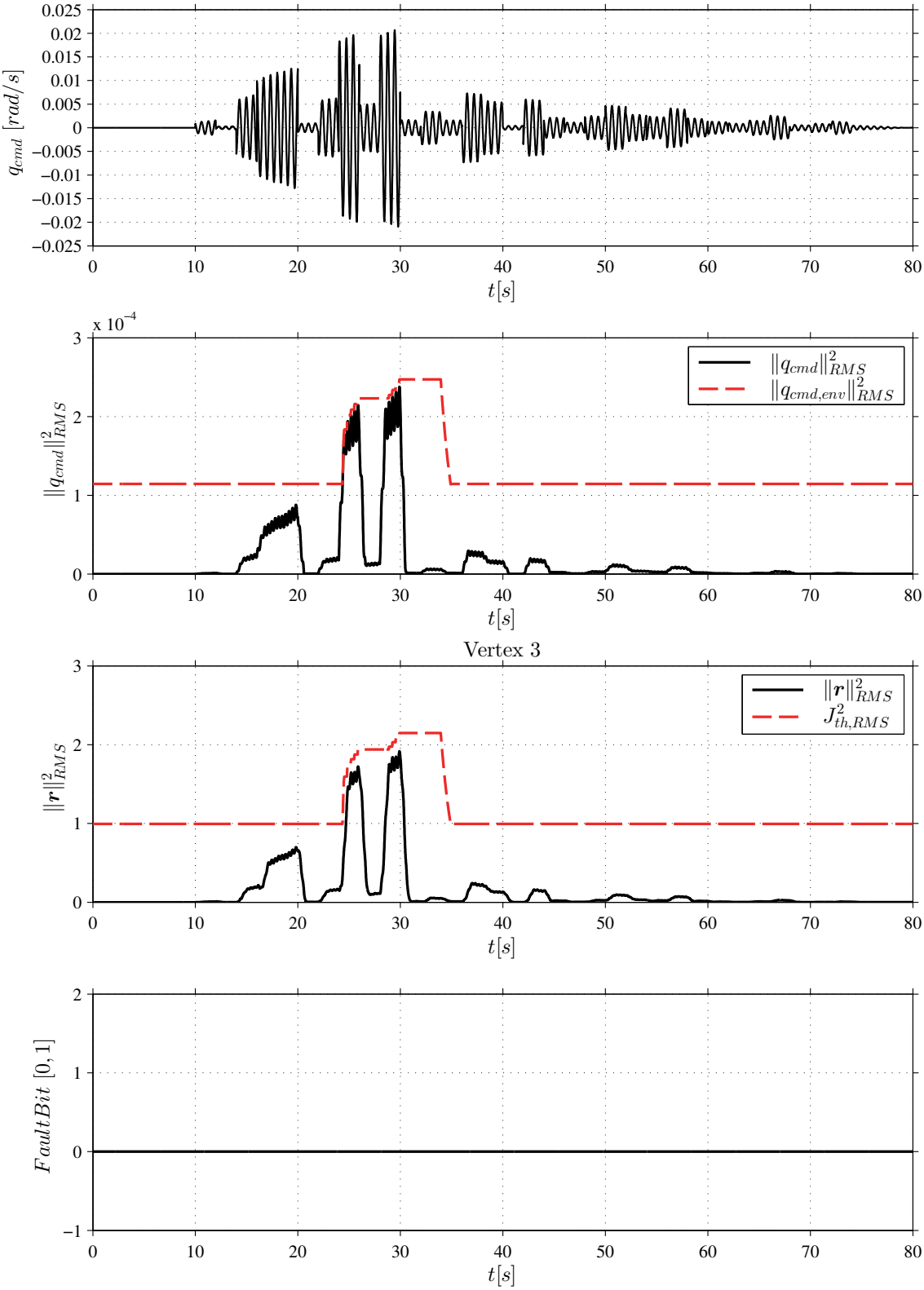

Figure 56 Results for envelope detector verification (TC 5.4)

4.3.2.4 Discussion of Results for Deterministic Fault Detection

In chapter 4.3.2.1 it has been verified that $\mathcal{H}_{\infty,max}$ for our residual dynamic system derived from the reference model with time-invariant polytopic model uncertainties is found at one of the for system vertices $\mathcal{V}$, i.e. $\mathcal{V}_{\infty,max}$.
Chapter 4.3.2.2 has demonstrated that the $\|\boldsymbol{r}\|^2_{RMS}$ indeed reaches but does not exceed the threshold $J^2_{th,RMS}$ for a sine command input q_{cmd} with $\omega_{\mathcal{H}_{\infty,max}}$ as expected from control theory (boundary case). It has also been shown that for step inputs $\|\boldsymbol{r}\|^2_{RMS} < J^2_{th,RMS}$. Furthermore the correct function of the $\|q_{cmd}\|^2_{RMS}$ envelope generator for the above cases has been demonstrated.
The correct behaviour of the envelope generator and the threshold calculation based on the envelope generator output $\left\|q_{cmd,env}\right\|^2_{RMS}$ for complicated inputs has been verified in chapter 4.3.2.3.
For the conditions tested it can therefore be concluded that *no* false alarms from the deterministic part of the fault detection system have to be expected. This has been the goal of chapter 4.3.2.

Remark 4-14: During early simulation runs for a demanding practical relevant failure case where the closed-loop aircraft becomes unstable it was found that allowing the system to vary in the full $\omega_{SP,L1}$-$\zeta_{SP,L1}$-parameter envelope (Table 7, p. 147) leads to a fault detection threshold that is too large in order to recover the aircraft from instability, especially within reasonable normal load factor $\left(n_{z,lim}\right)_K$ and angle of attack limits $\alpha_{K,lim}$. The above mentioned failure case will be discussed in detail in chapter 4.3.4, but it has to be mentioned here because it changed some assumptions for the rest of the simulation case study discussed in the next chapters. As a consequence of this finding the parameter envelope of acceptable closed loop performance was made smaller by defining new bounds $\omega_{SP,10\%} = \omega_{SP,nom} \pm 10\,\%$ and $\zeta_{SP,10\%} = \zeta_{SP,10\%} \pm 10\,\%$ (Table 12) and the threshold has been recalculated accordingly. While the author has to admit that this was not his original personal goal some important points have to be considered:

- With the new acceptable performance bounds, $\omega_{SP,10\%}$ and $\zeta_{SP,10\%}$, it will be demonstrated in chapter 4.3.4, that the fault detection delay is small enough so that aircraft can be successfully recovered from the above mentioned demanding failure case. This failure case can be considered the worst-case.
- The above discussed verifications of the theoretical results, obtained with $\omega_{SP,L1}$-$\zeta_{SP,L1}$ performance bounds, remain valid for the rest of the simulation case study, because $\omega_{SP,10\%}$- $\zeta_{SP,10\%}$ are a subset of the $\omega_{SP,L1}$-$\zeta_{SP,L1}$-parameter envelope and the underlying theory remains unchanged.

- Over all it demonstrates the flexibility of the FD system proposed in this thesis to adapt to different practical demands. This is easily done by just changing the range of acceptable *closed-loop* ω_{SP} and ζ_{SP}. Most important, those two parameters can be readily interpreted in physical and flying quality context. Especially they allow a direct comparison with the flying quality standards MIL-F-8785C (US DoD, 1996) and MIL-STD-1797B[14] (US DoD, 2012). To the author's opinion that is a huge practical advantage because it allows direct comparison to the requirements and gives the aerospace engineer a direct understanding what the effect of the parameter changes are.

End of Remark

Table 12 Summary of adapted short-period parameters for simulated flight conditions

FC ID	$\omega_{SP,lim}$ [rad/s]	$\omega_{SP,nom}$ [rad/s]	$\zeta_{SP,nom}$ [-]	$\omega_{SP,10\%}$	$\zeta_{SP,10\%}$
1	1.7 – 7.0	2.20	0.707	1.98-2.42	0.636-0.778
2		6.50		5.85-7.00	
3		3.22		2.90-3.54	
4		2.20		1.98-2.42	

4.3.2.5 Relation to Requirements and Summary Conclusion

For the conditions tested it has been demonstrated that the *deterministic* part of the integrated stochastic/deterministic FD system ensures that the AFCS is not inadvertently activated by the FD system, i.e. no false alarms have to be expected. The *deterministic* part of the integrated stochastic deterministic FD system is therefore *compliant* with Requirement 1-1 (p. 11) for the conditions tested.

[14] Restricted distribution, therefore information from MIL-F-8785C is used within this text.

4.3.3 Verification of Theoretical Results - Integrated Stochastic/Deterministic Fault Detection

4.3.3.1 Test Goal

The goal of the simulation case study of this chapter is to demonstrate that the False Alarm Rate (FAR) of the FD system $FAR_{\tilde{J}_{th,\chi^2}}$ is equal or lower the design FAR_{req}. $\widehat{FAR}_{\tilde{J}_{th,\chi^2}}$ is estimated from simulation.

4.3.3.2 Specific Simulation Setup

FAR estimation

In chapter 4.3.2 it was verified that $J^2_{th,RMS}$ is correctly determined. For the purpose of this chapter we use a generic $J^2_{th,RMS}$ to be able to prove the full range of interesting non-centrality parameters λ_{χ^2}. Furthermore we want to demonstrate that the design goal $FAR_{\tilde{J}_{th,\chi^2}} \leq FAR_{req}$ of Requirement 1-1 (p. 11) is achieved also for a $J^2_{th,RMS}$, which varies over the full simulated time frame $t_{sim} = 3\text{h}$. Because $J^2_{th,RMS}$ directly depends on the command input q_{cmd} according to (4-12), the threshold $J^2_{th,RMS}$ will also vary in practice. For this chapter $\left(J^2_{th,RMS}\right)_{sim}$ is thus simulated by a sine wave. This potentially needs some explanation. First we recall (3-222)

$$\begin{aligned} J^2_{th,2} &= \left\|\boldsymbol{G}_{rq_{cmd}}\right\|^2_{\infty} \|q_{cmd}\|^2_2 = N_{RMS}\left\|\boldsymbol{G}_{rq_{cmd}}\right\|^2_{\infty} \|q_{cmd}\|^2_{RMS} \\ &= J^2_{th,RMS} N_{RMS} \end{aligned}$$

As said before the correct determination of $J^2_{th,RMS}$ and therefore also $J^2_{th,2}$ was demonstrated already. In this chapter we want to show that the stochastic fault detection is correct for different $J^2_{th,RMS}$ in the range of interest and all vertices $\mathcal{V}_i$ of the parameter polytope. For obvious reasons this cannot be achieved using $\left\|\boldsymbol{G}_{rq_{cmd}}\right\|^2_{\infty} \|q_{cmd}\|^2_{RMS}$. Therefore we look for a way to simulate different generic $J^2_{th,RMS}$ but at the same time stay as close as possible to the real case, especially we want to keep the sliding window RMS in our simulation, because as explained in chapter 3.5.4.4, the window size influences the stochastic threshold. From (3-233) we have, as general definition of $J^2_{th,2}$,

$$J^2_{th,2} = \sup_{\boldsymbol{f}=\boldsymbol{0},\boldsymbol{\Delta}\neq\boldsymbol{0}} \|\boldsymbol{r}_{det}\|^2_2 = N_{RMS} \cdot \sup_{\boldsymbol{f}=\boldsymbol{0},\boldsymbol{\Delta}\neq\boldsymbol{0}} \|\boldsymbol{r}_{det}\|^2_{RMS}$$

where $\boldsymbol{r}_{det}$ is the deterministic part of residual $\boldsymbol{r}$.

Thus the way forward is to directly simulate $\sup_{\boldsymbol{f=0,\Delta\neq 0}}\|\boldsymbol{r}_{det}\|^2_{RMS}$. This is done by simulating different $\|\boldsymbol{r}_{det}\|^2_{RMS}$ in the range that can be reached thru $\left\|\boldsymbol{G}_{rq_{cmd}}\right\|^2_{\infty}\|q_{cmd}\|^2_{RMS}$ in a real application. To do so we use different $(\boldsymbol{r}_{det})_{sim}$ and then the sliding window RMS to get $\|\boldsymbol{r}_{det}\|^2_{RMS}$. For the boundary case we have according (3-234)

$$\lambda_{\chi^2} = J^2_{th,2} = \sup_{\boldsymbol{f=0,\Delta\neq 0}}\|\boldsymbol{r}_{det}\|^2_2 = N_{RMS}\cdot\sup_{\boldsymbol{f=0,\Delta\neq 0}}\|\boldsymbol{r}_{det}\|^2_{RMS}$$

For our simulation thus

$$\left(\lambda_{\chi^2}\right)_{sim} = \left(J^2_{th,2}\right)_{sim} = \|(\boldsymbol{r}_{det})_{sim}\|^2_2 = N_{RMS}\|(\boldsymbol{r}_{det})_{sim}\|^2_{RMS} \qquad (4\text{-}15)$$

To simulate the time varying $\boldsymbol{r}_{det}$ we use

$$(\boldsymbol{r}_{det})_{sim}(t) = (\check{\boldsymbol{r}}_{det})_{sim}\cdot\sin\left(\omega_{(\boldsymbol{r}_{det})_{sim}}\cdot t\right) \qquad (4\text{-}16)$$

The sine is sampled by a Zero Order Hold (ZOH) element to get $(\boldsymbol{r}_{det})_{sim}(k)$. The $(\boldsymbol{r}_{det})_{sim}$ parameters are summarized in Table 13.
The simulation setup is schematically depicted in Figure 57. The noise is taken from the residual without deterministic input for the respective vertex $\mathcal{V}_i$ tested. This means the noise has zero mean but the variance from the respective vertex residual dynamic system. The colored noise corrected $\chi^2_m(\lambda)$-threshold $\tilde{J}_{th,\chi^2}$ is calculated using the normal approximation according (3-249) as described in chapter 3.5.4.4.2.

Table 13 $(\boldsymbol{r}_{det})_{sim}$ parameters

Parameter	Amplitude $(\check{\boldsymbol{r}}_{det})_{sim}$					
	$\begin{bmatrix}0\\0\end{bmatrix}$	$\begin{bmatrix}0.1\\0.1\end{bmatrix}$	$\begin{bmatrix}0.5\\0.5\end{bmatrix}$	$\begin{bmatrix}1.0\\1.0\end{bmatrix}$	$\begin{bmatrix}2.5\\2.5\end{bmatrix}$	$\begin{bmatrix}5.0\\5.0\end{bmatrix}$
Amplitude $\left(\check{\lambda}_{\chi^2}\right)_{sim}$	0	1.2	30	120	750	3000
N_{RMS}	60					
$m_{\chi^2,RMS} = 2N_{RMS}$ Eq. (3-235)	120					
$\omega_{(\boldsymbol{r}_{det})_{sim}}$ [rad/s]	1.0					

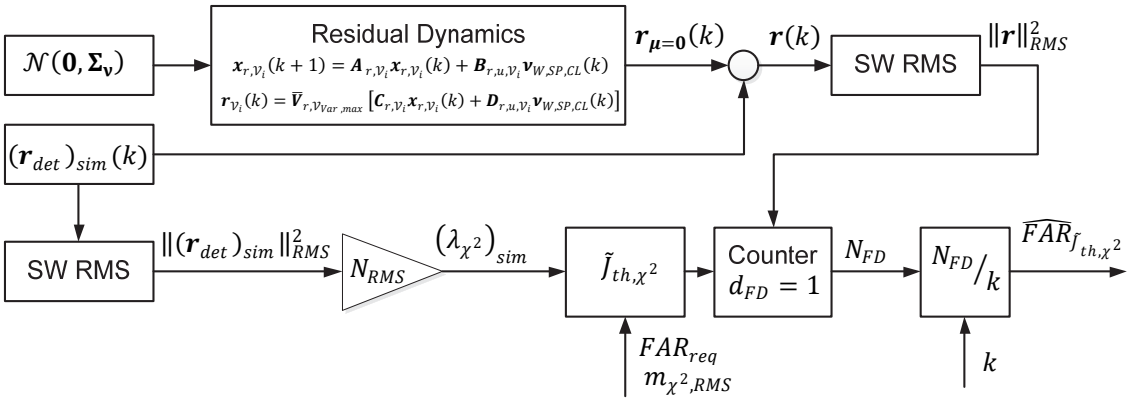

Figure 57 Schematic simulation setup for estimating the FAR

The FD decision logic is according (3-251)

$$d_{FD} = \begin{cases} 0 & if\ \|\boldsymbol{r}\|^2_{RMS} \leq \tilde{J}_{th,\chi^2} \Rightarrow nofault \\ 1 & if\ \|\boldsymbol{r}\|^2_{RMS} > \tilde{J}_{th,\chi^2} \Rightarrow fault \end{cases}$$

$\widehat{FAR}_{\tilde{J}_{th,\chi^2}}$ is estimated by counting the samples where $d_{FD} = 1$ and divide this value by the total simulation samples k at time t.

$$\widehat{FAR}_{\tilde{J}_{th,\chi^2}} = \frac{N_{FD}(k)}{k} \tag{4-17}$$

Variance correction factor

The variance correction factor $\varepsilon_{Var,1}(\lambda_{\chi^2}, FC)$, introduced in chapter 3.5.4.4.2, was determined by estimating the variance $\hat{\Sigma}_{\chi^2,RMS}(\lambda_{\chi^2})$ from simulation runs with the same setup as described above for the FAR estimation but with $(\boldsymbol{r}_{det})_{sim} = (\check{\boldsymbol{r}}_{det})_{sim} = const.$ $\varepsilon_{Var,1}(\lambda_{\chi^2}, FC)$ has then been calculated by (3-247):

$$\varepsilon_{Var,1}(\lambda_{\chi^2}) = \frac{\hat{\Sigma}_{\chi^2,RMS}(\lambda_{\chi^2})}{\Sigma_{\chi^2,RMS}(\lambda_{\chi^2})}$$

As explained in chapter 3.5.4.4.2, $\varepsilon_{Var,1}(\lambda_{\chi^2}, FC)$ has been stored in a look-up table for online interpolation as function of λ_{χ^2}. The results are summarized in Table 14.

Table 14 Variance correction factors

FC ID	λ_{χ^2}					
	0	1.2	30	120	750	3000
1	2.65	2.65	3.10	3.64	4.14	4.37
2	2.26	2.26	2.58	2.97	3.33	3.53
3	2.98	2.99	3.66	4.47	5.19	5.47
4	4.39	4.39	5.17	6.14	7.00	7.32

4.3.3.3 Test Conditions

The simulations for TC6.1t - 6.4t (FC 1-4) have been performed for six non-centrality parameters λ_{χ^2} (runs) for every vertex as well as the nominal dynamic system. Of course it is not possible to use the real FAR_{req} because as

$$FAR_{req} \leq \frac{1}{10^6 \cdot 3600/t_s} \tag{4-18}$$

with $t_s = 0.01$ it follows that $FAR_{req} \leq 2.78 \cdot 10^{-12}$. For a proper verification the simulation would have to be run several million simulated hours which is impracticable but also not important, as the theoretical considerations made for $\tilde{J}_{th,\chi^2}$ can also be verified for a larger FAR_{req}. For this chapter therefore $\left(FAR_{req}\right)_{sim}$ = 0.05 was chosen. This choice also ensures that enough samples with d_{FD} = 1, i.e. N_{FD} is large enough so that $\widehat{FAR}_{\tilde{J}_{th,\chi^2}}$ can be correctly estimated according (4-17). The simulated time frame has been t_{sim} = 3h. The acceptable closed-loop ω_{SP}-ζ_{SP} parameter envelope was set to $\omega_{SP,10\%}$ and $\zeta_{SP,10\%}$ according Table 12 (cf. Remark 4-14, p. 185).

4.3.3.4 Test Results

The estimated $\widehat{FAR}_{\tilde{J}_{th,\chi^2}}$ for every flight condition, vertex $\mathcal{V}_i$, and nominal system is shown in Table 15. For every FC the stochastic "worst-case" Vertex $\mathcal{V}_{Var,max}$ with the highest variance has been highlighted in bold face. As explained in chapter 3.5.4.4.1 the variance scaling filter $\bar{\boldsymbol{V}}_{r,\mathcal{V}_{Var,max}}$ of this vertex is also the filter integrated in the FD system. The maximum estimated $\widehat{FAR}_{\tilde{J}_{th,\chi^2},max}$ has been 0.0488 (FC 4, Vertex 4, Run 4).

Figure 58 exemplarily illustrates a representative trace to give the reader an impression of the different variables. The run with the highest $\widehat{FAR}_{\tilde{J}_{th,\chi^2},max} = 0.0488$ has been chosen (TC 6.4t, Vertex 4, Run 4). The time frame displayed has been randomly selected. The upper plot shows $\|\boldsymbol{r}\|^2_{RMS}$ (solid) and the threshold $\tilde{J}_{th,\chi^2}$ (dashed). According the decision rule d_{FD} every time the residual is $\|\boldsymbol{r}\|^2_{RMS} \geq \tilde{J}_{th,\chi^2}$ a fault is counted. $\widehat{FAR}_{\tilde{J}_{th,\chi^2}}$ is estimated by counting the samples where $d_{FD} = 1$ and divide this value by the total simulation samples k at time t according (4-17). The estimated $\widehat{FAR}_{\tilde{J}_{th,\chi^2}}$ (solid) and $\left(FAR_{req}\right)_{sim}$ (dashed) are depicted in the lower plot. As $\widehat{FAR}_{\tilde{J}_{th,\chi^2}}$ is a random process it slightly varies over time around the final value $\widehat{FAR}_{\tilde{J}_{th,\chi^2},max} = 0.0488$.

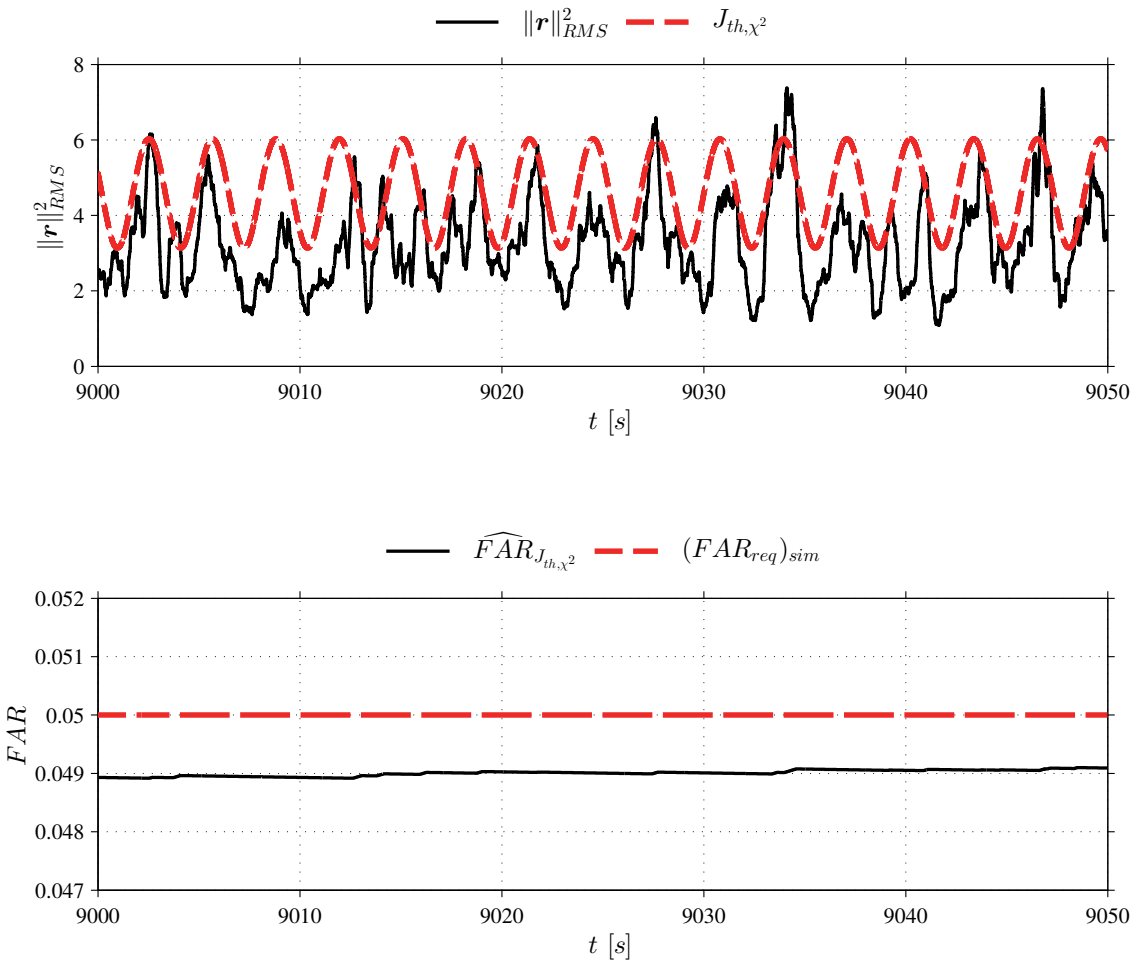

Figure 58 Example of FAR estimation (TC 6.4t, Vertex 4, Run 4)

Table 15 Results for FAR estimated from simulation (TC 6.1t - 6.4t)

FC ID	TC ID	System	$(\lambda_{\chi^2})_{sim}$					
			0	1.2	30	120	750	3000
Run ID			1	2	3	4	5	6
1	6.1t	Vertex 1	0.0147	0.0154	0.0214	0.0262	0.0300	0.0293
		Vertex 2	0.0001	0.0001	0.0002	0.0003	0.0007	0.0009
		Vertex 3	0.0001	0.0001	0.0003	0.0006	0.0012	0.0015
		Vertex 4	**0.0372**	**0.0382**	**0.0419**	**0.0429**	**0.0402**	**0.0356**
		Nominal	0.0012	0.0013	0.0023	0.0042	0.0068	0.0078
2	6.2t	Vertex 1	0.0101	0.0107	0.0157	0.0210	0.0275	0.0289
		Vertex 2	0.0000	0.0000	0.0001	0.0005	0.0022	0.0038
		Vertex 3	0.0001	0.0001	0.0004	0.0010	0.0031	0.0048
		Vertex 4	**0.0359**	**0.0364**	**0.0401**	**0.0408**	**0.0389**	**0.0347**
		Nominal	0.0008	0.0009	0.0021	0.0044	0.0089	0.0113
3	6.3t	Vertex 1	0.0287	0.0301	0.0375	0.0419	0.0427	0.0390
		Vertex 2	0.0000	0.0000	0.0000	0.0000	0.0000	0.0000
		Vertex 3	0.0000	0.0000	0.0000	0.0000	0.0000	0.0000
		Vertex 4	**0.0389**	**0.0398**	**0.0442**	**0.0455**	**0.0414**	**0.0359**
		Nominal	0.0004	0.0004	0.0007	0.0012	0.0021	0.0024
4	6.4t	Vertex 1	0.0133	0.0145	0.0205	0.0255	0.0287	0.0274
		Vertex 2	0.0000	0.0000	0.0001	0.0001	0.0004	0.0006
		Vertex 3	0.0000	0.0000	0.0000	0.0000	0.0000	0.0000
		Vertex 4	**0.0430**	**0.0441**	**0.0484**	**0.0488**	**0.0444**	**0.0394**
		Nominal	0.0000	0.0000	0.0000	0.0000	0.0000	0.0000

4.3.3.5 Discussion of Results with Respect to Test Goal

Table 15 verifies that for all vertices and flight conditions $\left(FAR_{req}\right)_{sim} \leq 0.05$ has been achieved. As explained in chapter 4.3.3.3 the realistic requirement $FAR_{req} \leq 2.78 \cdot 10^{-12}$ cannot be proven by simulation directly. For a proper verification the simulation would have to be run several million simulated hours which is impracticable. However this is also not important as the theoretical considerations made for threshold $\tilde{J}_{th,\chi^2}$ can also be verified with a larger FAR. In our case this has been done with $\left(FAR_{req}\right)_{sim} \leq 0.05$.

The simulation results also verify that the suggested extensions by the author for fault detection with systems subject to *deterministic polytopic model uncertainties and stochastic unknown inputs* are valid. Those extensions by the author are namely an approach to selection of the variance scaling filter $\boldsymbol{V}$ for the above mentioned systems (chapter 3.5.4.4.1) and the residual variance correction for colored noise (chapter 3.5.4.4.2).

4.3.3.6 Relation to Requirements

It has been demonstrated that the stochastic part of the integrated stochastic/deterministic FD system can ensure that the probability that the AFCS is inadvertently activated by the fault detection system is equal or less 10^{-6} per flight hour. The stochastic part of the integrated stochastic deterministic FD system is therefore *compliant* with Requirement 1-1 for the conditions tested.

4.3.3.7 Conclusion

The simulation results verify that the suggested extensions by the author (chapter 3.5.4.4.1 & 3.5.4.4.2) for fault detection with systems subject to *deterministic polytopic model uncertainties and stochastic unknown inputs* are valid.

It has been demonstrated that the stochastic part of the integrated stochastic/deterministic FD system can ensure that the probability that the AFCS is inadvertently activated by the fault detection system is equal or less 10^{-6} per flight hour. The stochastic part of the integrated stochastic deterministic FD system is therefore *compliant* with Requirement 1-1 for the conditions tested.

4.3.4 Fault Detection Performance for a Practical Relevant Failure Case – Closed-Loop Instability

We now discuss a practical relevant failure case where the closed-loop aircraft becomes unstable. This fault can be considered the worst-case from two points of view. First of all it clearly is a loss-off-control situation, i.e. a catastrophic failure, that has to be prevented by all means and the probability of occurrence has to be lower than 10^{-6} per FH for typical fighter aircraft, e.g. the Eurofighter Typhoon (cf. Table 4, p. 39). Secondly, due to the instability, it requires rapid fault detection to keep the aircraft safe. It can therefore be considered the worst-case scenario for a fault detection system like the one proposed in this thesis. This is also the reason why it has been selected as failure case for this simulation case study.
Two scenarios will be discussed: A purely deterministic one, e.g. without considering atmospheric turbulences, to demonstrate the performance of the deterministic FD part and the practical relevant case with atmospheric turbulence to show the capabilities of the integrated stochastic/deterministic FD system.

4.3.4.1 Test Goal

The goal of the simulation case study of this chapter is *to demonstrate that the fault detection delay is small enough* so that an AFCS is in principal able to stop the aircraft pitch-up movement of a closed-loop unstable aircraft, with realistic actuator system, within acceptable aircraft limits, i.e. angel of attack α and normal load factor n_z.

4.3.4.2 Specific Simulation Setup

4.3.4.2.1 Description of Simulated Fault Condition

At t = 6.5 s, a severe CFCS fault is simulated by setting the controller feedback gains to zero, i.e. $K_q = K_\alpha = 0$. This case is, to the author's opinion, interesting because it

- leads to a significant closed-loop pitch instability equal to the one of the open-loop plant with a time to double as low as $T_{2,OL}$ = 0.4 s (cf. Table 6, p. 146) and
- in additions triggers an elevator runaway, due to the feed forward gain H_q. This runaway creates an additional pitch up moment that makes the recovery even more difficult.

4.3.4.2.2 Description of Simulated AFCS Recovery Action

For this case study a simple simulation of a potential AFCS action to recover the aircraft from a closed-loop instability has been used. This simple simulation consists of an appropriate constant elevator command η_{cmd} = 25 deg (TC 7.1, 7.3 and 7.4)

and η_{cmd} = 10 deg (TC 2.2) to stop the movement induced by the system instability after the fault. The elevator command was given at 0.05 s after the fault has been detected by the FD system in order to incorporate a representative AFCS processing time delay ($T_{D,FCS}$ = 0.05 s).

Remark 4-15: If the author, in the following paragraphs, says that the recovery action has been successfully completed, this has to be seen in the context of the goal of the simulation case study of this chapter, i.e. *to demonstrate that the fault detection delay is small enough* so that an unstable plant with realistic actuator system is able to stop the aircraft pitch-up movement within acceptable system limits. The recovery action described above must be understood as simple simulation of a potential recovery action taken by an AFCS (not part of this thesis) after it has been activated by the fault-detection system (topic of this thesis). Or said in other words: This chapter aims to show that in principle the AFCS has sufficient time to recover the aircraft from a closed-loop instability under realistic conditions.

4.3.4.2.3 Actuator

As already mentioned in chapter 3.5.2.2.2 for this chapter the actuator dynamics have been included. The actuator was modelled as a linear second order system with rate and position limit as shown in Figure 59. The model is representative of a modern hydraulic actuator with position and rate feedback.

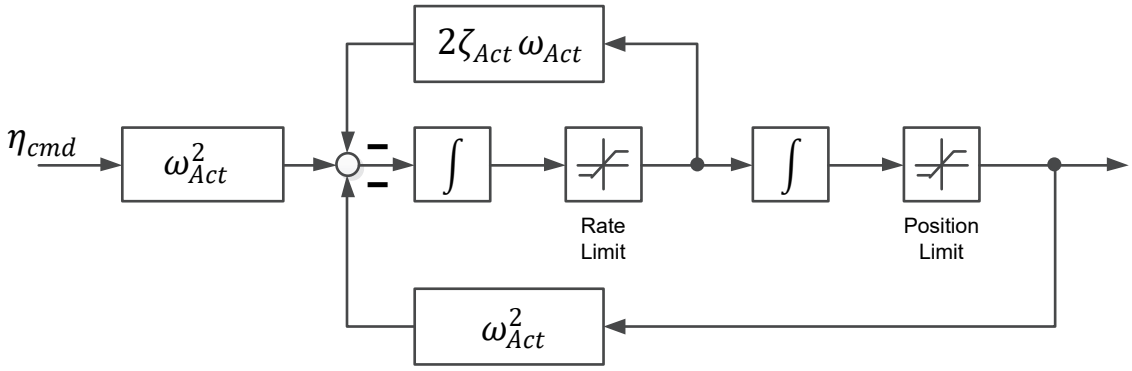

Figure 59 Actuator model

The model parameters used are summarized in Table 16. The values for the natural frequency ω_{Act} and damping ratio ζ_{Act} are taken from Brockhaus et al. (2011, p. 418), the value for the actuator rate limit from NATO RTO (2000, p. 55) and the position limit from the F-16 plant model as described in chapter A.6.

Table 16 Parameter values for the actuator model

Parameter	**Symbol**	**Value**
Natural frequency	ω_{Act}	60 rad/s
Damping ratio	ζ_{Act}	0.707
Rate Limit	$\dot{\eta}_{lim}$	±125 deg/s
Position Limit	η_{lim}	±25 deg

For the sake of completeness it shall be mentioned here, that the original F-16 elevator actuator system had a rate limit of 60 deg/s (Nguyen et al., 1979, p. 34). As stated in (NATO RTO, 2000, pp. 55-56) "a rate sufficient to reach full surface deflection from neutral in 0.2 seconds, provides a fast transient response and permits a full cycle of maximum amplitude oscillatory surface travel at about 5 rad/sec at the onset of rate saturation up to about 8 rad/sec, while fully rate saturated, if acceleration limiting is negligible." As we have adapted the original F-16 CG position to reach a smaller time to double, representative of more modern configurations like Eurofighter, it is reasonable to also choose an actuator rate limit more representative of a modern configuration. Based on the aforementioned requirement to reach full surface deflection from neutral in 0.2 seconds a rate limit of 125 deg/s was therefore chosen for this simulation case study.
Figure 59 allows deriving the actuator linear state space model (without position and rate limit):

$$\begin{aligned} \dot{\boldsymbol{x}}_{Act} &= \boldsymbol{A}_{Act}\boldsymbol{x}_{Act} + \boldsymbol{B}_{Act}\eta_{cmd} \\ \eta &= \boldsymbol{C}_{Act}\boldsymbol{x} \end{aligned} \tag{4-19}$$

with

$$\boldsymbol{A}_{Act} = \begin{bmatrix} -2\zeta_{Act}\omega_{Act} & -\omega_{Act}^2 \\ 1 & 0 \end{bmatrix} \qquad \boldsymbol{B}_{Act} = \begin{bmatrix} \omega_{Act}^2 \\ 0 \end{bmatrix}$$

$$\boldsymbol{C}_{Act} = [0 \quad 1]$$

$$\boldsymbol{x}_{Act} = \begin{bmatrix} \dot{\eta} \\ \eta \end{bmatrix}$$

The closed loop system with actuator dynamics is obtained from a series connection of (4-19) with (3-141) and then a feedback connection with feedback gain $\boldsymbol{K}_{Act} = [K_{q,Act} \quad K_{\alpha,Act}]$:

$$\begin{aligned} \dot{\boldsymbol{x}}_{SP,CL,Act} &= \boldsymbol{A}_{SP,CL,Act}\boldsymbol{x}_{SP,CL,Act} + \boldsymbol{B}_{SP,CL,Act}q_{cmd} \\ \boldsymbol{y}_{SP,CL,Act} &= \boldsymbol{C}_{SP,CL,Act}\boldsymbol{x}_{SP,CL,Act} + \boldsymbol{D}_{SP,CL,Act}q_{cmd} \end{aligned} \tag{4-20}$$

with

$$\boldsymbol{A}_{SP,CL,Act} = \begin{bmatrix} \boldsymbol{A}_{Act} & \begin{matrix} -K_{q,Act}\omega_{Act}^2 & -K_{\alpha,Act}\omega_{Act}^2 \\ 0 & 0 \end{matrix} \\ \boldsymbol{B}_{SP,OL}\boldsymbol{C}_{Act} & \boldsymbol{A}_{SP,OL} \end{bmatrix}$$

$$\boldsymbol{B}_{SP,CL,Act} = \begin{bmatrix} H_{q,Act}\omega_{Act}^2 \\ 0 \\ 0 \\ 0 \end{bmatrix}$$

$$\boldsymbol{C}_{SP,CL} = \begin{bmatrix} 1 & 0 \\ \boldsymbol{A}_{SP,CL,Act}(3,:) \end{bmatrix} \qquad \boldsymbol{D}_{SP,CL} = \begin{bmatrix} 0 \\ \boldsymbol{B}_{SP,CL,Act}(3,:) \end{bmatrix}$$

$$\boldsymbol{x}_{SP,CL} = \begin{bmatrix} \dot{\eta} \\ \eta \\ q_K \\ \alpha_K \end{bmatrix} \qquad \boldsymbol{y}_{SP,CL,Act} = \begin{bmatrix} q_K \\ \dot{q}_K \end{bmatrix}$$

The gain calculation was again done by the algorithm *evmin* provided with Srinathkumar (2011a, 2011b). As only two states are fed back only two poles can be influenced. In our case the short period poles have been placed at $\omega_{SP,nom}$ and $\zeta_{SP,nom}$ for the respective flight condition (Table 7, p. 147). The resulting actuator poles where accepted. Afterwards model (4-20) has been augmented with the wind model as described in chapter 3.5.3.1.2, discretized and used to calculate the Kalman observer gain $\bar{L}$ as explained in chapter 3.5.3.1.3. No uncertainties with respect to the actuator parameters ζ_{Act} and ω_{Act} were assumed (this could be changed in a future work if required). The Kalman filter therefore "knows" the actuator dynamics and thus makes the residual independent of it under nominal fault-free operating conditions.

4.3.4.3 Test Conditions

The simulation runs have been performed at FC 1-4 with a test setup equivalent to TC 1.1, TC 1.2, TC 1.3 and TC 1.4 (without considering atmospheric turbulences) and TC 1.1t, TC 1.2t, TC 1.3t and TC 1.4t (with turbulences, cf. chapters 4.2 & 4.3.1). Other than in those test cases, at t = 6.5 s a fault (closed-loop system instability) followed by an AFCS recovery action has been simulated as described in chapter 4.3.4.2. The acceptable closed-loop ω_{SP}-ζ_{SP} parameter envelope was set to $\omega_{SP,10\%}$ and $\zeta_{SP,10\%}$ according Table 12 (cf. Remark 4-14, p. 185). All test case parameters are summarized in Table 19 and Table 20.

4.3.4.4 Test Results

Remark 4-16: The plot scales have been intentionally kept the same for all TCs to facilitate comparability between the latters. Furthermore relation of the system response to the actual airframe limits in terms, especially $\alpha_{K,lim}$, $(n_{z,lim})_K$, and η_{lim}, is more important than to maximize the plot resolution for each TC.

4.3.4.4.1 Test Cases 7.1 and 7.1t

TC 7.1 (deterministic scenario without considering atmospheric turbulences)

Figure 60 illustrates the results of the simulation run in terms of system response and fault-detection performance for the *deterministic fault detection part* and consequently the scenario *without* atmospheric turbulences.
Up to T_F = 6.5 s the system exhibited the nominal system response as discussed for TC 1.1. As shown in the first plot, after fault occurrence at T_F = 6.5 s, the aircraft immediately started to pitch-up (dashed & solid line) with an angular velocity q_K greater than the nominal one (dotted line). The same observation can be made for the angle of attack α_K (second plot) and the normal load factor $(n_z)_K$ (third plot) though the effect is much less significant. The elevator deflection angle immediately started to run away in the negative (pitch-up) direction (fourth plot). While the ideal actuator (PT0) has been able to follow the step command, the realistic actuator (PT2, RL) followed the command at its rate limit of $|\dot{\eta}_{lim}|$ = 125 deg/s. At T_{FD} = 6.54 s the FD system has detected the fault and, at T_{FCS} = 6.59 s, after the processing time delay of the AFCS ($T_{D,FCS}$ = 0.05 s), the CFCS override bit has been activated (fifth plot). Consequently the elevator has received a full nose-down command of η_{cmd} = 25 deg (fourth plot). Again the ideal actuator has been capable of following the command instantly while the realistic actuator has been rate limited with $|\dot{\eta}_{lim}|$ = 125 deg/s. As a result it did not reach η_{cmd} = 25 deg before T_η = 6.89 s. The significantly different behaviour of the actuators did lead to noticeably different system responses as illustrated in the first three plots. At

$T_{q_k=0}$ = 7.15 s (realistic act.) the pitch-up rotation has been stopped (q_K = 0) and starts to decrease, followed by a respective reduction of α_K and $(n_z)_K$. At $T_{n_z=1}$ = 7.76 s (realistic act.) the normal load factor reaches its straight and level flight value of $(n_z)_K$ = 1 g.
The peak responses during the overall manoeuvre have been $q_{K,max}$ = 14.4 deg/s, $\alpha_{K,max}$ = 19.0 deg, and $(n_{z,max})_K$ = 1.6 g. *The fault detection time delay $T_{D,FD}$ has been just 0.04 s, equivalent just 4 samples at the FD systems sample rate of 100 Hz.* The results are summarized in Table 17 and Table 18.

TC 7.1t (stochastic/deterministic scenario with atmospheric turbulences)

Figure 61 illustrates the results of the simulation run in terms of system response and fault-detection performance for the *integrated stochastic/deterministic fault detection system with* atmospheric turbulences. In the following only significant differences to TC 7.1 will be discussed.
Up to T_F = 6.5 s the system exhibited the nominal system response as discussed for TC 1.1t. In contrast to TC 7.1 at T_F = 6.5 s the pitch rate q_K is already higher than $q_{K,nom}$ due to a disturbance through turbulence. The effect of turbulence is also visible for α_K (second plot) and $(n_z)_K$ (third plot) but less significant. The disturbance can be seen in at t = 6.5 s in Figure 33 (p. 153) as the difference between α_A and α_K which is according (3-160) the wind angle of attack α_W. The additional turbulence induced positive pitch rate, i.e. the difference between q_K and $q_{K,nom}$ just before T_F, makes the recovery after instability even *more* difficult. This is the reason T_F = 6.5 s has been chosen for the fault in order *not* to ease the task of the FD system.
At T_{FD} = 6.61 s the FD system has detected the fault (fifth plot). The FD delay has thus increased from $T_{D,FD,TC7.1}$ = 0.04 s to $T_{D,FD,TC7.1t}$ = 0.11 s.

Remark 4-17: The reason for the higher fault detection delay will be discussed in detail in chapter 4.3.4.5. It is due to the, in the case with stochastic disturbances (turbulence), necessarily higher fault detection threshold.

At T_{FCS} = 6.66 s the CFCS override bit has been activated (fifth plot). The elevator (realistic act.) did reach the recovery position η_{cmd} = 25 deg at T_η = 6.96 s (fourth plot). At $T_{q_k=0}$ = 7.71 s (realistic act.) the pitch-up rotation has been stopped (q_K = 0) and starts to decrease, followed by a respective reduction of α_K and $(n_z)_K$. At $T_{n_z=1}$ = 8.48 s (realistic act.) the normal load factor reaches its straight and level flight value of $(n_z)_K$ = 1 g.
The peak responses during the overall manoeuvre have been $q_{K,max}$ = 23.7 deg/s, $\alpha_{K,max}$ = 23.8 deg, and $(n_{z,max})_K$ = 1.9 g. Due to the negative influences of the atmospheric turbulence (see above) and the higher fault detection delay the maxi-

mum response values are necessarily higher than for TC 7.1. The angle of attack α_K nearly reached $\alpha_{K,lim}$ of the F-16 production FCS though this limit has informal character in our case study (see Remark 4-6, p. 148).
The fault detection time delay $T_{D,FD}$ has been just 0.11s, equivalent 11 samples at the FD systems sample rate of 100 Hz. The results are summarized in Table 17 and Table 18.

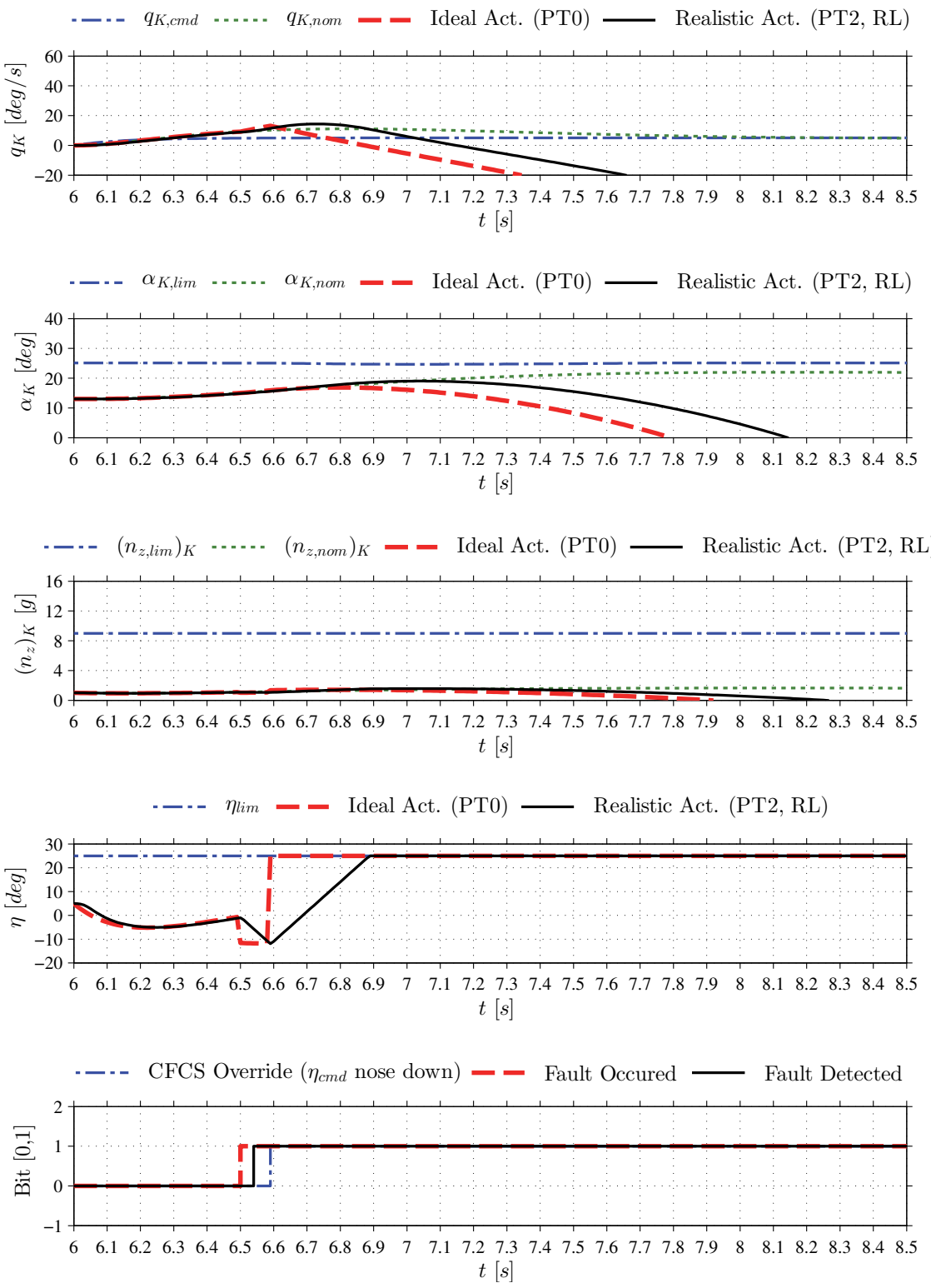

Figure 60 Fault-detection performance and system response for simulated closed-loop instability without atmospheric turbulence at FC 1 (TC 7.1)

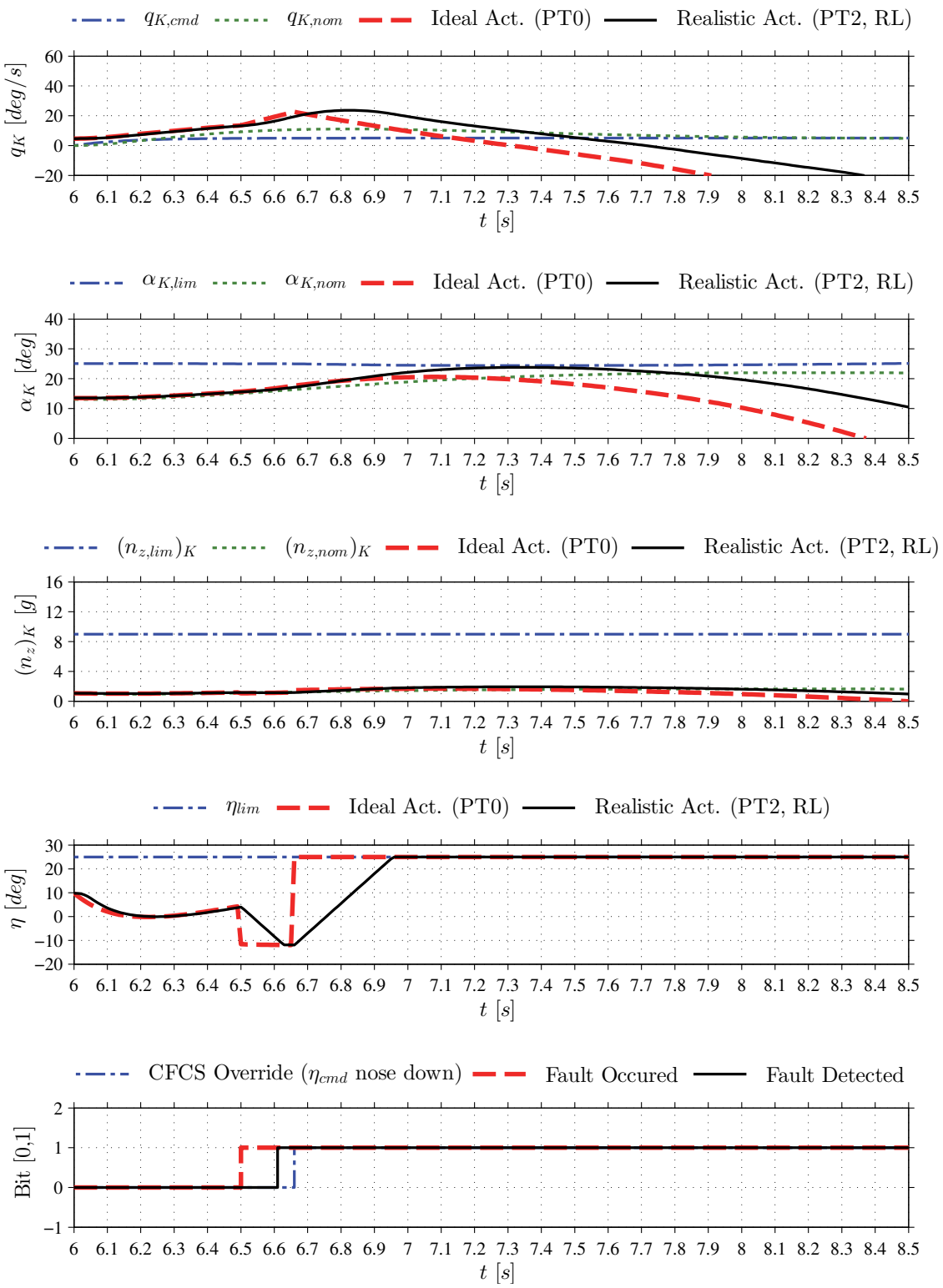

Figure 61 Fault-detection performance and system response for simulated closed-loop instability with atmospheric turbulence at FC 1 (TC 7.1t)

4.3.4.4.2 Test Cases 7.2 and 7.2t

TC 7.2 (deterministic scenario without considering atmospheric turbulences)

Figure 62 shows the results of the simulation run in terms of system response and fault-detection performance for the *deterministic fault detection part* and consequently the scenario *without* atmospheric turbulences.
The system exhibited the nominal system response as discussed for TC 1.2 up to T_F = 6.50 s. As illustrated in the first plot, after fault occurrence at T_F = 6.50 s, the aircraft immediately started to pitch-up (dashed & solid line) with an angular velocity q_K significantly higher than the nominal one (dotted line). In comparison to TC 7.1 the reaction is much more pronounced, as to be expected for a flight condition with 17.8 times higher dynamic pressure ($\bar{q}_{A,TC7.2}$ = 59.2 kPa, $\bar{q}_{A,TC7.1}$ = 3.32 kPa, see Table 6, p. 146) and a higher pitch rate command ($q_{K,cmd,TC7.2}$ = 14 deg/s, $q_{K,cmd,TC7.1}$ = 5 deg/s)
As for TC 7.1, the deviation from the nominal response in terms angle of attack α_K (second plot) is relatively small, however, in contrast to the latter, the fault induced increase in the normal load factor $(n_z)_K$ is very high reaching $(n_{z,max})_K$ = 12.6 g instead of $(n_{z,nom})_K$ = 8.5 g (third plot, solid line). In this regard it is also interesting to note that the lift generated by the recovery elevator deflection via Z_η leads to a normal load factor increase of $\Delta(n_z)_K$ = +2.4 g best seen from the curve of the ideal actuator at t = 6.58 s (dashed line). This was also the reason why the elevator deflection during recovery was reduced to η_{cmd} = 10 deg for TC 7.2 (cf. chapter 4.3.4.2, p. 194). Again the driving factor behind the strong reaction is the high dynamic pressure $\bar{q}_A$ of this flight condition. As for TC 7.1 after fault occurrence the elevator deflection angle immediately started to run away in the negative (pitch-up) direction. While the ideal actuator (PT0) has been able to follow the step command, the realistic actuator (PT2 with rate limiting) followed the command at its rate limit of $|\dot{\eta}_{lim}|$ = 125 deg/s.
At T_{FD} = 6.53 s the FD system has detected the fault and, at T_{FCS} = 6.58 s, after the processing time delay of the AFCS, the CFCS override bit has been activated. Consequently the elevator has received a full nose-down command of η_{cmd} = 10 deg (fourth plot). Again the ideal actuator has been capable of following the command instantly while the realistic actuator has been rate limited with $|\dot{\eta}_{lim}|$ = 125 deg/s. As a result it did not reach η_{cmd} = 10 deg before T_η = 6.72 s. The significantly different behaviour of the actuators did lead to noticeably different system responses as illustrated in the first three plots. At $T_{q_k=0}$ = 6.83 s (realistic actuator) the pitch-up rotation has been stopped (q_K = 0) and starts to decrease, followed by a respective reduction of α_K and $(n_z)_K$. At $T_{n_z=1}$ = 7.05 s (realistic actuator) the normal load factor reaches its straight and level flight value of $(n_z)_K$ = 1 g.

The peak responses during the overall manoeuvre have been $q_{K,max}$ = 42.7 deg/s, $\alpha_{K,max}$ = 7.5 deg, and $(n_{z,max})_K$ = 12.6 g. The normal load factor $(n_z)_K$ exceeds its operational limit $(n_{z,lim})_K$ = 9 g. This will be discussed further in chapter 4.3.4.5.
The fault detection time delay $T_{D,FD}$ has been just 0.03 s, equivalent 3 samples at the FD systems sample rate of 100 Hz. The results are summarized in Table 17 and Table 18.

TC 7.2t (stochastic/deterministic scenario with atmospheric turbulences)

Figure 63 illustrates the results of the simulation run in terms of system response and fault-detection performance for the *integrated stochastic/deterministic fault detection system with* atmospheric turbulences. In the following only significant difference to TC 7.2 will be discussed.
Up to T_F = 6.50 s the system exhibited the nominal system response as discussed for TC 1.2t. As for TC 7.1 at T_F = 6.50 s the pitch rate q_K is already higher than $q_{K,nom}$ due to a correspondent disturbance by turbulence (see Figure 35, p. 155).
At T_{FD} = 6.55 s the FD system has detected the fault (fifth plot). The FD delay has thus increased from $T_{D,FD,TC7.2}$ = 0.03 s to $T_{D,FD,TC7.2t}$ = 0.05 s (see Remark 4-17).
At T_{FCS} = 6.60 s, after the processing time delay of the AFCS, the CFCS override bit has been activated (fifth plot). The elevator (realistic act.) did reach the recovery position η_{cmd} = 10 deg at T_η= 6.74 s (fourth plot). At $T_{q_k=0}$ = 6.88 s (realistic act.) the pitch-up rotation has been stopped (q_K = 0) and starts to decrease, followed by a respective reduction of α_K and $(n_z)_K$. At $T_{n_z=1}$ = 7.12 s (realistic act.) the normal load factor reaches its straight and level flight value of $(n_z)_K$ = 1 g.
The peak responses during the overall manoeuvre have been $q_{K,max}$ = 52.7 deg/s, $\alpha_{K,max}$ = 9.2 deg, and $(n_{z,max})_K$ = 14.7 g. As for TC 7.1, due to the negative influences of the atmospheric turbulence (see above) and the higher fault detection delay, the maximum response values are necessarily higher for TC 7.2t than for TC 7.2. The normal load factor $(n_z)_K$ exceeds its operational limit $(n_{z,lim})_K$ = 9 g. This will be discussed further in chapter 4.3.4.5.
The fault detection time delay $T_{D,FD}$ has been just 0.05s, equivalent 5 samples at the FD systems sample rate of 100 Hz. The results are summarized in Table 17 and Table 18.

TC 7.2ta (stochastic/deterministic scenario with atmospheric turbulences)

To illustrate the influence of turbulence on the peak responses of $q_{K,max}$, $\alpha_{K,max}$, and $(n_{z,max})_K$, TC 7.2t was repeated with the exactly same parameters besides the time the instability occurred (Figure 64). T_F has now been set to 1.50 s a period where, due to turbulence, the pitch rate q_K is smaller than $q_{K,nom}$ (first plot). The

peak responses during the overall manoeuvre have now been $q_{K,max}$ = 43.4 deg/s, $\alpha_{K,max}$ = 8.0 deg, and $\left(n_{z,max}\right)_K$ = 13.2 g, i.e. *significantly lower* than for TC 7.2t. *The fault detection time delay* $T_{D,FD}$ *has been just 0.05s as for TC 7.2t.* The results are summarized in Table 17 and Table 18.

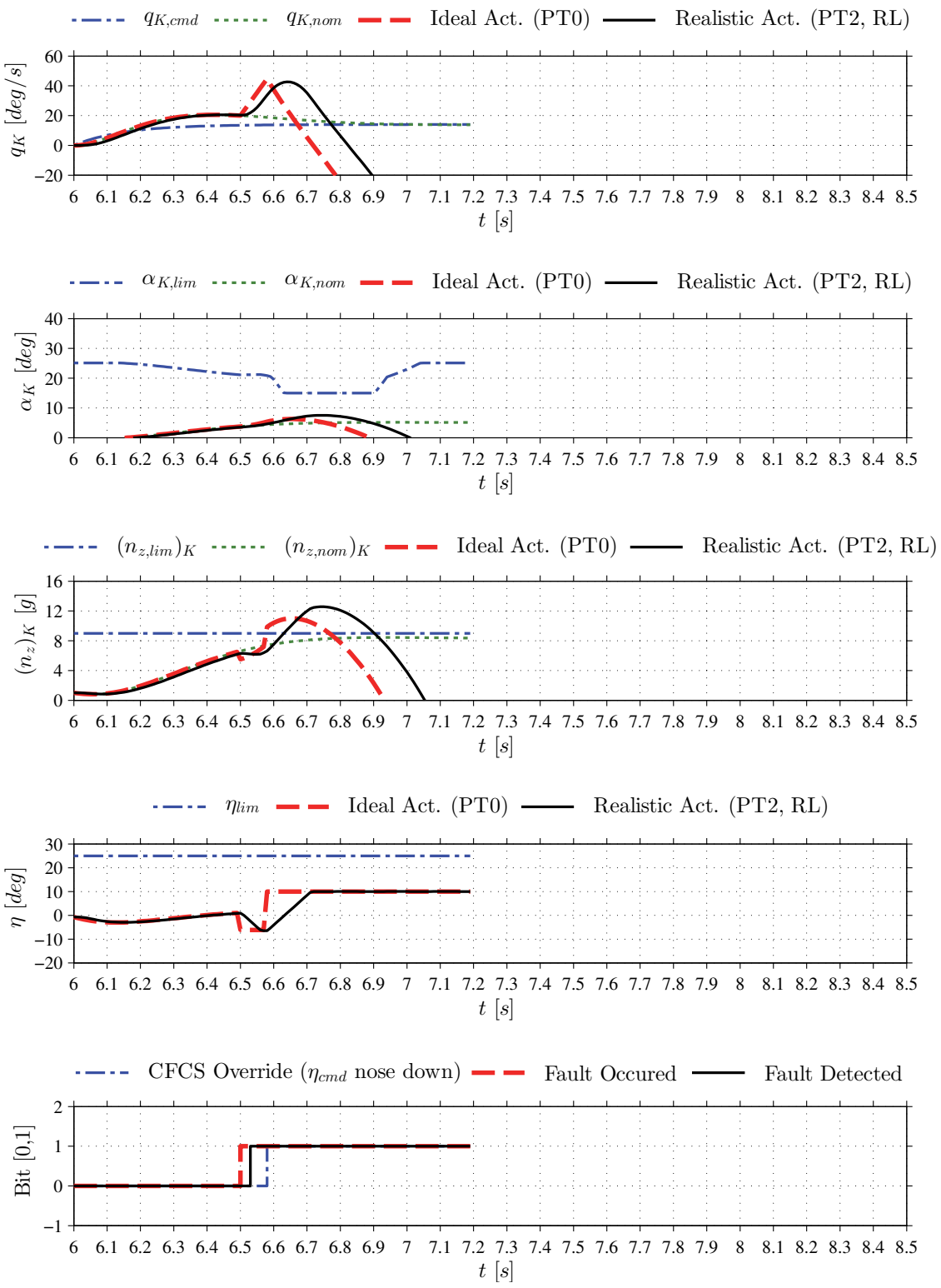

Figure 62 Fault-detection performance and system response for simulated closed-loop instability without atmospheric turbulence at FC 2 (TC 7.2)

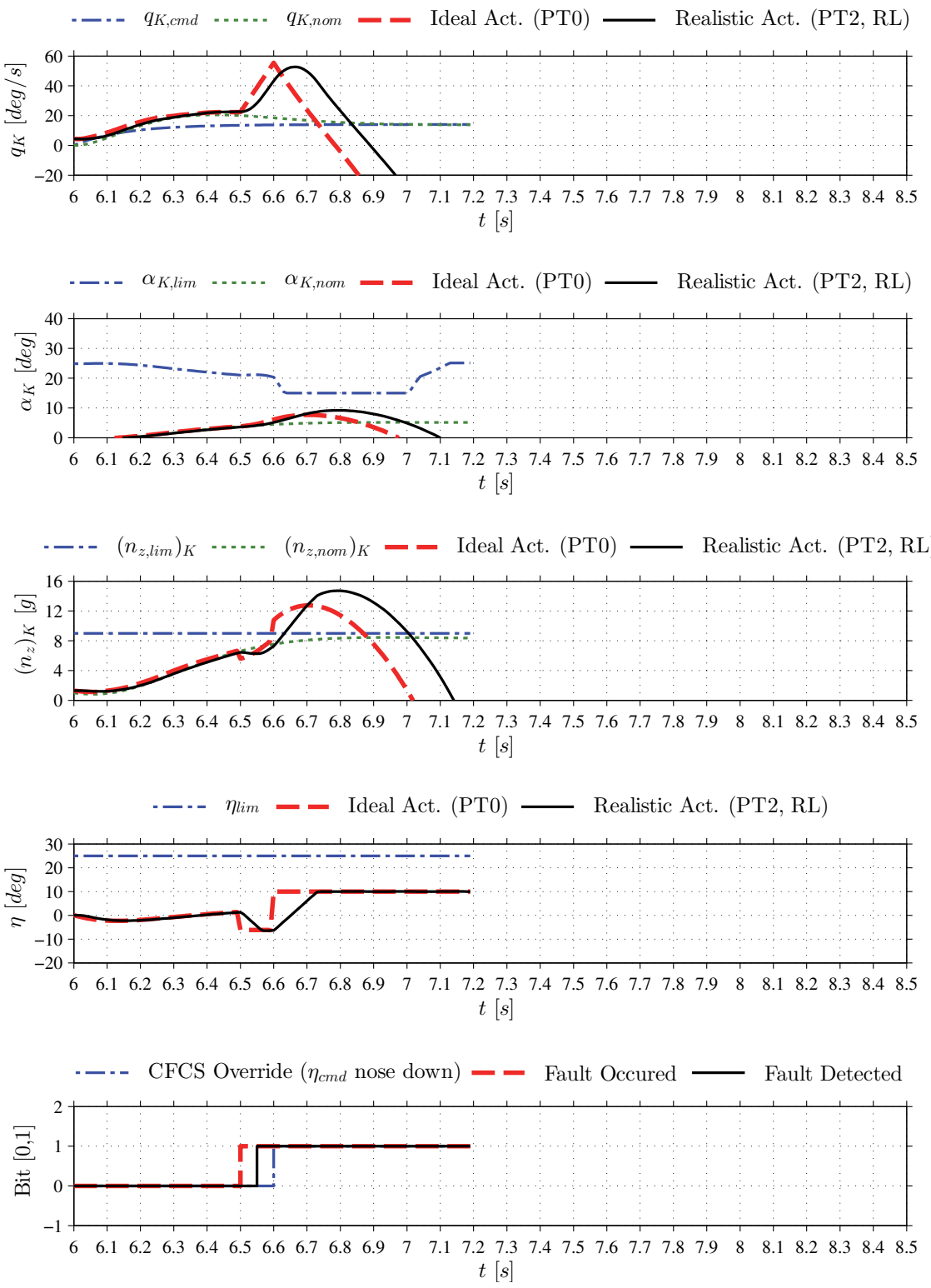

Figure 63 Fault-detection performance and system response for simulated closed-loop instability with atmospheric turbulence at FC 2 (TC 7.2t)

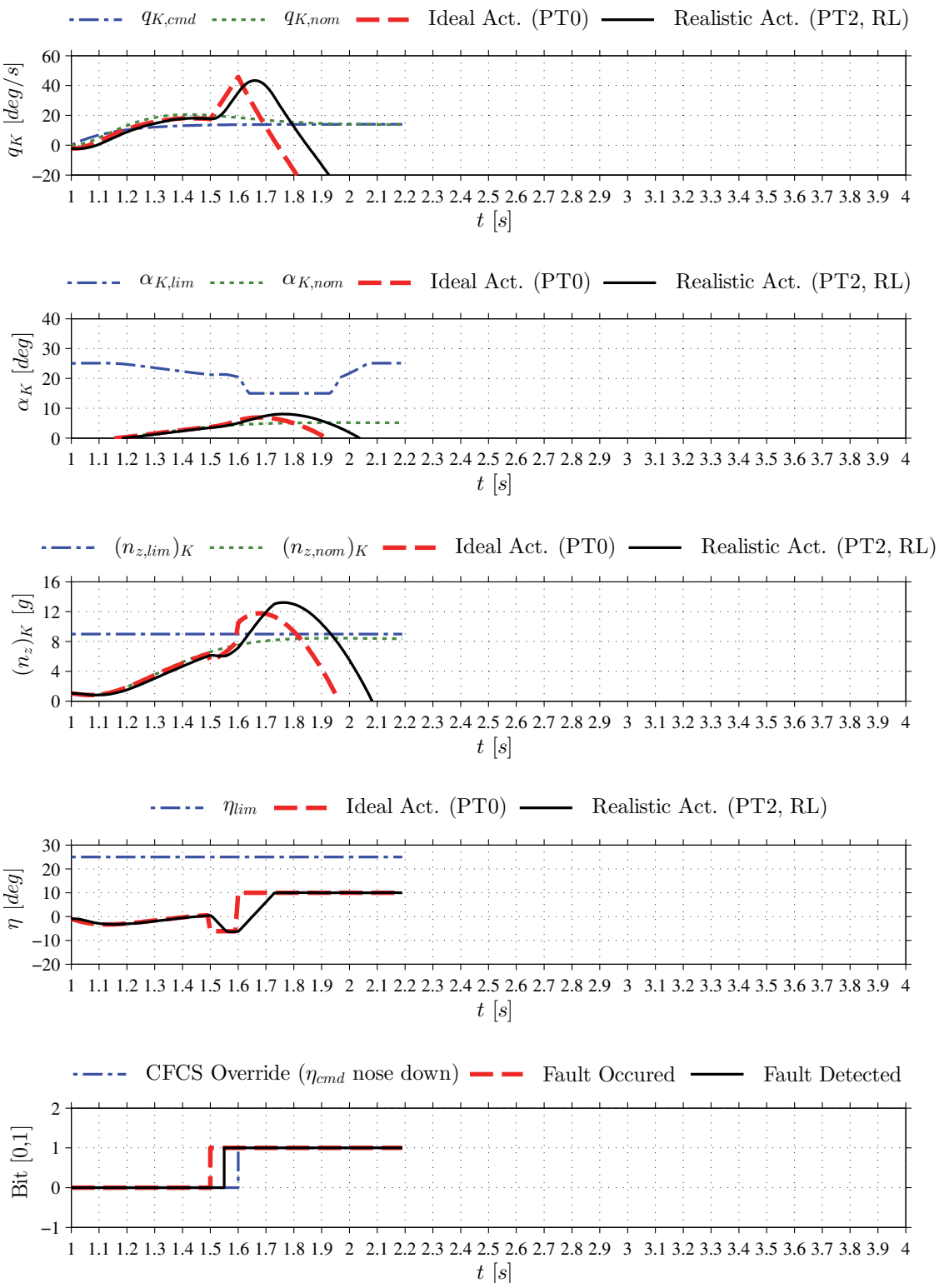

Figure 64 Fault-detection performance and system response for simulated closed-loop instability with atmospheric turbulence at FC 2 (TC 7.2ta)

4.3.4.4.3 Test Cases 7.3 and 7.3t

TC 7.3 (deterministic scenario without considering atmospheric turbulences)

Figure 65 shows the results of the simulation run in terms of system response and fault-detection performance for TC 7.3. The system exhibited the nominal system response as discussed for TC 1.3 up to T_F = 6.50 s.
As illustrated in the first plot, after fault occurrence at T_F = 6.50 s, the aircraft immediately started to pitch-up (dashed & solid line) with an angular velocity q_K significantly higher than the nominal one (dotted line). In comparison to TC 7.2, the reaction is less pronounced, as to be expected for a flight condition with less dynamic pressure ($\bar{q}_{A,TC7.2}$ = 59.2 kPa, $\bar{q}_{A,TC7.3}$ = 9.34 kPa, see Table 6, p. 146) and a smaller pitch rate command ($q_{K,cmd,TC7.3}$ = 5 deg/s, $q_{K,cmd,TC7.2}$ = 14 deg/s)
In contrast to TC 7.1 and TC 7.2, for the angle of attack α_K (second plot) the deviation from the nominal response is much more significant. While, with respect to TC7.2, this is clear from the difference in dynamic pressure (see above), the higher value in comparison to TC7.1 is less obvious. The pitch rate command is the same as for TC 7.1 and the dynamic pressure is even higher ($\bar{q}_{A,TC7.3}$ = 9.34 kPa, $\bar{q}_{A,TC7.1}$ = 3.32 kPa). However the time to double is significantly lower than for TC 7.1 ($T_{2,OL,TC7.3}$ = 0.98 s, $T_{2,OL,TC7.1}$ = 1.26 s, see Table 6, p. 146). The fault induced increase in the normal load factor $(n_z)_K$ is slightly higher than for TC 7.1 but significantly less than for TC 7.2. As for TC 7.2 a normal load factor increase due to the recovery elevator deflection is visible for the ideal actuator at t = 6.60 s (dashed line). The elevator deflection shows the same characteristics as discussed for TC 7.1 and 7.2 though the absolute deflection angles are of course different (fourth plot).
At T_{FD} = 6.56 s the FD system has detected the fault and, at T_{FCS} = 6.61 s, after the processing time delay of the FCS, the FCS override bit has been activated. Consequently the elevator has received a full nose-down command of η_{cmd} = 25 deg (fourth plot). Again the ideal actuator has been capable of following the command instantly while the realistic actuator has been rate limited with $|\dot{\eta}_{lim}|$ = 125 deg/s. As a result it did not reach η_{cmd} = 25 deg before T_η = 6.93 s. The significantly different behaviour of the actuators did lead to noticeably different system responses as illustrated in the first three plots. At $T_{q_k=0}$ = 7.11 s (realistic actuator) the pitch-up rotation has been stopped (q_K = 0) and starts to decrease, followed by a respective reduction of α_K and $(n_z)_K$. At $T_{n_z=1}$ = 7.62 s (realistic actuator) the normal load factor reaches its straight and level flight value of $(n_z)_K$ = 1 g.
The peak responses during the overall manoeuvre have been $q_{K,max}$ = 34.1 deg/s, $\alpha_{K,max}$ = 19.7 deg, and $(n_{z,max})_K$ = 4.6 g.
The fault detection time delay $T_{D,FD}$ has been just 0.06 s, equivalent 6 samples at the FD systems sample rate of 100 Hz. The results are summarized in Table 17 and Table 18.

TC 7.3t (stochastic/deterministic scenario with atmospheric turbulences)

Figure 66 illustrates the results of the simulation run in terms of system response and fault-detection performance for the *integrated stochastic/deterministic fault detection system with* atmospheric turbulences. In the following only significant difference to TC 7.3 will be discussed.

Up to T_F = 6.50 s the system exhibited the nominal system response as discussed for TC 1.3t. As for TC 7.1t and TC 7.2t, at T_F = 6.50 s, the pitch rate q_K is already higher than $q_{K,nom}$ due to a correspondent disturbance by turbulence. The effect is not very pronounced but can still be seen in Figure 37 (p. 157).

At T_{FD} = 6.58 s the FD system has detected the fault (fifth plot). The FD delay has thus increased from $T_{D,FD,TC7.3}$ = 0.06 s to $T_{D,FD,TC7.3t}$ = 0.08 s (see Remark 4-17).

At T_{FCS} = 6.63 s, after the processing time delay of the AFCS, the CFCS override bit has been activated (fifth plot). The elevator (realistic act.) did reach the recovery position η_{cmd} = 25 deg at T_η= 6.96 s (fourth plot). At $T_{q_k=0}$ = 7.18 s (realistic act.) the pitch-up rotation has been stopped (q_K = 0) and starts to decrease, followed by a respective reduction of α_K and $(n_z)_K$. At $T_{n_z=1}$ = 7.74 s (realistic act.) the normal load factor reaches its straight and level flight value of $(n_z)_K$ = 1 g.

The peak responses during the overall manoeuvre have been $q_{K,max}$ = 38.8 deg/s, $\alpha_{K,max}$ = 22.6 deg, and $(n_{z,max})_K$ = 5.2 g. As for TC 7.1 and TC 7.2, due to the negative influences of the atmospheric turbulence (see above) and the higher fault detection delay, the maximum response values are necessarily higher for TC 7.3t than for TC 7.3. The angle of attack α_K slightly exceeded $\alpha_{K,lim}$ of the F-16 production FCS between t = 7.05 s and t = 7.2 s, though this limit has informal character in our case study (see Remark 4-6, p. 148).

The fault detection time delay $T_{D,FD}$ has been just 0.08s, equivalent 8 samples at the FD systems sample rate of 100 Hz. The results are summarized in Table 17 and Table 18.

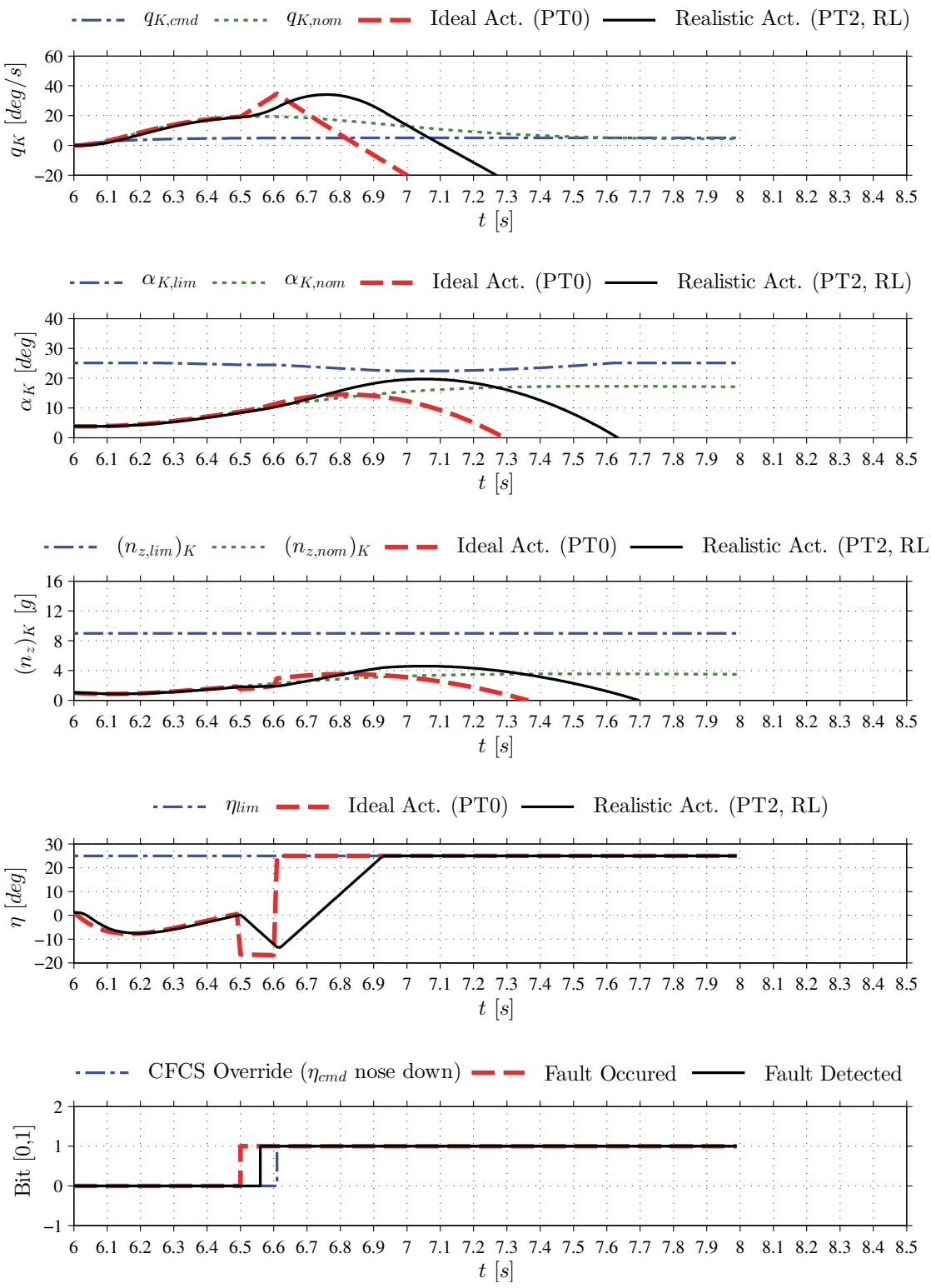

Figure 65 Fault-detection performance and system response for simulated closed-loop instability without atmospheric turbulence at FC 3 (TC 7.3)

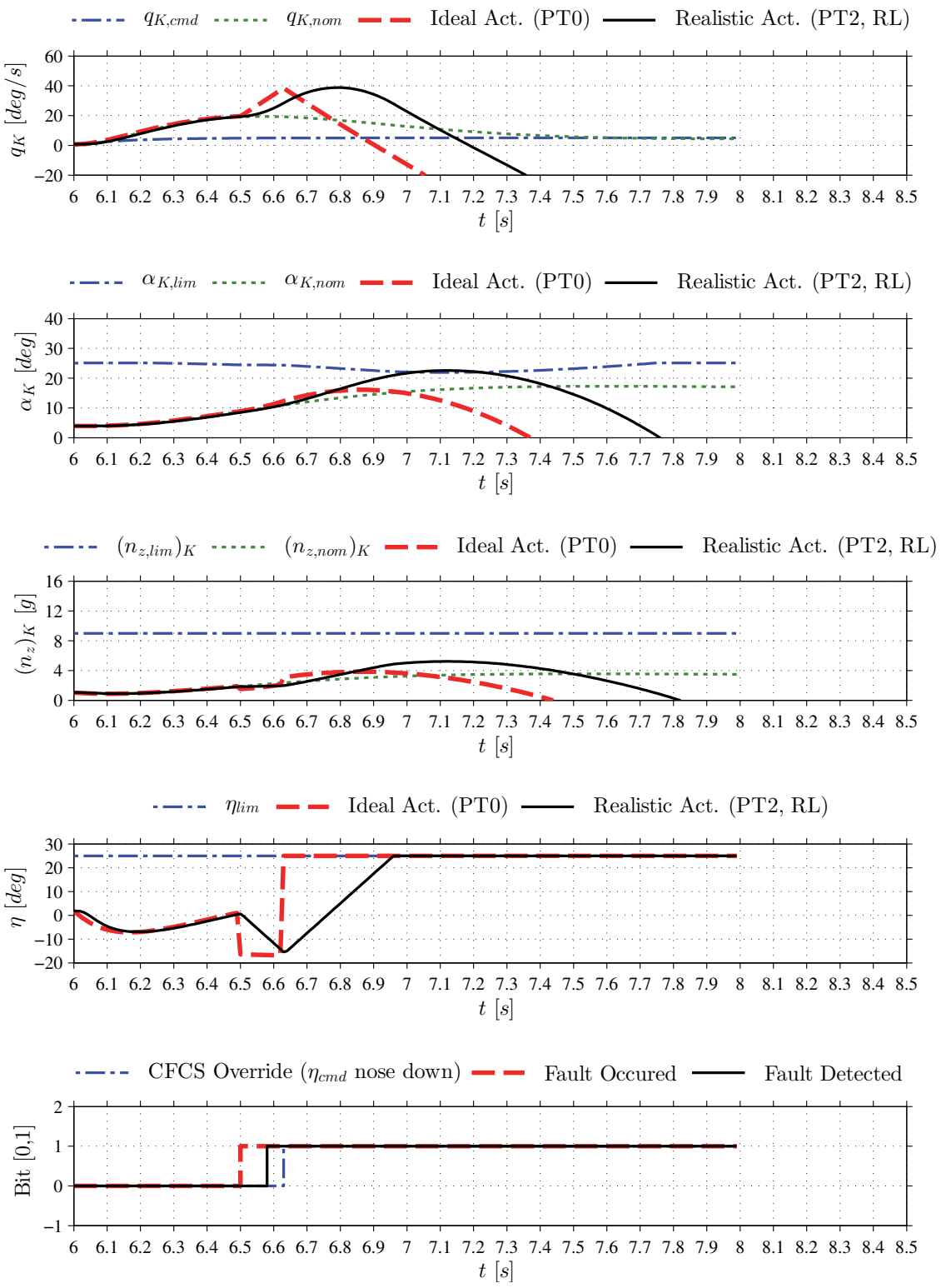

Figure 66 Fault-detection performance and system response for simulated closed-loop instability with atmospheric turbulence at FC 3 (TC 7.3t)

4.3.4.4.4 Test Cases 7.4 and 7.4t

TC 7.4 (deterministic scenario without considering atmospheric turbulences)

Figure 67 shows the results of the simulation run in terms of system response and fault-detection performance for TC 7.4. The system exhibited the nominal system response as discussed for TC 1.4 up to T_F = 6.50 s.
As illustrated in the first plot, after fault occurrence at T_F = 6.50 s, the aircraft immediately started to pitch-up (dashed & solid line) with an angular velocity q_K slightly higher than the nominal one (dotted line). The same observation can be made for the angle of attack α_K (second plot). The normal load factor $(n_z)_K$ (third plot) stayed close to its nominal value. Overall the absolute deviations of q_K, α_K, and $(n_z)_K$ have been very small in comparison to the other TCs discussed before. This should not be a surprise in view of FC 4, which is characterized by the lowest $\bar{q}_{A,TC7.4}$ = 2.15 kPa, largest time to double 2.68 s and smallest $q_{K,cmd,TC7.4}$ = 1.4 deg/s. The elevator deflection shows the same characteristics as discussed for TC 7.1, 7.2, and 7.3 though the absolute deflection angles are very pronounced (fourth plot) as to be expected for the low dynamic pressure of TC 7.4.
At T_{FD} = 6.56 s the FD system has detected the fault and, at T_{FCS} = 6.61 s, after the processing time delay of the FCS, the FCS override bit has been activated. Consequently the elevator has received a full nose-down command of η_{cmd} = 25 deg (fourth plot). Again the ideal actuator has been capable of following the command instantly while the realistic actuator has been rate limited with $|\dot{\eta}_{lim}|$ = 125 deg/s. As a result it did not reach η_{cmd} = 25 deg before T_η = 6.89 s. The significantly different behaviour of the actuators did lead to noticeably different system responses as illustrated in the first three plots. At $T_{q_k=0}$ = 7.21 s (realistic actuator) the pitch-up rotation has been stopped (q_K = 0) and starts to decrease, followed by a respective reduction of α_K and $(n_z)_K$. At $T_{n_z=1}$ = 7.96 s (realistic actuator) the normal load factor reaches its straight and level flight value of $(n_z)_K$ = 1 g.
The peak responses during the overall manoeuvre have been $q_{K,max}$ = 7.5 deg/s, $\alpha_{K,max}$ = 23.7 deg, and $(n_{z,max})_K$ = 1.2 g.
The fault detection time delay $T_{D,FD}$ has been just 0.06 s, equivalent 6 samples at the FD systems sample rate of 100 Hz. The results are summarized in Table 17 and Table 18.

TC 7.4t (stochastic/deterministic scenario with atmospheric turbulences)

Figure 68 illustrates the results of the simulation run in terms of system response and fault-detection performance for the *integrated stochastic/deterministic fault detection system with* atmospheric turbulences. In the following only significant difference to TC 7.4 will be discussed.

Up to T_F = 6.50 s the system exhibited the nominal system response as discussed for TC 1.4t. As for TC 7.1t, 7.2t, and 7.3t at T_F = 6.50 s the pitch rate q_K is already higher than $q_{K,nom}$ due to a correspondent disturbance by turbulence (see Figure 39, p. 159).

At T_{FD} = 6.68 s the FD system has detected the fault (fifth plot). The FD delay has thus increased from $T_{D,FD,TC7.4}$ = 0.06 s to $T_{D,FD,TC7.4t}$ = 0.18 s (see Remark 4-17).

At T_{FCS} = 6.73 s, after the processing time delay of the AFCS, the CFCS override bit has been activated (fifth plot). The elevator (realistic act.) did reach the recovery position η_{cmd} = 25 deg at T_η= 7.01 s (fourth plot). At $T_{q_k=0}$ = 7.71 s (realistic act.) the pitch-up rotation has been stopped (q_K = 0) and starts to decrease, followed by a respective reduction of α_K and $(n_z)_K$. At $T_{n_z=1}$ = 8.60 s (realistic act.) the normal load factor reaches its straight and level flight value of $(n_z)_K$ = 1 g.

The peak responses during the overall manoeuvre have been $q_{K,max}$ = 13.0 deg/s, $\alpha_{K,max}$ = 26.2 deg, and $(n_{z,max})_K$ = 1.3 g. As for TC 7.1t, 7.2t, and 7.3t due to the negative influences of the atmospheric turbulence (see above) and the higher fault detection delay, the maximum response values are necessarily higher for TC 7.4t than for TC 7.4. The angle of attack α_K slightly exceeded $\alpha_{K,lim}$ of the F-16 production FCS between t = 7.05 s and t = 7.9 s, though this limit has informal character in our case study (see Remark 4-6, p. 148).

The fault detection time delay $T_{D,FD}$ has been 0.18s, equivalent 18 samples at the FD systems sample rate of 100 Hz. The results are summarized in Table 17 and Table 18.

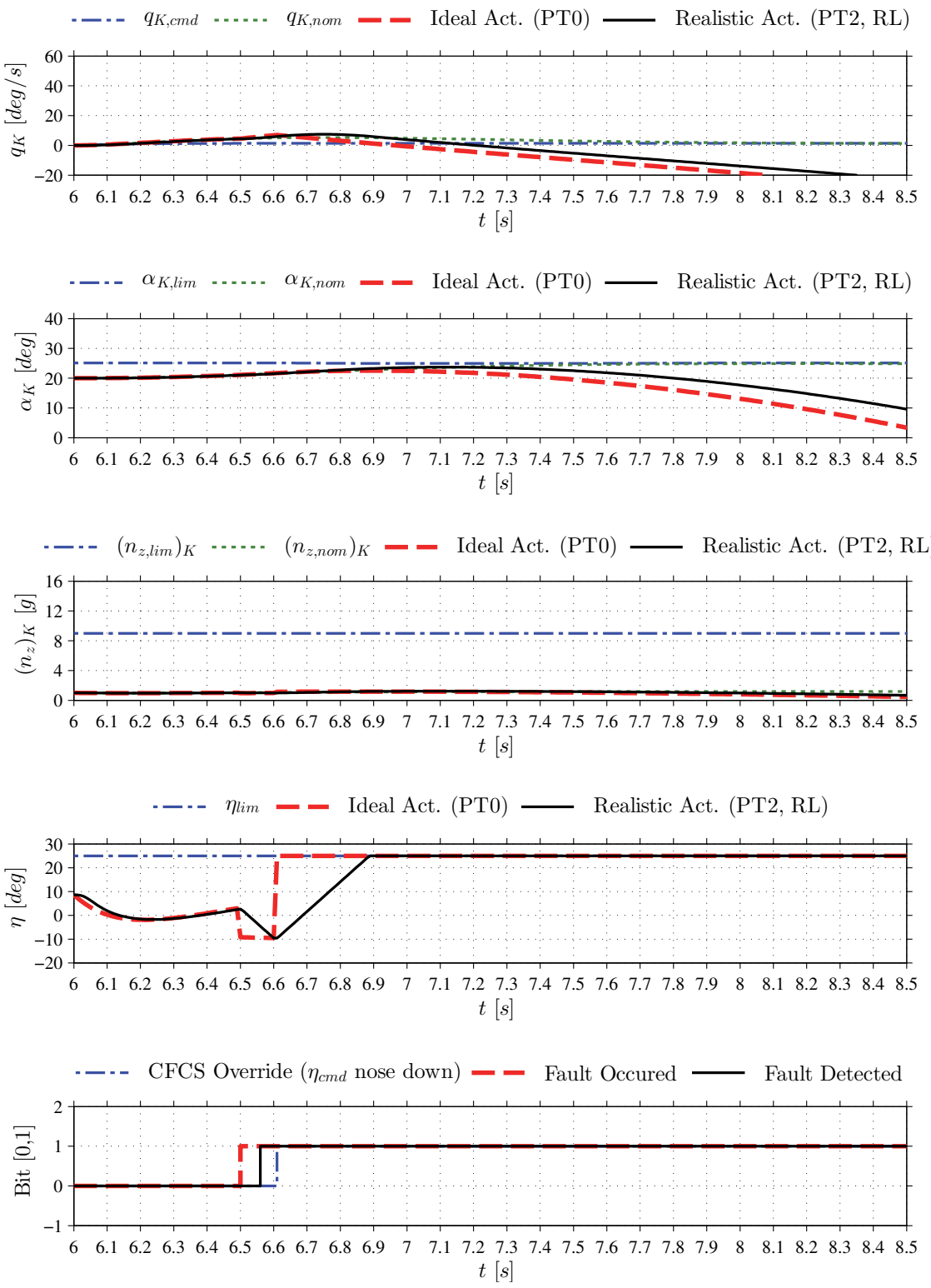

Figure 67 Fault-detection performance and system response for simulated closed-loop instability without atmospheric turbulence at FC 4 (TC 7.4)

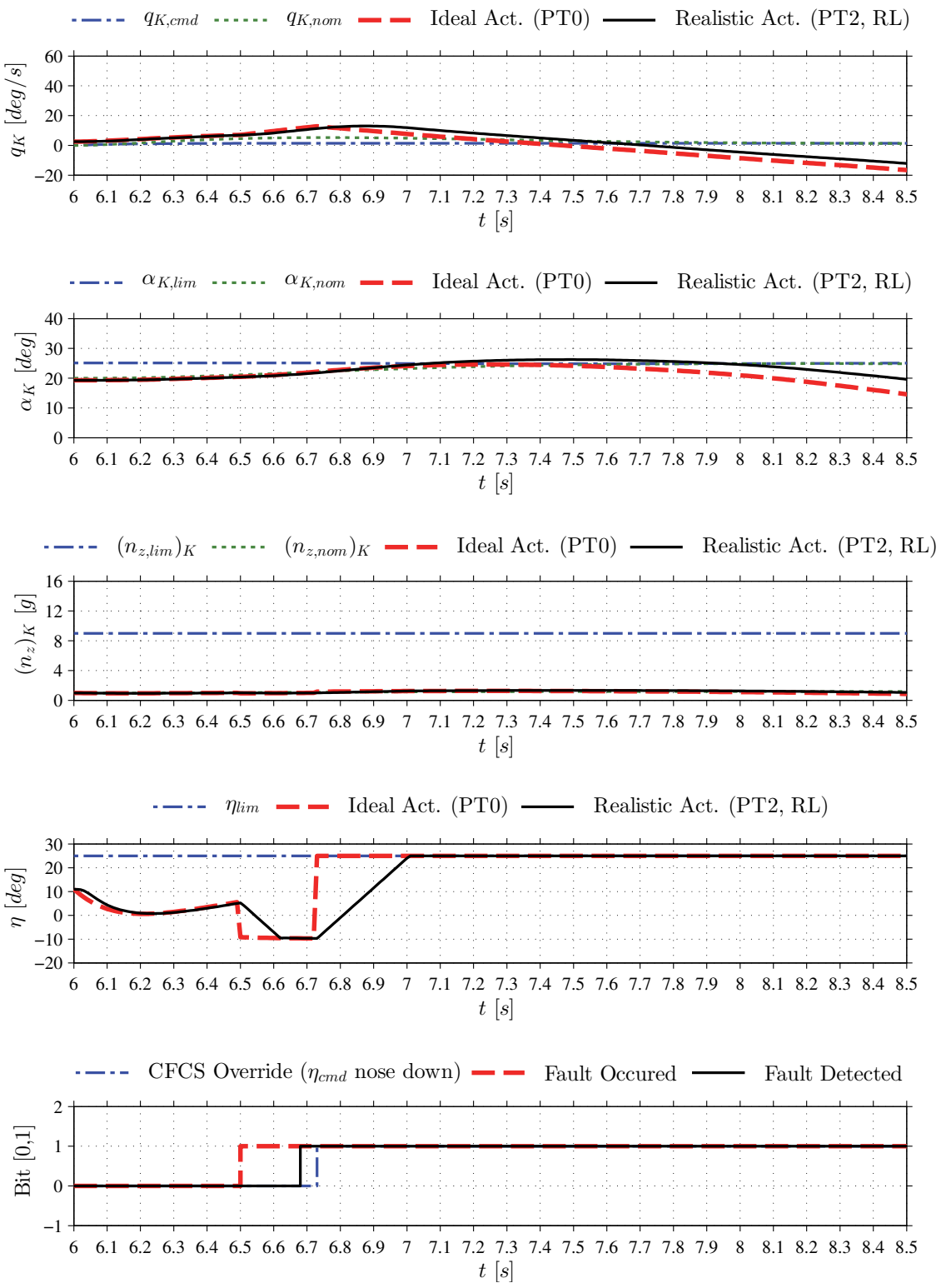

Figure 68 Fault-detection performance and system response for simulated closed-loop instability with atmospheric turbulence at FC 4 (TC 7.4t)

4.3.4.5 Discussion of Results with Respect to Test Goal

4.3.4.5.1 Fault Detection Delay

Test Cases 7.1 to 7.4 - Deterministic fault detection system

For TC 7.1 – 7.4 it has been shown that the fault detection delay of the FD system proposed in this work is small enough to stop the instability induced pitch-up motion from a severe fault where the closed-loop system has become unstable. The key results are summarized in Table 17 and Table 18.
$T_{D,FD}$ has varied between 0.03 s (TC 7.2) and 0.06 s (TC 7.3 & 7.4). For the FD system used, which operated at a sample rate of 100 Hz, this equalled just 3 samples and 6 samples respectively. A higher sample rate might potentially lower the delay further, but it should also have become clear that a typical FCS reaction in form of the processing time delay $T_{D,FCS}$ = 0.05 s and the time it takes the actuator/control surface (0.32 sec in TC 7.3) to reach is recovery position is much more dominant in the deterministic case.
In general it is also very import to recall Remark 6-1 (p. 247) at this point. A peculiarity of this simulation case study has been that we took the F-16 airframe (model), designed for a worst-case time to double of 1.5 s (cf. Table 1, p. 31), and artificially made it more unstable by a CG shift from $\left(x_{ref}^{G}\right)_B = 0.35\bar{c}$ to $(x^G)_B = 0.4\bar{c}$ (Table 22, p. 247) to get a time to double more representative of contemporary fighter aircraft (cf. Table 1, p. 31). This happened without adding additional pitch control power, i.e. increase M_η, something that would for sure not happen for a real aircraft design. Additional pitch control power would significantly simplify the recovery action. In this regard the tests conducted in this chapter can be seen as very conservative. Nevertheless, beside this conservatism, the instability induced pitch-up motion has been stopped successfully in all cases.
For completeness the residual $\|\boldsymbol{r}\|_{RMS}^2$ and the threshold $J_{th,RMS}$ are illustrated in Figure 69 for TC 7.1 - 7.4. A fault is detected (fault bit set to 1) when $\|\boldsymbol{r}\|_{RMS}^2 > J_{th,RMS}$. The residual signal will be discussed further in the next paragraph.

Test Cases 7.1t to 7.4t - Integrated stochastic/deterministic fault detection system

Also for TC 7.1t – 7.4t it has been shown that the fault detection delay of the FD system proposed in this work is small enough to stop the instability induced pitch-up motion from a severe fault where the closed-loop system has become unstable. The key results are summarized in Table 17 and Table 18.

$T_{D,FD}$ has varied between 0.05 s (TC 7.2t) and 0.18 s (TC 7.4), equal 5 and 18 samples respectively. Clearly the fault detection delay has increased in comparison to TC 7.1 – 7.4. As already mentioned in Remark 4-17 (p. 199) the reason is the, in the case with stochastic disturbances (turbulence), necessarily higher fault detection threshold. The theoretical explanation can be found in chapter 3.5.4.4. Here we want to have a look at the practical implications. We recall that a fault is detected (fault bit set to 1) when $\|\boldsymbol{r}\|^2_{RMS} > \tilde{J}_{th,\chi^2}$. Both values are depicted in Figure 70 for TC 7.1t - 7.4t. As a reference the deterministic threshold $J_{th,RMS}$ is also shown. It can be readily seen that $\tilde{J}_{th,\chi^2} \gg J_{th,RMS}$ as a result it takes more time till $\|\boldsymbol{r}\|^2_{RMS}$ passes $\tilde{J}_{th,\chi^2}$. $J_{th,\chi^2} \gg J_{th,RMS}$ is a necessity to ensure a FAR < 10^{-6} per FH despite the effect of atmospheric turbulence on the residual (cf. chapter 3.5.4.4).
By inspection of Figure 69 and Figure 70, we can also see that the residual $\|\boldsymbol{r}\|^2_{RMS}$, i.e. the fault signal, is much "stronger" (steep slope after fault occurrence at T_F = 6.50 s) for TC 7.2/7.2t and 7.3/7.3t than for TC 7.1/7.1t and 7.4/7.4t. The reason lies in the fact that the residual of this thesis has been generated only from the measurement of q_K and $\dot{q}_K$ due to Requirement 1-4 (minimize measurements, p. 11) and Requirement 1-5 (do not use an angle of attack measurement for fault detection, p. 11) and their related rationales. From flight mechanics theory it should be clear to the reader, that the aircraft reaction in terms of $\dot{q}_K$ and therefore q_K is much less pronounced at a flight condition with lower dynamic pressure $\bar{q}_A$ (FC 1 & 4; cf. Table 6, p. 146) than for a flight condition with higher dynamic pressure (FC 2 & 3). Of course this also manifests itself in a residual signal $\|\boldsymbol{r}\|^2_{RMS}$ generated from q_K and $\dot{q}_K$. Thus $\|\boldsymbol{r}\|^2_{RMS}$ is "weaker" in terms of initial slope after fault occurrence for TC 7.1/7.1t and 7.4/7.4t than for TC 7.2/7.2t and 7.3/7.3t. If we intent to get a stronger residual signal $\|\boldsymbol{r}\|^2_{RMS}$ to reduce $T_{D,FD}$ for those FCs, we have to add a signal to $\|\boldsymbol{r}\|^2_{RMS}$ that is stronger at those flight conditions. It should be clear that this would be the angle of attack α_K. But again, this was *not done herein by intention* because of the reasons described in the rationales of Requirement 1-4 and Requirement 1-5.

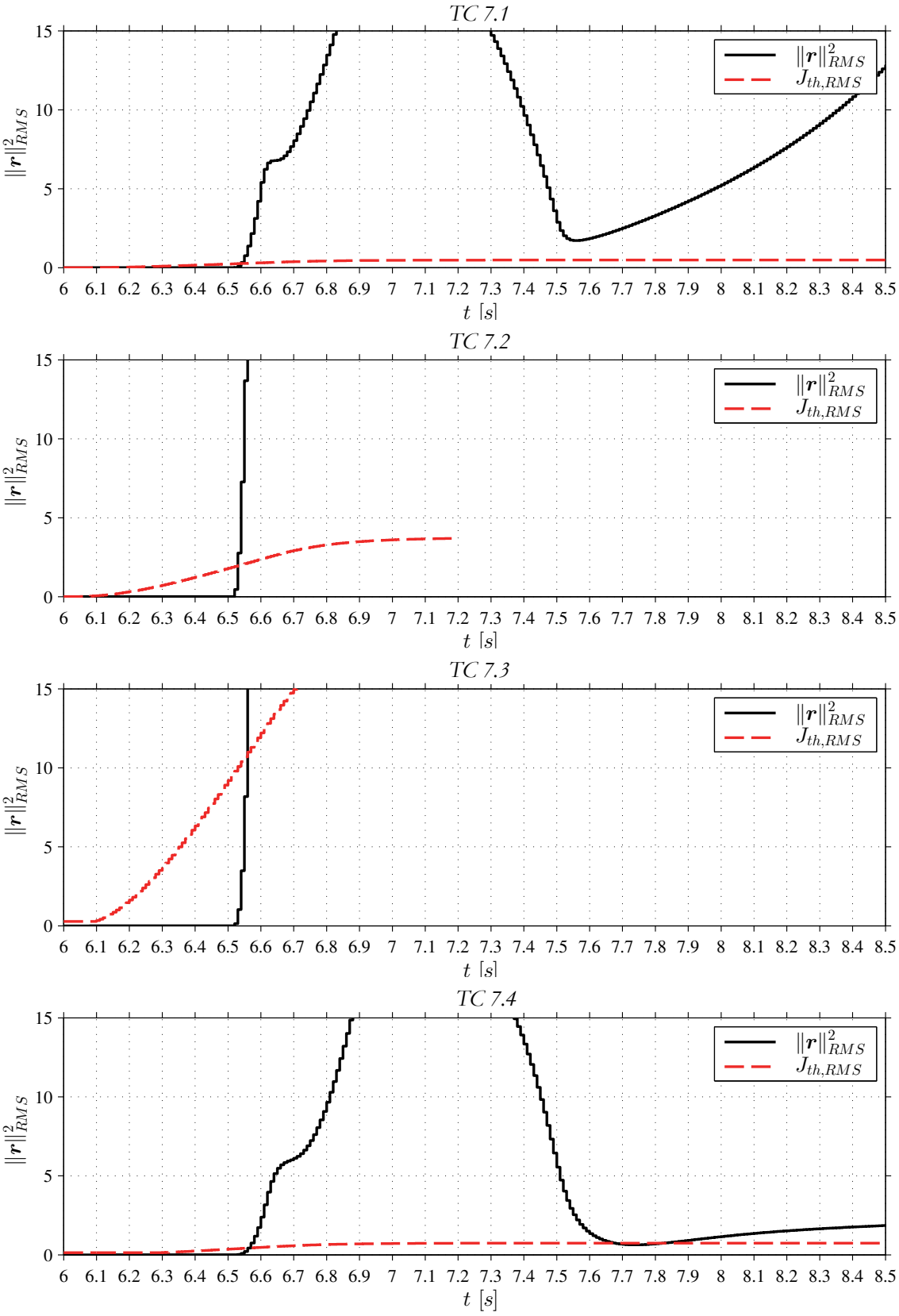

Figure 69 Comparison between residual and threshold (TC 7.1 - 7.4)

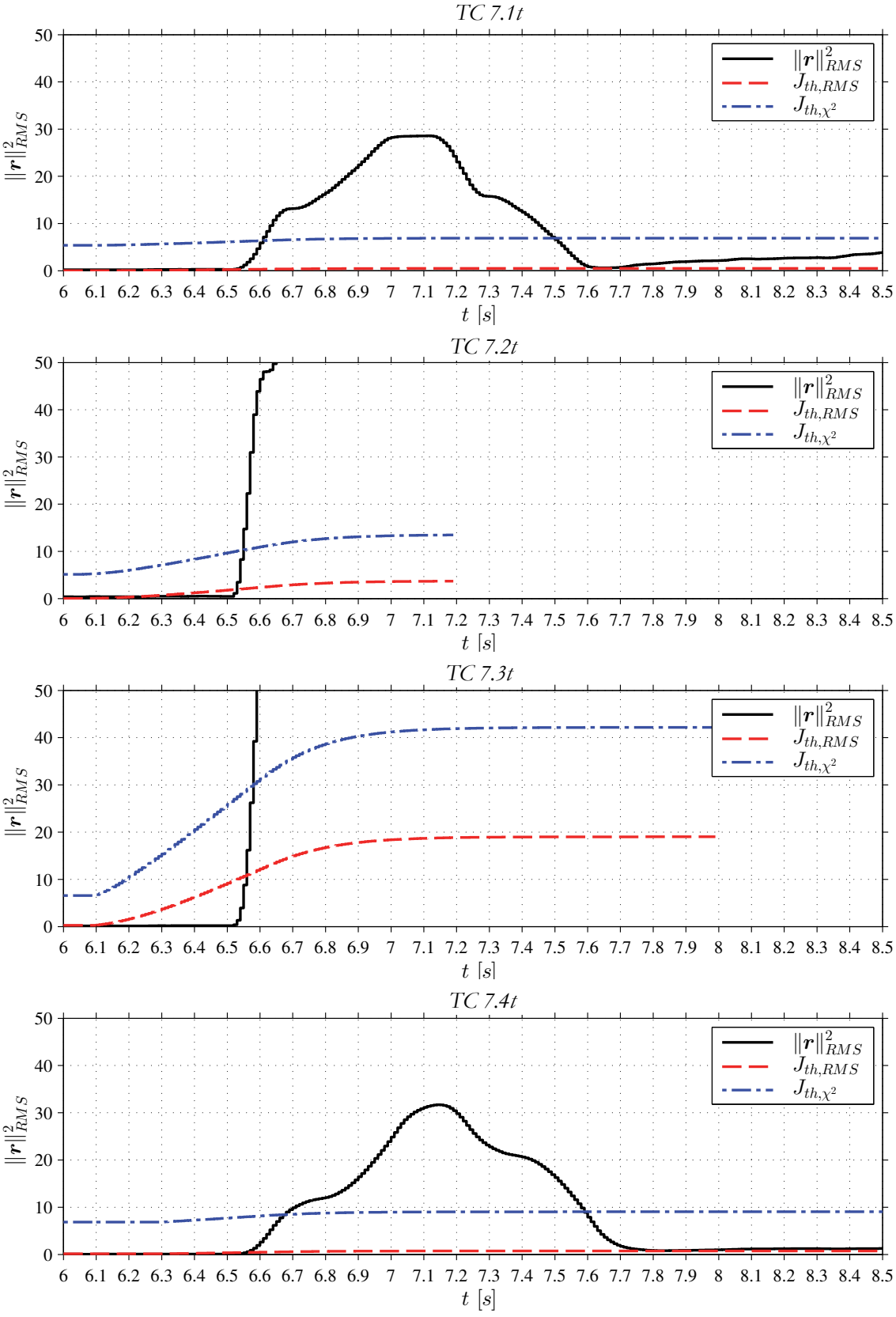

Figure 70 Comparison between residual and threshold (TC 7.1t - 7.4t)

4.3.4.5.2 Recovery within System Limits

Test Cases 7.1 to 7.4 - Deterministic fault detection system

Beside for TC 7.2, neither the F-16 production FCS operational angle of attack limit $\alpha_{K,lim}$ (cf. Remark 4-6, p. 148) nor the normal load factor limit $(n_{z,lim})_K$ = +9 g have been violated.
For TC 7.2 the maximum normal load factor during recovery $(n_{z,max})_K$ = 12.6 g exceeded the aforementioned normal operational limits, known as Design Limit Load (DLL). However we discuss a severe fault case. Thus the Design Ultimate Limit Load (DUL) which is the load up to which no structural failure must occur, is of greater importance. For a fighter aircraft it is typically 1.5x the DLL (Neubauer & Günther, 2001, p. 9-16; US DoD, 1987, p. 4). For our case with a DLL of $(n_{z,lim})_K$ = 9 g, this would lead to a DUL of $(n_{z,DUL})_K$ = +13.5 g thus no structural failure should occur at $(n_{z,max})_K$ = 12.6 g, though clearly the airframe DUL has nearly been reached. Beside that it should also be clear to the reader, that TC 7.2 represents a fault at high dynamic pressure $\bar{q}_A$ = 59.2 kPa (V_{EAS} = 311 m/s = 605 KEAS) and a high nominal (intended) normal load factor $(n_{z,nom})_K$ = 8.5 g. For sure a recovery after instability from such kind of fault conditions will be very difficult and potentially not be possible without violating the DUL when we take into considerations atmospheric turbulences. Finally the author wants to highlight that especially for TC 7.2 the FD delay $T_{D,FD}$ = 0.03 s has to be seen in relation to the overall reaction time T_F to T_η of 0.22 s, i.e. the deterministic scenario is clearly dominated by the FCS response time ($T_{D,FD}$ to T_η) of 0.19 s and not by $T_{D,FD}$.

Remark 4-18: With regard to the maximum normal load factor the question of aircrew physical limits might pop up. The author is for sure not a physician but by comparison with typical G-loads on aircrew during ejection (old ballistic seat: $n_{z,max}$ ~ 17-22 g, newer rocket propulsions seats: $n_{z,max}$ ~ 12-14 g) at least give a positive indication that a normal load factor $(n_{z,max})_K$ < 15 g can be survived without permanent injuries (see also Henzel, 1967). Another question related to aircrew will be the possibility of unconsciousness ("blackout") during recovery. In this regard it is for sure a good idea that the AFCS brings the aircraft to a relatively safe flight condition, e.g. wings level and shallow climb. Such functionality is already included in many modern CFCS.

Test Cases 7.1t to 7.4t - Integrated stochastic/deterministic fault detection system

For TC 7.3t and 7.4t the F-16 production FCS operational angle of attack limit $\alpha_{K,lim}$ has been slightly exceeded as shown in Figure 66 and Figure 68. The exceedance values have been $\alpha_{K,max}$ - $\alpha_{K,lim}$ = 22.6 – 21.9 deg = 0.7 deg for TC 7.3t and $\alpha_{K,max}$ - $\alpha_{K,lim}$ = 26.2 – 24.8 deg = 1.4 deg for TC 7.4t and can thus be considered insignificant. Furthermore as mentioned several times before $\alpha_{K,lim}$ has only informal character in our case study (see Remark 4-6, p. 148).
Beside for TC 7.2t, the normal load factor limit $(n_{z,lim})_K$ = +9 g has *not* been violated. For TC 7.2t the maximum normal load factor during recovery $(n_{z,max})_K$ = 14.7 g exceeded the Design Ultimate Limit Load $(n_{z,DUL})_K$ = +13.5 g. Thus a structural failure might occur though the time where $(n_z)_K > (n_{z,DUL})_K$ is only 0.2 s (t = 6.70 - 6.90 s). As mentioned before during discussion of TC 7.2 it should be clear that TC 7.2t represents a fault at high dynamic pressure $\bar{q}_A$ = 59.2 kPa (V_{EAS} = 311 m/s = 605 KEAS) and a high nominal (intended) normal load factor $(n_{z,nom})_K$ = 8.5 g and recovery after instability from such kind of fault conditions will be very difficult when we take into considerations atmospheric turbulences. To demonstrate the influence of turbulence on the peak responses of $q_{K,max}$, $\alpha_{K,max}$, and $(n_{z,max})_K$, TC 7.2t was repeated with the exactly same parameters besides the time the instability occurred (Figure 64). T_F has now been set to 1.50 s a period where, due to turbulence, the pitch rate q_K is smaller than $q_{K,nom}$ (first plot). The peak response $(n_{z,max})_K$ = 13.2 g has been *significantly lower* than for TC 7.2t and $(n_{z,DUL})_K$ = +13.5 g *has not been* violated for TC 7.2ta. Thus succesful recovery, in terms of not violating $(n_{z,DUL})_K$, for a TC 7.2t type condition significantly depends on the turbulence induced disturbances at time of fault occurrence T_F.

Table 17 Summary of key results for test cases TC 2.x

Test Case ID	$q_{K,cmd}$ [deg/s]	$q_{K,max}$ [deg/s]	$\alpha_{K,max}$ [deg]	$(n_{z,max})_K$ [g]	T_F [s]	T_{FD} [s]	T_{FCS} [s]	T_η [s]	$T_{q_k=0}$ [s]	$T_{n_z=1}$ [s]
7.1	5	14.4	19.0	1.6	6.50	6.54	6.59	6.89	7.15	7.76
7.1t	5	23.7	23.8	1.9	6.50	6.61	6.66	6.96	7.71	8.48
7.2	14	42.7	7.5	12.6	6.50	6.53	6.58	6.72	6.83	7.05
7.2t	14	52.7	9.20	**14.7**	6.50	6.55	6.60	6.74	6.88	7.12
7.2ta	14	43.4	8.0	13.2	1.50	1.55	1.60	1.74	1.85	2.07
7.3	5	34.1	19.7	4.6	6.50	6.56	6.61	6.93	7.11	7.62
7.3t	5	38.8	**22.6**	5.2	6.50	6.58	6.63	6.96	7.18	7.74
7.4	1.4	7.5	23.7	1.2	6.50	6.56	6.61	6.89	7.21	7.96
7.4t	1.4	13.0	**26.2**	1.3	6.50	6.68	6.73	7.01	7.71	8.60

Table 18 Summary of time delays with respect to fault occurrence (T_F = 6.50 s, TC 2.x)

Test Case ID	$T_{D,FD}$ [s]	$T_{D,FCS}$ [s]	$T_{D,\eta}$ [s]	$T_{D,q_k=0}$ [s]	$T_{D,n_z=1}$ [s]
7.1	0.04	0.09	0.39	0.65	1.26
7.1t	0.11	0.16	0.46	1.21	1.98
7.2	0.03	0.08	0.22	0.33	0.55
7.2t	0.05	0.10	0.24	0.38	0.62
7.3	0.06	0.11	0.43	0.61	1.12
7.3t	0.08	0.13	0.46	0.68	1.24
7.4	0.06	0.11	0.39	0.71	1.46
7.4t	0.18	0.23	0.51	1.21	2.10

4.3.4.6 Relation to an Operational System

For the TCs discussed in this chapter it has been shown that the delay of the FD system proposed in this work is small enough to stop the instability induced aircraft pitch-up motion from a severe fault where the closed-loop system has become unstable.

The exceedance of the F-16 production FCS operational angle of attack limit $\alpha_{K,lim}$ (cf. Remark 4-6, p. 148) can be considered *insignificant* and besides that $\alpha_{K,lim}$ has only informal character for our case study (see Remark 4-6, p. 148)

The Design Ultimate Load (DUL) limit $\left(n_{z,DUL}\right)_K$ = 13.5 g has only been violated 0.2 s for a fault at high dynamic pressure (V_{EAS} = 311 m/s = 605 KEAS) and a high nominal (intended) normal load factor $\left(n_{z,nom}\right)_K$ = 8.5 g where the turbulence induced disturbances were unfavourable at fault occurrence (TC 7.2t). It has been demonstrated that for more favourable turbulence induced disturbances at fault occurrence $\left(n_{z,DUL}\right)_K$ = 13.5 g will *not* be violated (TC 7.2ta).

For cases where the Design Limit Load $\left(n_{z,lim}\right)_K$ = 9 g is exceeded significant structural maintenance and repair actions have to be expected.

4.3.4.7 Relation to Requirements

It has been demonstrated that fault detection by the fault detection system is fast enough to give the active fault-tolerant flight control system a realistic chance to recover control of the air vehicle. The FD system is therefore *compliant* with Requirement 1-8 for the conditions tested.

It has been demonstrated that the fault detection by the fault detection system is fast enough to give the active fault-tolerant flight control system a realistic chance to recover control of the air vehicle within acceptable normal load factor limits. For a fault occurrence at high dynamic pressure and high nominal (intended) normal load factor the airframe DUL might be exceeded depending on the actual turbulence induced disturbances at fault occurrence, thus a recovery could be unsuccessful. The FD system is therefore *partially compliant* with Requirement 1-9 for the conditions tested.

4.3.4.8 Conclusion

For the conditions tested it has been demonstrated that the FD system proposed in this thesis has a fault detection delay that is small enough so that a AFCS has a realistic chance of successful recovering the aircraft, within acceptable normal load factor and angle of attack limits, from a severe fault condition where the closed-loop system has become unstable. For a fault occurrence at high dynamic pressure and high nominal (intended) normal load factor the airframe DUL might be exceeded depending on the actual turbulence induced disturbances at fault occurrence, thus a recovery could be unsuccessful.
The FD system proposed in this thesis is *compliant* with Requirement 1-8 and *partially compliant* with Requirement 1-9 for the conditions tested.

4.3.5 Test Matrix

Table 19 and Table 20 summarize all test conducted in the simulator case study as well as the related key parameters.

Table 19 Summary of key parameters for test cases

<table>
<tr><th>TC ID</th><th>q_{cmd} Type</th><th>q_{cmd} [deg/s]</th><th>Closed-loop Instability</th><th>σ_{wW} [m/s]</th><th>Acceptable SP Parameter Range</th><th>FAR_{req}</th></tr>
<tr><td>1.1</td><td rowspan="8">LP-filtered step input (K_{LP} = 1, T_{LP} = 0.15 s)</td><td>5</td><td rowspan="12">No</td><td>0</td><td rowspan="8">n/a</td><td rowspan="12">n/a</td></tr>
<tr><td>1.2</td><td>14</td></tr>
<tr><td>1.3</td><td>5</td></tr>
<tr><td>1.4</td><td>1.4</td></tr>
<tr><td>1.1t</td><td>5</td><td>6.96</td></tr>
<tr><td>1.2t</td><td>14</td><td>6.96</td></tr>
<tr><td>1.3t</td><td>5</td><td>7.04</td></tr>
<tr><td>1.4t</td><td>1.4</td><td>9.37</td></tr>
<tr><td>2.1</td><td colspan="2" rowspan="4">Not applicable.
See chapter 4.3.2.1 for details.</td><td rowspan="4">0</td><td rowspan="4">$\omega_{SP,L1}$
$\tilde{\zeta}_{SP,L1}$
(cf. Table 10)</td></tr>
<tr><td>2.2</td></tr>
<tr><td>2.3</td></tr>
<tr><td>2.4</td></tr>
</table>

	q_{cmd} Type	q_{cmd} [deg/s]	Closed-loop Instability	σ_{wW} [m/s]	Acceptable SP Parameter Range	FAR_{req}
3.1	Sine (ω = 15.0 rad/s)	5	No	0	$\omega_{SP,L1}$ $\tilde{\zeta}_{SP,L1}$ (cf. Table 10)	n/a
3.2	Sine (ω = 5.2 rad/s)	14				
3.3	Sine (ω = 14.7 rad/s)	5				
3.4	Sine (ω = 9.3 rad/s)	1.4				
4.1	Step	5				
4.2		14				
4.3		5				
4.4		1.4				
5.1	Combination of Sine, Step, Ramp, Random number acc. chapter 4.3.2.3.2.	5				
5.2		14				
5.3		5				
5.4		1.4				
6.1t	Not applicable. See chapter 4.3.3.2 for details.			6.96	$\omega_{SP,10\%}$ $\tilde{\zeta}_{SP,10\%}$ (cf. Table 12)	0.05
6.2t				6.96		
6.3t				7.04		
6.4t				9.37		
7.1	LP-filtered step input (K_{LP} = 1, T_{LP} = 0.15 s)	5	Yes, at T_F = 6.50 s by setting K_q = 0 K_α = 0 (TC7.2ta: T_F = 1.50 s)	0		n/a
7.2		14				
7.3		5				
7.4		1.4				
7.1t		5		6.96		2.8e-12
7.2t		14		6.96		
7.2ta		14		6.96		
7.3t		5		7.04		
7.4t		1.4		9.37		

Table 20 Summary of common key parameters for test cases

Parameter	Unit	Value
N_{RMS}	[-]	60
$(x^G)_B$	[m]	$0{,}4 \cdot \bar{c}$
$\sigma_{v_M,\dot{q}}$ (Jewell ASXC Angular Acceleration Sensor)	[rad/s²]	0.03
$\sigma_{v_M,q}$ (iMAR INS iNAV-FCAI–02 Angular Rate Sensor)	[rad/s]	3.3e-3
Sample Rate FD System	[Hz]	100
ISA standard day	n/a	n/a

5 Discussion of Thesis Results

5.1 Compliance to Requirements

In chapter 1.3 the objectives for the fault detection system proposed in this thesis have been defined. This chapter will discuss the compliance of the thesis results to those requirements.

Requirement 1-1: The probability that the AFCS is inadvertently activated by the fault detection system shall be equal or less 10^{-6} per flight hour. This shall be proven by stochastic and/or logical reasoning that supports a possible certification.

Chapter 3.5.4.3 has outlined the theory of the deterministic part of the proposed fault detection system. From theory no false alarms are expected. In chapter 4.3.2 it has been demonstrated, that, for the conditions tested, the *deterministic* part of the integrated stochastic/deterministic FD system ensures that the AFCS is not inadvertently activated by the FD system. The *deterministic* part of the integrated stochastic deterministic FD system is therefore *compliant* with Requirement 1-1 (p. 11) for the conditions tested.
In a similar way chapter 3.5.4.4 has outlined the theory for the *integrated stochastic deterministic* fault detection algorithm. The simulation results verify that the suggested extensions by the author (chapter 3.5.4.4.1 & 3.5.4.4.2) for fault detection with systems subject to *deterministic polytopic model uncertainties and stochastic unknown inputs* are valid. It has furthermore been demonstrated in chapter 4.3.3 that the *stochastic part* of the integrated stochastic/deterministic FD system can ensure that the probability that the AFCS is inadvertently activated by the fault detection system is equal or less 10^{-6} per flight hour. The integrated stochastic/deterministic fault detection system proposed in this work is therefore *compliant* with Requirement 1-1 for the conditions tested.

Requirement 1-2: The developed architecture must be able to be retrofitted to a conventional flight control systems.

Requirement 1-3: The architecture shall allow safe and efficient flight testing.

Requirement 1-4: The fault detection system shall minimize the amount of measurements required to function correctly.

Requirement 1-5: The fault detection system should not require angle of attack measurements to work correctly.

With respect to the signals required by the FD system it can be readily seen from Figure 26 (p. 94) that those are only the command input (herein q_{cmd}), the pitch rate q, and the pitch acceleration $\dot{q}$ measurements. Thus the FD system is *compliant with* the requirements of minimizing the amount of measurements necessary (Requirement 1-4, p. 11) and not using angle of attack measurements for fault detection (Requirement 1-5, p. 11). It is furthermore easily retrofitable, and therefore also *compliant* to Requirement 1-2 (p. 11), because the interface *of the FD system* to the existing aircraft flight control system is limited to the three measurements mentioned above. Finally it allows safe and efficient flight testing because, as long as the fault bit is not used for activation of the AFCS, no negative impact by the FD system can occur. In a proof of concept the FD system could for example be integrated into the Flight Test Instrumentation (FTI) for early data gathering flight tests to verify Requirement 1-1 in flight. The FD system is therefore also *compliant* to Requirement 1-3.

Requirement 1-6: The system shall not rely on an off-line defined set of failure models.

Requirement 1-7: The fault detection must not rely on the AFCS.

As outlined in chapter 3.5.4.3, the FD system uses the nominal (desired) closed-loop system dynamics as reference model. It does not require off-line pre-defined failure models and does not rely on the AFCS for fault detection it is therefore *compliant* to Requirement 1-6 and Requirement 1-7.

Requirement 1-8: The fault detection by the fault detection system shall be fast enough to give the active fault-tolerant flight control system a realistic chance to recover control of the air vehicle.

Requirement 1-9: The fault detection by the fault detection system shall be fast enough to give the active fault-tolerant flight control system a realistic chance to recover control of the air vehicle *within* acceptable normal load factor limits.

In chapter 4.3.4, it has been demonstrated for the conditions tested that the FD system proposed in this thesis has a fault detection delay that is small enough so that an AFCS has a realistic chance of successful recovering the aircraft, within acceptable normal load factor and angle of attack limits. The test case represents a severe fault condition where the closed-loop system has become unstable. For a fault occurrence at high dynamic pressure and high nominal (intended) normal load factor the airframe Design Ultimate Load (DUL) might be exceeded depending on the actual turbulence induced disturbances at fault occurrence, thus a recovery could be un-

successful. The FD system proposed in this thesis is thus *compliant* with Requirement 1-8 and *partially compliant* with Requirement 1-9 for the conditions tested.

5.2 Research Contributions

The research contributions by this thesis can be loosely grouped into two research areas. The first one is related to aircraft fault detection, namely to a fault detection algorithm to activate an Active fault-tolerant Flight Control System (AFCS) when the Conventional Flight Control System (CFCS) does no longer deliver an acceptable closed-loop performance. The second area of contributions is with respect to extensions of current Fault Detection (FD) methods. The latter have become necessary from the application of state of the art FD techniques to the above mentioned aircraft fault detection problem. Figure 71 graphically summarizes and structures the different research contributions. The elements shown will be discussed in the following chapters.

5.2.1 Aircraft Fault Detection Problem

The idea of combinging a conventional FCS with an active fault-tolerant one has only been very sparsely investigated in the past. Furthermore earlier work did either not focus on the required switching logic (Wohletz et al., 2000) or selected an approach where the fault-tolerant flight control system always works in parallel to the conventional one (for example D. G. Ward & Monaco, 2005). The latter inhibits a clear segregation of both systems (cf. chapter 1.4).
As for Wohletz et al. (2000) the approach chosen in this work is to activate the fault-tolerant control system only in case that the certified conventional flight control system delivers an unacceptable closed-loop performance. Such an approach would potentially allow keeping the Active fault-tolerant FCS (AFCS) largely outside certification scope. This will help to avoid/limit problems that may arise from the immature certification experience with respect to AFCS. Furthermore it will allow to *augment* the existing certified and proven CFCS of existing aircrafts instead of replacing them entirely, thus leading to significantly reduced costs and development risks. Such a setup of course needs reliable means to detect a CFCS problem that is severe enough so that it warrants switching to the AFCS. To the author's knowledge, the following aspects constitute new research contributions by this thesis:

5.2.1.1 FD System with Quantifiable, Guaranteed False Alarm Rate (FAR)

The idea of combining a CFCS with an AFCS, albeit not complete new, has only been very sparsely investigated in the past (Wohletz et al., 2000) and none of the work known to the author (cf. chapter 1.4) treats the problem of how to define a useable switching logic/threshold beyond mentioning its existence. This thesis fo-

cusses especially on the switching, i.e. fault detection algorithm. The above mentioned reasoning chain implies that the possibility that the fault-tolerant flight control system is *inadvertently activated* must be very remote, i.e. the False Alarm Rate (FAR) must be very low (cf. Requirement 1-1). To judge the possibility for inadvertent activation, the FAR must be quantifiable by a number. This work *uses a strict state of the art FAR-based design approach,* as suggested by Ding (2013), and applies it to the aircraft fault detection problem on hand. This strict FAR-based design approach is, to the author's knowledge, also new in the context of aircraft fault detection (Contribution 3-2, p. 94). Several extensions of the method, which will be discussed in chapter 5.2.2, have furthermore been required.

5.2.1.2 Closed-loop FD Based on a Reference Model with Model Uncertainties, Directly Derived from Flying Qualities Standards

Most of the current Fault Detection and Diagnosis (FDD) work treats the problem detecting faults in the uncontrolled plant. In case of aircraft, and potentially in many other applications, the user (e.g. pilot) is much more interested in the *closed-loop* performance of the system, because that is what is visible to him/her. The author therefore suggest to model *the acceptable closed-loop performance, directly derived from the respective flying qualities standards, as deterministic model uncertainties of reference model* used for fault detection. The approach to use the flying quality standard derived CAP-ζ_{SP} combination to define a ω_{SP}-ζ_{SP} parameter polytope of acceptable reference model uncertainties and consequently derive the norm-based residual threshold based on this reference model was developed by the author and is, to the author's knowledge, new (Contribution 3-3, p. 95).

5.2.1.3 Flexible Adaptation and Easy Interpretability of FD System Parameters in a Flying Quality Context

The FD system proposed in this thesis is to author opinion, very flexible to adapt to different practical demands. Adaptations are easily done by just changing the range of acceptable *closed-loop* natural frequencies and damping ratios. Most important, those two parameters can be readily interpreted in physical and flying quality context and they allow a direct comparison with the flying quality standards MIL-F-8785C (US DoD, 1996) and MIL-STD-1797B[15] (US DoD, 2012). To the author's opinion this is a significant practical advantage and furthermore gives the aerospace engineer a direct understanding what the effect of the parameter changes are (Contribution 3-4, p. 96).

[15] Restricted distribution, therefore information from MIL-F-8785C is used within this text.

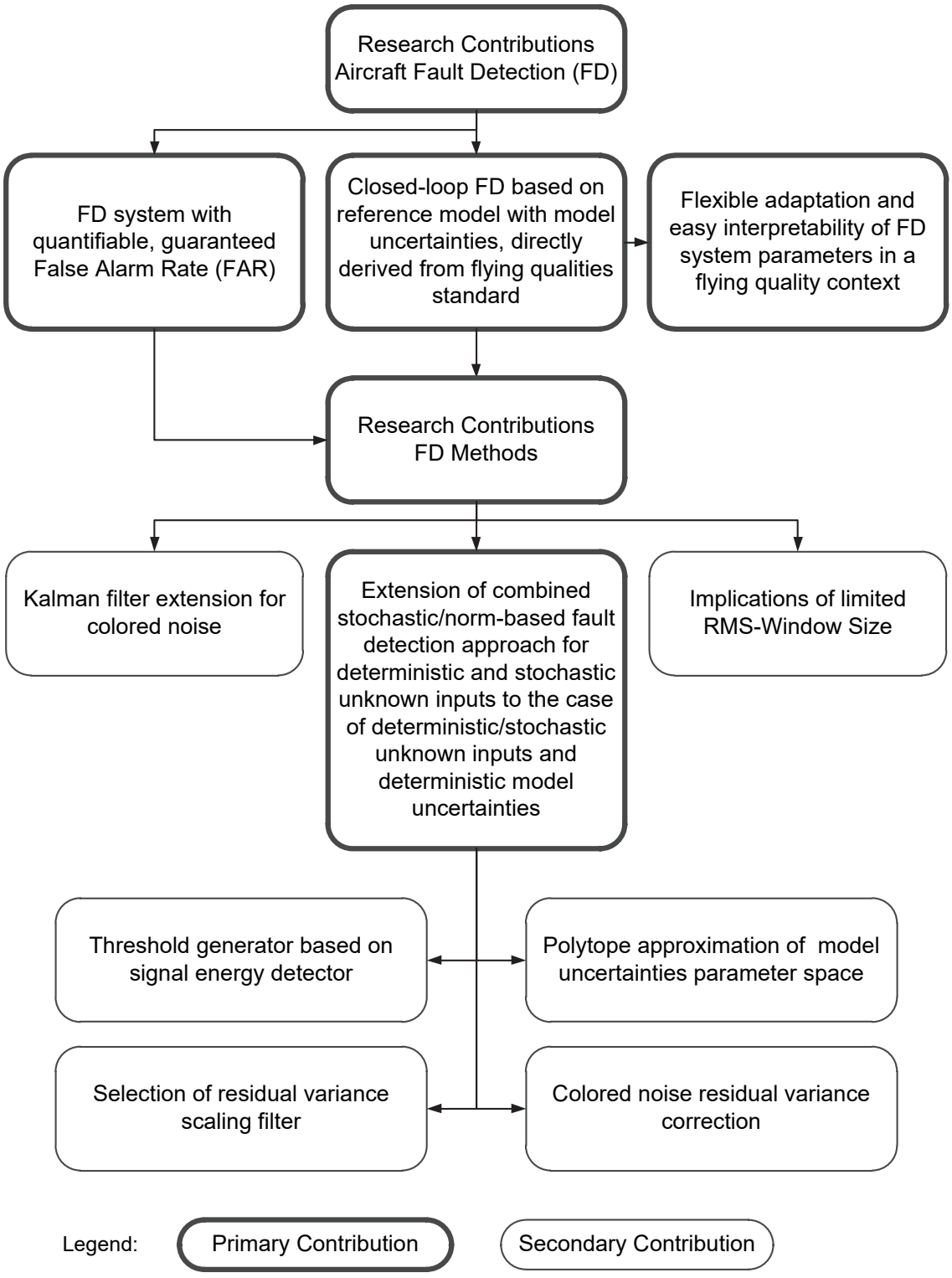

Figure 71 Overview Research Contributions

5.2.2 Fault Detection Methods

5.2.2.1 Extension of combined stochastic/norm-based fault detection approach for deterministic and stochastic unknown inputs to the case of deterministic/stochastic unknown inputs and deterministic model uncertainties

The aforementioned approach for the fault detection system required the extension of the combined stochastic/norm-based fault detection approach for deterministic and stochastic unknown *inputs,* as suggested by Ding (2013, pp. 339-345), to the much more complex case of deterministic/stochastic unknown inputs and *deterministic model uncertainties*. Several extensions are suggested in this work with respect to the aircraft application discussed above. The work thus adds research results to the, highlighted by Ding (2013, p. 17), very sparsely investigated research area of *residual evaluation* (Contribution 3-1, p. 59).

5.2.2.2 Threshold Generator Based on a Signal Energy Detector

Due to the incorporation of model uncertainties into the reference model also *known* system inputs affect the residual dynamics (cf. chapter 3.5.4.3.3). The author provides an approach for a signal envelope detector based adaptive fault detection threshold (threshold generator) that overcomes the problems of RMS-signals with limited observation time (cf. chapter 3.5.4.3.2). The threshold generator ensures validity of $J_{th,RMS}^2$ for the case of limited observation times *and* enables a fault detection threshold $J_{th,RMS}^2$ that is small enough to be useful in a practical context. The former has been demonstrated by simulation in chapter 4.3.2.2 and 4.3.2.3, the latter in chapter 4.3.4 (Contribution 3-8, p. 131).

5.2.2.3 Polytope Approximation of Model Uncertainties Parameter Space

To overcome the problem of a non-convex ω_{SP}-ζ_{SP} model uncertainty parameter space, the author suggests the use of an approximated parameter polytope as shown in Figure 29 (p. 115). In terms of the problem on hand, i.e. the aircraft longitudinal short period motion, this means that the allowable range of damping ratios ζ_{SP} is slightly reduced. However it is ensured that the approximation stays in the area of the desired level of flying qualities, i.e. on the "safe side". To the author's knowledge using such an approach in the context of a flying quality model is also new (Contribution 3-6, p. 115).

5.2.2.4 Selection of Residual Variance Scaling Filter

The in chapter 3.5.4.4.1 suggested approach for the selection of variance scaling filter $\overline{\boldsymbol{V}}$ in case of a residual subject to *stochastic unknown inputs* and *deterministic polytopic model uncertainties* is to the author's knowledge new (Contribution 3-9, p. 135). Alt-

hough the approach suggested provides a first empirical solution to the problem, the author strongly recommends some further work on the subject as it will be discussed in chapter 5.3.2.

5.2.2.5 Residual Variance Colored Noise Correction

The aircraft application warrants the use of a residual band-pass post filter to supress the impact of steady and very low frequency gains on the residual and to limit the higher frequency noise. Unfortunately, due to auto-correlation, the filtered residual noise is no longer white but colored, therefore violating one of the underlying assumptions of the χ^2-distribution required for stochastic residual evaluation. The suggested approach of using the $\chi^2_m(\lambda)$ normal distribution approximation with a colored noise corrected variance for the fault detection χ^2 -hypothesis testing problems is to the author's knowledge also new (Contribution 3-10, p. 138). Although the approach suggested provides a first solution to the problem, the author strongly recommends some further work on the subject as it will be discussed in chapter 5.3.3.

5.2.3 Kalman Filter Extension for Colored Noise

The colored process noise extension of the Kalman filter is to the author's knowledge not covered by contemporary FDD literature, e.g. Ding (2013). In the residual generation context it was introduced by the author to handle the problem of colored aircraft atmospheric turbulence. The theory is based on the respective known Kalman filter state observer colored noise extensions given for example in Lewis et al. (2007, p. 124-127) (Contribution 3-5, p. 101).

5.2.4 RMS-Window Size

To the author's knowledge the implications of using a limited RMS-window size for fault detection are not discussed in current FDD literature. The aspects discussed in chapter 3.5.4.3.2 are therefore also new (Contribution 3-7, p. 127).

5.3 Recommendations for Further Work

5.3.1 Deterministic Threshold with Polytopic Model Uncertainties

As discussed in chapter 3.5.4.3.1.3 there exist three possible approaches to calculation of the worst-case gain $\mathcal{K}_{\boldsymbol{G}_{rq_{cmd}},max}$ required to determine the deterministic threshold $J^2_{th,RMS}$. The first one is the *quadratic stability* approach that leads to an upper bound on the worst case gain $\mathcal{K}_{\boldsymbol{G}_{rq_{cmd}},max}$ for *time-varying* LPV systems with *arbitrary fast varying* parameters $\boldsymbol{\delta}$, i.e. $\dot{\boldsymbol{\delta}} \to \infty$ (cf. chapter 3.4.2.3.3). While this is for sure a powerful theoretical result, in our practical aircraft application we have to consider three things:

- The gains calculated by this approach are *very conservative*, i.e. they become *very large*. Therefore the fault detection performance for all cases where $\dot{\boldsymbol{\delta}} < \infty$ is significantly reduced. Actually the author's experience is that the gains obtained are useless in a practical aircraft fault detection problem.
- Arbitrary fast varying parameters constitute a dynamic in itself, that is for sure not in line with our flying quality requirements of specifications MIL-F-8785C (US DoD, 1996, p. 14) and MIL-STD-1797A (US DoD, 2004).
- At fault (damage) occurrence the parameters are potentially heavily time varying but this is a case we *for sure want to detect*, i.e. treating those time variations as normal parameter variations that occur during normal (fault-free) operations would be contradictory to our fault detection goal.

The approach was initially followed by the author but then discarded due to those three reasons. The second approach, finally chosen by the author, is to assume uncertain but time-invariant parameters $\boldsymbol{\delta}$, i.e. $\dot{\boldsymbol{\delta}} \cong \mathbf{0}$. This solved the three problems mentioned above. Nevertheless there is an important assumption in using this approach. Clearly in an aircraft context the parameters $\boldsymbol{\delta}$ *slowly vary* under fault-free operations with the flight condition. The assumption made is that the dynamics of these slowly varying parameters $\boldsymbol{\delta}$ are *insignificant* with respect to $\mathcal{K}_{\boldsymbol{G}_{rq_{cmd}},max}$. A similar assumption is made for nearly all gain-scheduled CFCS, i.e. closed-loop aircraft systems, used in production aircraft. Therefore it is reasonable to assume that it is also an acceptable assumption in our case, however, as for gain scheduled CFCS, a strict theoretical treatment would be desirable. In systems theory the concept of *robust stability* was developed which assumes bounds on the parameter change rates $\dot{\boldsymbol{\delta}}$. It contains the case of *time-invariant* parameters ($\dot{\boldsymbol{\delta}} = \mathbf{0}$) and *arbitrary fast time-varying parameters* ($\dot{\boldsymbol{\delta}} \to \infty$) as special cases (cf. e.g. Scherer & Weiland, 2016, pp. 9/25-13/25) and potentially offers the possibility of a strict theoretical treatment of *slowly varying* parameters $\boldsymbol{\delta}$ under fault-free operations in our fault detection con-

text. Nevertheless to derive bounds on the parameter rates $\dot{\boldsymbol{\delta}}$ for the aircraft under fault-free operation is potentially also not straight forward and requires careful analysis of all fault-free operation conditions (Further Work 3-1, p. 124).
The fact that we used an uncertain but time-invariant system allows us to calculate the maximum gain $\mathcal{K}_{\boldsymbol{G}_{rq_{cmd}},max}$ using the H_∞-norm. Inspired by the idea of *robust stability,* that contains the approach $\dot{\boldsymbol{\delta}} \cong \mathbf{0}$ as special case, the author deducted that the $\left\|\boldsymbol{G}_{rq_{cmd}}\right\|^2_{\infty,max}$ is found at one of the vertices $\mathcal{V}_i$. *While this has been verified by simulation* in chapter 4.3.2.1, it would be desirable to provide a strict theoretical proof that the maximum gain $\left\|\boldsymbol{G}_{rq_{cmd}}\right\|^2_{\infty,max}$, for the fault detection system of this text, is found at one of the vertices $\mathcal{V}_i$ (Further Work 3-2, p. 125).

5.3.2 Variance Scaling Filter

As discussed in chapter 3.5.4.4.1 the approach for selection of variance scaling ter $\overline{\boldsymbol{V}}$ for the integrated stochastic/deterministic fault detection scenario with *deterministic polytopic model uncertainties* suggested by the author and chosen in this thesis is:

- For every flight condition, identify the vertex $\mathcal{V}_{Var,max}$ (offline)
- Choose the correlation filter $\overline{\boldsymbol{V}}_{r,\mathcal{V}_{Var,max}}$ that belongs to this vertex (offline).
- Implement this filter $\overline{\boldsymbol{V}}_{r,\mathcal{V}_{Var,max}}$ for online processing of the residual, which is a simple multiplication of a matrix with a vector.

While the above suggested approach makes sense from an engineering judgment point of view and has also be verified by the simulation case study in chapter 4.3.3, a stringent theoretical understanding and solution would be desirable. This should be tackled in a follow on work (Further Work 3-4, p. 135). Furthermore in the simulation case study of this thesis certain points in the flight envelope have been used as dedicated flight conditions. For sure in a potential implementation in a real system some means have to be found for adaptation of $\overline{\boldsymbol{V}}$ between all flight conditions possible (e.g. like gain scheduling for controller gains). This is also an area of further work that has to be addressed for a practical application (Further Work 3-3, p. 135).

5.3.3 Residual Variance Colored Noise Correction

The aircraft application warrants the use of a residual band-pass post filter to supress the influence of steady and very low frequency gains on the residual and to limit the higher frequency noise (cf. chapter 3.5.3.2). Unfortunately, due to autocorrelation, the filtered residual noise is no longer white but colored, therefore violating one of the underlying assumptions of the χ^2-distribution required for stochastic residual evaluation. In chapter 3.5.4.4.2 the author suggests an approach of

using the $\chi_m^2(\lambda)$ normal distribution approximation and a *colored noise corrected* variance for fault detection χ^2 hypothesis testing problems. For this work the corrected variance has been estimated offline by simulation for five non-centrality parameters in the range of interest in this thesis and a correction factor has then been calculated accordingly. For every flight condition the correction factors have been stored in a look-up table as supporting points for online interpolation as function of λ_{χ^2} (Table 14, p. 190). However a method for calculating the corrected variance instead of estimating it from offline simulation would be more "elegant" and therefore desirable (Further Work 3-6, p. 137). In the simulation case study of this thesis only certain points in the flight envelope have been used as dedicated flight conditions. For sure in a potential implementation in a real system some means have to be found to adapt the variance correction factor $\varepsilon_{Var,1}$ between all flight conditions possible, e.g. like gain scheduling for controller gains. Even better would of course be a theoretical solution to the overall correction. This is for sure an area of further work that should be addressed for a practical application (Further Work 3-5, p. 137).
Unfortunately it was found in simulation that the above mentioned correction of the variance alone still leads to a False Alarm Rate (FAR) slightly higher than FAR_{req}. The reason is not fully understood yet and has to be investigated further in a follow on work (cf. chapter 3.5.4.4.2). For this thesis the correct FAR was obtained by an additional constant correction factor $\varepsilon_{Var,2}$ for all λ_{χ^2} and flight conditions. The use of $\varepsilon_{Var,2}$ to obtain correct FAR is for sure not fully satisfactory. *Although it has been verified by simulation* in chapter 4.3.3 that we can ensure the latter by $\varepsilon_{Var,2}$, and therefore fulfil Requirement 1-1 (p. 11), a theoretical profound understanding and solution would be highly desirable (Further Work 3-7, p. 138).

6 Summary

In the last three decades so called fault-tolerant flight control systems have drawn significant attention of the research community, authorities, and industry. The term fault-tolerant thereby refers to the potential of those systems to tolerate faults that cannot be dealt with by conventional flight control systems therefore reducing the risk of losing an aircraft due to loss of control. Despite their advantages fault-tolerant flight control systems have not yet seen widespread use beyond the scope of experimental aircraft, small UAVs, and a few fault-tolerant elements to detect actuator and sensor failures in production aircraft. To the author's opinion there exist two major reasons for the current situation. First of all, in aviation, certification is an inevitable requirement for all safety critical systems. Most active fault-tolerant methods are not yet compatible to the certification demands. Although there have been recently some improvements in this regard, the certification experience remains limited. Secondly most current approaches aim at *replacing* the *entire certified* conventional flight control systems already installed in current production aircraft or aircraft families. While this is certainly a valid long-term goal it neglects to the author's opinion an important practical truth: There already exist many excellent, certified, and operational proven conventional flight control systems installed in current production aircraft that have been designed by classical control methods. Due to economic constraints virtually no aircraft manufacturer will consider replacing them completely by new systems or developing a new FCS by solely relying on new control approaches.

This thesis was inspired by the idea to combine a Conventional Flight Control System (CFCS) with an active fault-tolerant one, were the latter is only activated in case that the CFCS is no longer able to provide an acceptable closed-loop performance, e.g. due to severe aircraft damage. Such an approach would potentially allow keeping the Active fault-tolerant FCS (AFCS) largely outside certification scope. This will help to avoid/limit problems that may arise from the immature certification experience with respect to AFCS. Furthermore it will allow to *augment* the existing certified and proven CFCS of existing aircrafts instead of replacing them entirely, thus leading to significantly reduced costs and development risks. Such a setup of course needs reliable means to detect a CFCS problem that is severe enough so that it warrants switching to the AFCS. The idea of combining a CFCS with an AFCS, albeit not complete new, has only been very sparsely investigated in the past (Wohletz et al., 2000) and none of the works known to the author (cf. chapter 1.4) do treat the problem of how to define a useable switching logic/threshold beyond mentioning its existence. This thesis suggests a possible approach to this Fault Detection (FD) problem utilizing a *model-based* FD approach. The above outlined reasoning chain implies that the possibility that the fault-tolerant flight control system is *inadvertently*

activated must be very remote, i.e. the False Alarm Rate (FAR) shall be very low (cf. Requirement 1-1). To judge the possibility for inadvertent activation, the FAR must be quantifiable by a number. Herein *a strict state of the art FAR-based design approach,* as suggested by Ding (2013), is applied to the aircraft fault detection problem on hand. The application of this strict FAR-based design approach is, to the author's knowledge, new in the context of aircraft fault detection.
Most of the current work on Fault Detection and Diagnosis (FDD) furthermore treats the problem detecting faults in the uncontrolled plant. In case of aircraft, and potentially in many other applications, the user (e.g. pilot) is much more interested in the *closed-loop* performance of the system, because that is what is visible to him/her. The author therefore suggest to model *the acceptable closed-loop performance directly derived from the respective flying qualities standards as deterministic model uncertainties of the reference model* used for fault detection. The approach to use the flying quality standard derived CAP-ζ_{SP} combination to define a ω_{SP}-ζ_{SP} parameter polytope of acceptable reference model uncertainties and consequently derive the norm-based residual threshold based on this reference model was developed by the author and is, to the author's knowledge. The major focus to this effect is in the task of *residual evaluation*, which, in general has only been very sparsely investigated in the past (cf. Ding, 2013, p. 17). The aforementioned approach required several extensions of the combined stochastic/norm-based fault detection method for deterministic and stochastic unknown *inputs*, as suggested by Ding (2013, pp. 339-345), to the much more complex case of deterministic/stochastic unknown inputs and *deterministic model uncertainties*. The extensions suggested by the author have been summarized in chapter 5.2.2.
Finally the FD system proposed in this thesis is to author opinion, very flexible to adapt to different practical demands. Adaptations are easily done by just changing the range of acceptable *closed-loop* natural frequencies and damping ratios. Most important, those two parameters can be readily interpreted in physical and flying quality context and they allow a direct comparison with the flying quality standards MIL-F-8785C (US DoD, 1996) and MIL-STD-1797B[16] (US DoD, 2012). To the author's opinion this is a significant practical advantage and furthermore gives the aerospace engineer a direct understanding what the effect of the parameter changes are.
Driven by the certification requirement the primary goal of this work was to provide an approach that guarantees a user selectable False Alarm Rate (FAR), because a false alarm would lead to an inadvertent activation of the AFCS. The FAR is therefore certification relevant. A secondary objective was to limit conservatism in the

[16] Restricted distribution, therefore information from MIL-F-8785C is used within this text.

assumptions in order to provide a fault detection performance that promises practical benefits of the suggested system. Both goals have, to the author's opinion, been achieved. The achievements of the detailed objectives outlined in chapter 1.3, are discussed in chapter 5.1. Concerning the secondary objective several potential additional improvements have been identified, that could be investigated in a follow-on work (chapter 5.3).

Chapter 3 discussed the theoretical studies conducted with respect to contemporary model-based fault detection and finally describes the fault detection system proposed in this work (chapter 3.5). The suggested fault detection system has been tested in a linear simulation case study based on a public F-16 model provided e.g. by Klein and Morelli (2006). The results of this simulation case study have been discussed in chapter 4.

Appendix A F-16 Non-Linear Simulation Model

This chapter is largely based on Kaminski (2012).

A.1 Flight Dynamic Plant Model

The aerodynamic, mass and propulsion data provided in Annex D of Klein and Morelli (2006, pp. 463-471), for a MATLAB-based simulation of the General Dynamics F-16, has been re-implemented in Simulink to provide a flexible non-linear six-degree of freedom open-loop flight simulation with facilities for trimming. The data has the advantage of being representative of a modern fighter aircraft configuration on one hand and being freely available *without any security related restrictions* on the other hand. The data set is based on the work of (Nguyen et al., 1979). The structure of the flight dynamic simulation model is shown in Figure 72 and explained in more detail in Chapters A.2 to A.6.

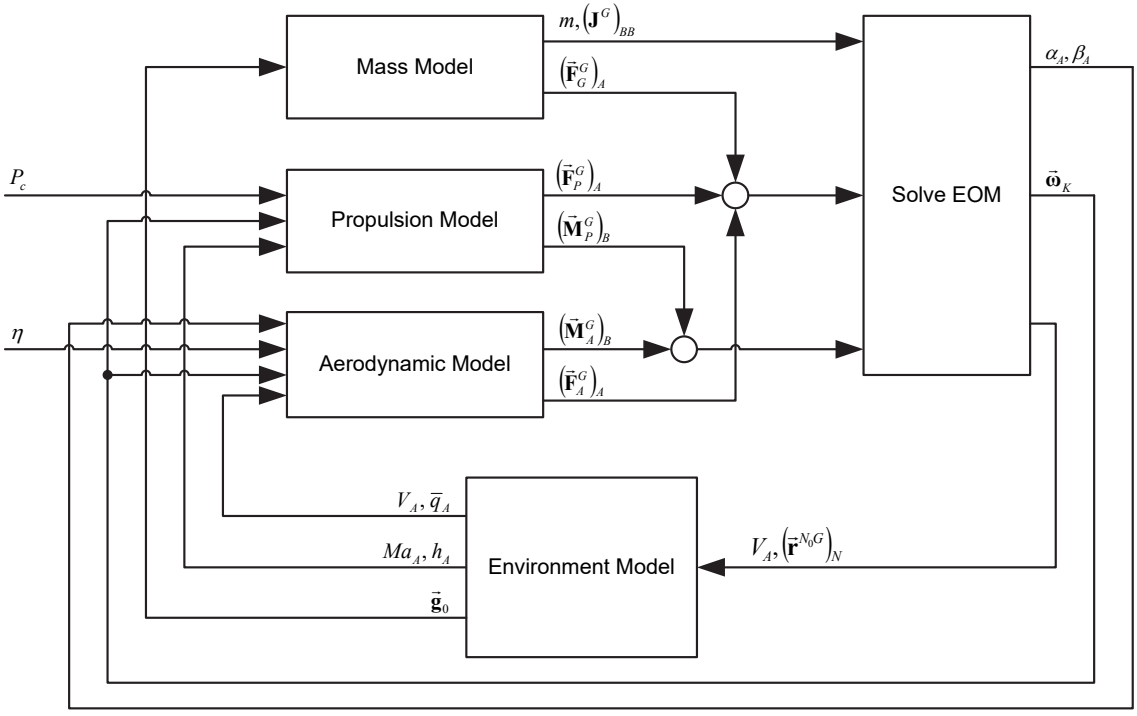

Figure 72 Structure of flight dynamic simulation model

A.2 Equations of Motion

For the simulation a flat and non-rotating earth was assumed. The resulting EOM are given by (6-1) to (6-4). The EOM have been solved using the Simulink "Custom Variable Mass 6DOF (Wind Axes)" block (2014, pp. 4-176 to 4-181).

$$\vec{\boldsymbol{a}}_K = \frac{\sum\left(\vec{\boldsymbol{F}}^G\right)_B}{m} = \left(\dot{\vec{\boldsymbol{v}}}_K^G\right)_B^{EB} + \left(\vec{\boldsymbol{\omega}}_K^{OB}\right)_B \times \left(\vec{\boldsymbol{v}}_K^G\right)_B^E \tag{6-1}$$

$$\begin{aligned}\dot{\vec{\boldsymbol{\omega}}}_K &= \left(\dot{\vec{\boldsymbol{\omega}}}_K^{OB}\right)_B^B \\ &= \left(\boldsymbol{J}^G\right)_{BB}^{-1} \cdot \left[\sum\left(\vec{\boldsymbol{M}}^G\right)_B - \left(\vec{\boldsymbol{\omega}}_K^{OB}\right)_B \times \left(\boldsymbol{J}^G\right)_{BB} \cdot \left(\vec{\boldsymbol{\omega}}_K^{OB}\right)_B\right]\end{aligned} \tag{6-2}$$

with

$$\sum\left(\vec{\boldsymbol{F}}^G\right)_B = \left(\vec{\boldsymbol{F}}_G^G\right)_B + \left(\vec{\boldsymbol{F}}_A^G\right)_B + \left(\vec{\boldsymbol{F}}_P^G\right)_B \tag{6-3}$$

$$\sum\left(\vec{\boldsymbol{M}}^G\right)_B = \left(\vec{\boldsymbol{M}}_A^G\right)_B + \left(\vec{\boldsymbol{M}}_P^G\right)_B \tag{6-4}$$

A.3 Environment Model

The environment model simulates the earth atmosphere and gravitational field. The atmosphere was modelled as ISA (ISO, 1997) using the Simulink "ISA Atmosphere Model" block (The MathWorks Inc., 2014, pp. 4-379 to 4-380) assuming that

$$h_A = -\left(r_z^{N_0 G}\right)_N \tag{6-5}$$

The gravitational acceleration was assumed to be constant with

$$\vec{\boldsymbol{g}}_0 = \begin{bmatrix} 0 \\ 0 \\ 9{,}81 \end{bmatrix} \frac{\mathrm{m}}{\mathrm{s}^2} \tag{6-6}$$

A.4 Mass Model

The time-invariant mass model used is identical to the one given in Annex D.6 of Klein and Morelli (2006, p. 471). The only exception to this is that for this case study a centre of gravity position $(x^G)_B = 0{,}4 \cdot \bar{c}$ has been chosen to obtain an open-loop unstable plant with time to doubles representative of contemporary fighter aircraft configurations. Nevertheless this has some implication with respect to control power available, which will be discussed in Remark 6-1 (p. 247).

Table 21 Mass and moments of inertia model

Parameter	**Symbol**	**Value**
Aircraft mass	m	$9295\ kg$
Moments of inertia	$(\boldsymbol{J}^G)_{BB}$	$\begin{bmatrix} 12874 & 0 & -13314 \\ 0 & 75671 & 0 \\ -13314 & 0 & 85549 \end{bmatrix} kgm^2$
Reference centre of gravity	$\left(x^G_{ref}\right)_B$	$0{,}35 \cdot \bar{c}$
Centre of gravity for simulation	$(x^G)_B$	$0{,}4 \cdot \bar{c}$

The calculation of the gravitational force was included in the mass model. Using $\vec{\boldsymbol{g}}_0$ of (6-6) the gravitational force in aerodynamic axis is given by

$$\left(\vec{\boldsymbol{F}}^G_G\right)_A = m \cdot [\boldsymbol{M}_{A0} \cdot \vec{\boldsymbol{g}}_0] \tag{6-7}$$

A.5 Propulsion Model

The propulsion model simulates the thrust force and moment of a single afterburning turbofan engine based on

$$\left(\vec{\boldsymbol{F}}^G_P\right)_A = \boldsymbol{M}_{\boldsymbol{AB}} \cdot \begin{bmatrix} X^G_P \\ 0 \\ 0 \end{bmatrix}_{\mathrm{B}} \text{ and } X^G_P = f(P_a, h, M) \tag{6-8}$$

$$\left(\vec{\boldsymbol{M}}^G_P\right)_B = \vec{\boldsymbol{\omega}}_K \times \begin{bmatrix} \mathrm{h_P} \\ 0 \\ 0 \end{bmatrix} \tag{6-9}$$

For the angular momentum $\mathrm{h_P}$ a fixed value of $217\,\frac{\mathrm{kgm^2}}{s}$ was used. Engine dynamics are modeled as a first order lag of the actual power level P_a to the commanded power level P_c.

$$\dot{P}_a = \frac{1}{\tau_{eng}}(P_c - P_a) \tag{6-10}$$

The model used is identical to the one given in Annex D.3 of Klein and Morelli (2006, pp. 468-469). A more detailed description can be found there.

A.6 Aerodynamic Model

The aerodynamic forces and moments acting on the air vehicle are calculated by

$$\left(\vec{F}_A^G\right)_A = \bar{q}_A \cdot S \cdot \boldsymbol{M_{AB}} \cdot \begin{bmatrix} C_X \\ C_Y \\ C_Z \end{bmatrix}_B \tag{6-11}$$

$$\left(\vec{M}_A^G\right)_B = \bar{q}_A \cdot S \cdot \begin{bmatrix} b \cdot C_l \\ \bar{c} \cdot C_m \\ b \cdot C_n \end{bmatrix}_B \tag{6-12}$$

with the non-linear coefficients in the body-fixed coordinate frame

$$C_X = C_{X0}(\alpha_A, \eta) + C_{Xq}(\alpha_A) \cdot q^* \tag{6-13}$$

$$\begin{aligned} C_Y = {} & -0.02\beta_A + 0.021\left(\frac{\xi}{20}\right) + 0.086\left(\frac{\zeta}{30}\right) \\ & + \left(\frac{b}{2V_A}\right)\left[C_{Yp}(\alpha_A) \cdot p + C_{Yr}(\alpha_A) \cdot r\right] \end{aligned} \tag{6-14}$$

$$C_Z = C_{Z0}(\alpha_A)\left[1 - \left(\frac{\beta_A \pi}{180}\right)^2\right] - 0.19\left(\frac{\eta}{25}\right) + C_{Zq}(\alpha_A) \cdot q^* \tag{6-15}$$

$$\begin{aligned} C_l = {} & C_{l0}(\alpha_A, \beta_A) + C_{l\xi}(\alpha_A, \beta_A)\left(\frac{\xi}{20}\right) + C_{l\zeta}(\alpha_A, \beta_A)\left(\frac{\zeta}{30}\right) \\ & + \left(\frac{b}{2V_A}\right)\left[C_{lp}(\alpha_A) \cdot p + C_{lr}(\alpha_A) \cdot r\right] - \left(\frac{\bar{c}}{b}\right)\left(x_{cg_{ref}} - x_{cg}\right) C_Y \end{aligned} \tag{6-16}$$

$$C_m = C_{m0}(\alpha_A, \eta) + C_{mq}(\alpha_A) \cdot q^* + \left(x_{cg_{ref}} - x_{cg}\right) C_Z \tag{6-17}$$

$$C_n = C_{n0}(\alpha_A, \beta_A) + C_{n\xi}(\alpha_A, \beta_A)\left(\frac{\xi}{20}\right) + C_{n\zeta}(\alpha_A, \beta_A)\left(\frac{\zeta}{30}\right) + \left(\frac{b}{2V_A}\right)\left[C_{np}(\alpha_A)\cdot p + C_{nr}(\alpha_A)\cdot r\right] - \left(\frac{\bar{c}}{b}\right)\left(x_{cg_{ref}} - x_{cg}\right)C_Y \quad (6\text{-}18)$$

where q^* is the non dimensionless pitch rate defined by

$$q^* = \frac{q\cdot\bar{c}}{2\cdot V_A} \quad (6\text{-}19)$$

The model used is identical to the one given in Annex D.4 of Klein and Morelli (2006, pp. 469-470). A more detailed description can be found there. Table 22 summarizes the constant aerodynamic parameters. The elevator deflection angles given represent the nominal values for the F-16 (cf. Nguyen et al., 1979, pp. 11 & 34-35). The case study conducted in this work will only analyse the longitudinal motion. Figure 73 shows the relevant aerodynamic coefficients $(C_{X0})_B$, $(C_{Z0})_B$ and $(C_{m0})_B$ as function of the angle of attack α_A for three different elevator deflection angles η. As it can been seen the slope of $(C_m)_B$ is positive in nearly all regions, i.e. the aircraft is statically unstable for $(x^G)_B = 0{,}4\ \cdot \bar{c}$.

Remark 6-1: It is important to note that, for $\alpha_A > 30\ deg$ and $\eta = +25\ deg$ (full nose down), $(C_m)_B$ becomes positive which means that no nose down moment can be created any longer. However this a particularity of the CG position chosen for this case study. In this regard we have to keep in mind that for the original F-16, with $\left(x^G_{ref}\right)_B = 0{,}35\ \cdot \bar{c}$, $(C_m)_B$ only becomes positive for $\alpha_A > 45\ deg$. Clearly if we would build a more unstable F-16 with $(x^G)_B = 0{,}4\ \cdot \bar{c}$ more pitch control power would be required, than with the original design.

Table 22 Summary of aerodynamic parameters

Parameter	**Symbol**	**Value**
Wing Area	S	$27.87\ m^2$
Wing Span	b	$9.14\ m$
Mean Aerodynamic Chord	$\bar{c}$	$3.45\ m$
Maximum elevator deflection angle	η	$\pm 25\ deg$
Maximum aileron deflection angle	ξ	$\pm 21{,}5\ deg$
Maximum ruder deflection angle	ζ	$\pm 30\ deg$

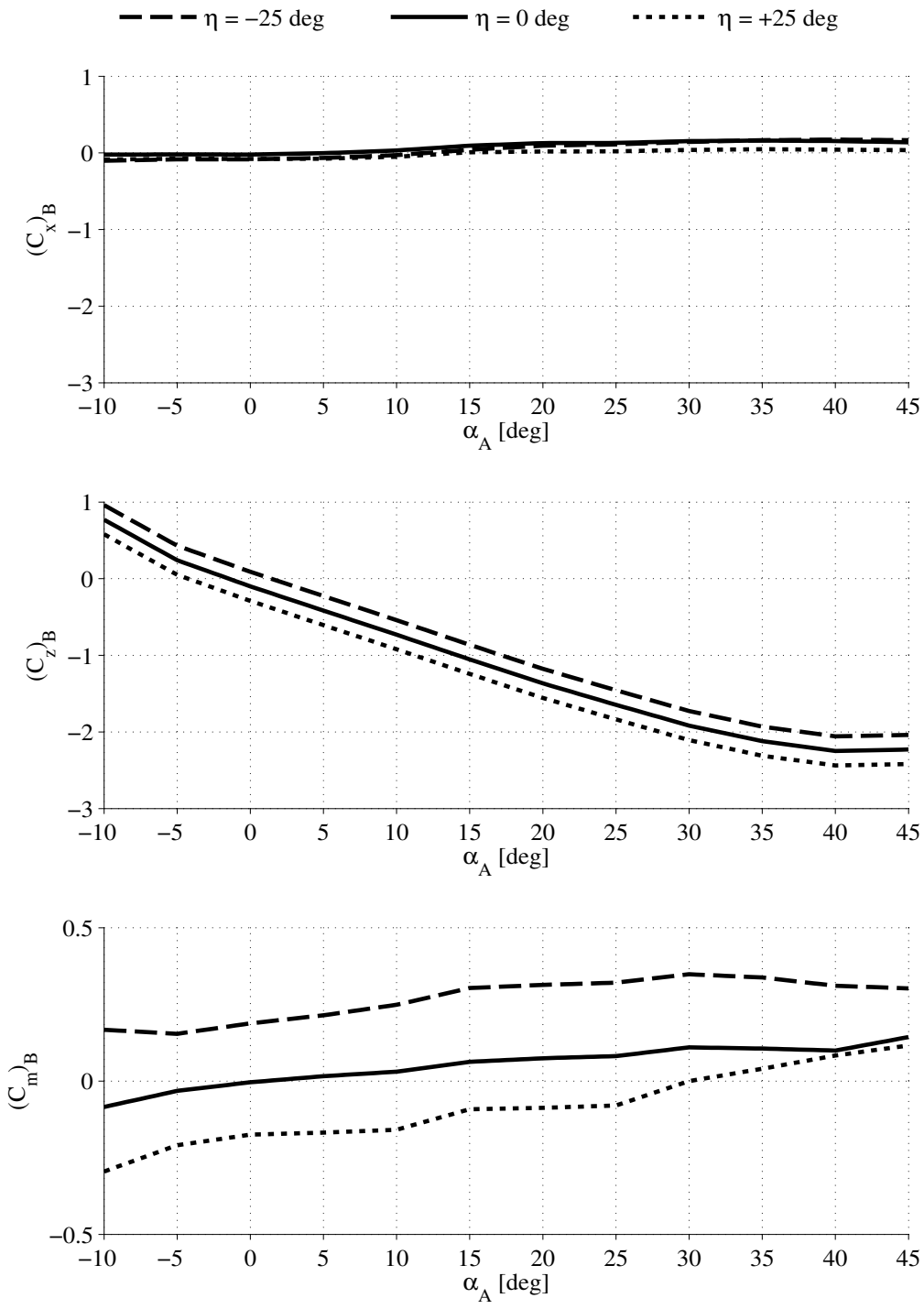

Figure 73 Longitudinal aerodynamic coefficients as function of the angle of attack

A.7 F-16 Angle-Of-Attack /G-Limiter

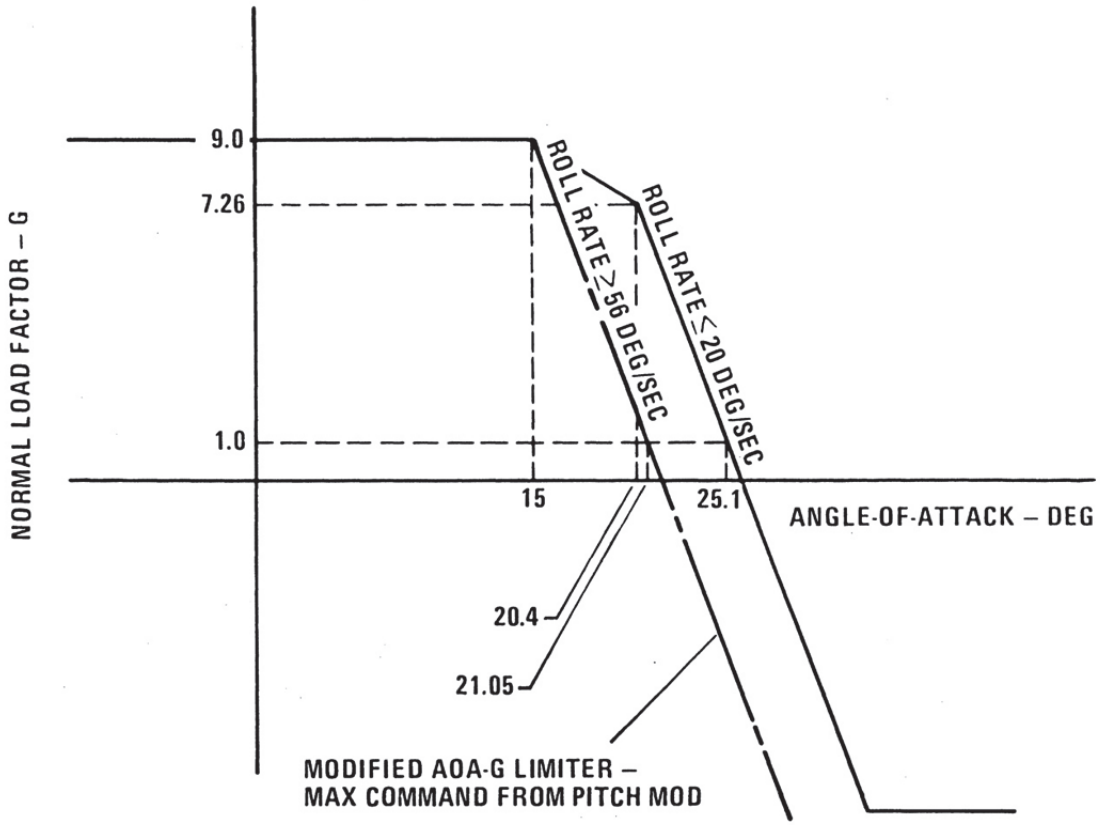

Figure 74 F-16 Angle-Of-Attack /G-Limiter (Droste & Walker, 2010, p. 94)

References

Aloni, S. (2006). *Israeli F-15 Eagle Units in Combat*. Oxford, UK: Osprey Publishing.

Alwi, H., Edwards, C., & Pin Tan, C. (2011). *Fault Detection and Fault-Tolerant Control Using Sliding Modes*. London: Springer.

Bartley, G. F. (2001). Boeing B-777: Fly-by-wire flight controls. In C. R. Spitzer (Ed.), *Digital Avionics Handbook*: CRC Press.

Basseville, M., & Nikiforov, I. V. (1993). *Detection of Abrupt Changes - Theory and Application*: Prentice-Hall.

Baumgarten, G., Buchholz, J., & Heine, W. (1995). A new reconfiguration concept for flight control systems *Guidance, Navigation, and Control Conference*: American Institute of Aeronautics and Astronautics.

Bodson, M., & Groszkiewicz, J. E. (1997). Multivariable adaptive algorithms for reconfigurable flight control. *Ieee Transactions on Control Systems Technology, 5*(2), 217-229. doi: 10.1109/87.556026

Boskovic, J., Bergstrom, S., Mehra, R., Urnes, J., Hood, M., & Lin, Y. (2005). Fast On-Line Actuator Reconfiguration Enabling (FLARE) System *AIAA Guidance, Navigation, and Control Conference and Exhibit*: American Institute of Aeronautics and Astronautics.

Boskovic, J., Prasanth, R., & Mehra, R. (2005). *Retrofit Reconfigurable Flight Control*. Paper presented at the AIAA Guidance, Navigation, and Control Conference and Exhibit, San Francisco, California.

Boskovic, J., Redding, J., & Knoebel, N. (2009). *An Adaptive Fault Management (AFM) System for Resilient Flight Control*. Paper presented at the AIAA Guidance, Navigation, and Control Conference, Chicago, Illinois. http://arc.aiaa.org/doi/abs/10.2514/6.2009-6263

Boskovic, J. D., Bergstrom, S., & Mehra, R. K. (2005). Robust Integrated Flight Control Design Under Failures, Damage, and State-Dependent Disturbances. *Journal of Guidance, Control, and Dynamics, 28*(5), 902-917. doi: 10.2514/1.11272

Boskovic, J. D., Bergstrom, S. E., & Mehra, R. K. (2005). *Retrofit reconfigurable flight control in the presence of control effector damage*. Paper presented at the American Control Conference.

Boskovic, J. D., & Mehra, R. K. (2002). *An adaptive retrofit reconfigurable flight controller*. Paper presented at the 41st IEEE Conference on Decision and Control.

Boskovic, J. D., Prasanth, R., & Mehra, R. K. (2007). Retrofit Fault-Tolerant Flight Control Design Under Control Effector Damage. *Journal of Guidance, Control, and Dynamics, 30*(3), 703-712. doi: 10.2514/1.25564

Bosworth, J. (2008). *Flight Results of the NF-15B Intelligent Flight Control System (IFCS) Aircraft with Adaptation to a Longitudinally Destabilized Plant*. Paper presented at the AIAA Guidance, Navigation and Control Conference and Exhibit, Honolulu, HI; United States.

Bosworth, J. T., & Williams-Hayes, P. S. (2007). *Flight Test Results from the NF-15B Intelligent Flight Control System (IFCS) Project with Adaptation to a Simulated Stabilator Failure*. NASA/TM-2007-214629. Edwards, CA, United States: NASA Dryden Flight Research Center.

Boyd, S., & Lall, S. (2014). *Introduction to Linear Dynamical Systems*. Lecture Notes (EE263, Autumn 2014-15). Electrical Engineering. Stanford University. Stanford, CA, United States.

Briat, C. (2015). *Linear Parameter-Varying and Time-Delay Systems: Analysis, Observation, Filtering & Control*. Berlin Heidelberg, Germany: Springer.

Brière, D., Favre, C., & Traverse, P. (2000). Electrical Flight Controls, From Airbus A320/330/340 to Future Military Transport Aircraft. In C. R. Spitzer (Ed.), *Digital Avionics Handbook, Second Edition*: CRC Press.

Brinker, J., & Wise, K. (1998). Reconfigurable flight control for a tailless advanced fighter aircraft *AIAA Guidance, Navigation, and Control Conference and Exhibit*: American Institute of Aeronautics and Astronautics.

Brinker, J., & Wise, K. (2000). *Flight testing of a reconfigurable flight control law on the X-36 tailless fighter aircraft*. Paper presented at the AIAA Guidance, Navigation, and Control Conference and Exhibit.

Brinker, J. S., & Wise, K. A. (2001). Flight Testing of Reconfigurable Control Law on the X-36 Tailless Aircraft. *Journal of Guidance, Control, and Dynamics, 24*(5), 903-909. doi: 10.2514/2.4826

Britt, R. T., Volk, J. A., Dreim, D. R., & Applewhite, K. A. (2000). *Aeroservoelastic Characteristics of the B-2 Bomber and Implications for Future Large Aircraft*. Paper presented at the NATO RTO AVT Specialists' Meeting on "Structural Aspects of Flexible Aircraft Control", Ottawa, Canada. https://www.cso.nato.int/Pubs/rdp.asp?RDP=RTO-MP-036

Brockhaus, R., Alles, W., & Luckner, R. (2011). *Flugregelung* (3 ed.). Berlin, Heidelberg: Springer.

Buchholz, J. J., Heine, W., & Baumgarten, G. (1996). Genetic algorithms for reconfiguration. *Zeitschrift für Flugwissenschaften und Weltraumforschung, 20*, pp. 129-136.

Burken, J., Hanson, C., Lee, J., & Kaneshige, J. (2009). *Flight Test Comparison of Different Adaptive Augmentations of Fault Tolerant Control Laws for a Modified F-15 Aircraft*. Paper presented at the AIAA Infotech@Aerospace Conference.

Burken, J., Maine, T., Burcham, F. J., & Kahler, J. (1996). *Longitudinal emergency control system using thrust modulation demonstrated on an MD-11 airplane*. Paper presented at the 32nd Joint Propulsion Conference and Exhibit.

Burken, J. J., Williams-Hayes, P., Kaneshige, J. T., & Stachowiak, S. J. (2006). *Reconfigurable Control with Neural Network Augmentation for a Modified F-15 Aircraft*. NASA/TM-2006-213678. Edwards, CA, United States: NASA Dryden Flight Research Center.

Buschbacher, M., & Maliska, H. (2006). *Flight Test of an Adaptive Controller and Simulated Failure/Damage on the NASA NF-15B*. Paper presented at the 7th Annual SFTE (Society of Flight Test Engineers) Symposium, Reno, NV, United States.

Calise, A., Kim, B. S., Kam, M., & Azam, M. (1992). *Neural networks for feedback linearization in aircraft control*. Paper presented at the Guidance, Navigation and Control Conference.

Calise, A., Lee, S., & Sharma, M. (1998). *Direct adaptive reconfigurable control of a tailless fighter aircraft*. Paper presented at the Guidance, Navigation, and Control Conference and Exhibit.

Calise, A. J., Bong-Jun, Y., & Craig, J. I. (2002). *Augmentation of an existing linear controller with an adaptive element*. Paper presented at the American Control Conference.

Chandler, P. R. (1984). *Self-repairing flight control system reliability and maintainability program executive overview*.

Chandler, P. R., Pachter, M., & Mears, M. (1995). System identification for adaptive and reconfigurable control. *Journal of Guidance, Control, and Dynamics, 18*(3), 516-524. doi: 10.2514/3.21417

DasGupta, A. (2011). *Probability for Statistics and Machine Learning: Fundamentals and Advanced Topics*. New York, NY, United States: Springer.

de Almeida, F., & Leißling, D. (2009). *Fault-Tolerant Model Predictive Control with Flight Test Results on ATTAS*. Paper presented at the AIAA Guidance, Navigation, and Control Conference.

de Almeida, F. A., & Leißling, D. (2010). Fault-Tolerant Model Predictive Control with Flight-Test Results. *Journal of Guidance, Control, and Dynamics, 33*(2), 363-375. doi: 10.2514/1.46108

Ding, S. X. (2013). *Model-Based Fault Diagnosis Techniques* (2 ed.). London: Springer.

DLR. (2008). VFW 614/ATTAS. Retrieved from http://www.dlr.de/DesktopDefault.aspx/tabid-4777/7916_read-11998/gallery-1/gallery_read-Image.1.5656/

Droste, C., & Walker, J. (2010). *The General Dynamics Case Study on the F-16 Fly-By-Wire Flight Control System*. Reston, VA, United States: American Institute of Aeronautics and Astronautics (AIAA).

Dryden, H. L. (1961). *A Review of the Statistical Theory of Turbulence*. New York, NY, United States: Interscience Publishers.

EASA. (2013). *Certification Specifications and Acceptable Means of Compliance for Large Aeroplanes* (CS-25 Amendment 14:2013).

Edwards, C., Lombaerts, T., & Smaili, H. (Eds.). (2010). *Fault Tolerant Flight Control*. Berlin Heidelberg: Springer.

Eterno, J. S., Weiss, J. L., Looze, D. P., & Willsky, A. (1985). *Design issues for fault tolerant-restructurable aircraft control*. Paper presented at the 24th IEEE Conference on Decision and Control

Gibson, J. C. (1999). *Development of a design methodology for handling qualities excellence in fly by wire aircraft*. (Doctoral Thesis), Delft University of Technology, Netherlands.

Goupil, P. (2010). Oscillatory failure case detection in the A380 electrical flight control system by analytical redundancy. *Control Engineering Practice, 18*(9), 1110-1119.

Goupil, P., & Marcos, A. (2010). Industrial Review. In C. Edwards, T. Lombaerts, & H. Smaili (Eds.), *Fault Tolerant Flight Control* (pp. 521-536). Berlin Heidelberg: Springer.

Gregory, I., Cao, C., Xargay, E., Hovakimyan, N., & Zou, X. (2009). *L1 Adaptive Control Design for NASA AirSTAR Flight Test Vehicle*. Paper presented at the AIAA Guidance, Navigation, and Control Conference.

Gregory, I., Xargay, E., Cao, C., & Hovakimyan, N. (2010). *Flight Test of an L1 Adaptive Controller on the NASA AirSTAR Flight Test Vehicle*. Paper presented at the AIAA Guidance, Navigation, and Control Conference.

Gu, D.-W., Petkov, P. H., & Konstantinov, M. M. (2013). *Robust Control Design with MATLAB* (2 ed.). London: Springer.

Hageman, J. J., Smith, M. S., & Stachowiak, S. (2003). *Integration of Online Parameter Identification and Neural Network for In-Flight Adaptive Control*. NASA/TM-2003-212028. Edwards, CA, United States: NASA Dryden Flight Research Center.

Hartnett, F. (2006). Ripped Off: The Story of No. 61-023. Retrieved April 17, 2014 from http://www.barksdale.af.mil/news/story.asp?id=123024862

Heine, W. (1999). *Alternative Flight Control Strategies For Multiple Effector Failures: ATTAS Flight Test Results and Lessons Learned*. Paper presented at the RTO SCI Symposium on "Flight in a Hostile Environment", Island, Maryland, United States.

Heller, M. (2013). *Flugdynamische Herausforderungen hochgradig-reglergestützter Konfigurationen*. Lecture Notes. Institut für Flugsystemdynamik. Technical University of Munich. Germany.

Henzel, J. H. (1967). *The Human Spinal Column And Upward Ejection Acceleration: An Appraisal Of Biodynamic Implications*. Wright-Patterson Air Force Base, Ohio, United States: Aerospace Medical Research Laboratories, Aerospace Medical Division, Air Force Systems Command. Retrieved June 11th, 2017 from http://www.dtic.mil.

Hodgkinson, J. (1999). *Aircraft Handling Qualities*. Reston, VA, United States: American Institute of Aeronautics and Astronautics (AIAA).

Holzapfel, F. (2011). *Flugsystemdynamik II*. Lecture Notes. Institute for Flight System Dynamics. Technical University of Munich. Germany.

Idan, M., Johnson, M., & Calise, A. J. (2002). Hierarchical Approach to Adaptive Control for Improved Flight Safety. *Journal of Guidance, Control, and Dynamics, 25*(6), 1012-1020. doi: 10.2514/2.5005

Isermann, R. (2006). *Fault-Diagnosis Systems. An Introduction from Fault Detection to Fault Tolerance*. Berlin Heidelberg: Springer.

Isermann, R., & Ballé, P. (1997). Trends in the application of model-based fault detection and diagnosis of technical processes. *Control Engineering Practice, 5*(5), 709-719. doi: 10.1016/S0967-0661(97)00053-1

ISO. (1997). *Standard Atmosphere* (ISO 2533:1975/Add.2:1997(E/F/R):1997).

Jategaonkar, R. V. (2006). *Flight Vehicle System Identification*: American Institute of Aeronautics and Astronautics.

Jourdan, D. B., Piedmonte, M. D., Gavrilets, V., Vos, D. W., & McCormick, J. (2010). *Enhancing UAV Survivability Through Damage Tolerant Control*. Paper presented at the AIAA Guidance, Navigation, and Control Conference, Toronto, Ontario, Canada.

Jovan, B., Joshua, R., & Raman, M. (2007). *Integrated Health Monitoring and Adaptive Reconfigurable Control*. Paper presented at the AIAA Guidance, Navigation and Control Conference and Exhibit.

Jovan, B., Ravi, P., & Raman, M. (2006). *Reconfigurable Fault-Tolerant Flight Control: Algorithms, Implementation and Metrics*. Paper presented at the AIAA Guidance, Navigation, and Control Conference and Exhibit.

Kaminski, M. (2012). *Proposal for online detection of changes in the flight dynamic characteristics, due to e.g. air vehicle damage, with subsequent re estimation of aerodynamic parameters*. Technische Universität München, Munich, Germany.

Kaul, H. J. (1992). *Flugsteuerung Jäger 90*. Paper presented at the DGLR Jahrestagung.

Kaul, H. J., Sella, F., & Walker, M. J. (1985). *The flight control system for the Experimental Aircraft Programme (EAP) demonstration aircraft*. Paper presented at the AGARD-CP-384.

Kim, B. S., & Calise, A. J. (1997). Nonlinear Flight Control Using Neural Networks. *Journal of Guidance, Control, and Dynamics, 20*(1), 26-33. doi: 10.2514/2.4029

Klein, V., & Morelli, E. A. (2006). *Aircraft System Identification: Theory and Practice*: American Institute of Aeronautics and Astronautics.

Koch, K.-R. (1999). *Parameter Estimation and Hypothesis Testing in Linear Models*. Berlin Heidelberg: Springer.

Lavigne, L., Cazaurang, F., Fadiga, L., & Goupil, P. (2014). New sequential probability ratio test: Validation on A380 flight data. *Control Engineering Practice, 22*(0), 1-9.

Lewis, F. L., Xie, L., & Popa, D. (2007). *Optimal and Robust Estimation: With an Introduction to Stochastic Control Theory* (2 ed.). Boca Raton, FL, United States: CRC Press.

Lombaerts, T., Smaili, H., & Breeman, J. (2010). Introduction. In C. Edwards, T. Lombaerts, & H. Smaili (Eds.), *Fault Tolerant Flight Control* (pp. pp. 3-45). Berlin Heidelberg: Springer.

Mason, D., ed. (1985). Eagle Eyed. *Flight International*.

Maybeck, P. S. (1979). *Stochastic Models, Estimation and Control Volume 1* (1 ed. Vol. 1). New York, New York, USA: Academic Press.

McDonough, R. N., & Whalen, A. D. (1995). *Detection of Signals in Noise* (2 ed.): Elsevier Science.

Mohammadpour, J., & Scherer, C. W. (2012). *Control of Linear Parameter Varying Systems with Applications*. New York: Springer.

Moir, I., & Seabridge, A. (2013). *Design And Development Of Aircraft Systems* (2nd ed.). West Sussex, UnitedKingdom: Wiley.

Monaco, J., Ward, D., Barron, R., & Bird, R. (1997). *Implementation and flight test assessment of an adaptive, reconfigurable flight control system*. Paper presented at the Guidance, Navigation, and Control Conference.

Monaco, J., Ward, D., & Bateman, A. (2004). *A Retrofit Architecture for Model-Based Adaptive Flight Control*. Paper presented at the AIAA 1st Intelligent Systems Technical Conference.

Moritz, N., & Osterhuber, R. (2006). *Three-Stage Gradient-Based Optimization Scheme in Design of Feedback Gains Within Eurofighter Primary Control Laws*. Paper presented at the AIAA Guidance, Navigation, and Control Conference and Exhibit, Keystone, Colorado.

Müller, K. (1996). *Entwurf robuster Regelungen* (1 ed.). Stuttgart: B. G. Teubner.

NASA. (1993, February 8). F-15A HIDEC. Retrieved from http://www.nasa.gov/sites/default/files/images/308230main_EC93-2081-1_full.jpg

NASA. (1997, October 30). X-36. Retrieved from http://www.nasa.gov/sites/default/files/styles/1600x1200_autoletterbox/public/images/354673main_EC97-44294-4_full.jpg?itok=EmXCZGm6

NASA. (1998, April 14). F-15B ACTIVE. Retrieved from http://www.nasa.gov/centers/armstrong/multimedia/imagegallery/F-15ACTIVE/index.html#lowerAccordion-set3-slide22

NATO AGARD. (1991a). *Flying Qualities*. Published Conference Proceedings AGARD-CP-508. Neuilly-sur-Seine, France: North Atlantic Treaty Organization Advisory Group for Aerospace Research and Development (NATO AGARD).

NATO AGARD. (1991b). *Handling Qualities of Unstable Highly Augmented Aircraft*. Published Report AGARD-AR-279. Neuilly-sur-Seine, France: North Atlantic Treaty Organization Advisory Group for Aerospace Research and Development (NATO AGARD). Retrieved Feb 14, 2015 from www.dtic.mil.

NATO RTO. (2000). *Flight Control Design – Best Practices*. Published Report RTO-TR-029. Neuilly-sur-Seine, France: North Atlantic Treaty Organization Science and Technology Organization (NATO RTO). Retrieved Feb 14, 2014 from https://www.cso.nato.int/Pubs/rdp.asp?RDP=RTO-TR-029.

Neubauer, M., & Günther, G. (2001). *Aircraft Loads*. Paper presented at the RTO AVT Lecture Series on "Aging Aircraft Fleets: Structural and Other Subsystem Aspects ", Sofia, Bulgaria. http://www.dtic.mil/get-tr-doc/pdf?AD=ADP010772

Neyman, J., & Pearson, E. S. (1933). On the Problem of the Most Efficient Tests of Statistical Hypotheses. *Philosophical Transactions of the Royal Society of London. Series A, Containing Papers of a Mathematical or Physical Character, 231*, 289-337. doi: 10.2307/91247

Nguyen, L. T., Ogburn, M. E., Gilbert, W. P., Kibler, K. S., Brown, P. W., & Deal, P. L. (1979). *Simulator study of stall/post-stall characteristics of a fighter airplane with relaxed longitudinal static stability*. Report NASA-TP-1538. Hampton, VA, United States: NASA Langley Research Center.

NTSB. (1990). *United Airlines Flight 232, McDonnell Douglas DC-10-10, Sioux Gateway Airport, Sioux City, Iowa, July 19, 1989*. Aircraft Accident Report NTSB/AAR-SO/06. Washington, D.C., USA: National Transportation Safety Board.

Oelker, H.-C., Osterhuber, R., & Hanel, M. (2009). *Experiences with Eurofighter Handling Qualities Testing*. Paper presented at the AIAA Atmospheric Flight Mechanics Conference.

Osterhuber, R., Hanel, M., & Hammon, R. (2004). *Realization of the Eurofighter 2000 Primary Lateral/Directional Flight Control Laws with Differential PI-Algorithm*. Paper presented at the AIAA Guidance, Navigation, and Control Conference and Exhibit, Providence, Rhode Island.

Page, A., Monaco, J., & Meloney, D. (2006). *Flight Testing of a Retrofit Reconfigurable Control Law Architecture Using an F/A-18C*. Paper presented at the AIAA Guidance, Navigation, and Control Conference and Exhibit.

Patton, R. J. (1997). *Fault-tolerant control systems: The 1997 situation*.

PennState. (2017). Probability Theory and Mathematical Statistics (STAT 414/415). Retrieved June 14, 2017 from https://onlinecourses.science.psu.edu/stat414/node/171

Pywell, M., Alonze, P. M., Hurricks, M. E., & Wellings, I. G. (1999). *The new enigma: Increased survivability with reduced cost?* Paper presented at the RTO SCI Symposium on "Flight in a Hostile Environment", Island, Maryland, United States.

Rice, J. W., & McCorkle, R. D. (1979). *Digital Flight Control Reliability - Effects of Redundancy Level, Architecture and Redundancy Management Technique*. Paper presented at the Guidance and Control Conference, Boulder, CO, United States.

Rysdyk, R., & Calise, A. (1998). *Fault tolerant flight control via adaptive neural network augmentation*. Paper presented at the AIAA Guidance, Navigation, and Control Conference and Exhibit.

SAE. (2007). *Aerospace - Flight Control Systems - General Specification For Design, Installation and Test of Piloted Military Aircraft* (AS94900:2007).

Scherer, C. W., & Weiland, S. (2015). *Linear Matrix Inequalities in Control.* Lecture Notes. University of Stuttgart, Department of Mathematics & Eindhoven University of Technology, Department of Electrical Engineering. Retrieved from http://www.mathematik.uni-stuttgart.de/opencms/opencms/fak8/imng/lehrstuhl/lehrstuhl_fuer_mathematische_systemtheorie/lehre_/lehrangebote/lmi/index.html

Scherer, C. W., & Weiland, S. (2016). *Linear Matrix Inequalities in Control.* Lecture Presentation. University of Stuttgart & Eindhoven University of Technology. Germany/The Netherlands. Retrieved from http://www.mathematik.uni-stuttgart.de/opencms/opencms/fak8/imng/lehrstuhl/lehrstuhl_fuer_mathematische_systemtheorie/lehre_/lehrangebote/lmi/index.html

Shamma, J. S. (1988). *Analysis and design of gain scheduled control systems.* (PhD thesis), Massachusetts Institute of Technology, United States.

Shamma, J. S., & Athans, M. (1992). Gain scheduling: potential hazards and possible remedies. *Control Systems, IEEE, 12*(3), 101-107. doi: 10.1109/37.165527

Slotine, J.-J., & Li, W. (1990). *Applied Nonlinear Control*. Upper Saddle River, New Jersey, United States: Prentice Hall.

Smith, S. W. (2003). *Digital Signal Processing*. Amsterdam: Newnes Elsevier.

Srinathkumar, S. (2011a). *Eigenstructure Control Algorithms: Applications to aircraft/rotorcraft handling qualities design*. London, United Kingdom: Institution of Engineering and Technology.

Srinathkumar, S. (2011b). *ESCORT User Manual*. Retrieved March 04, 2014 from http://www.escortool.com/toolbox/.

Steinberg, M. (2005). Historical Overview of Research in Reconfigurable Flight Control. *Proceedings of the Institution of Mechanical Engineers, Part G: Journal of Aerospace Engineering, 219*(4), 263-275. doi: 10.1243/095441005x30379

Tartakovsky, A., Nikiforov, I., & Basseville, M. (2015). *Sequential Analysis: Hypothesis Testing and Changepoint Detection*. Boca Raton, FL, United States: Chapman and Hall/CRC.

The MathWorks Inc. (2014). *Aerospace Blockset™ User's Guide R2014b* (Version 3.14 (Release 2014b) ed.). Natick, MA, USA: The MathWorks, Inc.

The MathWorks Inc. (2017a). *Control System Toolbox™ Reference*. Natick, MA, USA: The MathWorks, Inc.

The MathWorks Inc. (2017b). *MATLAB®Function Reference*. Natick, MA, USA: The MathWorks, Inc.

Tischler, M. B., & Remple, R. K. (2012). *Aircraft and Rotorcraft System Identification* (2 ed.). Reston, VA, United States: American Institute of Aeronautics and Astronautics.

Tomayko, J. E. (2003). *The Story of Self-Repairing Flight Control Systems*. Edwards, CA, United States: NASA Dryden Flight Research Center.

Traverse, P., Lacaze, I., & Souyris, J. (2004). *Airbus Fly-By-Wire: A Total Approach To Dependability*. Paper presented at the IFIP/WCC/topical event «fault-tolerance for trustworthy and dependable information infrastructure», Toulouse.

Tschirk, W. (2014). *Statistik: Klassisch oder Bayes*. Berlin Heidelberg: Springer.

TUM UB. (2014). *TUM-Zitierleitfaden*. Technische Universität München Universitätsbibliothek (TUM UB). Germany.

Unknown. (1964). 1963 Elephant Mountain B-52 crash. Retrieved April 21, 2014 from http://en.wikipedia.org/wiki/1963_Elephant_Mountain_B-52_crash

Unknown. (2014). Avions d'Israeal/ Aircrafts from Israel. Retrieved April 21, 2014, 2014 from http://israel-aircraft-avions.blogspot.de/p/f15.html

US DoD. (1975). *Flight Control Systems - Design, Installation And Test Of Piloted Aircraft* (MIL-F-9490D:1975).

US DoD. (1987). *Airplane Strength And Rigidity, General Specification For* (MIL-A-8860B:1987).

US DoD. (1996). *Flying Qualities of Piloted Airplanes* (MIL–F–8785C incl. Notice 1-2:1996).

US DoD. (2004). *Flying Qualities Of Piloted Aircraft* (MIL-STD-1797A including Notice 1-3:2004).

US DoD. (2012). *Flying Qualities of Piloted Aircraft* (MIL–STD–1797B incl. Notice 1:2012).

USAF. (1964). United States Air Force Film Report - Flight Without a Fin. Retrieved April 17, 2014 from https://www.youtube.com/watch?v=WJuEAQbxWRo

USAF. (2001). *Executive Summary, Aircraft Accident Investigation RQ-4A Global Hawk UAV Accident, Forward Operating Location, 30 December 2001*. Maxwell Air Force Base, Alabama, USA: United States Air Force (USAF). Retrieved April 18, 2014 from http://usaf.aib.law.af.mil/ExecSum2002/RQ-4A_FOL_30Dec01.pdf.

USAF. (2002). *Executive Summary, Aircraft Accident Investigation RQ-4A Global Hawk UAV Accident, Forward Operating Location, 10 July 2002*. Maxwell Air Force Base, Alabama, USA: United States Air Force (USAF). Retrieved April 18, 2014 from http://usaf.aib.law.af.mil/ExecSum2002/RQ-4A_CENTCOMAOR_10Jul02.pdf.

USAF. (2008). *Executive Summary, Aircraft Accident Investigation B-2A, T/N 89-0127, Anderson Air Force Base, Guam, 23 February 2008*. Maxwell Air Force Base, Alabama, USA: United States Air Force (USAF). Retrieved April 18, 2014 from http://usaf.aib.law.af.mil/ExecSum2008/B-2A_Andersen_23Feb08.pdf.

USAF. (2012, March 21). F-16 VISTA. Retrieved from http://www.edwards.af.mil/shared/media/photodb/photos/2012/12/110321-F-QG253-483.jpg

Verhaegen, M., Kanev, S., Hallouzi, R., Jones, C., Maciejowski, J., & Smail, H. (2010). Fault Tolerant Flight Control - A Survey. In C. Edwards, T. Lombaerts, & H. Smaili (Eds.), *Fault Tolerant Flight Control* (pp. 47-89). Berlin Heidelberg: Springer.

Ward, D. G., & Barron, R. L. (1995). *A self-designing receding horizon optimal flight controller*. Paper presented at the Proceedings Of the American Control Confernce, Seattle, Washington.

Ward, D. G., Barron, R. L., Carley, M. P., & Curtis, T. J. (1994). *Real-time parameter identification for self-designing flight control*. Paper presented at the IEEE 1994 National Aerospace and Electronics Conference, Dayton, OH, United States.

Ward, D. G., & Monaco, J. F. (2005). System identification for retrofit reconfigurable control of an F/A-18 aircraft. *Journal of Aircraft, 42*(1), 63-72. doi: 10.2514/1.2941

Ward, D. G., Monaco, J. F., & Bodson, M. (1998). Development and Flight Testing of a Parameter Identification Algorithm for Reconfigurable Control. *Journal of Guidance, Control, and Dynamics, 21*(6), 948-956. doi: 10.2514/2.4329

Wikipedia. (2016). Continuous gusts. Retrieved 22 September, 2016 from https://en.wikipedia.org/w/index.php?title=Continuous_gusts&oldid=740686944

Williams-Hayes, P. S. (2004). *Selected Flight Test Results for Online Learning Neural Network-Based Flight Control System*. TM-2004-212857. Edwards, CA, United States: NASA Dryden Flight Research Center.

Williams-Hayes, P. S. (2005). *Flight Test Implementation of a Second Generation Intelligent Flight Control System*. TM-2005-213669. Edwards, CA, United States: NASA Dryden Flight Research Center.

Wise, K. A., Brinker, J. S., Calise, A. J., Enns, D. F., Elgersma, M. R., & Voulgaris, P. (1999). Direct Adaptive Reconfigurable Flight Control For A Tailless Advanced Fighter Aircraft. *International Journal of Robust and Nonlinear Control, 9*(14), 999-1012.

Wohletz, J., Paduano, J., & Annaswamy, A. (1999). *Retrofit Systems For Reconfiguration In Civil Aviation*. Paper presented at the Guidance, Navigation, and Control Conference and Exhibit. http://dx.doi.org/10.2514/6.1999-3964

Wohletz, J., Paduano, J., & Maine, T. (2000). Retrofit Reconfiguration System For A Commercial Transport *AIAA Guidance, Navigation, and Control Conference and Exhibit*: American Institute of Aeronautics and Astronautics.

Yeager, J. C. (1998). *Implementation and Testing of Turbulence Models for the F18-HARV Simulation*. CR-1998-206937. Hampton, VA United States: NASA Langley Research Center. Retrieved Feb 20, 2016 from http://ntrs.nasa.gov/.

Yeh, Y. C. (1996). *Triple-triple redundant 777 primary flight computer*. Paper presented at the Aerospace Applications Conference.

Yeh, Y. C. (1998). *Design considerations in Boeing 777 fly-by-wire computers*. Paper presented at the Third IEEE International High-Assurance Systems Engineering Symposium.

Yeh, Y. C. (2001). *Safety critical avionics for the 777 primary flight controls system*. Paper presented at the 20th Digital Avionics Systems Conference.

Zhang, Y., & Jiang, J. (2008). Bibliographical review on reconfigurable fault-tolerant control systems. *Annual Reviews in Control, 32*(2), 229-252. doi: 10.1016/j.arcontrol.2008.03.008